Functions of leptin in tuberculosis and diabetes: multi-omics studies across species

Ding, Y.

Functions of leptin in tuberculosis and diabetes: multi-omics studies across species

Yi Ding

Colophon

Title: Functions of leptin in tuberculosis and diabetes: multi-omics studies across species

Author: Yi Ding

PhD thesis, Leiden University, Leiden, the Netherlands

Cover design & layout: Yi Ding

Printed: PrintSupport4U.nl

ISBN: 978-94-92597-85-4

The research described in this thesis was performed at the Animal Sciences and Health division of the Institute of Biology Leiden (IBL) and the Leiden Institute of Chemistry, Leiden University (Leiden, the Netherlands) and Institut für Medizinische Physik und Biophysik, Leipzig University (Leipzig, Germany).

The work was supported by China Scholarship Council.

The publication of this thesis was financially supported by Life Science Methods, IBL and Leiden University.

Functions of leptin in tuberculosis and diabetes: multi-omics studies across species

Proefschrift

ter verkrijging van

de graad van doctor aan de Universiteit Leiden,

op gezag van rector magnificus prof.dr.ir. H. Bijl,

volgens besluit van het college voor promoties

te verdedigen op dinsdag 7 december 2021

klokke 10.00 uur

door

Yi Ding

geboren te Chongqing, China

in 1989

Promotores: Prof. dr. H.P. Spaink

Prof. dr. A. Alia

Promotiecommissie:

Prof. dr. G. P. van Wezel

Prof. dr. A. H. Meijer

Prof. dr. T. Hankemeier

Prof. dr. J. Matysik (Universität Leipzig)

Prof. dr. J. P. Berry (Florida International University)

Table of contents

1

General introduction

Yi Ding[1], Herman P. Spaink[1]

[1] Institute of Biology, Leiden University, The Netherlands

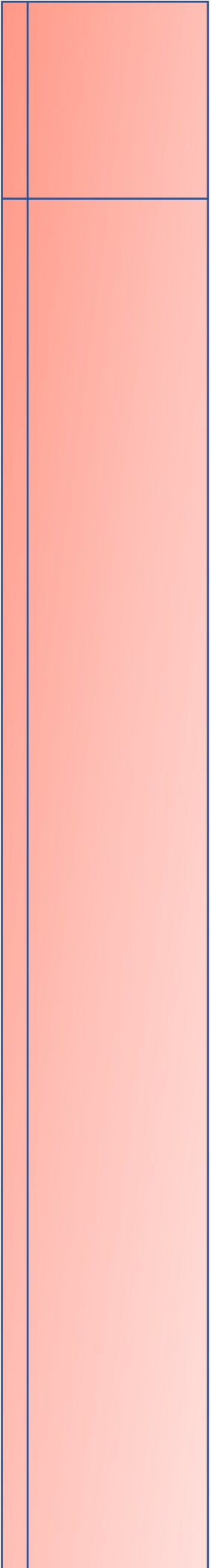

Functions of leptin in metabolic wasting syndrome

Metabolic wasting syndrome, also called cachexia, is a metabolic disorder characterized by unintentional excessive weight loss (greater than 5% of body weight in preceding 6 months) with the depletion of muscle and adipose tissues [1, 2]. It is different from the weight loss resulting from starvation, which can be recovered by ingestion of food. However, in the condition of wasting syndrome, the weight loss and body composition are hardly reversed by food supplementation [3]. This is because profound irreversible metabolic reprogramming takes place, which results in the degradation of muscle tissues [3, 4]. It usually occurs at the late stage of chronic diseases such as cancer [5], autoimmune disease (rheumatoid arthritis) [6], infectious diseases including AIDS and tuberculosis [7, 8], diabetes [9] and chronic kidney disease [10]. Cachexia increases the mortality and it accounts for 30% of death in patients with chronic diseases [11]. However, currently no pharmacological treatment exists [12, 13].

We have studied the function of the leptin gene in wasting syndrome. Leptin was firstly cloned and identified in obese mice by Friedman in 1994 [14]. It is a 167 amino acid long protein hormone with four-helix bundles (**Figure 1A**) and mainly secreted by adipose tissues. It has been shown that leptin is a key regulator of appetite, body weight, energy regulation, bone metabolism, immunity, reproduction and metabolic homeostasis [15, 16] (**Figure 1B**). Mutation of the *lep* gene (originally called *ob* gene) in mice (*ob/ob*) leads to extreme obesity, insulin resistance and type 2 diabetes mellitus [17]. The mutants in a later stage of diabetes, also display wasting syndrome characterized by the loss of muscle mass [18]. Therefore, *ob/ob* mice are commonly used as a diabetic animal model [17, 19].

This thesis is focused on metabolic effects of tuberculosis and leptin deficiency in mice (Mus musculus) and zebrafish (Danio rerio) animal models. We used different metabolomic tools including mass spectrometry (MS), nuclear magnetic resonance (NMR) and high-resolution magic-angle-spinning NMR (HR-MAS NMR) spectrometry to acquire the metabolic profiles of samples. Additionally, transcriptomics was used to investigate the mechanism underlying the metabolic disorders of TB and leptin mutation. Furthermore, we tested whether the adult leptin mutant zebrafish have a diabetic phenotype as well as kidney damage resulting from this. In this chapter we will give a short overview of various aspects that determine cachexia in tuberculosis and diabetes and explain the animal models and metabolomics methods that we used to study this.

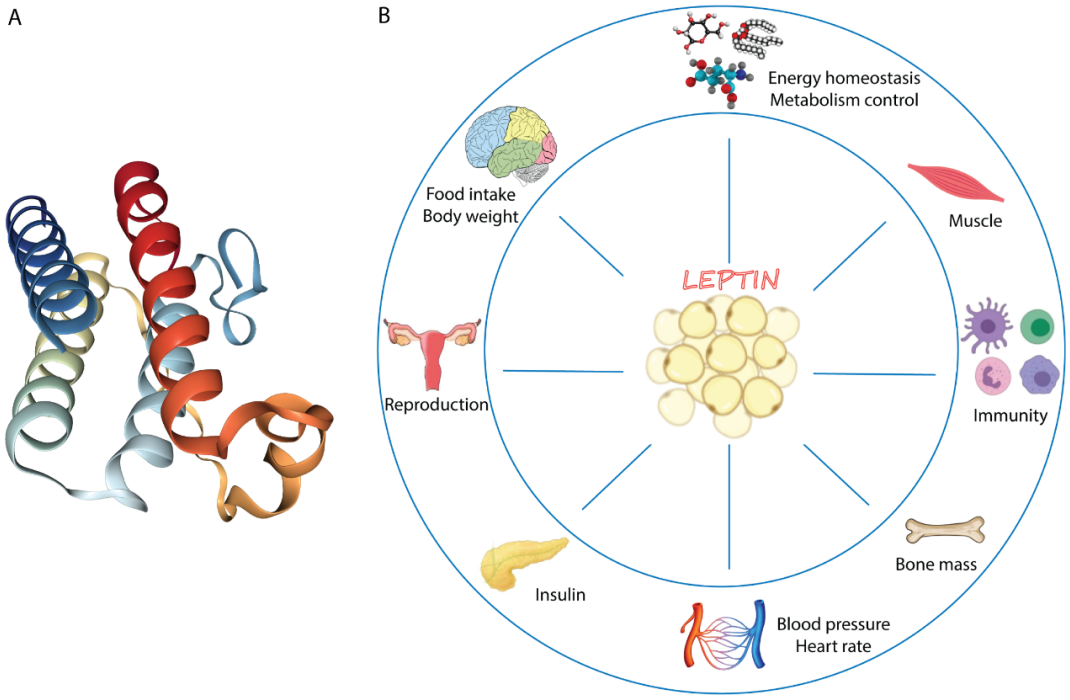

Figure 1. The structure and physiological functions of leptin. **A**. The structure of human leptin protein shows a four-helix bundles similar to that of the long-chain helical cytokine family [20]. **B**. Leptin is produced by a variety of tissues, for instance by white adipose tissues (in the middle) and it has diverse functions in several organs and molecules. Figure 1B is similar to the figure of Zabeau et al., 2016 [21].

Molecular basis of cachexia

Cachexia is an energy wasting syndrome in which energy expenditure exceeds energy intake resulting in muscle wasting and atrophy [22, 23]. Chronic diseases, such as cancer and tuberculosis, consume large amounts of energy, therefore the body triggers compensatory mechanisms to maintain energy homeostasis. The compensatory mechanisms are associated with important metabolic changes in carbohydrate, lipid and amino acid metabolism and the balance of protein synthesis and degradation [23]. In the condition of cachexia, protein synthesis is decreased and myofibrillar protein degradation is increased [24]. There are two main mechanisms for protein degradation: the ubiquitin-dependent proteasome and autophagy pathways [23, 25]. An increase in ubiquitin proteasome system (UPS) activity is involved in the degradation of muscle myofibrillar proteins [26]. In the case of skeletal muscle atrophy, this increase of UPS activity is accompanied by a higher expression level of atrogin-1 and MuRF-1, which are two key E3 ubiquitin ligases [27]. Autophagy is a well-known recycling process that ingests dysfunctional organelles such as mitochondria, eliminating intracellular pathogens as well as clearing up misfolded or aggregated proteins [28]. A block of autophagy signaling and mutation in autophagy genes lead to myofiber disorders and muscle weakness [29, 30]. Excessive activation of the activity of autophagy results in

detrimental consequences on muscle homeostasis and severe muscle loss [31, 32]. Therefore, a balanced autophagy flux is essential to maintain muscle mass and myofiber integrity.

A common effect of cachexia in mammals is chronic inflammation [33]. It is reported that inflammatory responses in many chronic diseases influence various metabolic changes related to wasting syndrome [34]. Chronic systemic production of pro-inflammatory cytokines decreases the appetite and increases the catabolism in the body [13]. Serum levels of the pro-inflammatory cytokines were found to be increased in human patients and in animal models of chronic diseases associated with wasting syndrome [24, 35]. The elevated levels of these cytokines inhibit the secretion and activity of growth hormones such as IGF-1. In addition, the high concentration of the cytokines directly induces signaling pathways that regulate enzymes leading to skeletal muscle protein turnover [24]. These cytokines include TNF-α, IL-6, IL-1β, interferon-γ, myostatin and activin A [13, 24, 36, 37]. TNF-α, originally named cachectin, is shown to induce cachexia in rats [37] and mice [38] and cause myotube atrophy *in vitro* via the activation of the UPS pathway [39]. Inhibition of IL-6 signaling attenuates cachexia development in mouse cancer models [40]. The blockade of the common receptor ActRIIB of myostatin and activin A, suppresses cachexia progression and reverses prior skeletal muscle loss in several mouse cancer cachexia models [41]. However, the molecular mechanisms underlying the regulation of wasting syndrome by cytokines at the systemic level are not yet known.

Tuberculosis

Tuberculosis (TB) remains one of the top 10 leading causes of human death worldwide because it is an infectious, contagious and often drug-resistant disease [42]. It spreads merely by aerosolized droplets carrying bacteria from the *Mycobacterium tuberculosis* (*Mtb*) complex [43]. It has been a threat to global public health for decades with about 10 million new cases and 1.4 million deaths reported in 2019 [42]. A quarter of the world's population is estimated to have latent TB infection, according to the World Health Organization (WHO) [42]. Approximately one tenth of latent TB is likely to develop to active TB disease at which stage the causative mycobacteria become highly transmittable [44]. The pathogen mainly targets the lung, although extra-pulmonary infection is also very frequently observed [43]. TB is characterized pathologically by the formation of granulomas that consist of clusters of infected macrophages and surrounding uninfected immune cells of various types (**Figure 2**). TB results in many symptoms including fever, cough, chest pains, hemolysis and weight loss [45, 46]. The causes of death by tuberculosis are mainly due to severe tissue damage, oxygen shortage and wasting syndrome [43]. It is claimed that TB has been existing throughout human history, leading to large epidemic proportions in the 18th, 19th and early 20th centuries [47, 48]. Although the disease was thought to be mostly eradicated by the end of the 20th

century, currently TB is spreading rapidly due to the emergence of many antibiotic resistant strains and a lack of proper diagnosis in many countries. The latter problem is aggravated by the current health problems due to the Covid-19 pandemic. Therefore, approaches to prevent *Mtb* transmission as well as to reduce TB morbidity and mortality, should not only rely on good preventions and effective therapies but also on efficient diagnoses [49].

Currently, several tests are applied for the diagnosis of TB [46, 50]. Those methods include tuberculin skin tests (TST), interferon-γ release assays (IGRA), sputum smear microscopy, mycobacterial culture-based methods, chest radiography such as chest X-rays and PET-CT, and commercial molecular tests [46]. TST is simple and cheap, however, it results in false positive responses for people who are Bacille Calmette-Guerin (BCG) vaccinated [51]. IGRA is more specific than the TST, but it gives false negative responses for people who suffer from immunosuppression [45]. Sputum smear microscopy is the most widely used test for TB, but it lacks sensitivity and misses a diagnosis of extra-pulmonary infections [46]. Mycobacterial culture-based methods are the golden standard diagnostic test with a high sensitivity for TB. However, it takes 3-4 weeks to obtain results, which delays diagnosis [52]. Chest radiography examines whether an abnormality is present, but it doesn't give information about the lesion's activity. Commercial molecular tests, such as GeneXpert MTB/RIF, although rapid and detecting antibiotic resistance of the pathogen, are expensive and have high requirements for infrastructure [53].

Given the limitations of the current diagnostic tests, there is an urgent need for the development of new efficient, reproducible and cost effective diagnostic methods to control the disease. Biomarker-based tests for the detection of TB, ideally performed on easily accessible samples such as blood or urine, provide great potential for the detection of TB [53, 54]. Since various biomarkers are used to define an endpoint in clinical trials distinguishing a normal and pathogenic biological state, they can be also directly used for advanced diagnostic tools [55]. Additionally, biomarkers can indicate the effectiveness of a therapeutic treatment and promote development of alternative therapy regimens. Reported biomarkers are either pathogen-derived such as lipoarabinomannan (LAM),or host-derived such as antibodies, cellular immune responses to *Mtb* antigens (i.e., cytokines and chemokines) or derived from both pathogen and host factors using omics-based approaches [53, 56, 57].

Omics-based approaches are capable of accurately predicting disease outcomes and providing insights for disease mechanisms [58]. Omics includes genomics, transcriptomics, proteomics and metabolomics approaches [58]. Trans-omics is defined as a discipline that seeks to reconstruct biomolecular networks not as a group of indirect statistical correlations, but as chains of direct mechanistic molecular interactions by using comprehensive multi-omics data measured under identical conditions, as opposed to heterogeneous sources of data [59, 60]. The metabolome

encompasses a complete set of metabolites in biological processes, and it is the ultimate downstream outcome of the processes measured by the other three omics levels. Therefore, any disruption at the other omics levels could affect the quantities of specific metabolites [61]. Identification and quantification of full metabolomes provide a great possibility for discovering biomarkers of diseases including TB [62]. To date, metabolomics has been applied to identify potential biomarkers of TB from blood [63], urine [64, 65] and sputum [66] of patients. However, they still need to be validated by comparisons of the outcomes of independent studies and tested in clinical trials before they can be used in the clinic. Additionally, TB animal models that for example use mice and zebrafish, provide basic tools to discover new biomarkers for diagnosis. The models can provide mechanistic insights into the biological relevance of the biomarkers, resulting in a more robust theoretical basis for the prediction of their effectiveness.

The zebrafish as a versatile model organism for tuberculosis studies

Animal models offer practical advantages to study the progression and the pathogenic mechanisms of TB, therefore they serve as important means for TB research [67]. Although *Mtb* infection in mouse recapitulates some aspects of human TB disease, *Mtb* is a dangerous pathogen to work with and it requires specialized and expensive facilities [43, 67]. Zebrafish larvae offer an excellent animal model for studying the pathogenesis of *Mtb* [68]. The optical transparency of zebrafish larvae allows the visualization of the infection of a fluorescently-labelled pathogen *in vivo*. *Mycobacterium marinum* (*M. marinum*), the closest known genetic relative of the *Mtb* complex, is a natural pathogen for zebrafish [69]. It is much less dangerous to work with than the *Mtb* pathogen because of its restricted temperature range of growth. Infection of zebrafish embryos with *M. marinum* results in the formation of characteristic necrotic and granulomatous lesions which is a hallmark of human TB (**Figure 2**). The granuloma is a highly organized structure characterized by aggregation of immune cells that engulf and confine the pathogens (**Figure 2**). Many publications show that the mechanisms of *M. marinum* infection in zebrafish larvae can be translated at the genetic, cellular and molecular signaling levels to tuberculosis progression in humans [70, 71]. Therefore, zebrafish larvae are a very powerful model organism to study the fundamental mechanism underlying TB progression.

Figure 2 (following page). Zebrafish as an excellent model organism for tuberculosis studies. Zebrafish embryos were injected with 30 colony forming units of *M. marinum* bacteria into the yolk at 4 hours post fertilization. Images were acquired at 5 days post infection. *M. marinum* strain M was transformed with a plasmid encoding the green fluorescent Wasabi protein, therefore it can be visualized with a fluorescent microscope. **A**. A whole zebrafish larva showing *M. marinum* infection in the yolk and tail (Y. Ding unpublished data). **B**. An enlargement of a mycobacterial cluster in the tail of the zebrafish larva. **C**. A

schematic diagram illustrates the morphology of the granuloma. The diagram is adapted from Masud et al., 2017 [72].

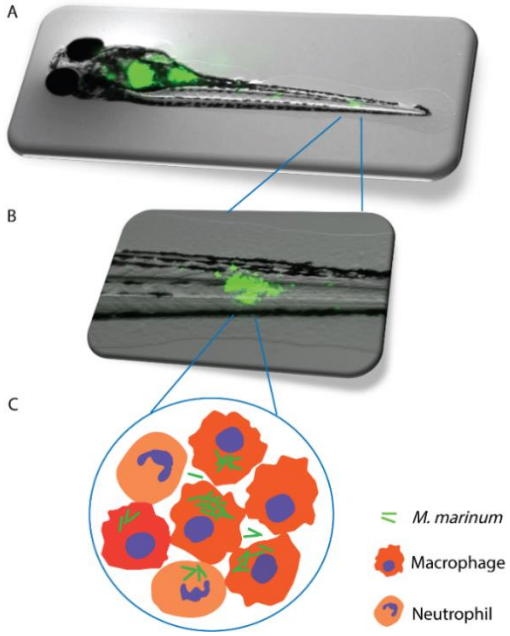

Diabetes

Diabetes mellitus (DM) is a chronic disease that is caused by a defect in insulin signaling in the body leading to limited glucose uptake from the blood stream. There were around 422 million cases and 1.6 million deaths all over the world per year [73]. Globally, currently one in eleven people are diagnosed with DM [73]. The morbidity and mortality of DM is steadily increasing, therefore, it exerts a big threat to global public health [73, 74]. DM is classified into type 1 diabetes mellitus (T1DM), type 2 diabetes mellitus (T2DM) and gestational diabetes mellitus (GDM) [75]. T1DM is most often caused by autoimmune disorders which results in the dysfunction or death of the beta cells leading to a failure of the pancreas to secret insulin. The frequency of T1DM is up to 10% of diabetic patients. T2DM is the most common type of diabetes and accounts for approximately 90% of all diabetic cases. It is a chronic metabolic disorder characterized by dysregulation of carbohydrate, fat and protein metabolism [76]. It is caused by peripheral insulin resistance that can lead to impaired insulin production [76]. GDM only occurs in pregnant women, and normally their blood glucose level will be back to normal after pregnancy. However, the risk of developing T2DM is higher both for the mother and child later on during their lifetime [77]. T2DM affects the whole body and is usually accompanied by many complications, including cardiovascular disease and chronic failure of organs such as kidney and eyes [78]. In addition, people with T2DM are more susceptible to infectious diseases including tuberculosis [79]. Obesity is reported to be the most

important factor in the development of metabolic diseases including T2DM [80]. Therefore, both obesity and T2DM are accompanied with insulin resistance [80]. This could be explained by the function of fat tissues in the secretion of hormones and cytokines, such as leptin, that can control whole body metabolism and cause insulin resistance [80]. Serum leptin levels are positively correlated with body mass index and percentage of body fat in T2DM patients [81]. Higher leptin levels have been observed in insulin-resistant patients with T2DM independently of body fat mass [82, 83]. However, several other studies show that leptin levels were decreased in non-obese patients with T2DM [84, 85]. Rodents with leptin deficiency are hyper obese and diabetic [86]. Therefore, leptin has been studied extensively for its role in diabetes [87, 88].

Leptin

Leptin in humans is a 167 amino peptide that is mainly produced and secreted by white adipose tissues, but also found in a variety of tissues including placenta, mammary gland, ovary, skeletal muscle, stomach, pituitary gland, and lymphoid tissue [89]. However, those tissues contribute relatively little to the circulating levels of leptin [90]. The concentration of circulating leptin is considered to be proportional to the amount of fat tissue [91]. Leptin, as both an adipokine and cytokine, plays a key role in various aspects including control of body weight, energy homeostasis and metabolism. In mammals, leptin exerts its role via binding to specific isoforms of the leptin receptor that have the structure of a class I cytokine receptor and are located on the cell membrane of multiple tissues [92]. Leptin binds to leptin receptors resulting in the activation of three main cellular downstream signaling pathways including JAK-STAT, SHP2-ERK and IRS-PI3K pathways (**Figure 3**).

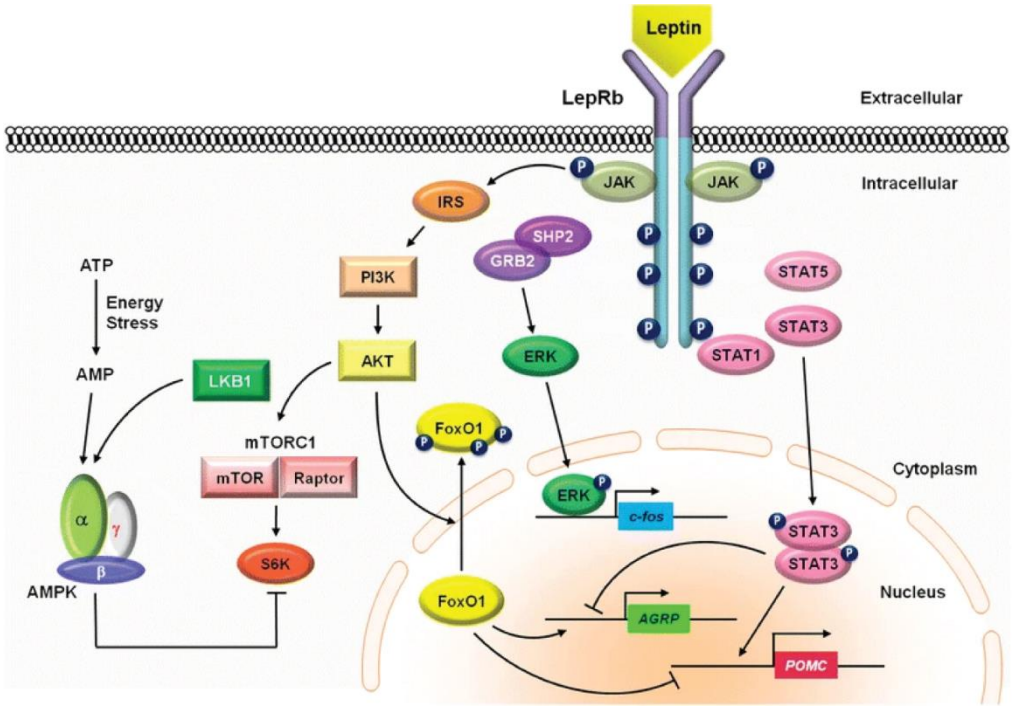

Figure 3 (previous page). Leptin signaling pathways. The figure is adapted from Kwon et al., 2016 [93]. Leptin binds to leptin receptor resulting in the activation of JAK-STAT, SHP2-ERK and IRS-PI3K pathways. The activated JAK prompts the phosphorylation of tyrosine residues which is involved in the dimerization of STAT3 and STAT5. Dimerized STAT3 and STAT5 then translocate into the nucleus and mediate the transcriptional expression of the targeted genes including POMC, which is involved in the regulation of appetite and body weight. In addition, the activation of tyrosine residues recruits SHP2 and GRB2, leading to the phosphorylation of ERK. The activated ERK translocates into the nucleus and regulates the expression of genes associated with energy homeostasis. Furthermore, upon leptin binding, activated JAK phosphorylates IRS, resulting in the activation of PI3K and AKT. This, on one hand, leads to the inactivation of FoxO1 by sequestering from nucleus to cytoplasm. On the other hand, AKT activates mTORC1 that subsequently activates S6K causing the phosphorylation of the AMPK α subunit and inhibition of AMPK activity. This pathway plays important roles in control of appetite and protein metabolism.

Leptin plays many functions in energy homeostasis and metabolism control. It maintains euglycemia by switching carbohydrate metabolism to fat metabolism during starvation [94]. In an early fasting state, glucose is mainly generated from hepatic breakdown of glycogen (glycogenolysis) [95]. In contrast, in a prolonged fasting state, *de novo* glucose production (gluconeogenesis), using lactate, pyruvate, amino acids and glycerol, is a main source for maintaining euglycemia level [95]. Gluconeogenesis is facilitated by changes of hormone levels such as glucagon, insulin, growth hormone and cortisol [95-97]. These signals stimulate lipolysis in fat tissues to generate ketone bodies through mitochondrial β oxidation and ketogenesis. The ketone bodies provide substrate to obligate glucose-utilizing organs such as the brain. The switch from glucose metabolism to fat metabolism is thought to be mainly driven by an increase of glucagon and a decrease of insulin levels. Perry et al [94] show that hypoleptinemia is a key regulator for this shift. A low level of plasma leptin stimulates the hypothalamic-pituitary-adrenal (HPA) axis, thereby mediating the degradation of white adipose tissue (WAT) (**Figure 4**). This results in an increase of hepatic acetyl-CoA content and pyruvate carboxylase flux, which is essential to maintain gluconeogenesis during prolonged starvation (**Figure 4**). The amount of hepatic acetyl-CoA and the activity of pyruvate carboxylase are key indicators for liver and whole body glucose and fat metabolism. Therefore, leptin is an essential regulator for glucose homeostasis during starvation.

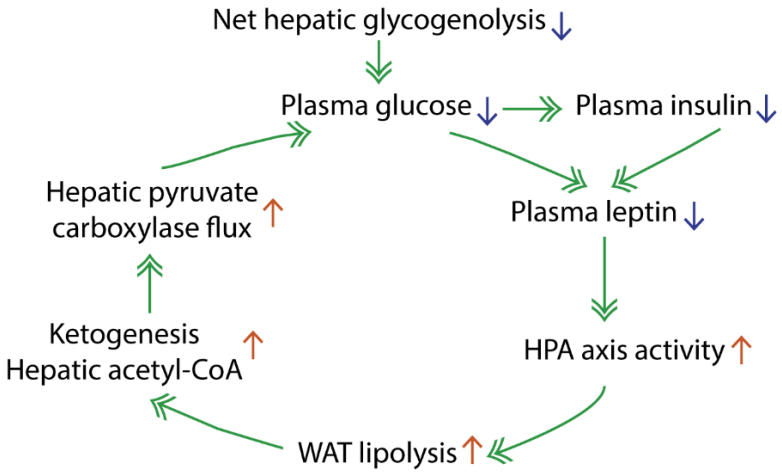

Figure 4. Leptin mediates a glucose-fatty acid cycle to maintain glucose homeostasis in starvation. The figure is adapted from Perry et al., 2018 [94]. In prolonged starvation, glucose generated from hepatic glycogenolysis is reduced, resulting in a decrease of plasma insulin and leptin concentrations. Hypoleptinemia is a critical signal to increase WAT lipolysis via the HPA axis activity. This accordingly results in an increase of hepatic acetyl-CoA content, ketogenesis and hepatic pyruvate carboxylase activity, therefore maintaining the glucose homeostasis during starvation. Orange arrows mean an increase and blue arrows mean a decrease. HPA: hypothalamic-pituitary-adrenal axis, WAT: white adipose tissues.

Congenital leptin mutations in human are extremely rare [98]. Patients with the disease are severely obese, hyperinsulinemic and dyslipidemic [99, 100]. The mean BMI of patients is distinctly decreased after 18 months of leptin replacement [99]. Furthermore, leptin administration normalizes serum glucose, insulin and lipid level [101]. Animal models in rodents with spontaneous mutations in the leptin (*ob/ob*) and leptin receptor (*db/db*) have existed for decades. Mice with the mutation in leptin signaling display hyperphagic, obese and diabetic phenotypes and the circulating leptin level is reduced [102]. Similar with the effects of leptin mutation in humans, recombinant leptin treatment in *ob/ob* mice successfully lowers the body weight, glucose and insulin level [102]. Leptin and leptin receptor are evolutionarily conserved from mammalian to nonmammalian species including zebrafish [103]. Zebrafish have one leptin receptor and two orthologs of the leptin gene, namely *leptin a* (*lepa*) and *leptin b* (*lepb*). Studies show that *lepr* mRNA is also highly expressed in the brain of zebrafish as it is in mammals [104]. The mutation in *lepa* results in an obesity phenotype in adult zebrafish [105]. However, the metabolic effects of leptin mutation in the early development are still largely unknown.

Metabolomics

Metabolomics is defined as large-scale studies of metabolite compositions that are substrates, intermediates and products of biological processes [106]. It focuses on global sets of small molecules with a molecular weight smaller than 1500 Da within cells, tissues, organs and organisms at any given time [107]. The small molecules include sugars, amino acids, organic acids, and lipids. Metabolomics is a powerful approach because the studied metabolites are the end products of cellular processes and they therefore represent an important element of the molecular phenotype [108]. Therefore, the level of metabolites can directly reflect the underlying biochemical condition in a biological sample.

The most common used analytical tools for metabolomics are mass spectrometry (MS) and nuclear magnetic resonance (NMR) spectrometry [109]. In comparison, they both have their specific advantages and disadvantages shown in **Table 1**. MS is a powerful analytical technique as it offers the merits of high sensitivity, selectivity, and high throughput ability [110]. MS provides a mass-to-charge ratio (m/z) of charged molecules to identify components in a sample by determining the molecular weight and its isotopic abundance [107]. MS instruments consist of three main parts: an ionization source, a mass analyzer and a detector. The ionization source converts targeted analytes from liquid and solid phase into gas phase ions [111]. The ions travel through a fixed distance in a mass analyzer before reaching to the detector. The higher m/z ions achieve lower velocity than the lower m/z ions as the ion velocities are inversely proportional to their m/z. Therefore, the ion m/z can be determined by measuring the time of traveling in the mass analyzer [112]. However, samples for MS measurement are destructive. NMR spectroscopy compensates for this limitation of MS.

NMR spectroscopy enables the identification and quantification of metabolites in complex biological samples with a high reproducibility [113]. By applying an external magnetic field, nuclei of molecules can behave like a magnet due to their charge and spin. Thus, the molecular structure of components in a sample can be analyzed by measuring the interaction of nuclear spins. There are solid-state and solution-state NMR methods. In biology, NMR spectrometry is usually applied for the analysis of liquid samples obtained by extraction of tissues with organic solvents. To apply NMR for the analysis of (semi-) solid samples, such as intact tissues, another advanced technique, called high-resolution magic-angle-spinning NMR (HR-MAS NMR) was developed [114]. The most important advantage of HR-MAS NMR is that it directly measures intact samples. It thereby prevents the loss and degradation of metabolites by extraction which are required for the measurements by MS and solution-state NMR. HR-MAS NMR spectrometry spins samples at a magic angle of approximately 54.7° at a frequency of a few thousands of Hertz to reduce the hetero- and homonuclear dipolar coupling of the samples [115, 116]. In this way, it makes it possible to acquire high-resolution spectra of heterogeneous samples based on a small volume (50 microliter).

Therefore, HR-MAS NMR spectrometry has contributed greatly to the metabolomic analysis of small intact organisms such as zebrafish larvae for instance in the work described in this thesis.

Table 1. Advantages and disadvantages of mass spectrometry in comparison with nuclear magnetic resonance spectroscopy as standard analytical tools for metabolomics research [116-118].

	MS	NMR
Sensitivity	High and detection limit reach nanomolar, but can suffer from ion suppression in complex and salty mixtures	Low but can be improved with the use of higher field strength, cryoprobes and dynamic nuclear polarization
Selectivity	Can be used for both selective and nonselective (targeted and nontargeted) analyses	Even though few selective experiments are available such as selective TOCSY, it is in general used for nonselective analysis
Number of detectable metabolites	300-1000+	30-100
Target analysis	Superior for targeted analysis	Inferior for targeted analysis
Sample preparation	More demanding; Needs different LC columns and optimization of ionization conditions	Needs minimal sample preparation
Sample measurement	Usually needs different chromatography techniques for different classes of metabolites	All metabolites that are within the limit of NMR sensitivity can be detected in one measurement
Sample recovery	Destructive technique, but needs a small amount of samples	Nondestructive for HR-MAS NMR; Samples can be recovered and stored for a long time, several analyses can be carried out on the same sample
Tissue samples	Requires tissue extraction. MS can be used to identify metabolites in tissues using MALDI-MS	Using HR-MAS NMR tissue samples can be analyzed directly
In vivo studies	Not possible	Widely used for ^{1}H magnetic resonance spectroscopy (and to a lesser degree ^{31}P and ^{13}C)

Transcriptomics

Transcriptomics investigates all RNA transcripts of cells, tissues and organisms. It serves as an intermediatory omics tool used to study the level of transcription of the entire genome and can also be used to analyze RNA modification, stability and localization [119]. Measuring the expression levels of genes under a particular condition provides information on how the genes are regulated, thereby contributing to better understanding of the genetic functions underlying developmental or disease processes in terms of molecular mechanism. RNA sequencing (RNA-seq) has evolved over a decade and has become an indispensable method to study differential expression of genes [120, 121]. It is a medium throughput technology that has to be combined with computational methodologies to map the sequencing data to the genome. The most commonly used RNA-seq technology is marketed by Illumina, which is mainly used for short read sequencing to a length of 50-500bp [120]. We also used this RNA-seq method extensively in this thesis. The general workflow of short read sequencing starts with RNA isolation of specimens, followed by mRNA enrichment or rRNA depletion, RNA fragmentation, cDNA synthesis, adaptor ligation, PCR amplification, sequencing and analysis (**Figure 5A**). For analysis of eukaryotic gene transcription, the prepared library is commonly sequenced to a read depth of 10-30 million reads per run [120]. The principle of this method is based on detection of four colored fluorophores that are incorporated in synthetic cDNA derived from the RNA (**Figure 5B**). Transcripts can be sequenced in one direction (single-end) as well as both directions (paired-end). The bioinformatic analysis of RNAseq data requires alignment of sequencing reads to an annotated reference genome and normalization between samples [122]. Differential gene expression (DGE) analysis and further analysis such as gene ontology (GO) enrichment are common research tools for the use of RNAseq data sets. The short-read sequencing techniques have the advantages of high throughput, better knowledge of biases and error profiles and applications for degraded RNA. However, imperfections and bias can be introduced due to reproducibility problems in sample preparation and computational analysis. In many eukaryotes, a majority of genes are alternatively spliced to form two or more distinct transcripts. For short-read cDNA sequencing, a significant percentage of reads map ambiguously when an exon is shared between isoforms (**Figure 5C**). This complicates analysis and interpretations of results. Long-read sequencing methods can generate full-length transcript reads, thereby improving differential isoform expression analysis. There are two long read technologies: long-read cDNA sequencing and long-read direct RNA-seq (**Figure 5A**). The long-read cDNA method shares many of the steps of library construction with the short-read method (**Figure 5A**). In the absence of RNA fragmentation, read lengths up to 50kb can be generated. The library preparation of the long-read direct RNA-seq method only requires adaptor ligation with minimal steps. The maximum read length of this method is currently 10kb, but is rapidly improving [123]. The long-read sequencing approaches overcome the limitation of short-read method. It reduces

the ambiguity in the mapping of sequence reads and high rates of false positive splice junction detection (**Figure 5C**). Longer transcripts can be identified, resulting in a more complete capture of transcript diversity. Despite that they are still relatively expensive, it might soon present a challenge to the dominance of Illumina short-read sequencing.

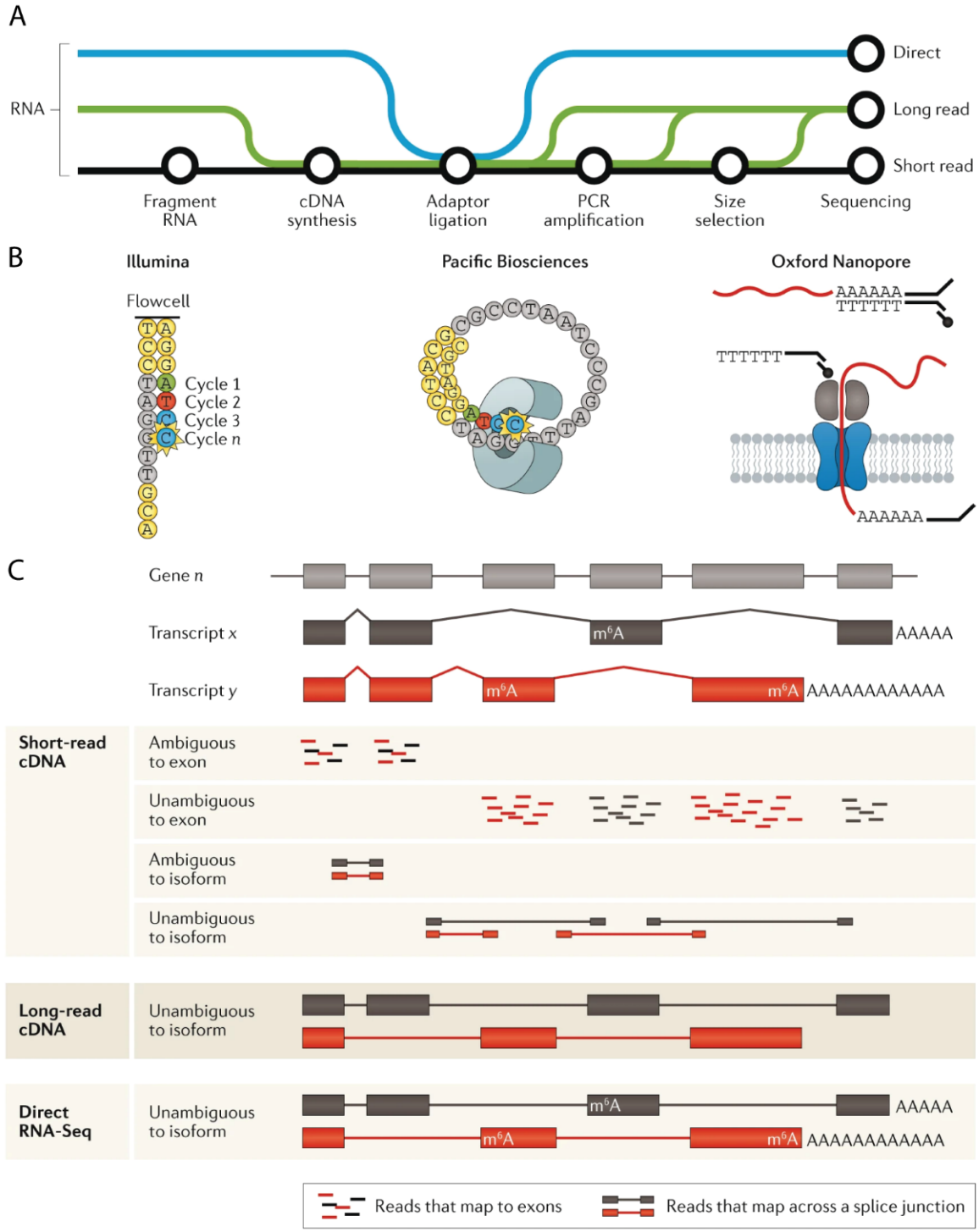

Figure 5 (previous page). Short-read, long-read and direct RNA-seq technologies and workflows. The figure is adapted from Stark 2019 et al [120]. **A.** An overview of library preparation methods for different RNA-seq methods. Black: short-read sequencing. Green: long-read cDNA sequencing. Blue: long-read direct RNA sequencing. **B**. An overview is shown of three main sequencing technologies for RNA-seq. **C.** Comparison of short-read, long-read and direct RNA-seq analysis.

Outline of this thesis

In this thesis, my aims are to study 1) metabolic alterations in tuberculosis related to wasting syndrome in human patients as well as in rodent and fish animal models. 2) effects of the mutation of the leptin gene on cachexia and diabetes in rodent and zebrafish animal models. 3) how tuberculosis infection and resulting metabolic reprogramming are dependent on leptin signaling in mice and zebrafish larvae.

In **Chapter 2**, we obtained metabolic profiles of the blood of TB patients and *Mtb*-infected C57BL/6 mice, and *M. marinum*-infected entire zebrafish larvae and their respective controls measured by MS. Despite that there were huge differences among the tested samples, we found that they shared 10 common biomarkers which could distinguish the disease and healthy state. Furthermore, we confirmed the 10 common biomarkers in zebrafish larvae by using another metabolomic tool NMR spectroscopy.

In **Chapter 3**, we generated and acquired a *lepb* mutant zebrafish line. The leptin mutation in mice leads to hyperphagic, severe obese, insulin resistance and T2DM. In this chapter we described the investigation of the effect of leptin mutation on fat accumulation in tissues and glucose metabolism in adult zebrafish. We found that *lepb* deficiency in zebrafish leads to higher body weight, more visceral fat tissues and higher glucose level, indicating there was a diabetic phenotype similar to that observed in *ob/ob* mice. Moreover, we showed that there was a mild diabetic complication showing in kidneys as observed by thicker glomerular basement membranes.

In **Chapter 4**, we tested and compared the metabolomic profiles of leptin mutants in mice and zebrafish larvae. We found that there are great similarities in terms of metabolite changes in the two species measured by different metabolomic approaches. These metabolites also shared a common set of biomarkers that are found in tuberculosis. To further investigate the mechanisms of the metabolic alterations, we performed deep RNA sequencing. We showed that the transcriptomic signature sets of the mutants of the two species were both enriched in genes with the common GO terms proteolysis and arachidonic acid signaling. In summary, leptin mutation leads to the same evolutionarily conserved metabolic syndrome in adult mice and zebrafish larvae.

In chapter 4, we found there was a connection of metabolite alteration in mycobacterial infection and leptin mutation as well as the reported connection of TB and diabetes in clinical condition. Therefore, in **Chapter 5**, we investigated how mycobacterial infection and leptin mutation affect each other. We tested the metabolic profiles in the leptin mutant mice and zebrafish larvae in the presence and absence of infection. We found that leptin mutation and mycobacterial infection led non-synergistically to a similar metabolic syndrome. In contrast, the RNAseq data of zebrafish larvae samples showed that mycobacteria induce a very different transcriptome signature in the *lepb* mutant compared to the wild type sibling control. Therefore, we concluded that leptin and mycobacterial infection led to a similar dysregulation of metabolism via different genetic mechanisms.

In **Chapter 6**, I summarized and discussed our results and findings described in this thesis and suggested future directions of research.

References

[1] Berardi E, Madaro L, Lozanoska-Ochser B, Adamo S, Thorrez L, Bouche M, et al. A Pound of Flesh: What Cachexia Is and What It Is Not. Diagnostics 2021;11(1).

[2] Laviano A, Paldino A. Diagnosing cachexia. Clinical practice 2014;11(1):71.

[3] Fearon K, Strasser F, Anker SD, Bosaeus I, Bruera E, Fainsinger RL, et al. Definition and classification of cancer cachexia: an international consensus. The Lancet Oncology 2011;12(5):489-95.

[4] Rosen ED, Spiegelman BM. Adipocytes as regulators of energy balance and glucose homeostasis. Nature 2006;444(7121):847-53.

[5] Fonseca GW, Farkas J, Dora E, von Haehling S, Lainscak M. Cancer Cachexia and Related Metabolic Dysfunction. International Journal of Molecular Sciences 2020;21(7).

[6] Kerekes G, Nurmohamed MT, González-Gay MA, Seres I, Paragh G, Kardos Z, et al. Rheumatoid arthritis and metabolic syndrome. Nature Reviews Rheumatology 2014;10(11):691-6.

[7] Grinspoon S, Mulligan K, Department of H, Human Services Working Group on the P, Treatment of W, Weight L. Weight Loss and Wasting in Patients Infected with Human Immunodeficiency Virus. Clinical Infectious Diseases 2003;36(Supplement_2):S69-S78.

[8] Schwenk A, Macallan DC. Tuberculosis, malnutrition and wasting. Current Opinion in Clinical Nutrition & Metabolic Care 2000;3(4).

[9] Perry BD, Caldow MK, Brennan-Speranza TC, Sbaraglia M, Jerums G, Garnham A, et al. Muscle atrophy in patients with Type 2 Diabetes Mellitus: roles of inflammatory pathways, physical activity and exercise. Exerc Immunol Rev 2016;22:94-109.

[10] Koppe L, Fouque D, Kalantar-Zadeh K. Kidney cachexia or protein-energy wasting in chronic kidney disease: facts and numbers. J Cachexia Sarcopenia Muscle 2019;10(3):479-84.

[11] von Haehling S, Anker MS, Anker SD. Prevalence and clinical impact of cachexia in chronic illness in Europe, USA, and Japan: facts and numbers update 2016. J Cachexia Sarcopenia Muscle 2016;7(5):507-9.

[12] Advani SM, Advani PG, VonVille HM, Jafri SH. Pharmacological management of cachexia in adult cancer patients: a systematic review of clinical trials. BMC Cancer 2018;18(1):1174-.

[13] Webster JM, Kempen LJAP, Hardy RS, Langen RCJ. Inflammation and Skeletal Muscle Wasting During Cachexia. Frontiers in Physiology 2020;11:1449.

[14] Zhang Y, Proenca R, Maffei M, Barone M, Leopold L, Friedman JM. Positional cloning of the mouse obese gene and its human homologue. Nature 1994;372(6505):425-32.

[15] Park H-K, Ahima RS. Physiology of leptin: energy homeostasis, neuroendocrine function and metabolism. Metabolism: clinical and experimental 2015;64(1):24-34.

[16] Farooqi IS, O'Rahilly S. Leptin: a pivotal regulator of human energy homeostasis. The American Journal of Clinical Nutrition 2009;89(3):980S-4S.

[17] Wang B, Chandrasekera PC, Pippin JJ. Leptin- and leptin receptor-deficient rodent models: relevance for human type 2 diabetes. Curr Diabetes Rev 2014;10(2):131-45.

[18] Sáinz N, Rodríguez A, Catalán V, Becerril S, Ramírez B, Gómez-Ambrosi J, et al. Leptin administration favors muscle mass accretion by decreasing FoxO3a and increasing PGC-1α in ob/ob mice. PloS one 2009;4(9):e6808.

[19] King AJF. The use of animal models in diabetes research. Br J Pharmacol 2012;166(3):877-94.

[20] Zhang F, Basinski MB, Beals JM, Briggs SL, Churgay LM, Clawson DK, et al. Crystal structure of the obese protein Ieptin-E100. Nature 1997;387(6629):206-9.
[21] Zabeau L, Peelman F, Tavernier J. Leptin and Leptin Receptor. In: Choi S, editor Encyclopedia of Signaling Molecules. New York, NY: Springer New York; 2016, p. 1-6.
[22] Rohm M, Zeigerer A, Machado J, Herzig S. Energy metabolism in cachexia. EMBO Rep 2019;20(4):e47258.
[23] Argilés JM, Busquets S, Stemmler B, López-Soriano FJ. Cancer cachexia: understanding the molecular basis. Nature reviews Cancer 2014;14(11):754-62.
[24] Yoshida T, Delafontaine P. Mechanisms of Cachexia in Chronic Disease States. Am J Med Sci 2015;350(4):250-6.
[25] Sakuma K, Aoi W, Yamaguchi A. Molecular mechanism of sarcopenia and cachexia: recent research advances. Pflugers Archiv : European journal of physiology 2017;469(5-6):573-91.
[26] Kitajima Y, Yoshioka K, Suzuki N. The ubiquitin–proteasome system in regulation of the skeletal muscle homeostasis and atrophy: from basic science to disorders. The Journal of Physiological Sciences 2020;70(1):40.
[27] Bodine SC, Baehr LM. Skeletal muscle atrophy and the E3 ubiquitin ligases MuRF1 and MAFbx/atrogin-1. Am J Physiol Endocrinol Metab 2014;307(6):E469-E84.
[28] Glick D, Barth S, Macleod KF. Autophagy: cellular and molecular mechanisms. J Pathol 2010;221(1):3-12.
[29] Xia Q, Huang X, Huang J, Zheng Y, March ME, Li J, et al. The Role of Autophagy in Skeletal Muscle Diseases. Frontiers in physiology 2021;12:638983-.
[30] Masiero E, Sandri M. Autophagy inhibition induces atrophy and myopathy in adult skeletal muscles. Autophagy 2010;6(2):307-9.
[31] Masiero E, Agatea L, Mammucari C, Blaauw B, Loro E, Komatsu M, et al. Autophagy Is Required to Maintain Muscle Mass. Cell Metabolism 2009;10(6):507-15.
[32] Sandri M, Coletto L, Grumati P, Bonaldo P. Misregulation of autophagy and protein degradation systems in myopathies and muscular dystrophies. Journal of Cell Science 2013;126(23):5325-33.
[33] Webster JM, Kempen LJAP, Hardy RS, Langen RCJ. Inflammation and Skeletal Muscle Wasting During Cachexia. Frontiers in physiology 2020;11:597675-.
[34] Webster JM, Kempen LJAP, Hardy RS, Langen RCJ. Inflammation and Skeletal Muscle Wasting During Cachexia. Frontiers in Physiology 2020;11(1449).
[35] Di Francia M, Barbier D, Mege JL, Orehek J. Tumor necrosis factor-alpha levels and weight loss in chronic obstructive pulmonary disease. American journal of respiratory and critical care medicine 1994;150(5 Pt 1):1453-5.
[36] Mannelli M, Gamberi T, Magherini F, Fiaschi T. The Adipokines in Cancer Cachexia. International Journal of Molecular Sciences 2020;21(14).
[37] Fong Y, Moldawer LL, Marano M, Wei H, Barber A, Manogue K, et al. Cachectin/TNF or IL-1 alpha induces cachexia with redistribution of body proteins. The American journal of physiology 1989;256(3 Pt 2):R659-65.
[38] Oliff A, Defeo-Jones D, Boyer M, Martinez D, Kiefer D, Vuocolo G, et al. Tumors secreting human TNF/cachectin induce cachexia in mice. Cell 1987;50(4):555-63.

[39] Li YP, Chen Y, John J, Moylan J, Jin B, Mann DL, et al. TNF-alpha acts via p38 MAPK to stimulate expression of the ubiquitin ligase atrogin1/MAFbx in skeletal muscle. FASEB journal : official publication of the Federation of American Societies for Experimental Biology 2005;19(3):362-70.
[40] Narsale AA, Carson JA. Role of interleukin-6 in cachexia: therapeutic implications. Curr Opin Support Palliat Care 2014;8(4):321-7.
[41] Zhou X, Wang JL, Lu J, Song Y, Kwak KS, Jiao Q, et al. Reversal of Cancer Cachexia and Muscle Wasting by ActRIIB Antagonism Leads to Prolonged Survival. Cell 2010;142(4):531-43.
[42] World Health Organization. Global Tuberculosis Report. 2020.
[43] Smith I. Mycobacterium tuberculosis pathogenesis and molecular determinants of virulence. Clin Microbiol Rev 2003;16(3):463-96.
[44] Kiazyk S, Ball TB. Latent tuberculosis infection: An overview. Can Commun Dis Rep 2017;43(3-4):62-6.
[45] Fogel N. Tuberculosis: a disease without boundaries. Tuberculosis (Edinburgh, Scotland) 2015;95(5):527-31.
[46] Pai M, Behr MA, Dowdy D, Dheda K, Divangahi M, Boehme CC, et al. Tuberculosis. Nature reviews Disease primers 2016;2:16076.
[47] Barberis I, Bragazzi NL, Galluzzo L, Martini M. The history of tuberculosis: from the first historical records to the isolation of Koch's bacillus. J Prev Med Hyg 2017;58(1):E9-E12.
[48] Daniel TM. The history of tuberculosis. Respiratory medicine 2006;100(11):1862-70.
[49] Jensen PA, Lambert LA, Iademarco MF, Ridzon R. Guidelines for preventing the transmission of Mycobacterium tuberculosis in health-care settings, 2005. 2005.
[50] Furin J, Cox H, Pai M. Tuberculosis. Lancet (London, England) 2019;393(10181):1642-56.
[51] Mancuso JD, Mody RM, Olsen CH, Harrison LH, Santosham M, Aronson NE. The Long-term Effect of Bacille Calmette-Guérin Vaccination on Tuberculin Skin Testing: A 55-Year Follow-Up Study. Chest 2017;152(2):282-94.
[52] Chopra KK, Singh S. Tuberculosis: Newer diagnostic tests: Applications and limitations. Indian Journal of Tuberculosis 2020;67(4, Supplement):S86-S90.
[53] MacLean E, Broger T, Yerlikaya S, Fernandez-Carballo BL, Pai M, Denkinger CM. A systematic review of biomarkers to detect active tuberculosis. Nature microbiology 2019;4(5):748-58.
[54] Goletti D, Lee MR, Wang JY, Walter N, Ottenhoff THM. Update on tuberculosis biomarkers: From correlates of risk, to correlates of active disease and of cure from disease. Respirology (Carlton, Vic) 2018;23(5):455-66.
[55] Wallis RS, Peppard T. Early Biomarkers and Regulatory Innovation in Multidrug-Resistant Tuberculosis. Clinical infectious diseases : an official publication of the Infectious Diseases Society of America 2015;61Suppl 3:S160-3.
[56] Goletti D, Petruccioli E, Joosten SA, Ottenhoff THM. Tuberculosis Biomarkers: From Diagnosis to Protection. Infect Dis Rep 2016;8(2):6568-.
[57] Yong YK, Tan HY, Saeidi A, Wong WF, Vignesh R, Velu V, et al. Immune Biomarkers for Diagnosis and Treatment Monitoring of Tuberculosis: Current Developments and Future Prospects. Frontiers in Microbiology 2019;10(2789).
[58] Hasin Y, Seldin M, Lusis A. Multi-omics approaches to disease. Genome Biol 2017;18(1):83-.
[59] Yugi K, Kubota H, Hatano A, Kuroda S. Trans-Omics: How To Reconstruct Biochemical Networks Across Multiple 'Omic' Layers. Trends in Biotechnology 2016;34(4):276-90.

[60] Yugi K, Kuroda S. Metabolism-Centric Trans-Omics. Cell Systems 2017;4(1):19-20.
[61] Preez Id, Luies L, Loots DT. Metabolomics biomarkers for tuberculosis diagnostics: current status and future objectives. Biomarkers in Medicine 2017;11(2):179-94.
[62] Parida SK, Kaufmann SHE. The quest for biomarkers in tuberculosis. Drug Discovery Today 2010;15(3):148-57.
[63] Weiner J, 3rd, Parida SK, Maertzdorf J, Black GF, Repsilber D, Telaar A, et al. Biomarkers of inflammation, immunosuppression and stress with active disease are revealed by metabolomic profiling of tuberculosis patients. PloS one 2012;7(7):e40221.
[64] Banday KM, Pasikanti KK, Chan ECY, Singla R, Rao KVS, Chauhan VS, et al. Use of Urine Volatile Organic Compounds To Discriminate Tuberculosis Patients from Healthy Subjects. Analytical Chemistry 2011;83(14):5526-34.
[65] Luier L, Loots DT. Tuberculosis metabolomics reveals adaptations of man and microbe in order to outcompete and survive. Metabolomics 2016;12(3):40.
[66] Schoeman JC, du Preez I, Loots DT. A comparison of four sputum pre-extraction preparation methods for identifying and characterising Mycobacterium tuberculosis using GCxGC-TOFMS metabolomics. Journal of Microbiological Methods 2012;91(2):301-11.
[67] Bucsan AN, Mehra S, Khader SA, Kaushal D. The current state of animal models and genomic approaches towards identifying and validating molecular determinants of Mycobacterium tuberculosis infection and tuberculosis disease. Pathog Dis 2019;77(4):ftz037.
[68] Meijer AH. Protection and pathology in TB: learning from the zebrafish model. Seminars in immunopathology 2016;38(2):261-73.
[69] Tobin DM, Ramakrishnan L. Comparative pathogenesis of Mycobacterium marinum and Mycobacterium tuberculosis. Cellular microbiology 2008;10(5):1027-39.
[70] Cronan MR, Tobin DM. Fit for consumption: zebrafish as a model for tuberculosis. Disease models & mechanisms 2014;7(7):777-84.
[71] Berg RD, Ramakrishnan L. Insights into tuberculosis from the zebrafish model. Trends in Molecular Medicine 2012;18(12):689-90.
[72] Masud S, Torraca V, Meijer AH. Modeling Infectious Diseases in the Context of a Developing Immune System. Current topics in developmental biology 2017;124:277-329.
[73] Lin X, Xu Y, Pan X, Xu J, Ding Y, Sun X, et al. Global, regional, and national burden and trend of diabetes in 195 countries and territories: an analysis from 1990 to 2025. Scientific Reports 2020;10(1):14790.
[74] Roglic G. WHO Global report on diabetes: A summary. International Journal of Noncommunicable Diseases 2016;1(1):3.
[75] Association AD. Diagnosis and classification of diabetes mellitus. Diabetes care 2014;37(Supplement 1):S81-S90.
[76] DeFronzo RA, Ferrannini E, Groop L, Henry RR, Herman WH, Holst JJ, et al. Type 2 diabetes mellitus. Nature Reviews Disease Primers 2015;1(1):15019.
[77] Kim C, Newton KM, Knopp RH. Gestational Diabetes and the Incidence of Type 2 Diabetes. A systematic review 2002;25(10):1862-8.
[78] American Diabetes A. Diagnosis and classification of diabetes mellitus. Diabetes care 2009;32 Suppl 1(Suppl 1):S62-S7.

[79] Dooley KE, Chaisson RE. Tuberculosis and diabetes mellitus: convergence of two epidemics. Lancet Infect Dis 2009;9(12):737-46.
[80] Al-Goblan AS, Al-Alfi MA, Khan MZ. Mechanism linking diabetes mellitus and obesity. Diabetes, metabolic syndrome and obesity: targets and therapy 2014;7:587.
[81] Asakawa H, Tokunaga K, Kawakami F. Relationship of leptin level with metabolic disorders and hypertension in Japanese type 2 diabetes mellitus patients. Journal of Diabetes and its Complications 2001;15(2):57-62.
[82] Fischer S, Hanefeld M, Haffner SM, Fusch C, Schwanebeck U, Köhler C, et al. Insulin-resistant patients with type 2 diabetes mellitus have higher serum leptin levels independently of body fat mass. Acta Diabetologica 2002;39(3):105-10.
[83] Facey A, Dilworth L, Irving R. A review of the leptin hormone and the association with obesity and diabetes mellitus. Journal of Diabetes & Metabolism 2017;8(3).
[84] Mohammadzadeh G, Zarghami N. Serum leptin level is reduced in non-obese subjects with type 2 diabetes. Int J Endocrinol Metab 2013;11(1):3-10.
[85] Sayeed MA, Azad Khan AK, Mahtab H, Ahsan KA, Banu A, Khanam PA, et al. Leptin Is Reduced in Lean Subjects With Type 2 Diabetes in Bangladesh. Diabetes Care 2003;26(2):547-.
[86] Wang B, Chandrasekera PC, Pippin JJ. Leptin- and leptin receptor-deficient rodent models: relevance for human type 2 diabetes. Curr Diabetes Rev 2014;10(2):131-45.
[87] Meek TH, Morton GJ. The role of leptin in diabetes: metabolic effects. Diabetologia 2016;59(5):928-32.
[88] Amitani M, Asakawa A, Amitani H, Inui A. The role of leptin in the control of insulin-glucose axis. Frontiers in Neuroscience 2013;7(51).
[89] Park H-K, Ahima RS. Physiology of leptin: energy homeostasis, neuroendocrine function and metabolism. Metabolism 2015;64(1):24-34.
[90] Kelesidis T, Kelesidis I, Chou S, Mantzoros CS. Narrative review: the role of leptin in human physiology: emerging clinical applications. Ann Intern Med 2010;152(2):93-100.
[91] Zhang Y, Chua S, Jr. Leptin Function and Regulation. Compr Physiol 2017;8(1):351-69.
[92] Gorska E, Popko K, Stelmaszczyk-Emmel A, Ciepiela O, Kucharska A, Wasik M. Leptin receptors. Eur J Med Res 2010;15 Suppl 2(Suppl 2):50-4.
[93] Kwon O, Kim KW, Kim MS. Leptin signalling pathways in hypothalamic neurons. Cellular and molecular life sciences : CMLS 2016;73(7):1457-77.
[94] Perry RJ, Wang Y, Cline GW, Rabin-Court A, Song JD, Dufour S, et al. Leptin Mediates a Glucose-Fatty Acid Cycle to Maintain Glucose Homeostasis in Starvation. Cell 2018;172(1):234-48.e17.
[95] Rui L. Energy metabolism in the liver. Comprehensive Physiology 2014;4(1):177-97.
[96] Aronoff SL, Berkowitz K, Shreiner B, Want L. Glucose Metabolism and Regulation: Beyond Insulin and Glucagon. Diabetes Spectrum 2004;17(3):183.
[97] Kuo T, McQueen A, Chen T-C, Wang J-C. Regulation of Glucose Homeostasis by Glucocorticoids. Adv Exp Med Biol 2015;872:99-126.
[98] Farooqi IS, O'Rahilly S. 20 YEARS OF LEPTIN: Human disorders of leptin action. Journal of Endocrinology 2014;223(1):T63-T70.
[99] Paz-Filho G, Wong ML, Licinio J. Ten years of leptin replacement therapy. Obesity Reviews 2011;12(5):e315-e23.

[100] Montague CT, Farooqi IS, Whitehead JP, Soos MA, Rau H, Wareham NJ, et al. Congenital leptin deficiency is associated with severe early-onset obesity in humans. Nature 1997;387(6636):903-8.
[101] Licinio J, Caglayan S, Ozata M, Yildiz BO, de Miranda PB, O'Kirwan F, et al. Phenotypic effects of leptin replacement on morbid obesity, diabetes mellitus, hypogonadism, and behavior in leptin-deficient adults. Proceedings of the National Academy of Sciences of the United States of America 2004;101(13):4531-6.
[102] Pelleymounter M, Cullen M, Baker M, Hecht R, Winters D, Boone T, et al. Effects of the obese gene product on body weight regulation in ob/ob mice. Science 1995;269(5223):540-3.
[103] Denver RJ, Bonett RM, Boorse GC. Evolution of Leptin Structure and Function. Neuroendocrinology 2011;94(1):21-38.
[104] Liu Q, Chen Y, Copeland D, Ball H, Duff RJ, Rockich B, et al. Expression of leptin receptor gene in developing and adult zebrafish. General and Comparative Endocrinology 2010;166(2):346-55.
[105] Audira G, Sarasamma S, Chen J-R, Juniardi S, Sampurna BP, Liang S-T, et al. Zebrafish Mutants Carrying Leptin a (lepa) Gene Deficiency Display Obesity, Anxiety, Less Aggression and Fear, and Circadian Rhythm and Color Preference Dysregulation. International Journal of Molecular Sciences 2018;19(12).
[106] Clish CB. Metabolomics: an emerging but powerful tool for precision medicine. Cold Spring Harb Mol Case Stud 2015;1(1):a000588-a.
[107] Turi KN, Romick-Rosendale L, Ryckman KK, Hartert TV. A review of metabolomics approaches and their application in identifying causal pathways of childhood asthma. Journal of Allergy and Clinical Immunology 2018;141(4):1191-201.
[108] Johnson CH, Ivanisevic J, Siuzdak G. Metabolomics: beyond biomarkers and towards mechanisms. Nat Rev Mol Cell Biol 2016;17(7):451-9.
[109] Pan Z, Raftery D. Comparing and combining NMR spectroscopy and mass spectrometry in metabolomics. Analytical and Bioanalytical Chemistry 2007;387(2):525-7.
[110] Ren J-L, Zhang A-H, Kong L, Wang X-J. Advances in mass spectrometry-based metabolomics for investigation of metabolites. RSC Advances 2018;8(40):22335-50.
[111] Awad H, Khamis MM, El-Aneed A. Mass Spectrometry, Review of the Basics: Ionization. Applied Spectroscopy Reviews 2015;50:158 - 75.
[112] Glish GL, Vachet RW. The basics of mass spectrometry in the twenty-first century. Nature Reviews Drug Discovery 2003;2(2):140-50.
[113] Emwas A-H, Roy R, McKay RT, Tenori L, Saccenti E, Gowda G, et al. NMR spectroscopy for metabolomics research. Metabolites 2019;9(7):123.
[114] Power WP. High Resolution Magic Angle Spinning-Applications to Solid Phase Synthetic Systems and Other Semi-Solids. ANNUAL REPORTS OF NMR SPECTROSCOPY 2003;51:261-96.
[115] Corsaro C, Cicero N, Mallamace D, Vasi S, Naccari C, Salvo A, et al. HR-MAS and NMR towards Foodomics. Food Research International 2016;89:1085-94.
[116] Augustijn D, de Groot HJM, Alia A. HR-MAS NMR Applications in Plant Metabolomics. Molecules 2021;26(4).
[117] Emwas A-HM, Salek RM, Griffin JL, Merzaban J. NMR-based metabolomics in human disease diagnosis: applications, limitations, and recommendations. Metabolomics 2013;9(5):1048-72.
[118] Emwas A-HM. The strengths and weaknesses of NMR spectroscopy and mass spectrometry with particular focus on metabolomics research. Metabonomics. Springer; 2015, p. 161-93.

[119] Lowe R, Shirley N, Bleackley M, Dolan S, Shafee T. Transcriptomics technologies. PLoS computational biology 2017;13(5):e1005457.
[120] Stark R, Grzelak M, Hadfield J. RNA sequencing: the teenage years. Nature reviews Genetics 2019;20(11):631-56.
[121] Wang Z, Gerstein M, Snyder M. RNA-Seq: a revolutionary tool for transcriptomics. Nature reviews Genetics 2009;10(1):57-63.
[122] Conesa A, Madrigal P, Tarazona S, Gomez-Cabrero D, Cervera A, McPherson A, et al. A survey of best practices for RNA-seq data analysis. Genome Biol 2016;17(1):13.
[123] Amarasinghe SL, Su S, Dong X, Zappia L, Ritchie ME, Gouil Q. Opportunities and challenges in long-read sequencing data analysis. Genome Biol 2020;21(1):30.

Chapter 2

Tuberculosis causes highly conserved metabolic changes in human patients, mycobacteria-infected mice and zebrafish larvae

Yi Ding[1], Robert Jan Raterink[2], Rubén Marín-Juez[1,6], Wouter J. Veneman[1], Koen Egbers[2] , Susan van den Eeden[3], Mariëlle C. Haks[3], Simone A. Joosten[3], Tom H.M. Ottenhoff[3], Amy C. Harms[2], A. Alia[4,5], Thomas Hankemeier[2], Herman P. Spaink[1*]

[1] Institute of Biology, Leiden University, The Netherlands
[2] Leiden Academic Centre for Drug Research, Leiden University, The Netherlands
[3] Department of Infectious Diseases, Leiden University Medical Center, The Netherlands
[4] Leiden Institute of Chemistry, Leiden University, 2333 Leiden, The Netherlands.
[5] Institute for Medical Physics and Biophysics, University of Leipzig, 04107 Leipzig, Germany.
[6] Department of Developmental Genetics, Max Planck Institute for Heart and Lung Research, 61231 Bad Nauheim, Germany
*Corresponding author, email: H.P.Spaink@biology.leidenuniv.nl

Scientific Reports 2020;10(1):11635

ABSTRACT

Tuberculosis is a highly infectious and potentially fatal disease accompanied by wasting symptoms, which cause severe metabolic changes in infected people. In this study we have compared the effect of mycobacteria infection on the level of metabolites in blood of humans and mice and whole zebrafish larvae using one highly standardized mass spectrometry pipeline, ensuring technical comparability of the results. Quantification of a range of circulating small amines showed that the levels of the majority of these compounds were significantly decreased in all three groups of infected organisms. Ten of these metabolites were common between the three different organisms comprising: methionine, asparagine, cysteine, threonine, serine, tryptophan, leucine, citrulline, ethanolamine and phenylalanine. The metabolomic changes of zebrafish larvae after infection were confirmed by nuclear magnetic resonance spectroscopy. Our study identified common biomarkers for tuberculosis disease in humans, mice and zebrafish, showing across species conservation of metabolic reprogramming processes as a result of disease. Apparently, the mechanisms underlying these processes are independent of environmental, developmental and vertebrate evolutionary factors. The zebrafish larval model is highly suited to further investigate the mechanism of metabolic reprogramming and the connection with wasting syndrome due to infection by mycobacteria.

Introduction

Infection with *Mycobacterium tuberculosis (Mtb)* can result in tuberculosis (TB) that currently is newly affecting over 10 million people per year and leading to 1.6 million deaths annually [1]. However, the majority of people that have been infected with *Mtb*, estimated to be in the order of 2 billion, do not experience any symptoms in the presence of positive immunological (blood or skin) test results. In patients diagnosed with TB, the disease is uniformly characterized by a metabolic wasting syndrome that leads to heavy weight loss that concurs with a strong reduction of muscle mass. TB has therefore historically earned the name of "consumption".

Novel tools for control of TB should include not only better treatments, including attention to the deleterious effects of wasting syndrome, but also needs to include cost-effective assays for robust and sensitive diagnosis of TB [2]. Recent metabolomics studies have identified valuable diagnostic metabolic blood markers that can discriminate TB patients from healthy individuals [3-13]. This appeared to be applicable to very different population groups, ranging from trans-Africa, China, Georgia, and Indonesia, and therefore highlighting that blood metabolites are robust and validating biomarkers for TB progression. These studies used mostly mass spectrometry (MS) and in some cases nuclear magnetic resonance (NMR) spectrometry [4]. Compared to MS, NMR offers the advantages of high reproducibility, minimal sample preparation, fast measurement, non-invasive, non-selectivity, non-destructive such that samples also could be stored and used for other detections. The limitation of NMR is its relatively low sensitivity, which however can be improved by using higher magnetic fields (frequencies commonly used range between 300 and 700 MHz), and large numbers of samples [14, 15]. MS studies of metabolites from blood samples showed that many amino acids, such as histidine, cysteine, glutamine, tryptophan, citrulline, and creatine were decreased in TB patients from South Africa [3]. A few metabolites were increased in abundance including kynurenine, phenylalanine and pyroglutamine in the active TB group [3]. Similar patterns of metabolic changes due to TB were found in a recent MS study on blood samples from a cohort of Indonesian TB patients even if the patients suffered from a combination of TB and type II diabetes [16]. By comparing metabolic profiles of TB patients from patients with other respiratory diseases, Weiner et al. identified metabolic profiles that are specific to TB [11]. In this study it was shown that changes in various metabolites were predictive for the onset of clinical TB as early as 12 months prior to TB diagnosis in a trans-African population [11]. Using MS, Yi et al. demonstrated that histidine, arachidonic acid and biliverdin were decreased in Chinese TB patients compared to the group of healthy individuals, but could be restored to normal levels following TB cure [12]. In an MS study that compared the effects of curing patients from Gambia of an infection of *Mtb* or *M. africanum* on metabolism, it was shown that in both cases the levels of many amino acids such as histidine, ornithine, tryptophan and leucine were increasing strongly after 6 months of antibiotic treatment [7]. In a study that used NMR for analysis of blood metabolites, markers for Chinese TB patients were found, although there were major differences with the published MS studies, such as an increased plasma level of glutamine [4].

There are only few studies investigating the metabolic profile of *Mtb* in animal models, such as cattle, guinea pigs and mice using NMR. A study with calves that were infected with three *Mtb* strains including *M.bovis*, *H37Rv* and *Mtb1458* through intratracheal injection and followed for 33 weeks showed that serum levels of isoleucine, leucine, tyrosine, valine were decreased in case of all three strains [17]. Using ^{1}H Magic Angle Spinning NMR, Somashekar et al. revealed that alanine was significantly elevated after 15 and 60 days infection with *Mtb H37Rv* in lung tissue of challenged guinea pigs [18]. A few metabolites such as ethanolamine, glutamine and ATP were significantly decreased after 30 and 60 days of infection in serum of guinea pigs [19]. Clear separation between control and *Mtb*-infected groups was also observed in organs (lung, liver, spleen) and serum samples of mice [20]. A majority of these metabolites including tyrosine, glutamine, leucine, isoleucine were increased in lung, liver, spleen and serum [20]. Although these NMR studies identified metabolic markers for TB, there was little correlation with the markers identified in human studies using MS.

Zebrafish has been shown to be an excellent model for the study of TB [21-25]. Because zebrafish have large amounts of offspring at one time and the availability of high throughput automated infection methods [26], many zebrafish larvae can be tested for TB in a short time. The test system is independent of food intake and adaptive immune responses that only start later during development. In order to validate our platform for identification of TB biomarkers, we also performed metabolomic studies in zebrafish larvae. It is an important model for TB research based on the infection of zebrafish larvae with *Mycobacterium marinum (M. marinum)*. It has been shown that this infection leads already after several days to many inflammatory responses and state that are highly comparable to progression of TB in humans [27, 28]. The sensitivity of our mass spectrometry platform has been shown to be sufficient for the analysis of single zebrafish larva for the detection of large set of small metabolites [29].

Here, we have compared the effect of TB infection on the level of metabolites in blood of humans and mice and whole zebrafish larvae using one highly standardized mass spectrometry pipeline, ensuring technical comparability of the results. Subsequently we used the zebrafish model to further investigate the metabolic changes after infection using NMR analyses based on a large number of specimens. Our results show a common conservation of metabolic reprogramming processes during TB infection and disease in humans, mice and zebrafish. The NMR analysis of zebrafish larvae confirmed the MS data and also identified new markers for infection including identifying general effects on metabolism such as a change of glucose levels.

Results

Metabolite profiles of TB patients measured by mass spectrometry

To measure metabolite profiles in TB patients compared to healthy people, 20 blood samples from each group were analysed by MS. Using a highly standardized platform we could measure 59 small

amine-containing compounds. The normalized data sets showed a significant separation of the metabolite profiles of the patient and control group using Partial Least Squares Discriminant Analysis (PLS-DA) (**Fig.1A**). Using a false discovery rate cut-off value of 0.05 we could classify 31 of the 59 identified small amine-containing compounds as associated with the TB disease state (**Fig.1B**, **Supplementary Table S2**). There were 26 metabolites showing significantly lower abundance in patients compared to healthy individuals (**Fig.1B**). Only a few metabolites, namely putrescine, methionine sulfoxide, aspartic acid and glutamic acid, were increased in patients compared to controls (**Fig.1B**). Considering the relatively large number of metabolites of which the levels were significantly affected, the data suggest a drastic metabolic reprogramming in TB patients. For 8 of these metabolites it was previously shown that they were biomarkers for TB, namely methionine, glutamine, threonine, tryptophan, histidine, citrulline, cysteine and homoserine [3, 11, 16]. Antibiotic treatment for 6 weeks did not have a major effect on separation of the metabolic profiles of TB patients from the control group although minor effects were observed (**Supplementary Fig.S1**). Some markers appeared to be responding in an anti-correlated fashion compared to published TB cohorts studies, such as lowered level of phenylalanine (**Fig.1B**) that was shown to be increased in patients in the study of Weiner et al, 2012 [3] and Vrieling et al, 2019 [13]. However, in a study of a TB patient cohort from South Africa, also a decreased level of phenylalanine was reported compared to the control group [30].

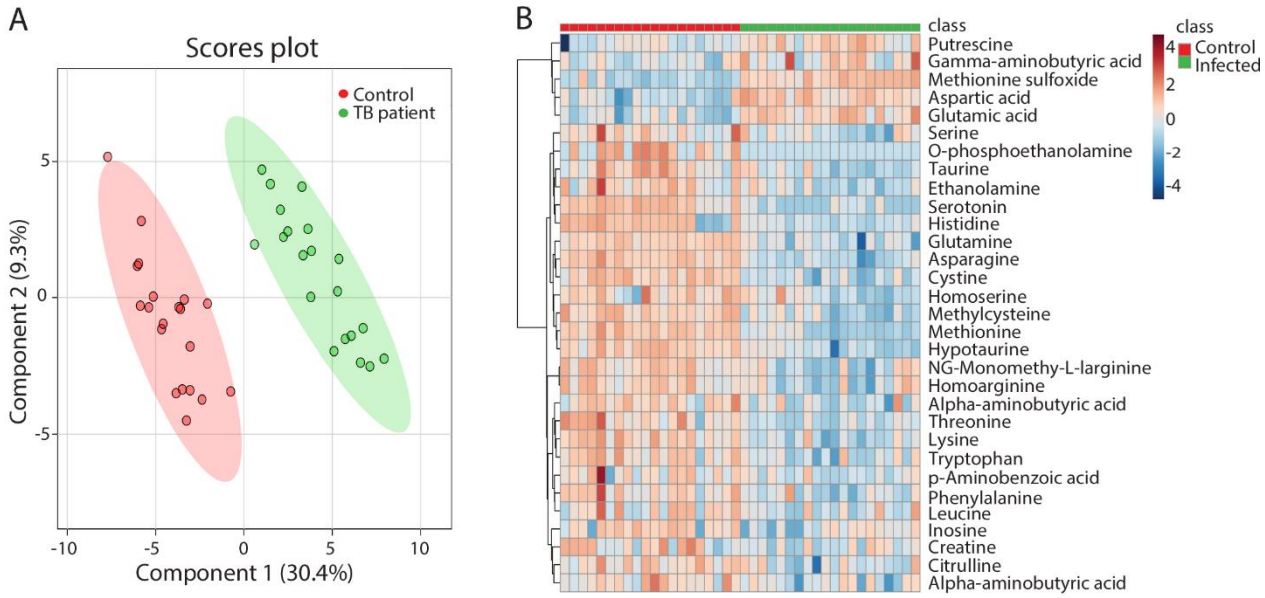

Figure 1. Partial least squares discriminant analysis and heat map of metabolomic profiles from patients with active TB and healthy controls. (**A**) PLS-DA analysis of blood of the healthy control group (Control), patients with active TB disease (TB patient), n = 20. (**B**) Heat map of the 31 metabolites which have a significantly different concentration in TB infected patients and the healthy control group in a T-test with $p<0.05$.

Metabolite profiles of *Mtb* infected mice measured by mass spectrometry

Metabolic profiles of the blood of *Mtb*-infected C57BL/6 mice and an uninfected control group were measured by MS to identify and compare profiles in a rodent model of TB. PLS-DA scores plot of the 40 identified metabolites showed clear differences between the control group and the *Mtb*-infected mice, indicating there were significant alterations in the metabolism after infection (**Fig.2A**). The data showed significant differences and ratios of metabolite quantities for 31 of the 40 identified molecules between infected mice and controls by applying a t-test at a significant threshold of 0.05 (**Fig.2B**, **Supplementary Table S3**). The relative abundances of all the significantly identified metabolites were reduced after infection (**Fig.2B**). Of these signature metabolites 14 were also lower in human TB patients compared to controls (**Fig.3A**). In contrast to the human data set, there was no increase of any metabolite after infection.

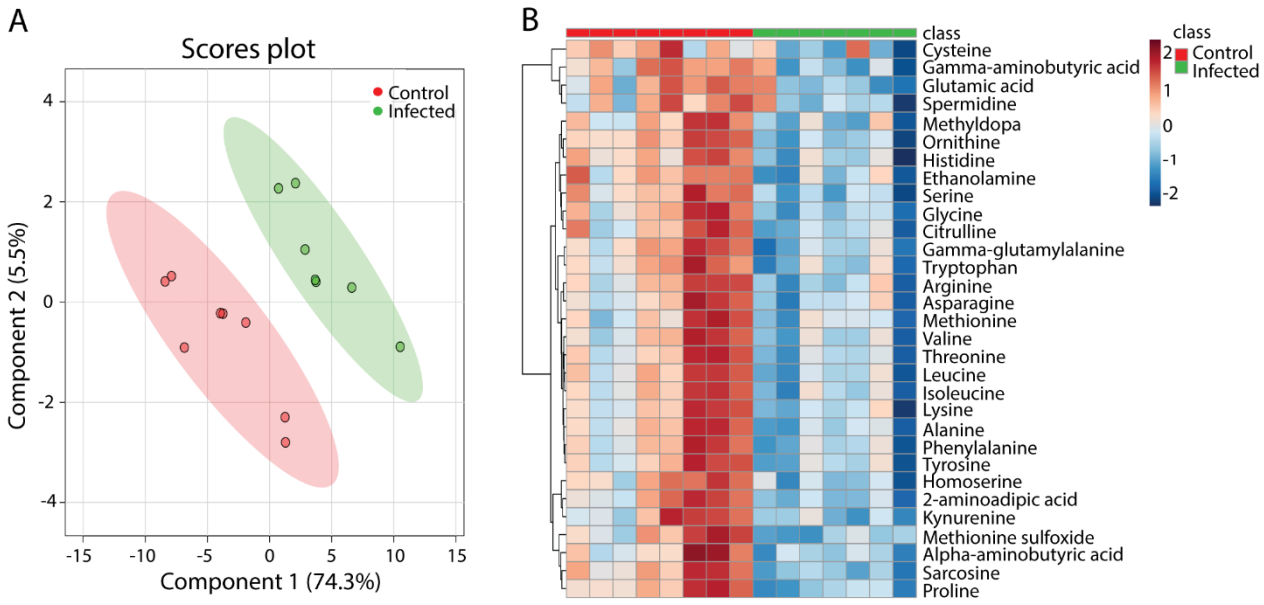

Figure 2. Partial least squares discriminant analysis and heat map of metabolomic profiles from mice with or without *Mtb* infection. (**A**) PLS-DA analysis of blood of the wild type mouse strain C57BL/6 after 8 weeks of nasal infection with *M. tuberculosis* H37Rv, n = 8. (**B**) Heat map of the 31 metabolites which have a significantly different concentration in *Mtb*-infected and uninfected mice in a T-test with $p<0.05$.

A

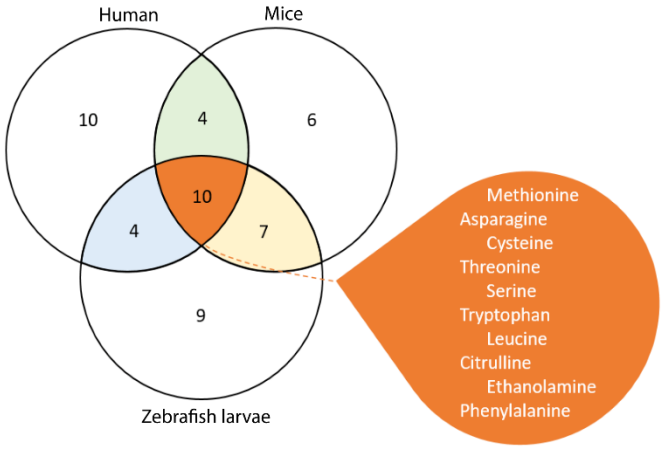

B

Metabolite	HMDB identifier	Human FDR	Human Ratio	Mouse FDR	Mouse Ratio	Zebrafish FDR	Zebrafish Ratio
Asparagine	HMDB00168	5,35E-11	0.42	9,04E-03	0.69	8,31E-05	0.58
Citrulline (1,2,3)	HMDB00904	2,00E-03	0.67	2,11E-03	0.57	3,68E-03	0.67
Cysteine (1,2)	HMDB00192	2,47E-09	0.4	2,36E-02	0.97	2,25E-02	0.25
Ethanolamine	HMDB00149	2,50E-04	0.75	1,31E-03	0.67	9,70E-07	0.41
Leucine	HMDB00687	3,50E-02	0.84	1,58E-03	0.55	4,97E-06	0.46
Methionine (1)	HMDB00696	1,01E-11	0.22	1,79E-02	0.63	1,15E-05	0.63
Phenylalanine	HMDB00159	4,16E-04	0.79	2,62E-03	0.56	2,16E-05	0.55
Serine	HMDB00187	8,84E-03	0.8	3,07E-04	0.63	7,26E-05	0.54
Threonine (1,3)	HMDB00167	2,94E-05	0.66	2,78E-03	0.54	2,71E-05	0.62
Tryptophan (1,2,3)	HMDB00929	2,55E-04	0.72	1,23E-03	0.48	1,38E-06	0.45
Histidine (1,2,3)	HMDB00177	3,72E-04	0.46	9,87E-04	0.66	NS	0.87
Lysine	HMDB00182	1,90E-06	0.73	5,77E-03	0.59	NS	0.98
Alpha-aminobutyric acid	HMDB00452	9,00E-04	0.75	4,11E-03	0.65	-	ND
Homoserine (3)	HMDB00719	2,46E-03	0.75	1,21E-03	0.59	-	ND
Glutamine (1,2,3)	HMDB00641	1,21E-06	0.33	NS	0.83	1,10E-05	0.58
Putrescine	HMDB01414	1,51E-03	3.18	NS	0.81	1,08E-04	1.52
Asymmetric dimethylarginine	HMDB01539	1,16E-02	0.79	-	ND	7,94E-04	0.54
Methylcysteine	HMDB02108	4,05E-08	0.48	-	ND	4,04E-03	0.48
Alanine (3)	HMDB00161	NS	0.9	1,69E-03	0.61	4,35E-03	0.77
Arginine	HMDB00517	NS	0.92	3,15E-03	0.61	5,34E-04	0.65
Isoleucine	HMDB00172	NS	0.92	2,94E-03	0.57	1,79E-06	0.42
Ornithine (3)	HMDB00214	NS	0.87	1,38E-04	0.52	2,01E-06	0.58
Proline	HMDB00162	NS	0.82	1,92E-04	0.53	6,02E-05	0.67
Tyrosine	HMDB00158	NS	0.87	3,89E-03	0.52	8,11E-05	0.45
Valine	HMDB00883	NS	0.89	5,51E-03	0.54	1,16E-06	0.48

Figure 3. Common metabolic responses in TB patients, infected mice and zebrafish. (**A**) A Venn diagram is shown of the common metabolites that respond significantly towards infection with mycobacteria in patients with TB disease, infected mice and zebrafish larvae. Anti-correlated values are not included in the overlap of the Venn diagram. (**B**) A table shows the ratio of common metabolites in humans, mice and zebrafish larvae. Abbreviations: ND, non-detectable; NS, not significant. (1) Metabolites that have been reported to have significantly different levels between patients with TB as compared to healthy controls [3]. (2) Metabolites of which the levels have been reported to be predictive for the development of TB in African patients [11]. (3) Metabolites that are significantly decreased in TB patients [13].

Metabolic profiles of *M.marinum* infected zebrafish larvae measured by mass spectrometry

In order to test whether the metabolic responses observed in humans and mice could be translated to results in zebrafish, larvae infected for 5 days with *M.marinum* strain E11 were studied by MS. Metabolomic profiles of the 44 identified metabolites of complete infected and uninfected larvae could be clearly discriminated using PLS-DA (**Fig.4A**). A set of 35 out of 44 identified small amine-

containing metabolites was significantly different with an FDR cut-off value of 0.05 (**Fig.3B**, **Supplementary Table S4**). The majority of the 30 metabolites was significantly decreased in the infected zebrafish larvae (**Fig.3B**, **Supplementary Table S4**). Five metabolites, namely glutathione, putrescine, beta-alanine, 5-hydroxylysine and O-phospoethanolamine, were increased in the infected group compared to the control group (**Fig.4B**). There was an overlap of 17 metabolites with the TB signature metabolites observed in mice and of 14 metabolites with the TB signature metabolites observed in humans (**Fig.3A**).

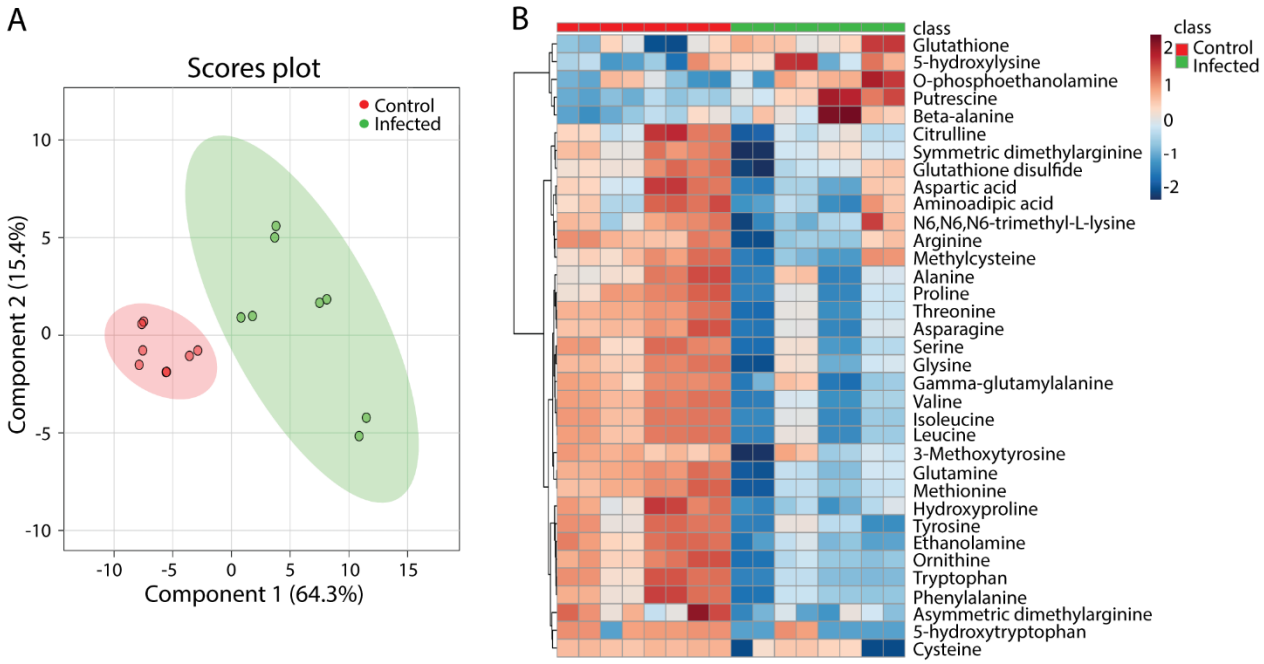

Figure 4. Partial least squares discriminant analysis and heat map of metabolomic profiles from *M. marinum* infected and uninfected zebrafish larvae. (**A**) PLS-DA analysis of entire zebrafish larvae uninfected (Control) or after infection with *M. marinum* strain E11 in the yolk at 2 h post fertilization (Infected). All the larvae were collected at 5 dpf and then measured with mass spectrometry. Each dot represents one larva, n = 8. (**B**) Heat map of the 35 metabolites which have a significantly different concentration in zebrafish larvae in the infected and the control group. *dpf* days post fertilization.

A core set of metabolites are markers for tuberculosis in humans, mice and zebrafish

Interestingly and consistently, the three metabolomics data sets identified a relatively high number of common metabolites that were decreased after infection with mycobacteria in the human, mouse and zebrafish samples. The comparisons of common metabolites from the humans, mice and zebrafish larvae are shown in the Venn diagram of **Fig.3A**. As shown in **Fig.3B**, the ten common metabolites, methionine, asparagine, cysteine, threonine, serine, tryptophan, leucine, citrulline, ethanolamine and phenylalanine, were significantly decreased in all three sample sets. It should be noted that the overlap between species was limited by the fact that some metabolites that were detected in the human blood samples could not be detected in the mouse or zebrafish samples. This

result is true for both the original and normalized values of these ten common metabolites (**Fig.5**). Therefore these metabolites represent good markers for TB disease activity. Remarkably, five metabolites (citrulline, cysteine, methionine, threonine and tryptophan) of this marker set have been previously identified as markers for TB disease in different human populations [3, 16]. Three (citrulline, cysteine and tryptophan) of these markers have also been shown to be predictive for progression of TB. Furthermore, in some cases, such as histidine in the zebrafish samples, a positive correlation was observed, but the threshold of significance was not achieved for inclusion in the overlap set (**Fig.3B**). In case of zebrafish, this could be the result of the small size of single larva of approximately 0.3 microliter that limits the amount of material analyzed [31]. In order to verify the zebrafish data in more detail we therefore undertook an NMR study with larger numbers of pooled zebrafish larvae.

Figure 5 (following page). Quantification of the common 10 amino acids that have a decreased concentration in the infected groups of humans, mice and zebrafish. The data for the 10 common metabolites which all display a significantly decreased concentration ($p<0.05$) in all the infected groups are shown for (**A**) the patients with active TB disease, (**B**) mice, and (**C**) zebrafish larvae, with the original and normalized values.

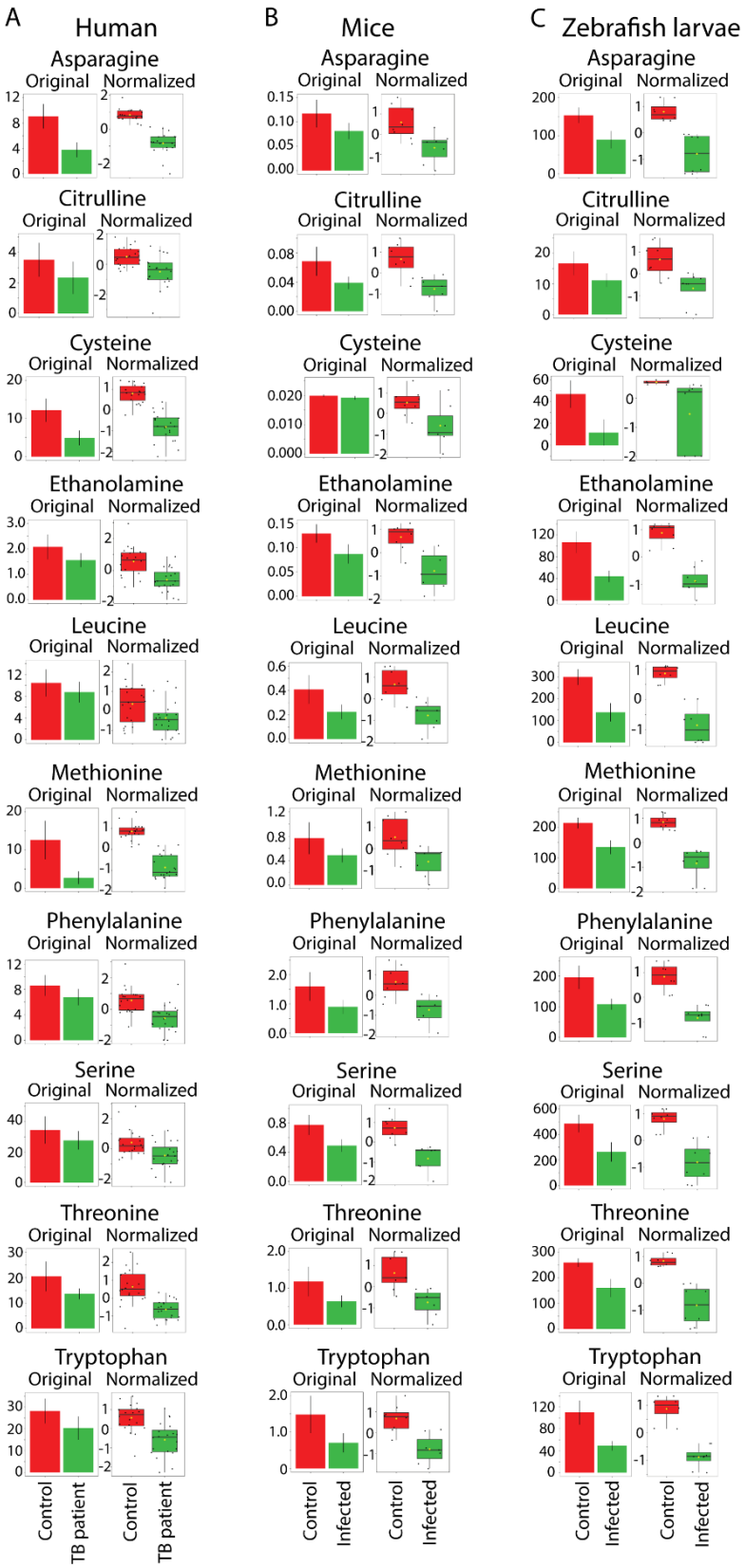
A
Human
B
Mice
C
Zebrafish larvae
Asparagine
Citrulline
Cysteine
Ethanolamine
Leucine
Methionine
Phenylalanine
Serine
Threonine
Tryptophan
Original
Normalized
Control
TB patient
Infected

Metabolic profiles in *M.marinum* infected zebrafish larvae measured by nuclear magnetic resonance spectroscopy

In order to obtain metabolic profiles of zebrafish after infection with *M. marinum* measured by another metabolomic technique and compare with MS, ^{1}H-nuclear magnetic resonance was used. Metabolic profiles of extracted zebrafish embryos infected for 5 days with the *M. marinum* M strain were obtained by one-dimensional (1-D) and two-dimensional (2-D) ^{1}H NMR. Representative 1D ^{1}H-NMR spectra from mock-injected control and infected group are shown in **Fig.6A**. 1D ^{1}H-NMR of *M. marinum*-injected embryos chemical shift were compared to controls (**Fig.6A**). The ^{1}H-NMR spectra of control and *M. marinum*-injected embryos were investigated by multivariate analysis with PLS-DA modeling to probe if control and infected embryos can be discriminated. The PLS-DA scores plot of the first two principle components explains 38.5% of the total variance, and clustering of the control and infected larvae groups could be observed in the score plot of PLS-DA1 vs PLS-DA2 (**Fig.6B**). Comparisons (based on 1-D NMR chemical shifts) to the Human Metabolome Database (HMDB), along with 2-D NMR techniques (i.e.,^{1}H-^{1}H COSY) enabled unambiguous identification and subsequent quantitation of metabolites (**Supplementary Fig.S4**).

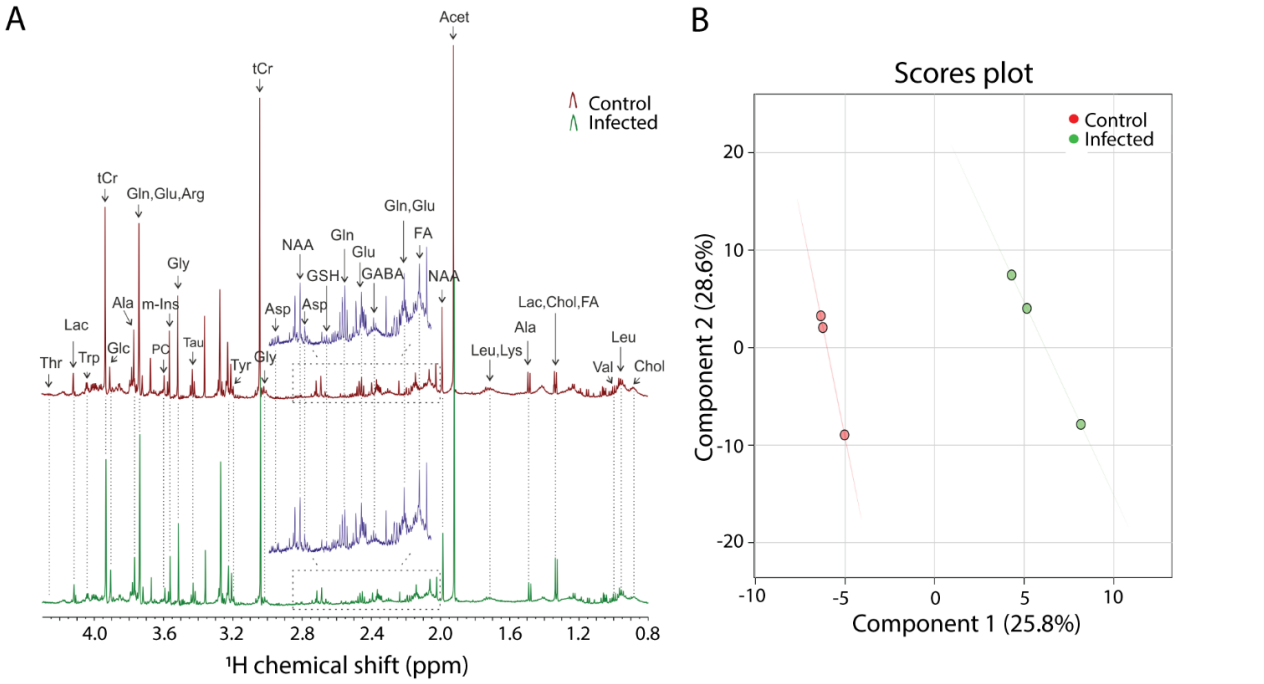

Figure 6. One-dimensional ^{1}H NMR spectra of *M. marinum*-infected and uninfected zebrafish larvae. (**A**) Zebrafish larvae at 4 h post fertilization were infected with the *M. marinum* M strain in the yolk and NMR measurements were carried out at 5 dpf. Spectra from chemical shift 0.8 to 4.3 were assigned to specific metabolites. *Thr* threonine, *Lac* lactate, *Trp* Tryptophan, *tCr* total creatine (creatine + phosphocreatine), *Glc* Glucose, *Ala* alanine, *Gln* glutamine, *Glu* glutamate, *Arg* arginine, *PC* phosphocholine, *m-Ins* myo-inositol, *Gly* glycine, *Tau* taurine, *Tyr* tyrosine, *Asp* aspartate, *NAA* N-acetyl aspartate, *GSH* glutathione, *GABA* gammaaminobutyric acid, *FA* fatty acid, *Leu* leucine, *Lys* lysine, *Val* valine, *Chol* cholesterol. Lilac color stands for a magnification of the chemical shift in the dashed rectangle box. (**B**) PLS-DA shows a clear separation of control and infected groups, n = 3, each replicate represents 120 pooled larvae.

Nuclear magnetic resonance confirms data from mass spectrometry in zebrafish larvae

To compare the consistency of metabolic changes in zebrafish performed by MS and NMR, quantification and comparison of the most abundant metabolites from two approaches between control and *M. marinum*-infected zebrafish embryos are shown in Fig.7. Quantitative analysis of metabolites which were identified in both MS and NMR showed the same trend of changes for all metabolites (**Fig.7A, B**). The significant changes included 12 decreased metabolites (**Fig.7A**) that included the entire group of the 10 common biomarker set from the MS analyses. A common biomarker in the human and mouse data set, histidine, which was not significant in the MS analysis in zebrafish, however was significantly decreased in the infected group in the NMR analysis (**Fig.7C**). Notably, the increased level of putrescine after infection was confirmed by NMR analysis of the zebrafish larvae (**Fig.7A, B**). NMR could detect additional significantly changed metabolites which were not found in MS, as shown in **Fig.7C**: lactate, taurine and GABA were reduced in the infected group, while glucose, mannose, and NADH were significantly increased after infection.

Discussion

Measurements of metabolites in human TB patients have shown to be a promising method for diagnostic purposes. However, in the absence of knowledge about genetic, physiological and environmental factors that could influence the measurements at different stages of the disease, clinical implications are still uncertain. Our data of metabolic changes in a small contingent of tuberculosis patients in the Netherlands confirm the notion that the observed changes compared to healthy individuals are very common for patients in highly different geographic locations and showed the consistency of our highly-standardized metabolite analysis pipeline [32, 33]. In this study we also compared host metabolic changes during human TB disease to infection with *Mtb* in a rodent model and infection with *M. marinum* in a zebrafish using identical pipelines. Our results show highly consistent metabolic changes in all three models. This internal validation of the findings in quite different models enhances the biological broad impact of the findings in the human patients. This is surprising because the analyzed samples of this comparative infection study are in many respects extremely different in that the species represent quite diverse examples from the vertebrate subphylum, that differ for example in metabolic rate, body size, body temperature and examined developmental stages. Since zebrafish larvae are not yet fed during the timeframe of the experiment, but solely use their yolk for nutrition, this shows that difference in food intake are not involved in the observed metabolic changes. Considering these differences, it is striking that in the three studies we found 10 common metabolites that were significantly decreased during infection or disease from a total of 89 metabolites that were detectable with our mass spectrometry platform. These data suggest that this set of metabolites is strongly conserved during mycobacterial infection and disease in all species.

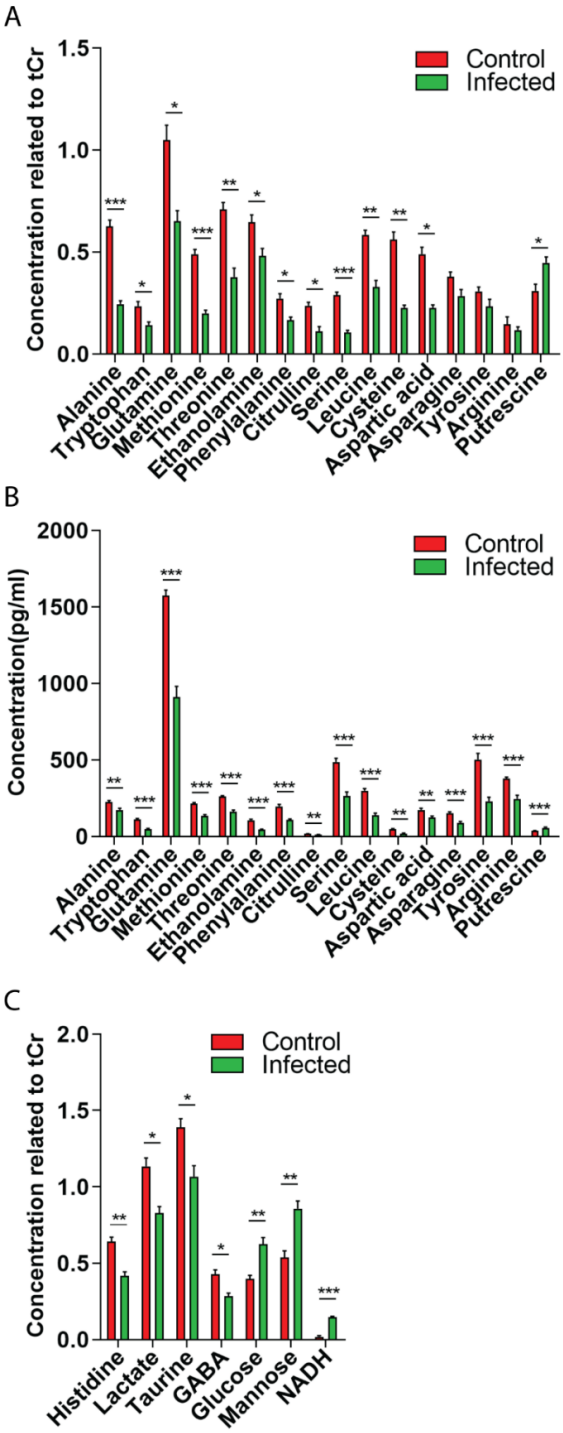

Figure 7. Comparison of the effect of *M. marinum* infection in zebrafish on the metabolic profiles measured by ^{1}H NMR spectroscopy and mass spectrometry. (**A**) Quantification of metabolite concentrations obtained by NMR spectroscopy. Values are average ± SE of mean (p<0.05). tCr represents total creatine. (**B**) MS data of the corresponding metabolites shown in Fig.4 and Table S4. (**C**) Metabolites which are significantly changed in concentration identified by NMR, but not by MS. Asterisks represent significant p-values obtained by a comparative T-test. *p<0.05, **p<0.01, ***p<0.001.

NMR was used to confirm the mass spectrometry results in the case of zebrafish. These results confirm results from earlier studies that metabolic changes during TB are very significant. Importantly, here we show for the first time that the metabolic changes during TB are highly similar within different vertebrates, at least for the metabolites measured. Apparently, these metabolic changes are so fundamental to mycobacterial infection that they are not affected by the many factors that we mention above. This observation strengthens the biological significance of the finding in human patients, and also supports the potential utility of these metabolites as biomarkers for TB in different trans-species settings, including humans and animal TB, and also diseases caused by non-tuberculosis mycobacteria such as *M. marinum*. In addition, the conservation of these biomarkers in model organisms provides a way to further investigate the mechanism underlying the changes in biomarker levels during TB. Since these biomarkers are common between humans, mice and fish, kinetic analyses that will contribute significantly to pathophysiologic and mechanistic insights can be performed in animal models.

Out of the 10 identified common biomarkers whose levels are decreased in our study, 5 represent amino acids that are essential in human diet [34]. Several of the other decreased biomarkers that are not conserved in all three trans species data sets are also essential amino acids or are derived from these essential amino acids such as tyrosine that is derived from phenylalanine. The decreased levels of these amino acid biomarkers are consistent with earlier reports by Weiner et al, 2012, Weiner et al, 2018, and Vrieling et al, 2019 (**Fig.3B**). These results indicate that differences in diet or biosynthesis are unlikely to be causing the decreased levels of the identified common group of metabolites. The fact that these biomarkers are also reduced in zebrafish larvae infected with mycobacteria shows an uncoupling of the biomarkers with food intake. One could argue that the decreased levels of these metabolites are the result of consumption of circulating host metabolites by the mycobacteria. This hypothesis seems rather unlikely in the light of the observation that short term treatment with antibiotics did not alter the levels of these metabolites in human patients, despite strongly reducing the number of viable bacilli. It is therefore more likely that the direct cause of the decreased levels of metabolites is the consumption of these metabolites by host cells as a result of inflammation resulting in wasting syndrome. This would be in line with the fact that infection with mycobacteria leads to a metabolic wasting syndrome that can last 6 months or longer after initial antibiotic treatment of the disease [35]. In a previous study, treatment of TB patients with antibiotics indeed lead to recovery of the levels of amino acids after 26 weeks, but this recovery was not yet complete after 8 weeks of treatment [16].

Currently the mechanisms underlying the strong effects of mycobacterial infection on host metabolism are still poorly understood. Previous studies have suggested that some metabolites might be indicative of changes in particular enzymes involved in host metabolism linked to *Mtb* infection. During TB, an increased level of the enzyme indoleamine 2,3 dioxygenase 1 (IDO1) that converts tryptophan to kynurenine might be responsible for decreased levels of tryptophan and an increased level of kynurenine [3, 36]. Our results also indicate a decreased level of tryptophan in the infected state of all three species, but, we have not been able to detect increased levels of

kynurenine in the human Groningen contingent and zebrafish samples. Surprisingly, we found a decrease of kynurenine after infection in the mouse experiments (**Supplementary Table S3**). Other amino acids that are changed in our data sets such as citrulline, ornithine, arginine and aspartic acid are intermediates in the urea cycle that functions in the conversion of ammonia to urea. The only consistently decreased metabolite of these urea cycle intermediates in all three species is citrulline. Interestingly, previous studies have shown that arginine depletion as a result of arginase activity can be replenished from citrulline in macrophages and T-cells and thereby plays a role in immune defense [37, 38]. Although in zebrafish larvae, the T-cells are not yet developed [39], functional macrophages that can express arginase are present [40]. In addition, zebrafish larvae produce various cytokines that have been found to correlate with decreased amino acid levels in human patients [3]. Therefore, the reduced citrulline levels in zebrafish larvae could indicate a link with innate immune responses. The zebrafish infection model as also used in this study has been recently analyzed using a mathematical model which can predict zebrafish metabolism from gene expression. The results showed that the model predicts reduced histidine metabolism in *M. marinum* infected zebrafish larvae at 4 days post injection [41]. In accordance with the model, a reduction of histidine levels in infected zebrafish larvae was shown to be significant as measured by NMR.

In conclusion, our study provides robust, cross species and validating metabolic marker changes during TB and provides important leads to investigate mechanisms underlying this metabolic reprogramming in animal models. Moreover, further studies should address whether the observed metabolic changes during TB can result in meaningful biomarkers for *Mtb* infection and disease [42]. Animal models can be used to analyse the effect of genetic mutants in key metabolic pathways that could play a role in the observed changes of metabolism. In our future studies we will be interested in genes that play a role at the interface of immune response and metabolism for which knock out mutants are available such as genes in toll-like receptor, leptin [43] and glucocorticoid receptor [44] signalling pathways. These studies could not only help elucidating the observed changes in metabolism during infection, but could also lead to the development of new medicines for treatment of TB or wasting syndrome using innovative host-directed therapeutic approaches [45].

Methods

Biological material

Human plasma samples were collected at the specialized UMCG clinical center for TB treatment, Beatrixoord in Haren, Groningen, The Netherlands. All patients were diagnosed with active pulmonary and/or extrapulmonary *M. tuberculosis* infection. Patients were diagnosed with active pulmonary or extrapulmonary TB using mycobacterial culture or PCR of sputum or tissue specimens. For all culture positive specimens, drug sensitivity was determined to guide clinical

treatment. All patients improved clinically upon treatment with anti-TB drugs. Patients were admitted to the TB ward for clinical treatment and received a 6 month antibiotic regimen based on Dutch guidelines. Patients originated from various countries, including TB endemic regions. A second blood sample was collected from all individuals 6 weeks after inclusion into the study (referred to as on treatment sample in **Supplementary Fig.S1**). In addition, a control group was recruited at the Leiden University Medical Center, comprised of healthy skin test negative individuals. All human sample collection and research was performed in accordance with the guidelines and regulations of the Leiden University Medical School at time of recruitment under protocol P07.48. The age and gender of the patients and healthy persons are given in Supplementary Table S1A and S1B showing that there is a highly unequal distribution of the gender in the patient group. For the mice experiments, two groups of male mice (strain C57BL/6) were obtained from Charles River Laboratories. Male mice were chosen because they have less variation due to the hormonal cycle. Eight male mice nasally-infected with *M. tuberculosis* strain H37Rv at 6 weeks age, and eight mock infected male mice were kept under standard conditions for 8 weeks. The results showed that the mice were systemically infected as shown by plating of bacteria from isolated organ material (**Supplementary Fig.S2B** and **C**). One mouse of the group of 8 infected mice had to be killed at an early stage due to unexpected symptoms. There was no significant difference in body weights in the infected groups (**Supplementary Fig.S2A**). Zebrafish breeding and embryo collection were performed as described previously [46]. Zebrafish embryos at 2 to 4 hours post fertilization (hpf) were used for *M. marinum* injection. For mass spectrometry analysis we used *M. marinum* strain E11 labelled with a mCherry-expressing pSMT3 vector [26]. For the NMR experiments we used *M. marinum* strain M labelled with mWasabi plasmid pTEC15 vector [22]. *M. marinum* preparation and injection were followed by the protocol of a previous study [26]. Infection levels were checked with fluorescence microscopy (**Supplementary Fig.S3A**, **B**, **C** and **D**). One larva per sample (n=8) obtained from different crossings that show batch effects in the clustering was used for LC-MS/MS analysis. Regarding the limitation of NMR sensitivity, 120 larvae per sample (n=3) with *M. marinum* injection or 2% polyvinylpyrrolidone 40 (PVP40) mock injection were used for NMR measurements.

LC-MS

Human plasma was derived from heparinized tubes. Mice serum was derived of clotted blood tubes, aliquoted, and stored at −80 °C until analysis. A zebrafish embryo has a volume of approximately 0.3 µL [31]. Because of this small volume it is important to dilute the sample as minimal as possible in order to obtain a comprehensive metabolic profile. For this reason the derivatization volumes were downscaled to 4µL:16µL (AccQ:borate) which made the sample 2,5 times less diluted. Although the sample composition didn't change by this optimization step, the sample was too organic (20% ACN) to give the polar metabolites good chromatography. This problem was solved by diluting the sample four times with water, so the ACN concentration in the sample went to 5%. To compensate for this dilution factor, the sample injection volume was increased with the same

factor, so from 1µL injection to 4 µL injection. When the larvae are ready to be analyzed, they are transferred to (1.5mL) centrifuge tubes and are placed in a random order for the washing and quenching by methanol. After homogenization, the proteins were removed from the sample by centrifuging and collecting the supernatant. After collecting the supernatant (75µL), a small portion (5µL) is used for a QC pool which was depending on the batch size aliquoted over 5 centrifuge tubes. The QCs and samples are all placed randomly in the evaporator and derivatized afterwards. After derivatization the samples were diluted with water four times and transferred into vials that were randomly placed in the auto sampler of the LC.

The amine platform covers amino acids and biogenic amines employing an Accq-Tag derivatization strategy adapted from the protocol supplied by Waters [47]. 5.0 µL of each sample was spiked with an internal standard solution. Then proteins were precipitated by the addition of MeOH. The supernatant was taken to dryness in a speedvac. The residue was reconstituted in borate buffer (pH 8.5) with AQC reagent. 1.0 µL of the reaction mixture was injected into the UPLC-MS/MS system. Chromatographic separation was achieved by an Agilent 1290 Infinity II LC System on an Accq-Tag Ultra column (Waters). The UPLC was coupled to electrospray ionization on a triple quadrupole mass spectrometer (AB SCIEX Qtrap 6500). Analytes were detected in the positive ion mode and monitored in Multiple Reaction Monitoring (MRM) using nominal mass resolution. Acquired data were evaluated using MultiQuant Software for Quantitative Analysis (AB SCIEX, Version 3.0.2). The data are expressed as relative response ratios (target area/ISTD area; unit free) using proper internal standards. For analysis of amino acids their $^{13}C^{15}N$-labeled analogs were used. For other metabolites, the closest-eluting internal standard was employed. In-house developed algorithms were applied using the pooled QC samples to compensate for shifts in the sensitivity of the mass spectrometer over the batches. After quality control correction, metabolite targets complied with the acceptance criteria of RSDqc<15%. Using this platform we were able to identify maximally 89 metabolites in blood samples from humans, mice and total zebrafish larvae. Not all these metabolites could be detected in each of the species.

MS data analysis

Data was analysed using the software package MetaboAnalyst 4.0 [48]. MetaboAnalyst offers the possibility to provide automated data reports which we used for archiving data sets. In brief, default settings were used with log transformation and auto scaling of the data for normalisation (Fig. 5). PLS-DA was performed with PLS regression using the plsr function provided by R pls package. The classification and cross-validation are performed using the corresponding wrapper function offered by the caret package[49]. Naming of the metabolites is based on reference compounds using standard nomenclature of the human metabolome database (http://www.hmdb.ca/). We have categorized cystine and cysteine as one metabolite.

NMR spectroscopy

For NMR spectroscopy, metabolites from zebrafish larvae were extracted based on an adapted protocol from a previous study [50]. In brief, 120 zebrafish larvae per sample were crashed in the mixture of methanol: water (1:1, v/v). Subsequently, 1ml chloroform was added. The mixture was sonicated for 15 minutes and then centrifuged at 5000rpm for 5 minutes. After centrifugation, two layers were formed: the upper layer is methanol and water. The dried methanol:water layer with metabolites was dissolved in 1ml of 100mM deuterated phosphate buffer (KD_2PO4, PH=7.0) containing 0.02% trimethyl-silylpropanoic acid (TSP) as internal standard and subsequently filtered with Millipore filter (Millex-HV 0.45-lmFilterUnit). Metabolites in zebrafish larvae were measured with a Bruker DMX 600MHz NMR spectrometer at 4°C equipped with a 5mm inverse triple high-resolution probe with an actively shielded gradient coil. The ^{1}H NMR spectra were accumulated with 65,000 data points, a 2-s relaxation delay, a sweep width of 12.4 kHz, and 256 scans which were required to obtain a satisfactory signal-to-noise ratio. Two-dimensional homonuclear ^{1}H-^{1}H experiments were carried out using the chemical shift correlated spectroscopic (COSY) sequence. The parameters used for COSY were 2048 data points collected in the t2 domain over the spectral width of 4k, 512 t1 increments were collected with 16 transients, relaxation delay 2 sec, acquisition time 116 msec, and pre-saturated water resonance during relaxation delay. The resulting data were zero filled with 2048 data points, and were weighted with sine bell window functions in both dimensions prior to Fourier Transformation. The chemical shifts are relative to TSP.

NMR analysis

NMR analysis was performed based on an adjusted version from previous studies [33, 51]. In brief, the one-dimensional ^{1}H NMR spectra obtained from both in control and infection group were corrected for baseline and phase shifts using the MestReNova software version 11.0 (Mestrelab Research S.L., Santiago de Compostela, Spain). The spectra were then subdivided in the range between 0 and 10 ppm into buckets of 0.04 ppm. The region of 4.20-6.00 ppm was excluded from the analysis to remove the water peak. The resulting data matrix was exported into Microsoft office excel (Microsoft Corporation). This was then imported into MetaboAnalyst 4.0 for PLSDA. Correlation coefficients with $p<0.05$ were considered statistically significant. Quantification of metabolites was performed using Chenomx NMR Suite 8.3, which allowed for qualitative and quantitative analysis of an NMR spectrum by fitting spectral signatures from an HMDB database to the spectrum. Metabolite concentrations were subsequently calculated as ratio to tCr. Statistical analysis (t-tests) of the NMR quantification results was performed with GraphPad Prism 8 and *p*-values smaller than 0.05 were considered significant.

Data availability

All data underlying this study are included within the manuscript, supplementary material and supporting information file.

Acknowledgements

We thank Dr. Slavik Koval for assistance with the MetaboAnalyst program.

Ethical licenses and consent of patients for publication

Zebrafish lines were handled in accordance with the local animal welfare regulations and maintained according to standard protocols (https://zfin.org). This local regulation serves as the implementation of Guidelines on the protection of experimental animals by the Council of Europe, Directive 86/609/EEC, which allows zebrafish embryos to be used up to the moment of free-living (5 days after fertilization). Since embryos used in this study were no more than 5 days old, no license is required by Council of Europe (1986), Directive 86/609/EEC or the Leiden University ethics committee. The mice experiments were performed under ethical license number DEC 14080 (10-07-2014) of Leiden University. The study with human patients material was approved by the Ethical Committee of the Faculty of Medicine, Leiden University Medical Center, and written informed consent was voluntarily signed by all patients and control subjects registered under protocol P07.48 (March 17, 2008).

Competing interest statement

The authors declare that there are no competing interests.

Author contributions

R.J.R. and K.E. performed mass spectrometry experiments, Y.D., performed NMR experiments, R.J.R., Y.D., A.A. and H.P.S. bioinformatic analysis, Y.D., W.J.V., M.C.H., S.v.E and R.M.J. performed animal experiments, S.A.J., M.C.H. and W.J.V. obtained samples and ethical permission, A.C.H., T.H., A.A., T.H.M.O. and H.P.S. supervised technical facilities, A.A., S.A.J., M.C.H.,T.H.M.O. and H.P.S. supervised research, Y.D. and H.P.S. wrote first draft of manuscript and made figures and tables, R.M.J., H.P.S., S.A.J., R.J.R., T.H., M.C.H., T.H.M.O. and A.A. conceived the study, H.P.S., R.J.R., Y.D., R.M.J., W.J.V., S.A.J., M.C.H., and A.A. planned experiments and interpreted results, all authors reviewed the manuscript.

References

[1] World Health Organization. Global Tuberculosis Report. 2019.

[2] World Health Organization. Early detection of tuberculosis: an overview of approaches, guidelines and tools[R]. Geneva: World Health Organization, 2011.

[3] Weiner J, 3rd, Parida SK, Maertzdorf J, Black GF, Repsilber D, Telaar A, et al. Biomarkers of inflammation, immunosuppression and stress with active disease are revealed by metabolomic profiling of tuberculosis patients. PLoS One 2012;7(7):e40221.

[4] Zhou A, Ni J, Xu Z, Wang Y, Lu S, Sha W, et al. Application of (1)h NMR spectroscopy-based metabolomics to sera of tuberculosis patients. J Proteome Res 2013;12(10):4642-9.

[5] Che N, Cheng J, Li H, Zhang Z, Zhang X, Ding Z, et al. Decreased serum 5-oxoproline in TB patients is associated with pathological damage of the lung. Clin Chim Acta 2013;423:5-9.

[6] Frediani JK, Jones DP, Tukvadze N, Uppal K, Sanikidze E, Kipiani M, et al. Plasma metabolomics in human pulmonary tuberculosis disease: a pilot study. PLoS One 2014;9(10):e108854.

[7] Tientcheu LD, Maertzdorf J, Weiner J, Adetifa IM, Mollenkopf HJ, Sutherland JS, et al. Differential transcriptomic and metabolic profiles of M. africanum- and M. tuberculosis-infected patients after, but not before, drug treatment. Genes Immun 2015;16(5):347-55.

[8] Feng S, Du YQ, Zhang L, Zhang L, Feng RR, Liu SY. Analysis of serum metabolic profile by ultra-performance liquid chromatography-mass spectrometry for biomarkers discovery: application in a pilot study to discriminate patients with tuberculosis. Chin Med J (Engl) 2015;128(2):159-68.

[9] Lau SK, Lee KC, Curreem SO, Chow WN, To KK, Hung IF, et al. Metabolomic Profiling of Plasma from Patients with Tuberculosis by Use of Untargeted Mass Spectrometry Reveals Novel Biomarkers for Diagnosis. J Clin Microbiol 2015;53(12):3750-9.

[10] Collins JM, Walker DI, Jones DP, Tukvadze N, Liu KH, Tran VT, et al. High-resolution plasma metabolomics analysis to detect Mycobacterium tuberculosis-associated metabolites that distinguish active pulmonary tuberculosis in humans. PLoS One 2018;13(10):e0205398.

[11] Weiner J, 3rd, Maertzdorf J, Sutherland JS, Duffy FJ, Thompson E, Suliman S, et al. Metabolite changes in blood predict the onset of tuberculosis. Nature communications 2018;9(1):5208.

[12] Yi WJ, Han YS, Wei LL, Shi LY, Huang H, Jiang TT, et al. l-Histidine, arachidonic acid, biliverdin, and l-cysteine-glutathione disulfide as potential biomarkers for cured pulmonary tuberculosis. Biomed Pharmacother 2019;116:108980.

[13] Vrieling F, Alisjahbana B, Sahiratmadja E, van Crevel R, Harms AC, Hankemeier T, et al. Plasma metabolomics in tuberculosis patients with and without concurrent type 2 diabetes at diagnosis and during antibiotic treatment. Scientific reports 2019;9(1):18669.

[14] de Falco B, Lanzotti V. NMR spectroscopy and mass spectrometry in metabolomics analysis of Salvia. Phytochemistry Reviews 2018;17(5):951-72.

[15] Bjerrum JT. Metabonomics: analytical techniques and associated chemometrics at a glance. Methods Mol Biol 2015;1277:1-14.

[16] Vrieling, F. *et al.* Dynamic plasma metabolomics in tuberculosis patients with and without concurrent type 2 diabetes at diagnosis and during antibiotic treatment. Manuscript sumbitted for publication (2019). .

[17] Tyagi AK, Chen Y, Wu J, Tu L, Xiong X, Hu X, et al. 1H-NMR Spectroscopy Revealed Mycobacterium tuberculosis Caused Abnormal Serum Metabolic Profile of Cattle. PloS one 2013;8(9).

[18] Somashekar BS, Amin AG, Rithner CD, Troudt J, Basaraba R, Izzo A, et al. Metabolic profiling of lung granuloma in Mycobacterium tuberculosis infected guinea pigs: ex vivo 1H magic angle spinning NMR studies. J Proteome Res 2011;10(9):4186-95.

[19] Somashekar BS, Amin AG, Tripathi P, MacKinnon N, Rithner CD, Shanley CA, et al. Metabolomic signatures in guinea pigs infected with epidemic-associated W-Beijing strains of Mycobacterium tuberculosis. J Proteome Res 2012;11(10):4873-84.

[20] Shin JH, Yang JY, Jeon BY, Yoon YJ, Cho SN, Kang YH, et al. (1)H NMR-based metabolomic profiling in mice infected with Mycobacterium tuberculosis. J Proteome Res 2011;10(5):2238-47.

[21] Berg RD, Ramakrishnan L. Insights into tuberculosis from the zebrafish model. Trends in molecular medicine 2012;18(12):689-90.

[22] Takaki K, Davis JM, Winglee K, Ramakrishnan L. Evaluation of the pathogenesis and treatment of Mycobacterium marinum infection in zebrafish. Nat Protoc 2013;8(6):1114-24.

[23] Berg RD, Levitte S, O'Sullivan MP, O'Leary SM, Cambier CJ, Cameron J, et al. Lysosomal Disorders Drive Susceptibility to Tuberculosis by Compromising Macrophage Migration. Cell 2016;165(1):139-52.

[24] Cambier CJ, O'Leary SM, O'Sullivan MP, Keane J, Ramakrishnan L. Phenolic Glycolipid Facilitates Mycobacterial Escape from Microbicidal Tissue-Resident Macrophages. Immunity 2017;47(3):552-65.e4.

[25] Roca FJ, Whitworth LJ, Redmond S, Jones AA, Ramakrishnan L. TNF Induces Pathogenic Programmed Macrophage Necrosis in Tuberculosis through a Mitochondrial-Lysosomal-Endoplasmic Reticulum Circuit. Cell 2019;178(6):1344-61.e11.

[26] Veneman WJ, Marin-Juez R, de Sonneville J, Ordas A, Jong-Raadsen S, Meijer AH, et al. Establishment and optimization of a high throughput setup to study Staphylococcus epidermidis and Mycobacterium marinum infection as a model for drug discovery. J Vis Exp 2014(88):e51649.

[27] Tobin DM, May RC, Wheeler RT. Zebrafish: a see-through host and a fluorescent toolbox to probe host-pathogen interaction. PLoS Pathog 2012;8(1):e1002349.

[28] Tobin DM, Ramakrishnan L. Comparative pathogenesis of Mycobacterium marinum and Mycobacterium tuberculosis. Cell Microbiol 2008;10(5):1027-39.

[29] Raterink R-J, van der Kloet FM, Li J, Wattel NA, Schaaf MJM, Spaink HP, et al. Rapid metabolic screening of early zebrafish embryogenesis based on direct infusion-nanoESI-FTMS. Metabolomics : Official journal of the Metabolomic Society 2013;9(4):864-73.

[30] Vrieling F, Ronacher K, Kleynhans L, van den Akker E, Walzl G, Ottenhoff THM, et al. Patients with Concurrent Tuberculosis and Diabetes Have a Pro-Atherogenic Plasma Lipid Profile. EBioMedicine 2018;32:192-200.

[31] Guo Y, Veneman WJ, Spaink HP, Verbeek FJ. Three-dimensional reconstruction and measurements of zebrafish larvae from high-throughput axial-view in vivo imaging. Biomed Opt Express 2017;8(5):2611-34.

[32] He M, Harms AC, van Wijk E, Wang M, Berger R, Koval S, et al. Role of amino acids in rheumatoid arthritis studied by metabolomics. Int J Rheum Dis 2019;22(1):38-46.

[33] Roy U, Conklin L, Schiller J, Matysik J, Berry JP, Alia A. Metabolic profiling of zebrafish (Danio rerio) embryos by NMR spectroscopy reveals multifaceted toxicity of beta-methylamino-L-alanine (BMAA). Scientific reports 2017;7(1):17305.

[34] Reeds PJ. Dispensable and indispensable amino acids for humans. J Nutr 2000;130(7):1835s-40s.

[35] Wipperman MF, Fitzgerald DW, Juste MAJ, Taur Y, Namasivayam S, Sher A, et al. Antibiotic treatment for Tuberculosis induces a profound dysbiosis of the microbiome that persists long after therapy is completed. Scientific reports 2017;7(1):10767.

[36] Adu-Gyamfi CG, Snyman T, Hoffmann CJ, Martinson NA, Chaisson RE, George JA, et al. Plasma Indoleamine 2, 3-Dioxygenase, a Biomarker for Tuberculosis in Human Immunodeficiency Virus-Infected Patients. Clin Infect Dis 2017;65(8):1356-8.

[37] Lange SM, McKell MC, Schmidt SM, Hossfeld AP, Chaturvedi V, Kinder JM, et al. l-Citrulline Metabolism in Mice Augments CD4(+) T Cell Proliferation and Cytokine Production In Vitro, and Accumulation in the Mycobacteria-Infected Lung. Front Immunol 2017;8:1561.

[38] Lange SM, McKell MC, Schmidt SM, Zhao J, Crowther RR, Green LC, et al. l-Arginine Synthesis from l-Citrulline in Myeloid Cells Drives Host Defense against Mycobacteria In Vivo. J Immunol 2019;202(6):1747-54.

[39] Traver D, Herbomel P, Patton EE, Murphey RD, Yoder JA, Litman GW, et al. The zebrafish as a model organism to study development of the immune system. Advances in immunology 2003;81:253-330.

[40] Wiegertjes GF, Wentzel AS, Spaink HP, Elks PM, Fink IR. Polarization of immune responses in fish: The 'macrophages first' point of view. Mol Immunol 2016;69:146-56.

[41] van Steijn L, Verbeek FJ, Spaink HP, Merks RMH. Predicting Metabolism from Gene Expression in an Improved Whole-Genome Metabolic Network Model of Danio rerio. Zebrafish 2019;16(4):348-62.

[42] Kaufmann SH, Fortune S, Pepponi I, Ruhwald M, Schrager LK, Ottenhoff TH. TB biomarkers, TB correlates and human challenge models: New tools for improving assessment of new TB vaccines. Tuberculosis (Edinburgh, Scotland) 2016;99 Suppl 1:S8-s11.

[43] Zabeau L, Jensen CJ, Seeuws S, Venken K, Verhee A, Catteeuw D, et al. Leptin's metabolic and immune functions can be uncoupled at the ligand/receptor interaction level. Cell Mol Life Sci 2015;72(3):629-44.

[44] Facchinello N, Skobo T, Meneghetti G, Colletti E, Dinarello A, Tiso N, et al. nr3c1 null mutant zebrafish are viable and reveal DNA-binding-independent activities of the glucocorticoid receptor. Scientific reports 2017;7(1):4371.

[45] Korbee CJ, Heemskerk MT, Kocev D, van Strijen E, Rabiee O, Franken K, et al. Combined chemical genetics and data-driven bioinformatics approach identifies receptor tyrosine kinase inhibitors as host-directed antimicrobials. Nature communications 2018;9(1):358.

[46] Benard EL, van der Sar AM, Ellett F, Lieschke GJ, Spaink HP, Meijer AH. Infection of zebrafish embryos with intracellular bacterial pathogens. J Vis Exp 2012(61).

[47] Noga MJ, Dane A, Shi S, Attali A, van Aken H, Suidgeest E, et al. Metabolomics of cerebrospinal fluid reveals changes in the central nervous system metabolism in a rat model of multiple sclerosis. Metabolomics : Official journal of the Metabolomic Society 2012;8(2):253-63.

[48] Xia J, Wishart DS. Using MetaboAnalyst 3.0 for Comprehensive Metabolomics Data Analysis. Current protocols in bioinformatics 2016;55:14.0.1-.0.91.

[49] Wehrens R, Mevik B-H. The pls package: principal component and partial least squares regression in R. 2007.

[50] Kabli S, Spaink HP, De Groot HJ, Alia A. In vivo metabolite profile of adult zebrafish brain obtained by high-resolution localized magnetic resonance spectroscopy. J Magn Reson Imaging 2009;29(2):275-81.

[51] Berry JP, Roy U, Jaja-Chimedza A, Sanchez K, Matysik J, Alia A. High-Resolution Magic Angle Spinning Nuclear Magnetic Resonance of Intact Zebrafish Embryos Detects Metabolic Changes Following Exposure to Teratogenic Polymethoxyalkenes from Algae. Zebrafish 2016;13(5):456-65.

Supplementary materials

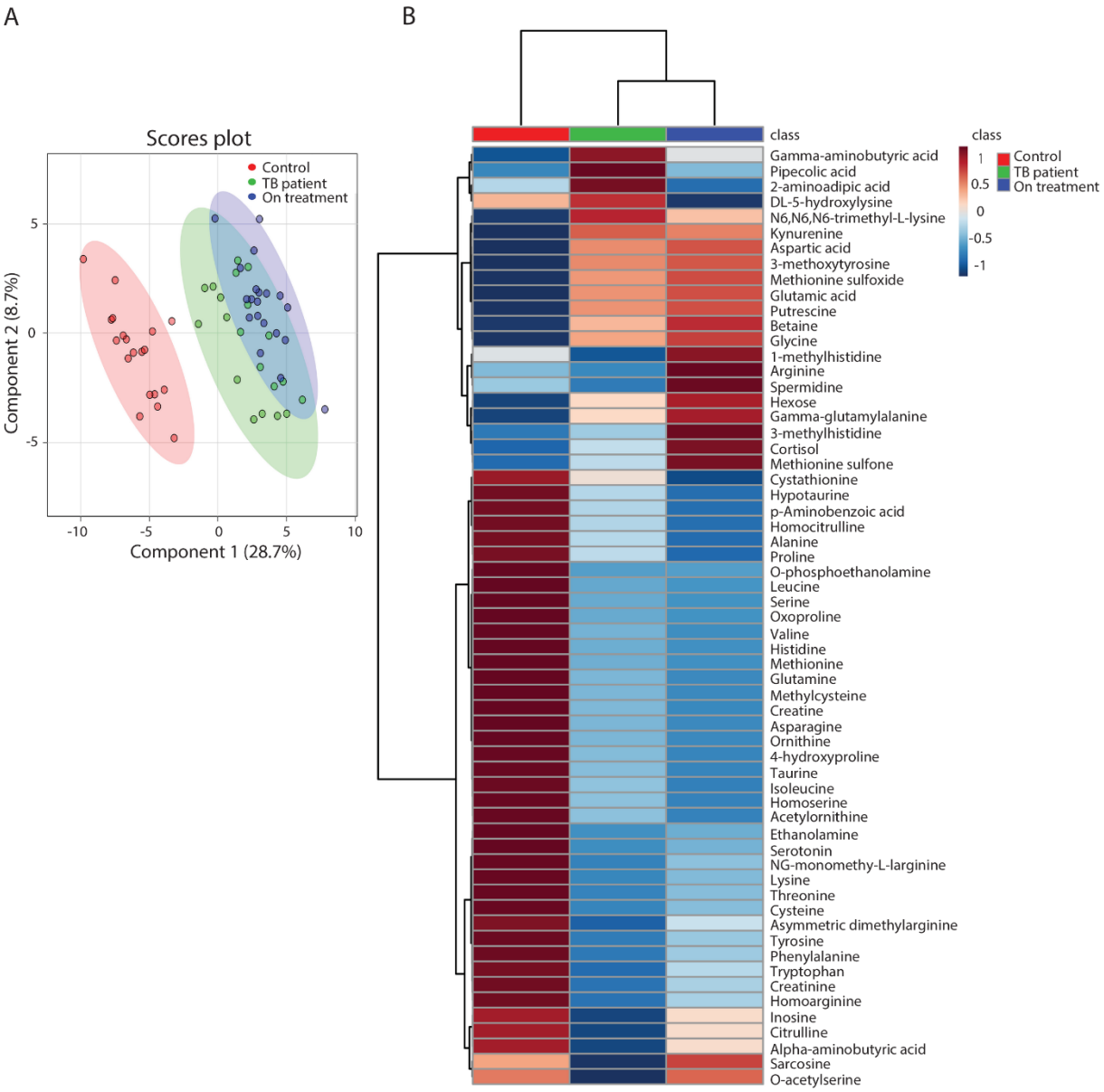

Supplementary Figure S1. Partial least squares discriminant analysis and heat map of metabolomic profiles from healthy control, TB patient, and on treatment groups. A. Analysis of blood of the healthy control group (Control), patients with active TB disease (TB patients), and the same patients treated for 6 weeks with antibiotics (On treatment), n=20. **B**. Heat map of all metabolites of blood of the healthy control group (Control), TB infected patients (TB patient) and the same patients treated for 6 weeks with antibiotics (On treatment).

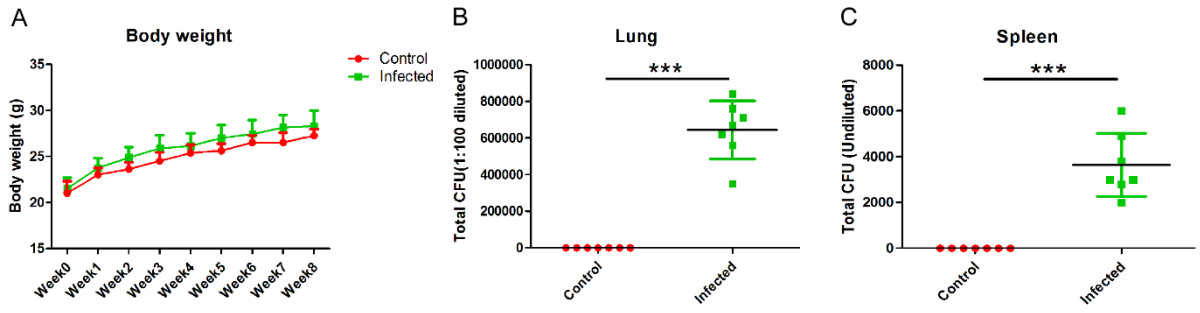

Supplementary Figure S2. Body weight and total colony forming unit of isolated organs in mice. A. Body weight of control and infected mice from week 0 to week 8. **B.** Total colony forming unit (cfu) (1:100 diluted) of isolated lung from control and infected mice after 8 weeks of systemically infection with *Mtb*. **C.** Total cfu (Undiluted) of isolated spleen from control and infected mice after 8 weeks of systemically infection with *M.tb*. ***p<0.001. Abbreviation: cfu, colony forming unit.

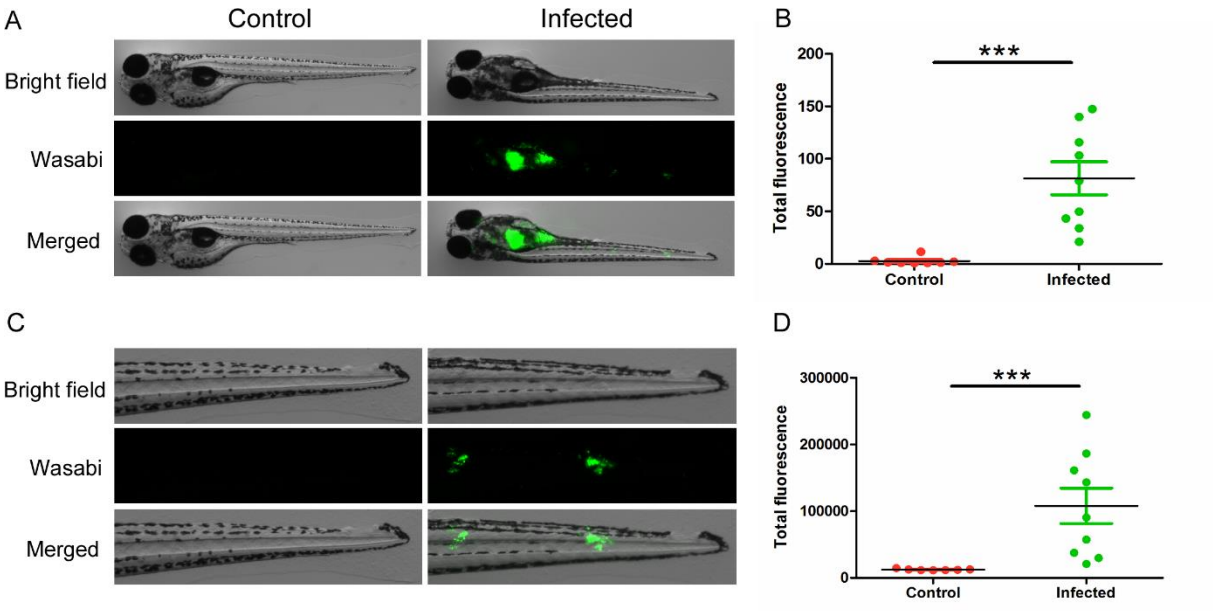

Supplementary Figure S3. Representative images and quantification of *M.m* infection in zebrafish larvae. A. The representative images of whole larva from control and infected group. **B.** Quantification of total fluorescence of wasabi from whole larva in two groups. **C.** The representative images of tail part from control and infected group. **D.** Quantification of total fluorescence of wasabi from tail part in two groups.

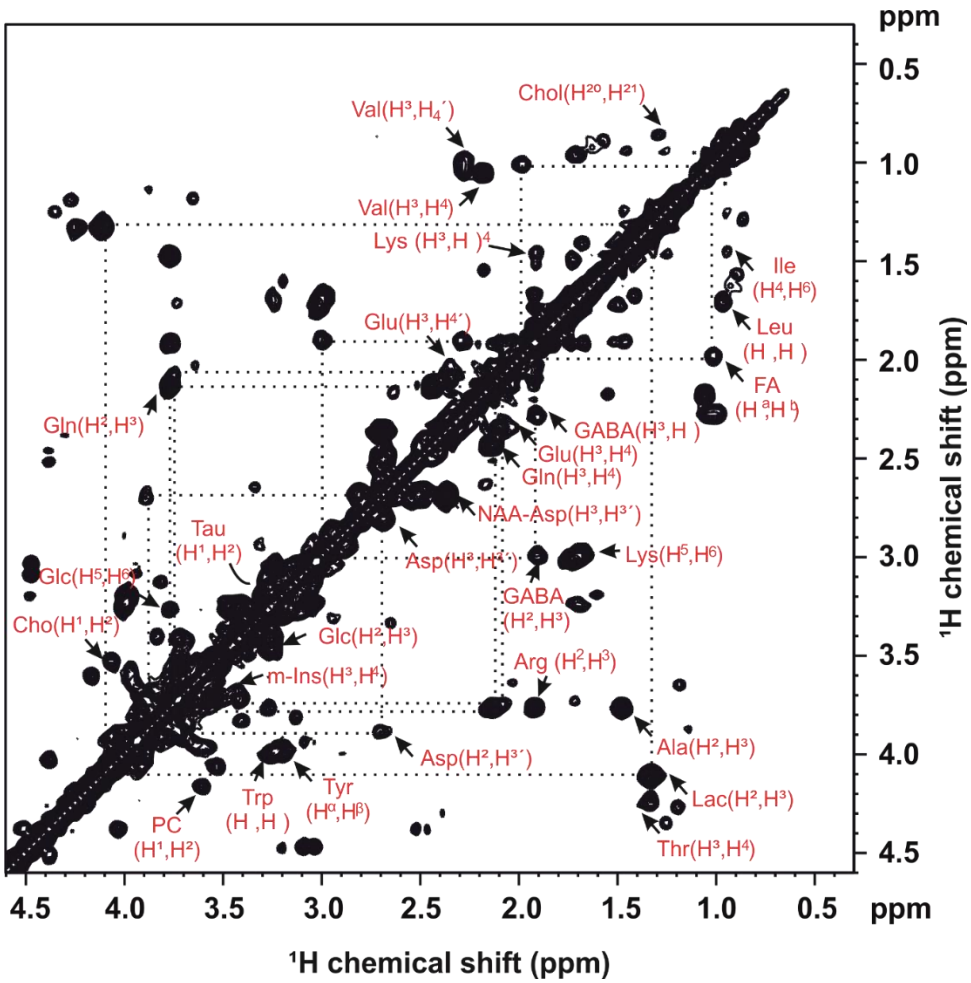

Supplementary Figure S4. Representative high resolution 2D ^{1}H-^{1}H homonuclear correlation spectrum in control zebrafish larvae. The extracted metabolites of zebrafish larvae obtained using the chemical shift correlated spectroscopic (COSY) sequence.

Supplementary Table S1.A

Gender and Age	Control n=20	TB patient n=20
Gender(male/female)	7/13	18/2
Age (years)	34.5+12.4	32.9+14.8

Supplementary Table S1.B

Sample	Label	Gender	Age
C5_1	Control	female	33
C5_3	Control	female	33
C5_7	Control	male	25
C5_10	Control	female	41
C5_13	Control	female	42
C5_14	Control	female	26
C5_15	Control	female	31
C5_18	Control	female	44
C5_20	Control	male	18
C5_21	Control	female	54
C5_24	Control	female	22
C5_25	Control	female	22
C5_27	Control	male	69
C5_28	Control	female	23
C5_29	Control	male	36
C5_30	Control	male	32
C5_32	Control	female	43
C5_33	Control	male	33
C5_34	Control	male	41
C5_38	Control	female	22
TR001	TB patient	male	22
TR002	TB patient	male	31
TR003	TB patient	male	27
TR004	TB patient	male	24

TR005	TB patient	male	44
TR006	TB patient	male	31
TR007	TB patient	male	34
TR008	TB patient	male	48
TR009	TB patient	male	41
TR010	TB patient	male	26
TR011	TB patient	male	29
TR012	TB patient	male	23
TR013	TB patient	male	21
TR014	TB patient	male	29
TR016	TB patient	female	85
TR017	TB patient	male	43
TR018	TB patient	female	32
TR019	TB patient	male	24
TR020	TB patient	male	17
TR021	TB patient	male	26

Supplementary Table S1. Gender and age information in healthy people and TB patients. A. Summarized gender and age information from two groups. **B.** Individual gender and age information from two groups.

Supplementary Table S2

Metabolites	HMDB identifier	Human FDR	Human Ratio
Methionine	HMDB00696	1,01E-11	0.22
Methionine sulfoxide	HMDB02005	1,47E-11	5.78
Serotonin	HMDB00259	5,35E-11	0.003
Asparagine	HMDB00168	5,35E-11	0.42
Cysteine	HMDB00574	2,47E-09	0.40
Methylcysteine	HMDB02108	4,05E-08	0.48
Hypotaurine	HMDB00965	9,09E-08	0.23
Aspartic acid	HMDB00191	4,04E-07	1.93

Glutamic acid	HMDB00148	1,04E-06	1.97
Glutamine	HMDB00641	1,21E-06	0.33
Lysine	HMDB00182	1,90E-06	0.73
O-phosphoethanolamine	HMDB00224	1,59E-05	0.0003
Threonine	HMDB00167	2,94E-05	0.66
Taurine	HMDB00251	5,84E-05	0.60
NG-Monomethy-L-arginine	HMDB29416	1,72E-04	0.57
Ethanolamine	HMDB00149	2,50E-04	0.75
Tryptophan	HMDB00929	2,55E-04	0.72
Histidine	HMDB00177	3,72E-04	0.46
Phenylalanine	HMDB00159	4,16E-04	0.79
Homoarginine	HMDB00670	7,77E-04	0.62
Alpha-aminobutyric acid	HMDB00452	9,00E-04	0.75
Putrescine	HMDB01414	1,51E-03	3.18
Citrulline	HMDB00904	2,00E-03	0.67
Homoserine	HMDB00719	2,46E-03	0.75
Serine	HMDB00187	8,84E-03	0.80
Asymmetric dimethylarginine	HMDB01539	1,16E-02	0.79
Inosine	HMDB00195	1,46E-02	0.16
Gamma-aminobutyric acid	HMDB00112	1,85E-02	1.47
p-Aminobenzoic acid	HMDB01392	2,30E-02	0.79
Creatine	HMDB00064	3,35E-02	0.67
Leucine	HMDB00687	3,50E-02	0.84

Supplementary Table S2. Ratio of metabolite quantities in blood of TB patients compared to the control group. Ratios of metabolite quantities in human blood samples. The levels of 31 metabolites are significantly altered in TB disease compared to healthy people.

Supplementary Table S3

Metabolites	HMDB identifier	Mice FDR	Mice ratio
Sarcosine	HMDB00271	4,63E-05	0.36
Ornithine	HMDB00214	1,38E-04	0.52
Proline	HMDB00162	1,92E-04	0.53
Serine	HMDB00187	3,07E-04	0.63
2-aminoadipic acid	HMDB00510	5,80E-04	0.40
Glycine	HMDB00123	5,90E-04	0.63
Gamma-glutamylalanine	HMDB06248	8,43E-04	0.47
Histidine	HMDB00177	9,87E-04	0.66
Homoserine	HMDB00719	1,21E-03	0.59

Tryptophan	HMDB00929	1,23E-03	0.48
Methionine sulfoxide	HMDB02005	1,28E-03	0.51
Ethanolamine	HMDB00149	1,31E-03	0.67
Leucine	HMDB00687	1,58E-03	0.55
Alanine	HMDB00161	1,69E-03	0.61
Citrulline	HMDB00904	2,11E-03	0.57
Phenylalanine	HMDB00159	2,62E-03	0.56
Threonine	HMDB00167	2,78E-03	0.54
Isoleucine	HMDB00172	2,94E-03	0.57
Arginine	HMDB00517	3,15E-03	0.61
Kynurenine	HMDB00183	3,47E-03	0.55
Tyrosine	HMDB00158	3,89E-03	0.52
Alpha-aminobutyric acid	HMDB00452	4,11E-03	0.65
Methyldopa	HMDB11754	4,30E-03	0.52
Gamma-aminobutyric acid	HMDB00112	4,38E-03	0.57
Valine	HMDB00883	5,51E-03	0.54
Lysine	HMDB00182	5,77E-03	0.59
Asparagine	HMDB00168	9,04E-03	0.69
Glutamic acid	HMDB00148	9,68E-03	0.64
Methionine	HMDB00696	1,79E-02	0.63
Cysteine	HMDB00192	2,36E-02	0.97
Spermidine	HMDB01257	2,63E-02	0.49

Supplementary Table S3. Ratio of metabolite quantities in blood of *Mtb*-infected mice compared to the control group. Ratios of metabolite quantities in mice blood samples. The levels of 31 metabolites are significantly altered in the infected compared to the control group.

Supplementary Table S4

Metabolites	HMDB identifier	ZF FDR	ZF ratio
Ethanolamine	HMDB00149	9,70E-07	0.41
Valine	HMDB00883	1,16E-06	0.48
Tryptophan	HMDB00929	1,38E-06	0.45
Isoleucine	HMDB00172	1,79E-06	0.42
Ornithine	HMDB00214	2,01E-06	0.58
Leucine	HMDB00687	4,97E-06	0.46
Glutamine	HMDB00641	1,10E-05	0.58
Methionine	HMDB00696	1,15E-05	0.63
Hydroxyproline	HMDB06055	2,05E-05	0.46
Phenylalanine	HMDB00159	2,16E-05	0.55

Threonine	HMDB00167	2,71E-05	0.62
Proline	HMDB00162	6,02E-05	0.67
Serine	HMDB00187	7,26E-05	0.54
Tyrosine	HMDB00158	8,11E-05	0.45
Asparagine	HMDB00168	8,31E-05	0.58
Putrescine	HMDB01414	1,08E-04	1.52
Gamma-glutamylalanine	HMDB06248	2,60E-04	0.41
Glycine	HMDB00123	3,43E-04	0.63
Arginine	HMDB00517	5,34E-04	0.65
Asymmetric dimethylarginine	HMDB01539	7,94E-04	0.54
Aspartic acid	HMDB00191	3,01E-03	0.72
Citrulline	HMDB00904	3,68E-03	0.67
Methylcysteine	HMDB02108	4,04E-03	0.48
Alanine	HMDB00161	4,35E-03	0.77
Symmetric dimethylarginine	HMDB03334	6,04E-03	0.46
Glutathione	HMDB00125	6,18E-03	1.46
3-methoxytyrosine	HMDB01434	7,16E-03	0.71
5-hydroxytryptophan	HMDB00472	8,78E-03	0.28
Beta-alanine	HMDB00056	9,06E-03	1.23
Glutathione disulfide	HMDB03337	1,22E-02	0.78
Aminoadipic acid	HMDB00510	1,37E-02	0.78
Cysteine	HMDB00192	2,25E-02	0.25
O-phosphoethanolamine	HMDB00224	2,32E-02	1.17
5-hydroxylysine	HMDB00450	3,52E-02	1.49
N6,N6,N6-trimethyl-L-lysine	HMDB01325	3,59E-02	0.62

Supplementary Table S4. Ratio of metabolite quantities in *M.marinum*-infected zebrafish larvae versus control group obtained by MS. The concentration of 35 metabolites that are significantly changed in the mycobacterial infected group compared to the control group. ZF ratio: zebrafish larvae with *M.marinum* strain E11 infection compared with control.

Chapter 3

Leptin deficiency affects glucose homeostasis and results in adiposity in zebrafish

Junling He[1,2,*], Yi Ding[2,*], Natalia Nowik[2,3], Charel Jager[1], Muhamed N H Eeza[4], A Alia [4,5], Hans J Baelde[1] and Herman P Spaink[2]

[1] Department of Pathology, Leiden University Medical Center, Leiden, The Netherlands
[2] Department of Animal Sciences and Health, Institute of Biology, Leiden University, Leiden, The Netherlands
[3] Department of Animal Anatomy, Faculty of Veterinary Medicine, University of Warmia and Mazury in Olsztyn, Olsztyn, Poland
[4] Institute of Medical Physics and Biophysics, University of Leipzig, Leipzig, Germany
[5] Leiden Institute of Chemistry, Leiden University, Leiden, The Netherlands
Correspondence should be addressed to H P Spaink: h.p.spaink@biology.leidenuniv.nl
*(J He and Y Ding contributed equally to this work)

Journal of Endocrinology 249(2): 125-134.

ABSTRACT

Leptin is a hormone which functions in the regulation of energy homeostasis via suppression of appetite. In zebrafish, there are two paralogous genes encoding leptin, called *lepa* and *lepb*. In a gene expression study, we found that the *lepb* gene, not the *lepa* gene, was significantly downregulated under the state of insulin-resistance in zebrafish larvae, suggesting that the *lepb* plays a role in glucose homeostasis. In the current study, we characterized *lepb*-deficient ($lepb^{-/-}$) adult zebrafish generated via a CRISPR-CAS9 gene editing approach by investigating whether the disruption of the *lepb* gene would result in the development of type 2 diabetes mellitus (T2DM) and diabetic complications. We observed that $lepb^{-/-}$ adult zebrafish had an increase in body weight, length and visceral fat accumulation, compared to age-matched control zebrafish. In addition, $lepb^{-/-}$ zebrafish had significantly higher blood glucose levels compared to control zebrafish. These data collectively indicate that $lepb^{-/-}$ adult zebrafish display the features of T2DM. Furthermore, we showed that $lepb^{-/-}$ adult zebrafish had glomerular hypertrophy and thickening of the glomerular basement membrane, compared to control zebrafish, suggesting that $lepb^{-/-}$ adult zebrafish develop early signs of diabetic nephropathy. In conclusion, our results demonstrate that *lepb* regulates glucose homeostasis and adiposity in zebrafish, and suggest that $lepb^{-/-}$ mutant zebrafish are a promising model to investigate the role of leptin in the development of T2DM and are an attractive model to perform mechanistic and therapeutic research in T2DM and its complications.

Key Words leptin, glucose homeostasis, adiposity, diabetic nephropathy, adult zebrafish

Introduction

Human leptin is a 16-kDa protein hormone which is predominantly secreted by adipocytes (Zhang *et al.* 1994). Leptin plays a role in diverse physiological processes including energy homeostasis (Ahima *et al.* 1998), immune regulation (Lord *et al.* 1998, Matarese *et al.* 2005), endocrine regulation (Meier & Gressner 2004), and reproduction (Caprio *et al.* 2001, Licinio *et al.* 2004). Congenital leptin deficiency causes extreme obesity in children (Farooqi *et al.* 1999, Funcke *et al.* 2014). Rodents lacking the gene encoding leptin are commonly characterized by hyperphagia, obesity, insulin resistance and impaired glucose tolerance. For instance, leptin-deficient mice (*ob/ob* mice) exhibit the features of obesity and type 2 diabetic mellitus (T2DM) (Drel *et al.* 2006). Growing evidence suggests that leptin treatment has a beneficial effect on glucose metabolism (Yu *et al.* 2008, Fujikawa *et al.* 2010, Hedbacker *et al.* 2010, German *et al.* 2011) and insulin resistance (Muzzin *et al.* 1996, Pocai *et al.* 2005, Park *et al.* 2008, German *et al.* 2009), indicating that leptin might be a crucial factor in the development of T2DM. However, the function of leptin in the pathogenesis of T2DM is still obscure.

Leptin and leptin receptor are highly conserved across mammalian species. The most widely used animal models in T2DM research are the congenial leptin- or leptin receptor-deficient rodent models, such as *ob/ob* and *db/db* mice. Besides, the basic structural features and intracellular signaling mechanisms of leptin and its receptor appear to be conserved throughout vertebrates (Denver *et al.* 2011). Several studies have reported that administration of exogenous leptin in fish reduces food intake, indicating the conservation of the function of the leptin signaling system throughout vertebrates (Volkoff *et al.* 2003, Murashita *et al.* 2008, Aguilar *et al.* 2011). In recent decades, zebrafish have become a promising animal model with numerous advantages, including fast development and generation time, small size, easily accessible larvae, and cost-effective breeding. In zebrafish, there are two divergent leptin paralogous: *lepa* and *lepb*, and one leptin receptor gene (*lepr*) (Gorissen *et al.* 2009). Michel *et al.* (2016) demonstrated that *lepr*-deficient zebrafish larvae have increased numbers of β-cells and increased insulin mRNA expression, compared to control zebrafish larvae. They also found that the leptin receptor deficiency contributes to higher blood glucose levels in adult zebrafish. Their findings indicated that the regulation of glucose homeostasis by the leptin receptor is conserved across vertebrates. However, they observed no significant difference in the whole body adiposity phenotype between *lepr*-deficient zebrafish and control zebrafish at the adult stage. On the other hand, Chisada *et al.* (2014) showed that the deletion of leptin receptor in medaka results in a modest increase in visceral fat accumulation compared to the WT medaka fish. More recently, Audira *et al.* (2018) found that *lepa*-deficient adult zebrafish display an obesity phenotype. Thus, there are some conflicting results in the literature regarding the relationship between disruption of leptin signaling and adiposity in zebrafish. In a previous study, our group found that the *lepb* gene, not the *lepa* gene, was significantly downregulated in zebrafish larvae under an insulin-resistance state, resulting from acute hyperinsulinemia, which suggests that *lepb* plays a role in insulin homeostasis in zebrafish

(Marin-Juez *et al.* 2014). Since the roles of *lepa* and *lepr* in zebrafish have already been investigated by other groups, therefore, the focus in the current work is to study the function of the *lepb* gene in zebrafish at an adult stage to obtain more insights into the relationship between the leptin signaling pathway and T2DM.

This study aims to investigate whether *lepb* deficiency contributes to the development of T2DM in adult zebrafish. To address this question, we examined the body weight and length, blood glucose levels, and the body fat distribution in 1.5 years old $lepb^{-/-}$ adult zebrafish and compared them to age-matched WT controls. Furthermore, we examined the renal histopathologic changes of these zebrafish by performing hematoxylin and eosin (HE) or periodic-acid schiff (PAS) staining, and transmission electron microscopy (TEM) methods.

Methods and materials

Animals

Zebrafish strains were handled in compliance with the local animal welfare regulations and maintained according to standard protocols (zfin.org). The use of adult zebrafish was approved by the local animal welfare committee (DEC) of the University of Leiden (license number: AVD1060020171767) and adhered to the international guidelines specified by the EU Animal Protection Directive 2010/63/EU.

The CRISPR-CAS9 gene editing approach was used to knock out the *lepb* in the ABTL zebrafish to generate the *lepb*-deficient zebrafish. The sgRNA CTACCCAATCCCGAGACCCC targeted the exon 2 in *lepb*. The *lepb* primer (for: 5′-*AGGAACTGGCCGTCTCACAG*-3′; rev: *5′-CGGGGAAGGCTGTTTCTTCTT-3′*) was used for *lepb*-deficient zebrafish genotyping. Sanger sequencing showed that a 7bp ($lepb^{7-/7-}$) or 8bp ($lepb^{8-/8-}$) stretch of nucleotides was missing in the *lepb* gene in two different mutant lines (**Supplementary Fig. 1A**, see section on supplementary materials given at the end of this article). Both deletions resulted in a frameshift mutation of *lepb* (**Supplementary Fig. 1B**). The deletion of the *lepb* gene was in codon 110 in zebrafish, which is close to the non-sense mutation in codon 105 of the leptin gene of C57BL/6J *ob/ob* mice. In the C57BL/6J *ob/ob* mice, this mutation in the leptin gene leads to a truncated protein that cannot bind to the leptin receptor anymore (Zhang *et al.* 1994). Therefore, although we cannot be sure that our mutant has a complete null phenotype, it is very likely that our truncation in the *lepb* gene leads to a leptin b protein which cannot bind to the leptin receptor in the zebrafish.

The $lepb^{+/+}$ and $lepb^{-/-}$ zebrafish were obtained from an incross of *lepb* heterozygous fish ($lep^{+/-}$); (**Supplementary Fig. 1C**). $Lepb^{+/+}$, $lepb^{+/-}$ and $lepb^{-/-}$ zebrafish were mixed and raised in the same tank before genotyping. After genotyping, $lepb^{+/+}$, $lepb^{+/-}$ and $lepb^{-/-}$ fish were separated and raised in different sizes of tanks depending on the number of fish per volume of water. The ABTL (control)

fish of 1.5 years old were kept in the big-sized-tanks. We raised all zebrafish in the same circulating water system and maintained the normal mixed-sex environment. Adult zebrafish were fed twice per day. One meal is a mixture of GEMMA Micro 300 and GEMMA Diamond (Skretting; Nutreco company) whose amount is based on 5% of zebrafish body weight. Another is the life Artemia (ZebCare). Both amounts are positively proportional to the number of fish per tank and given by highly skilled caretakers.

We included both *lepb*$^{7-/7-}$ and *lepb*$^{8-/8-}$ mutants in the current study since two independent mutants have more certainty to rule out off-target effects of CRISPR-CAS9 approach. The age-matched ABTL adult zebrafish of the same lineage as used for the CRISPR-CAS9 procedure were used as the controls. In an independent study, a WT (*lepb*$^{+/+}$) zebrafish line, resulting from an incross of heterozygotes *lepb*$^{7+/-}$ was compared with the ABTL control, showing no significant difference in blood glucose levels (**Supplementary Fig. 2**; female: $t(3)= -0.149$, $P = 0.891$; male: $t(3)= -2.820$, $P = 0.067$), further excluding off-target effects of the CRISPR-CAS9 procedure. For the current study, adult zebrafish (ABTL female fish, $n = 9$; *lepb*$^{-/-}$ female fish, $n = 11$; ABTL male fish, $n = 9$; *lepb*$^{-/-}$ male fish, $n = 15$) were sacrificed at the age of 1.5 years, since we observed that all *lepb*$^{-/-}$ mutants displayed an obese phenotype, compared to control zebrafish. Because there was no difference in body weight, body length, body mass index (BMI), and 2 h postprandial blood glucose levels between *lepb*$^{7-/7-}$, *lepb*$^{8-/8-}$ and *lepb*$^{7-/8-}$ mutants (**Supplementary Fig. 3**), we pooled *lepb*$^{7-/7-}$, *lepb*$^{8-/8-}$ and *lepb*$^{7-/8-}$ mutants into one group which is named as *lepb*$^{-/-}$ for the subsequent analysis.

Body weight and body length measurement

Two hours after feeding, fish were sacrificed by putting them into ice-cold aquarium water which was filled with ice chips to maintain the temperature near 0°C for 3–6 s. After there was no response of the fish to external stimuli, the euthanized fish was placed on a paper tissue, drying the body as much as possible. Then, the fish size (from the tip of the mouth to the caudal peduncle) was measured with a calliper, and the fish were weighed with a precision analytical scale.

Blood collection

A steel blade was used to cut the fish between anal fin and caudal fin just after euthanasia to collect zebrafish blood. The blood was collected into a 500 µL Eppendorf tube with a 20 µL micro-pipet. Following the blood collection, the remaining body of the zebrafish was fixed in 4% paraformaldehyde (PFA). After 2 h of coagulation at room temperature, the blood was spun down in a centrifuge at 13000 ***g*** for 10 min. Subsequently, the blood serum and the blood cells were separated into different Eppendorf tubes and kept at −80°C for the further analysis.

Blood glucose level measurement

A PicoProbeTM Glucose Fluorometric Assay kit (Biovision, Milpitas, CA) was used to measure the glucose levels in the serum of zebrafish. The serum samples were diluted 50× with milli-Q water. Nine microliters of the diluted serum was added into a 96-well white plate, and then the total volume was adjusted to 50 μL with 36 μL glucose assay buffer and 5 μL reaction mix which was composed of 0.5 μL PicoProbeTM, 1 μL glucose substrate mix, 1 μL glucose enzyme mix and 2.5 μL glucose assay buffer. The 100 mM glucose standard was diluted into a series of wells in 96-well plates to generate 0, 1.5, 3, 6, 9, 12, 15 μM/well for making the glucose standard curve. The volumes of different concentrations of glucose standards were also adjusted to 50 μL with glucose assay buffer and reaction mix. The samples were incubated for 30 min at 37°C, protected from light. Fluorescence was measured at excitation/emission = 535/587 nm in a microtiter plate reader. The concentrations of glucose in the serum of zebrafish were calculated according to the glucose standard curve.

MRI measurement

After one week fixation in 4% PFA at 4°C, the whole adult fish were washed twice with PBS and then transferred to MR silent liquid (Fomblin, perfluoropolyether) for MRI measurement. All MRI scans were performed at 300 MHz Bruker vertical wide-bore system, using a birdcage radiofrequency coil with an inner diameter of 10 mm. Data acquisition and processing were performed with Para Vision 5.1 (Bruker Biospin, Germany). Before each measurement, the magnetic field homogeneity was optimized by shimming. Each session of measurements began with a multi-slice orthogonal gradient-echo sequence for position determination and selection of the desired region for subsequent experiments.

For anatomical images, a rapid acquisition with relaxation enhancement (RARE) sequences was used. Basic measurement parameters used for the RARE sequence were: echo time (TE) = 8.5 ms with an effective echo time of 18.1 ms; repetition time (TR) = 3000 ms; number of scans (ns) = 12; total scan time = 17 min; RARE factor = 4. The field of view (FOV) was 1.2 cm with a matrix size of 256 × 256, the slice thickness was 0.2 mm, and the interslice distance was also 0.2 mm.

For selective fat imaging, a Chemical Shift Selective (CHESS) sequence was used. The CHESS consists of a single frequency-selective excitation pulse with a flip angle of $\pi/2$ followed by a dephasing gradient (homogeneity spoiling gradient). The procedure leaves the spin system in a state where no net magnetization of the unwanted component is retained while the wanted component remains entirely unaffected in the form of z-magnetization. A narrow bandwidth of 90° Gaussian pulse was used for on resonance frequency selective excitation. Further basic parameters used are as follows: TE = 13.3 ms; TR = 800 ms; ns = 16; Scan time 27 min.

For quantitative analysis of fat in CHESS images, the image slices were exported and analyzed in ImageJ software (https://imagej.nih.gov/ij/). By using a plugin, the area of the fish was defined, and a certain threshold was adjusted to eliminate any contribution of noise. Subsequently, the hyperintense signal of fat was calculated. The data were exported to Origin Pro v. 8 software for further analysis.

Renal histopathology

After 1 week fixation in 4% PFA at 4°C, the whole adult zebrafish were washed twice with PBS and then transferred to EDTA (100 mM, pH 8) for the decalcification at room temperature for another 1 week, followed by embedding in paraffin. The zebrafish tissue was cut (4-μm thickness) on a Leica microtome (Wetzlar) and then stained with HE or PAS using standard protocols.

Stained slides were digitalized using a Philips Ultra- Fast Scanner 1.6 RA (Philips Electronics, Amsterdam, the Netherlands). The surface areas (μm^2) of Bowman's capsule, space, and glomerular tuft were measured in the digitalized PAS-stained slides using ImageJ software. All available glomeruli (5–11 glomeruli per slide) in each zebrafish were included in the measurements.

Transmission electron microscopy (TEM)

Zebrafish kidneys were harvested and fixed in EM fixation buffer (1.5% GA/1% PF) for 24 h. Subsequently, the renal tissue was fixed with 2.5% glutaraldehyde/1.2% acrolein in fixation buffer (0.1 mol/L cacodylate, 0.1 mol/L sucrose, pH 7.4) and 1% osmium tetroxide, and embedded in epon resin. Ultrathin sections were stained with uranyl acetate. The images were collected using a JEM-1200 EX transmission electron microscope (JEOL, Tokyo, Japan).

The thickness of the glomerular basement membrane (GBM) of zebrafish was analyzed with ImageJ software. One glomerulus per fish was analyzed. Photos of eight distinct areas (25,000×) of the glomerular capillaries from each glomerulus at randomly selected places were taken. The mean thickness of the GBM in each photograph was determined by measuring the thickness of 15 nonoverlapping places of the GBM area. The mean of these 8 distinct areas was taken as the thickness for each glomerulus.

Statistical analyses

Statistical analysis was performed using SPSS Statistics 25 (IBM, Armonk, NY). Differences between groups were analyzed using Student's *t*-test. Data are presented as the mean ± s.d. Differences with $P < 0.05$ were considered as statistically significant.

Results

Deficiency of *lepb* has an effect on body weight, length and blood glucose levels in adult zebrafish

In this study, we first examined the basic parameters, including body weight, length and blood glucose levels, in control and *lepb*$^{-/-}$ adult zebrafish in both genders at the age of 1.5 years. The body weight of *lepb*$^{-/-}$ zebrafish in both genders was significantly increased compared to their respective controls (**Fig. 1A**; female: $t(8.191) = 4.219$, $P = 0.003$; male: $t(16) = 2.396$, $P = 0.029$). Accordingly, the body length of *lepb*$^{-/-}$ zebrafish was also significantly increased compared to the controls, in both genders (**Fig. 1B**; female: $t(12) = 2.680$, $P = 0.020$; male: $t(16) = 3.266$, $P = 0.005$). Two hours postprandial blood glucose levels (**Fig. 1C**; female: $t(12) = 0.357$, $P = 0.727$; male: $t(14) = 2.230$, $P = 0.043$) and fasting blood glucose levels (**Supplementary Fig. 4**; female: $t(4) = 0.999$, $P = 0.374$; male: $t(4) = 3.289$, $P = 0.030$) in *lepb*$^{-/-}$ male zebrafish group were significantly higher compared to control male zebrafish group, but we did not find that in the female group.

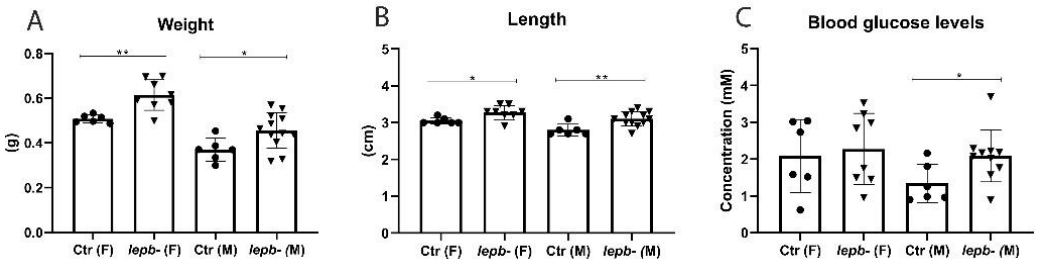

Figure 1. Body weight, length and blood glucose levels in control and *lepb*-deficient adult zebrafish. (A) The body weight of control and *lepb*$^{-/-}$ female (**$p < 0.01$) and male (*$p < 0.05$) adult zebrafish. (B) The body length of control and *lepb*$^{-/-}$ female (*$p < 0.05$) and male (**$p < 0.01$) adult zebrafish. (C) Two hours postprandial blood glucose levels in control and *lepb*$^{-/-}$ female and male (*$p < 0.05$) adult zebrafish. Ctr, control zebrafish; *lepb*–, *lepb*$^{-/-}$ zebrafish; F, female; M, male.

Lepb-deficient adult zebrafish have more visceral fat accumulation

After observing the obese phenotype in *lepb*$^{-/-}$ zebrafish, we examined the body fat distribution in zebrafish with a non-invasive MRI approach. Successive slices were imaged from top to bottom in the coronal plane of control and *lepb*$^{-/-}$ zebrafish in both genders (**Fig. 2**). We observed a substantial increase in visceral fat accumulation in both *lepb*$^{-/-}$ female (**Fig. 2B**) and male (**Fig. 2D**) zebrafish compared to control female (**Fig. 2A**) and male (**Fig. 2C**) zebrafish. Furthermore, we performed the chemical shift selective (CHESS) imaging to acquire clear fat distribution images (**Fig. 2A′, B′, C′** and **D′**). A quantitative analysis of body fat from CHESS images clearly showed a significant increase in fat accumulation in *lepb*$^{-/-}$ zebrafish in both genders compared to their respective controls (**Fig. 2E**; female: $t(10) = 7.057$, $P < 0.001$; male: $t(10) = 5.231$, $P < 0.001$).

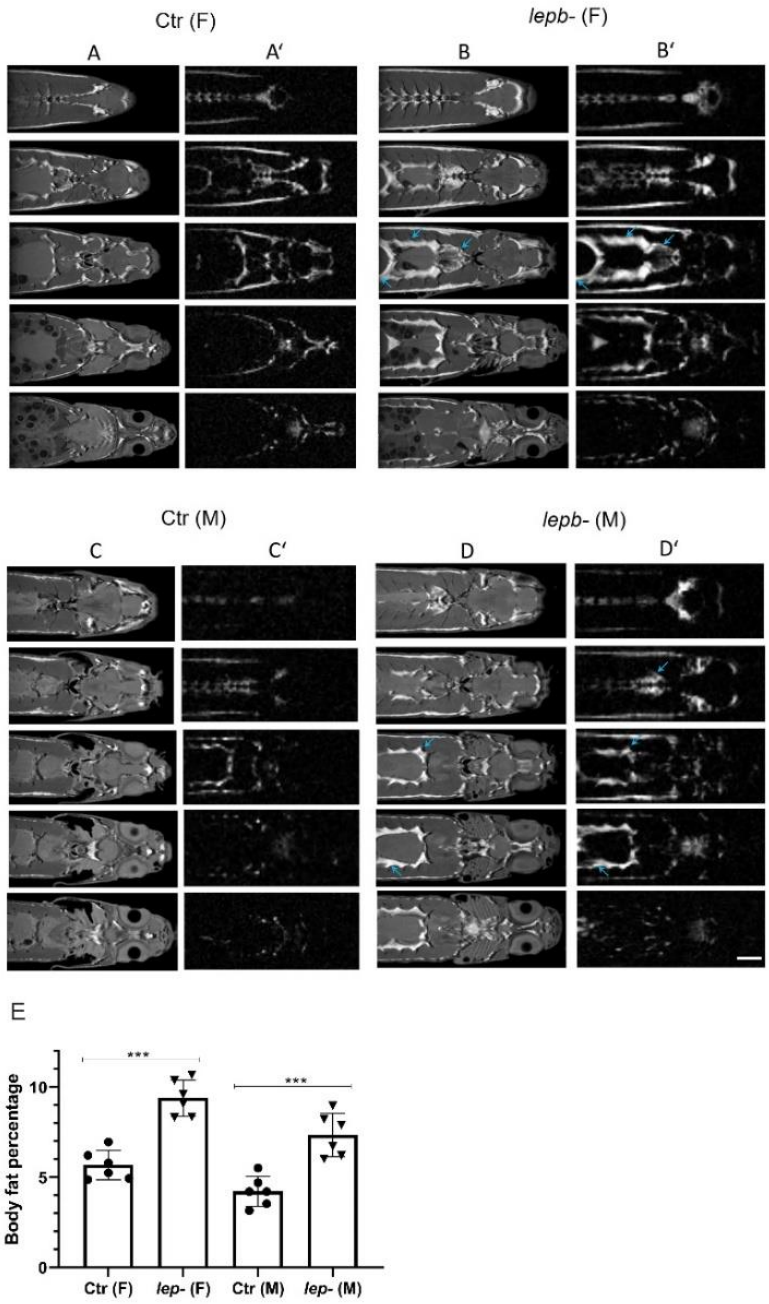

Figure 2. Magnetic resonance anatomical imaging and selective fat imaging in control and *lepb*-deficient female and male adult zebrafish. (A, B, C and D) Successive slices (top to bottom) in the coronal plane obtained using T_2 weighted RARE pulse sequence at a magnetic field strength of 300MHz (7T). (A', B', C' and D') Successive images (top to bottom) of fat distribution in the coronal plane, acquired with Chemical Shift Selective (CHESS) pulse sequence at a magnetic field strength of 300MHz. (A, A') Control female; (B, B') *lepb*$^{-/-}$ female; (C, C') Control male; (D, D') *lepb*$^{-/-}$ male adult zebrafish. A substantial visceral fat accumulation was seen in *lepb*$^{-/-}$ adult zebrafish (arrows) as compared to control adult zebrafish (female and male). Scale bar: 2.5 mm. (E) Quantification of body fat in control and *lepb*$^{-/-}$ female (***$p < 0.001$) and male (***$p < 0.001$) adult zebrafish was measured from CHESS MR images. Ctr, control zebrafish; *lepb*−, *lepb*$^{-/-}$ zebrafish; F, female; M, male.

Lepb-deficient male adult zebrafish develop glomerular hypertrophy

Subsequently, we investigated the histopathology of the zebrafish kidney, an organ with a high vulnerability under the diabetic condition. We found a substantial increase in the surface area of the glomeruli of *lepb*$^{-/-}$ male zebrafish (**Fig. 3B**), compared to control male zebrafish (**Fig. 3A**), on PAS-stained slides. A quantitative analysis of the surface area of the glomeruli showed significant enlargement of Bowman's in *lepb*$^{-/-}$ male zebrafish compared to control male zebrafish, indicating that *lepb*$^{-/-}$ male zebrafish develop glomerular hypertrophy. The surface area of Bowman's space was also larger in *lepb*$^{-/-}$ male zebrafish compared to controls. However, this difference did not reach statistical significance (**Fig. 3E**; $t(13) = 2$.capsule (**Fig. 3C**; $t(13) = 3.725$, $P = 0.003$) and glomerular tuft (**Fig. 3D**; $t(13) = 3.176$, $P = 0.007$) 108, $P = 0.055$). Besides, we did not observe severe mesangial matrix expansion in the glomeruli of *lepb*$^{-/-}$ male zebrafish. Tubular injury and interstitial fibrosis, the final events of chronic tubular injury, contribute to the loss of kidney function. The tubular histology of *lepb*$^{-/-}$ male zebrafish was as normal as control male zebrafish on both PAS- (**Fig. 3A** and **B**) and HE-stained slides (**Fig. 3F** and **G**), and no signs of the tubular atrophy and interstitial fibrosis were observed.

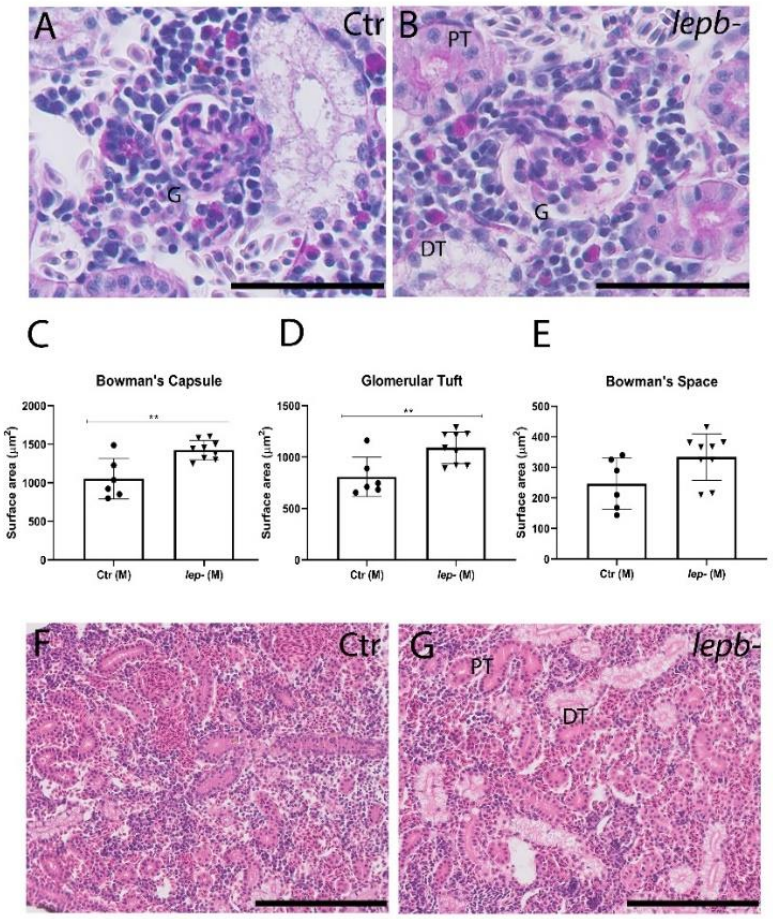

Figure 3. *Lepb*-deficient male adult zebrafish develop glomerular hypertrophy. (A and B) Representative images of the glomeruli of control (A) and *lepb*$^{-/-}$ (B) male adult zebrafish; the scale bars represent 50 µm; PAS staining. (C) Summary of the surface areas of Bowman's capsule of control and *lepb*$^{-/-}$ male adult zebrafish (**$p < 0.01$). (D) Summary of the surface areas of Glomerular tuft of control and *lepb*$^{-/-}$ male adult zebrafish (**$p < 0.01$). (E) Summary of the surface areas of Bowman's space of control and *lepb*$^{-/-}$ male adult zebrafish. (F and G) Representative images of the tubules of control (F) and *lepb*$^{-/-}$ (G) male adult zebrafish; the scale bars represent 50 µm; HE staining. Ctr, control zebrafish; *lepb*−, *lepb*$^{-/-}$ zebrafish; M, male; G, glomeruli; PT, proximal tubule; DT, distal tubule.

Lepb-deficient male adult zebrafish show a thickening of the GBM

Thickening of the GBM is an early sign of diabetic nephropathy (DN). We found a significant increase (2.6 times) in the thickness of GBM in *lepb*$^{-/-}$ male zebrafish (**Fig. 4A, B, C, D** and **H**; $t(4) = 10.281$, $P < 0.001$) compared to controls via TEM approach. Furthermore, we observed some fibers surrounding the GBM in the glomeruli of *lepb*$^{-/-}$ male zebrafish (**Fig. 4G**), suggesting there might have the extracellular matrix accumulation. However, we did not observe obvious podocyte foot process effacement and endothelial cell damage in the glomeruli of *lepb*$^{-/-}$ male zebrafish. Besides, the ultrastructure of the renal proximal tubules of *lepb*$^{-/-}$ male zebrafish was normal and indistinguishable when comparing to control male zebrafish (**Fig. 4E** and **F**), which is consistent with the findings from HE and PAS staining.

Discussion

In the current study, we generated *lepb*-deficient zebrafish by using the CRISPR/CAS9 gene editing approach. We demonstrated that 1.5 years old *lepb*$^{-/-}$ adult zebrafish in both genders had an increase in body weight, length and visceral fat accumulation compared to their respective controls. Furthermore, we found that the blood glucose levels in *lepb*$^{-/-}$ male adult zebrafish were significantly higher than control male adult zebrafish. Lastly, we showed that *lepb*$^{-/-}$ male adult zebrafish developed early signs of DN.

There are conflicting reports whether the disruption of leptin signaling induces adiposity in zebrafish. Audira *et al.* reported that *lepa*-deficient adult zebrafish display an obese phenotype (Audira *et al.* 2018). On the other hand, Michel *et al.* (2016) did not detect an increased fat mass or higher body weight in *lepr*-deficient adult zebrafish. In the current study, we observed that all *lepb* mutants had an increased body weight and body length compared to controls at the adult stage. However, no difference in BMI between control and *lepb*$^{-/-}$ zebrafish, in both genders, was found (**Supplementary Fig. 3C**; female: $t(12) = 1.120$, $P = 0.285$; male: $t(16) = 0.070$, $P = 0.945$). It is well known that increased visceral fat accumulation is a typical feature of obesity. In addition, it has been suggested in the literature that body fat percentage and visceral fat level can predict type II diabetes (Lebovitz & Banerji 2005) or insulin resistance (Kurniawan *et al.* 2018) better than BMI.

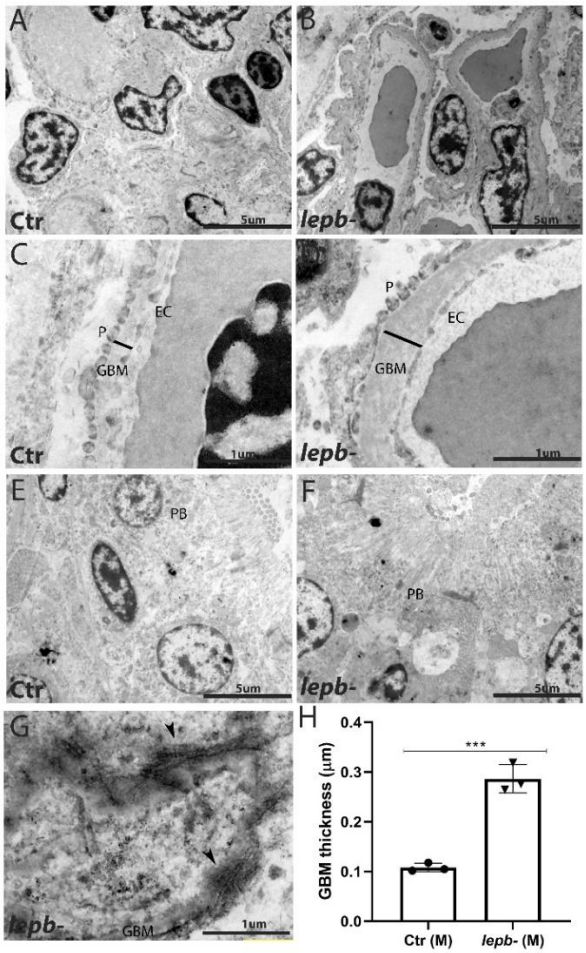

Figure 4. Transmission electron microscopy pictures of glomeruli and tubules from control and *lepb*-deficient male adult zebrafish. (A and B) Representative images of glomeruli from control (A) and *lepb*$^{-/-}$ (B) male adult zebrafish; magnification 5000×. (C and D) High magnification view of one segment of a glomerular capillary from control (C) and *lepb*$^{-/-}$ (D) male adult zebrafish (the thickness of GBM was marked by black lines); magnification 25,000×. (E and F) Representative images of the tubular brash border of the proximal tubule of control (E) and *lepb*$^{-/-}$ (F) male adult zebrafish; magnification 5000×. (G) High magnification of the fibrillar mesangial matrix in *lepb*$^{-/-}$ male adult zebrafish (black arrowheads); magnification 50,000×. (H) Summary of the thickness of GBM in the control and *lepb*$^{-/-}$ male adult zebrafish. The thickness of GBM in *lepb*$^{-/-}$ male zebrafish is 2.6 times thicker than that in control male zebrafish (***$p < 0.001$). Ctr, control zebrafish; *lepb*−: *lepb*$^{-/-}$ zebrafish; M, male; GBM, glomerular basement membrane; P, podocytes; EC, endothelial cells; PB, proximal tubular brush border.

To more precisely compare the body fat distribution between control and *lepb*$^{-/-}$ zebrafish, the successive slices from top to bottom in the coronal plane were imaged via an MRI approach. We found a significantly increased visceral fat accumulation in the *lepb*$^{-/-}$ zebrafish compared to control zebrafish in both genders. The increase of body weight and visceral fat accumulation in *lepb*$^{-/-}$ zebrafish in both genders jointly suggested that *lepb* deficiency results in adiposity in zebrafish. How can we reconcile our findings with the study of Michel *et al.* (2016) showing that *lepr*-deficient zebrafish did not develop obesity? The different findings between these two studies might be due to the different age of zebrafish investigated, or different feeding protocols.

Alternatively, leptin signaling in zebrafish might also have functions that are independent of the leptin receptor. Besides, to exclude off-target effects in our study, we investigated three different mutants, including *lepb*$^{7-/7-}$, *lepb*$^{8-/8-}$ and *lepb*$^{7-/8-}$ mutants, in the *lepb*-deficient (*lepb*$^{-/-}$) group. We found that all these three mutants of *lepb*$^{-/-}$ adult zebrafish had an increased body weight and body length, compared to the controls, which makes it unlikely that our results are caused by the off-target effects of the CRISPR-CAS9 procedure.

Recently, researchers have generated different diabetic models in zebrafish. For instance, Zhang *et al.* developed a zebrafish model for T2DM by overfeeding 4~6 months old fish with diet-induced obesity (DIO) food over 8 weeks, and they showed that these obese fish have increased fasting blood glucose levels (Zang *et al.* 2017). Olsen *et al.* induced a type 1 diabetes mellitus (T1DM) in 4~6 months old zebrafish by injecting streptozotocin (STZ) to ablate beta cells from the pancreas (Olsen *et al.* 2010). This STZ-induced T1DM zebrafish model represents several diabetic complications, such as retinal thinning (an early sign of retinopathy) and GBM thickening (an early sign of nephropathy). However, to further investigate diabetes in zebrafish, there is still a lack of a congenital diabetic zebrafish line which does not require time-consuming feeding schemes or invasive procedures which might cause side effects when inducing the diabetic symptoms.

Diabetes is characterized by hyperglycemia which plays a crucial role in the development of diabetes complications. In the current study, we found that 2 hours postprandial blood glucose levels and fasting blood glucose levels of *lepb*$^{-/-}$ male zebrafish were significantly higher than the levels of control male zebrafish. However, we did not detect this difference in female zebrafish. A review from Wang *et al.* illustrated that diabetic manifestations in some of the rodent models do not develop in females or are not as apparent as in males (Wang *et al.* 2014). Therefore, it is very interesting that we got similar results in the current study in a fish model. The increased body weight, length and visceral fat accumulation and higher blood glucose levels in *lepb*$^{-/-}$ male zebrafish collectively indicate that *lepb*-deficient male adult zebrafish display the features of T2DM. To further explore the glucose homeostasis in the *lepb*-deficient zebrafish model, it would be very interesting to investigate whether the whole-body glucose level has already increased in the *lepb*-deficient zebrafish at larvae stage.

Growing literature provides evidence that leptin has a glucose-lowering effect. A previous study reported that the infusion of leptin into the brain could normalize the hyperglycemia in *ob/ob* mice (Kamohara *et al.* 1997). Insulin has a robust role in the regulation of glucose homeostasis, and insulin resistance is a fundamental aspect of the etiology of T2DM. Several studies have demonstrated that leptin can improve insulin sensitivity (Shimomura *et al.* 1999, German *et al.* 2009). An experimental study from Morton *et al.* suggested that reduced leptin in the mediobasal hypothalamus leads to severe insulin resistance and glucose intolerance in Koletsky rats, and phosphatidylinositol-3-OH kinase signaling is a vital mediator of this effect (Morton *et al.* 2005). In addition, Yu *et al.* reported that leptin could reverse the hyperglycemia and ketosis by

suppressing the action of glucagon on the liver and improving the utilization of glucose in the skeletal muscle in insulin-deficient diabetic rodents (Yu *et al.* 2008). These studies indicated that leptin acts on glucose metabolism in both insulin-dependent and insulin-independent ways. Earlier work from our laboratory had demonstrated that *lepb* was significantly downregulated in zebrafish larvae under an insulin-resistance state (Marin- Juez *et al.* 2014). Future studies should investigate whether the diabetic phenotype of *lepb* mutants is caused by disruption of the insulin signaling pathway.

The segmental anatomy of the nephron is conserved among the vertebrates (McCampbell & Wingert 2014). Olsen *et al.* found that STZ-induced T1DM zebrafish have a thickening of the GBM (an early sign of DN) (Olsen *et al.* 2010). In the current study, we want to address whether *lepb*$^{-/-}$ adult zebrafish develop DN or not. We found that the *lepb*$^{-/-}$ male group had higher blood glucose levels compared to the control male group, but not in the female group. Therefore, the kidney in male zebrafish was further investigated by performing histopathological examination. Glomerular hypertrophy, mesangial expansion, and thickening of the GBM are the particular characteristics of the histopathology of DN (Tervaert *et al.* 2010). We found that *lepb*$^{-/-}$ male zebrafish develop glomerular hypertrophy and thickening of the GBM, compared to control male zebrafish. However, we did not observe severe mesangial expansion, podocyte damage, or tubular cell damage in the kidney tissue of *lepb*$^{-/-}$ male zebrafish. These findings collectively indicate that the renal injury in *lepb*$^{-/-}$ male zebrafish is relatively mild.

In summary, we demonstrated that *lepb* regulates glucose homeostasis and adiposity in zebrafish, and deletion of the *lepb* gene results in the development of T2DM and the early stage of DN. These results suggest that *lepb*-deficient zebrafish can be used as a T2DM model, and further investigation would give us new insights into the mechanistic function of leptin in T2DM.

Declaration of interest

The authors declare that there is no conflict of interest that could be perceived as prejudicing the impartiality of the research reported.

Funding

The work was supported by the Polish National Science Center (grant number 2016/21/N/NZ6/01162).

Author contribution statement

J H and Y D designed the study, analyzed and interpreted the data, and wrote the manuscript. J H, Y D, N N, C J, and M N H E performed experiments and the data collection. A A provided technical support and conceptual advice. H J B provided conceptual advice, the experimental design of the study and revisions of the scientific content of the manuscript. H P S conceived the ideas and the experimental design of the study, provided revisions of the scientific content of the manuscript, and supervised the whole study. All authors approved the final version of the manuscript and are fully accountable for all aspects of the study.

Acknowledgements

The first authors (J He and Y Ding) were supported by the China Scholarship Council (CSC). We would like to thank Peter Neeskens for the technical support of the transmission electron microscopy (TEM).

References

1. Aguilar AJ, Conde-Sieira M, Lopez-Patino MA, Miguez JM & Soengas JL 2011 In vitro leptin treatment of rainbow trout hypothalamus and hindbrain affects glucosensing and gene expression of neuropeptides involved in food intake regulation. *Peptides* **32** 232–240. (https://doi.org/10.1016/j.peptides.2010.11.007)
2. Ahima RS, Prabakaran D & Flier JS 1998 Postnatal leptin surge and regulation of circadian rhythm of leptin by feeding. Implications for energy homeostasis and neuroendocrine function. *Journal of Clinical Investigation* **101** 1020–1027. (https://doi.org/10.1172/JCI1176)
3. Audira G, Sarasamma S, Chen JR, Juniardi S, Sampurna BP, Liang ST, Lai YH, Lin GM, Hsieh MC & Hsiao CD 2018 Zebrafish mutants carrying leptin a (lepa) gene deficiency display obesity, anxiety, less aggression and fear, and circadian rhythm and color preference dysregulation. *International Journal of Molecular Sciences* **19** 4038. (https://doi.org/10.3390/ijms19124038)
4. Caprio M, Fabbrini E, Isidori AM, Aversa A & Fabbri A 2001 Leptin in reproduction. *Trends in Endocrinology and Metabolism* **12** 65–72. (https://doi.org/10.1016/s1043-2760(00)00352-0)
5. Chisada S, Kurokawa T, Murashita K, Ronnestad I, Taniguchi Y, Toyoda A, Sakaki Y, Takeda S & Yoshiura Y 2014 Leptin receptor-deficient (knockout) medaka, Oryzias latipes, show chronical up-regulated levels of orexigenic neuropeptides, elevated food intake and stage specific effects on growth and fat allocation. *General and Comparative Endocrinology* **195** 9–20. (https://doi.org/10.1016/j.ygcen.2013.10.008)
6. Denver RJ, Bonett RM & Boorse GC 2011 Evolution of leptin structure and function. *Neuroendocrinology* **94** 21–38. (https://doi. org/10.1159/000328435)
7. Drel VR, Mashtalir N, Ilnytska O, Shin J, Li F, Lyzogubov VV & Obrosova IG 2006 The leptin-deficient (ob/ob) mouse: a new animal model of peripheral neuropathy of type 2 diabetes and obesity. *Diabetes* **55** 3335–3343. (https://doi.org/10.2337/db06-0885)
8. Farooqi IS, Jebb SA, Langmack G, Lawrence E, Cheetham CH, Prentice AM, Hughes IA, Mccamish MA & O'Rahilly S 1999 Effects of recombinant leptin therapy in a child with congenital leptin deficiency. *New England Journal of Medicine* **341** 879–884. (https://doi. org/10.1056/NEJM199909163411204)
9. Fujikawa T, Chuang JC, Sakata I, Ramadori G & Coppari R 2010 Leptin therapy improves insulin-deficient type 1 diabetes by CNS-dependent mechanisms in mice. *PNAS* **107** 17391–17396. (https://doi.org/10.1073/pnas.1008025107)
10. Funcke JB, Von Schnurbein J, Lennerz B, Lahr G, Debatin KM, Fischer- Posovszky P & Wabitsch M 2014 Monogenic forms of childhood obesity due to mutations in the leptin gene. *Molecular and Cellular Pediatrics* **1** 3. (https://doi.org/10.1186/s40348-014-0003-1)
11. German J, Kim F, Schwartz GJ, Havel PJ, Rhodes CJ, Schwartz MW & Morton GJ 2009 Hypothalamic leptin signaling regulates hepatic insulin sensitivity via a neurocircuit involving the vagus nerve. Endocrinology 150 4502–4511. (https://doi.org/10.1210/en.2009- 0445)
12. German JP, Thaler JP, Wisse BE, Oh-I S, Sarruf DA, Matsen ME, Fischer JD, Taborsky GJ, Schwartz MW & Morton GJ 2011 Leptin activates a novel CNS mechanism for insulin-independent normalization of severe diabetic hyperglycemia. Endocrinology 152 394–404. (https://doi.org/10.1210/en.2010-0890)
13. Gorissen M, Bernier NJ, Nabuurs SB, Flik G & Huising MO 2009 Two divergent leptin paralogues in zebrafish (Danio rerio) that originate early in teleostean evolution. Journal of Endocrinology 201 329–339. (https://doi.org/10.1677/JOE-09-0034)

14. Hedbacker K, Birsoy K, Wysocki RW, Asilmaz E, Ahima RS, Farooqi IS & Friedman JM 2010 Antidiabetic effects of IGFBP2, a leptin-regulated gene. Cell Metabolism 11 11–22. (https://doi.org/10.1016/j. cmet.2009.11.007)
15. Kamohara S, Burcelin R, Halaas JL, Friedman JM & Charron MJ 1997 Acute stimulation of glucose metabolism in mice by leptin treatment. Nature 389 374–377. (https://doi.org/10.1038/38717)
16. Kurniawan LB, Bahrun U, Hatta M & Arif M 2018 Body mass, total body fat percentage, and visceral fat level predict insulin resistance better than waist circumference and body mass index in healthy young male adults in Indonesia. Journal of Clinical Medicine 7 96. (https:// doi.org/10.3390/jcm7050096)
17. Lebovitz HE & Banerji MA 2005 Point: visceral adiposity is causally related to insulin resistance. Diabetes Care 28 2322–2325. (https://doi. org/10.2337/diacare.28.9.2322)
18. Licinio J, Caglayan S, Ozata M, Yildiz BO, De Miranda PB, O'Kirwan F, Whitby R, Liang L, Cohen P, Bhasin S, et al. 2004 Phenotypic effects of leptin replacement on morbid obesity, diabetes mellitus, hypogonadism, and behavior in leptin-deficient adults. PNAS 101 4531–4536. (https://doi.org/10.1073/pnas.0308767101)
19. Lord GM, Matarese G, Howard JK, Baker RJ, Bloom SR & Lechler RI 1998 Leptin modulates the T-cell immune response and reverses starvation-induced immunosuppression. Nature 394 897–901. (https://doi. org/10.1038/29795)
20. Marin-Juez R, Jong-Raadsen S, Yang S & Spaink HP 2014 Hyperinsulinemia induces insulin resistance and immune suppression via Ptpn6/Shp1 in zebrafish. Journal of Endocrinology 222 229–241. (https://doi.org/10.1530/JOE-14-0178)
21. Matarese G, Moschos S & Mantzoros CS 2005 Leptin in immunology. Journal of Immunology 174 3137–3142. (https://doi.org/10.4049/ jimmunol.174.6.3137)
22. McCampbell KK & Wingert RA 2014 New tides: using zebrafish to study renal regeneration. Translational Research 163 109–122. (https://doi. org/10.1016/j.trsl.2013.10.003)
23. Meier U & Gressner AM 2004 Endocrine regulation of energy metabolism: review of pathobiochemical and clinical chemical aspects of leptin, ghrelin, adiponectin, and resistin. Clinical Chemistry 50 1511–1525. (https://doi.org/10.1373/clinchem.2004.032482)
24. Michel M, Page-Mccaw PS, Chen W & Cone RD 2016 Leptin signaling regulates glucose homeostasis, but not adipostasis, in the zebrafish. PNAS 113 3084–3089. (https://doi.org/10.1073/pnas.1513212113)
25. Morton GJ, Gelling RW, Niswender KD, Morrison CD, Rhodes CJ & Schwartz MW 2005 Leptin regulates insulin sensitivity via phosphatidylinositol-3-OH kinase signaling in mediobasal hypothalamic neurons. Cell Metabolism 2 411–420. (https://doi. org/10.1016/j.cmet.2005.10.009)
26. Murashita K, Uji S, Yamamoto T, Ronnestad I & Kurokawa T 2008 Production of recombinant leptin and its effects on food intake in rainbow trout (Oncorhynchus mykiss). Comparative Biochemistry and Physiology: Part B, Biochemistry and Molecular Biology 150 377–384. (https://doi.org/10.1016/j.cbpb.2008.04.007)
27. Muzzin P, Eisensmith RC, Copeland KC & Woo SL 1996 Correction of obesity and diabetes in genetically obese mice by leptin gene therapy. PNAS 93 14804–14808. (https://doi.org/10.1073/pnas.93.25.14804) Olsen AS, Sarras Jr MP & Intine RV 2010 Limb regeneration is impaired in an adult zebrafish model of diabetes mellitus. Wound Repair and Regeneration 18 532–542. (https://doi.org/10.1111/j.1524- 475X.2010.00613.x)

28. Park S, Hong SM, Sung SR & Jung HK 2008 Long-term effects of central leptin and resistin on body weight, insulin resistance, and beta-cell function and mass by the modulation of hypothalamic leptin and insulin signaling. Endocrinology 149 445–454. (https://doi. org/10.1210/en.2007-0754)
29. Pocai A, Morgan K, Buettner C, Gutierrez-Juarez R, Obici S & Rossetti L 2005 Central leptin acutely reverses diet-induced hepatic insulin resistance. Diabetes 54 3182–3189. (https://doi.org/10.2337/ diabetes.54.11.3182)
30. Shimomura I, Hammer RE, Ikemoto S, Brown MS & Goldstein JL 1999 Leptin reverses insulin resistance and diabetes mellitus in mice with congenital lipodystrophy. Nature 401 73–76. (https://doi. org/10.1038/43448)
31. Tervaert TW, Mooyaart AL, Amann K, Cohen AH, Cook HT, Drachenberg CB, Ferrario F, Fogo AB, Haas M, De Heer E, et al. 2010 Pathologic classification of diabetic nephropathy. Journal of the American Society of Nephrology 21 556–563. (https://doi.org/10.1681/ ASN.2010010010)
32. Volkoff H, Eykelbosh AJ & Peter RE 2003 Role of leptin in the control of feeding of goldfish Carassius auratus: interactions with cholecystokinin, neuropeptide Y and orexin A, and modulation by fasting. Brain Research 972 90–109. (https://doi.org/10.1016/s0006- 8993(03)02507-1)
33. Wang B, Chandrasekera PC & Pippin JJ 2014 Leptin- and leptin receptor-deficient rodent models: relevance for human type 2 diabetes. Current Diabetes Reviews 10 131–145. (https://doi.org/10.2174/157339981066 6140508121012)
34. Yu X, Park BH, Wang MY, Wang ZV & Unger RH 2008 Making insulin-deficient type 1 diabetic rodents thrive without insulin. PNAS 105 14070–14075. (https://doi.org/10.1073/pnas.0806993105)
35. Zang L, Shimada Y & Nishimura N 2017 Development of a novel zebrafish model for type 2 diabetes mellitus. Scientific Reports 7 1461. (https://doi.org/10.1038/s41598-017-01432-w)
36. Zhang Y, Proenca R, Maffei M, Barone M, Leopold L & Friedman JM 1994 Positional cloning of the mouse obese gene and its human homologue. Nature 372 425–432. (https://doi.org/10.1038/372425a0)

Supplementary materials

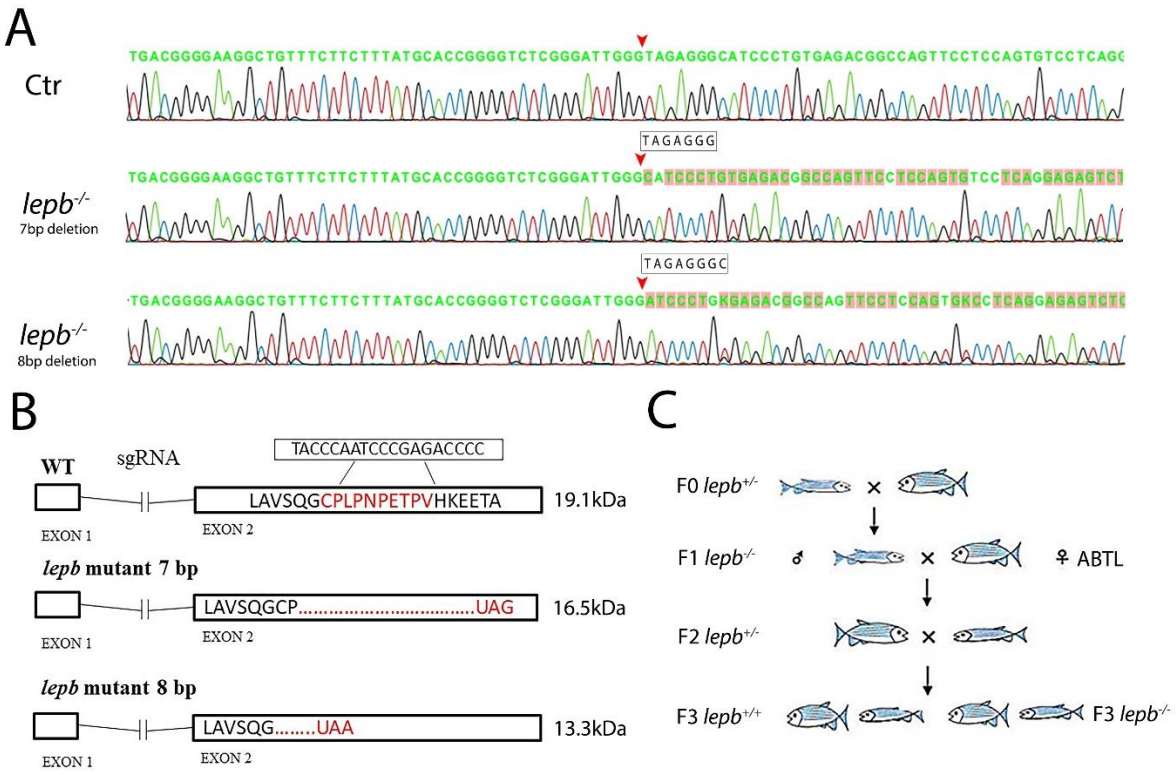

Supplementary Figure 1. *Lepb*-deficient zebrafish line (A) The wild type zebrafish (Ctr) is showing a partial sequence of the *lepb* gene. Seven base pairs (TAGAGGG) were deleted in *lepb*$^{7-/7-}$ zebrafish and eight base pairs (TAGAGGGC) were deleted in *lepb*$^{8-/8-}$ zebrafish. The arrowheads show the start point of the deletion. (B) The wild type *lepb* gene translates into the predicted 19.1 kDa lepb protein in zebrafish. The seven base pairs deletion creates a premature stop codon UAG in exon 2, which results in a truncated 16.5 kDa protein. And the eight base pairs deletion causes a premature stop codon UAA in exon 2, which results in a truncated 13.3 kDa protein. (C) Homozygous F1 carriers were outcrossed once against the wild type zebrafish (ABTL) and the offspring (heterozygote *lepb*$^{+/-}$) were subsequently incrossed, resulting in the used *lepb*$^{+/+}$ and *lepb*$^{-/-}$ siblings. Because of the limitations of the number of adult zebrafish during this study, we used adult WT-ABTL (Ctr) and all *lepb*$^{-/-}$ (*lepb*$^{7-/7-}$, *lepb*$^{8-/8-}$ and *lepb*$^{7-/8-}$) for the experiments.

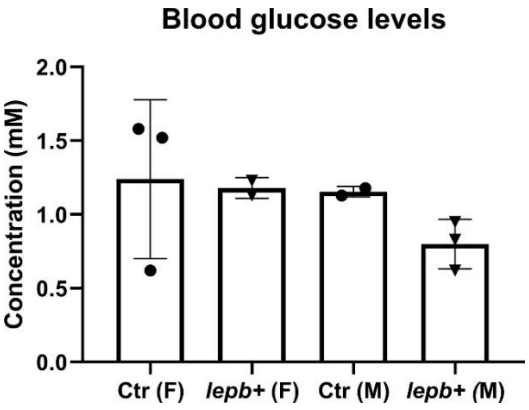

Supplementary Figure 2. Blood glucose levels in *lepb*$^{+/+}$ adult zebrafish and age-matched ABTL control zebrafish Two hours postprandial blood glucose levels in ABTL control and *lepb*$^{+/+}$ zebrafish (female and male). Ctr: ABTL control zebrafish; *lepb*+: *lepb*$^{+/+}$ zebrafish; F: female; M: male.

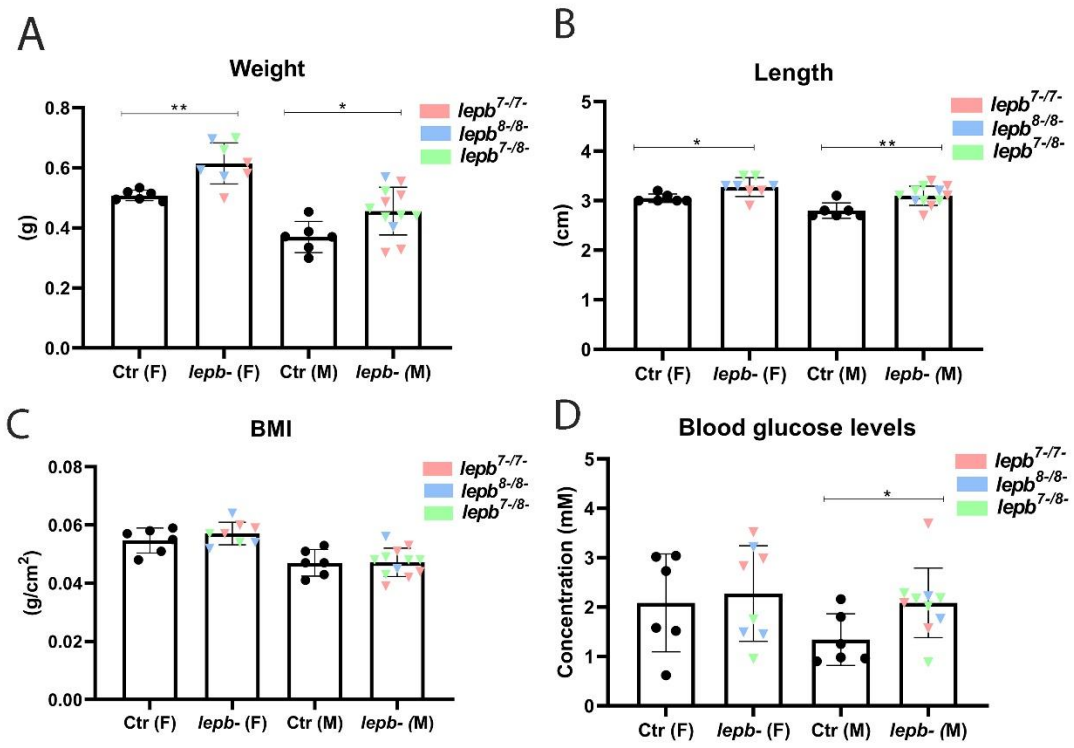

Supplementary Figure 3. Body weight, length, BMI and blood glucose levels in different *lepb*$^{-/-}$ mutants (A) The body weight of control and *lepb*$^{-/-}$ female (**$p < 0.01$) and male (*$p < 0.05$) adult zebrafish. (B) The body length of control and *lepb*$^{-/-}$ female (*$p < 0.05$) and male (**$p < 0.01$) adult zebrafish. (C) The BMI of control and *lepb*$^{-/-}$ female and male adult zebrafish. (D) Two hours postprandial blood glucose levels in control and *lepb*$^{-/-}$ female and male (*$p < 0.05$) adult zebrafish. Different *lepb*$^{-/-}$ mutants were marked in different colors. *lepb*$^{7-/7-}$ in red, *lepb*$^{8-/8-}$ in blue and *lepb*$^{7-/8-}$ in green. Ctr: control zebrafish; *lepb*-: *lepb*$^{-/-}$ zebrafish; F: female; M: male.

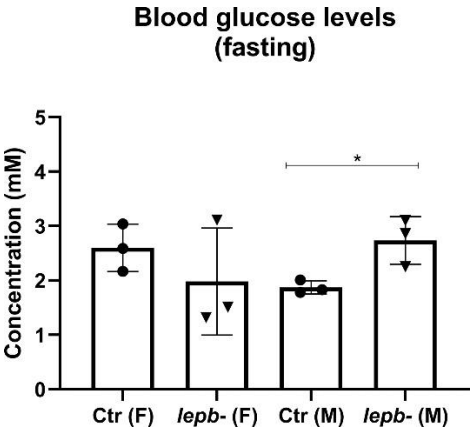

Supplementary Figure 4. Fasting blood glucose levels in control and *lepb*-deficient adult zebrafish (*$p < 0.05$). Ctr: control zebrafish; *lepb*-: *lepb*$^{-/-}$ zebrafish; F: female; M: male.

Chapter 4

Metabolomic and transcriptomic profiling of adult mice and larval zebrafish leptin mutants reveal a common pattern of changes in metabolites and signalling pathways

Yi Ding[1], Marielle C. Haks[2], Gabriel Forn-Cuni[1], Junling He[1], Natalia Nowik[1,3], Amy C. Harms[4], Thomas Hankemeier[4], Muhamed N. H. Eeza[5,6], Jorg Matysik[6], A. Alia[5,7] and Herman P. Spaink[1*]

[1] Institute of Biology, Leiden University, Leiden, The Netherlands
[2] Department of Infectious Diseases, Leiden University Medical Center, Leiden, The Netherlands
[3] Department of Animal Anatomy, Faculty of Veterinary Medicine, University of Warmia and Mazury, Oczapowskiego 13, 10-719 Olsztyn, Poland
[4] Leiden Academic Centre for Drug Research, Leiden University, Leiden, The Netherlands
[5] Institute of Medical Physics and Biophysics, University of Leipzig, 04107 Leipzig, Germany
[6] Institute of Analytical Chemistry, University of Leipzig, Linnéstraße 3, D-04103, Leipzig, Germany
[7] Leiden Institute of Chemistry, Leiden University, Leiden, The Netherlands
*Corresponding author, email: h.p.spaink@biology.leidenuniv.nl

Cell Biosci (2021) 11:126

ABSTRACT

Background

Leptin plays a critical role in the regulation of metabolic homeostasis. However, the molecular mechanism and cross talks between leptin and metabolic pathways leading to metabolic homeostasis across different species are not clear. This study aims to explore the effects of leptin in mice and zebrafish larvae by integration of metabolomics and transcriptomics. Different metabolomic approaches including mass spectrometry, nuclear magnetic resonance (NMR) and high-resolution magic-angle-spinning NMR spectroscopy were used to investigate the metabolic changes caused by leptin deficiency in mutant *ob/ob* adult mice and *lepb* zebrafish larvae. For transcriptome studies, deep RNA sequencing was used.

Results

Thirteen metabolites were identified as common biomarkers discriminating *ob/ob* mice and *lepb* zebrafish larvae from their respective wild type controls: alanine, citrulline, ethanolamine, glutamine, glycine, histidine, isoleucine, leucine, methionine, phenylalanine, putrescine, serine and threonine. Moreover, we also observed that glucose and lipid levels were increased in *lepb* zebrafish larvae compared to the *lepb* group. Deep sequencing showed that many genes involved in proteolysis and arachidonic acid metabolism were dysregulated in *ob/ob* mice heads and *lepb* mutant zebrafish larvae compared to their wild type controls, respectively.

Conclusions

Leptin deficiency leads to highly similar metabolic alterations in metabolites in both mice and zebrafish larvae. These metabolic changes show similar features as observed during progression of tuberculosis in human patients, mice and zebrafish larvae. In addition, by studying the transcriptome, we found similar changes in gene regulation related to proteolysis and arachidonic acid metabolism in these two different in vivo models.

Keywords: *Ob/ob* mice, Leptin mutant zebrafish, Diabetes, Metabolomics, Transcriptomics, Wasting syndrome

Background

Leptin, the first discovered adipokine, plays a critical role in the regulation of energy balance and homeostasis of metabolism [1, 2]. Congenital leptin deficiency in humans results in extreme obesity, hyperphagia and many complications such as type 2 diabetes [3]. Leptin administration therapy with metreleptin, a recombinant human leptin analogue, has been approved for the treatment of the metabolic abnormalities linked to dyslipidemia [4]. Metabolic effects of leptin have been studied in rodent animal models [5]. Leptin signaling deficient rodent mutants, such as *ob/ob* mice, *db/db* mice and Zucker rats, have been commonly used as animal models in leptin studies [5]. Similar to the rare cases of congenital human leptin deficiency, these rodent mutants display hyperphagia, obesity and an insulin resistant phenotype. Several studies have shown metabolic disorders in *ob/ob* mice [6-8], *db/db* mice [6, 9, 10] and obese Zucker rats [11] measured by mass spectrometry (MS) or ^{1}H solution nuclear magnetic resonance (NMR). Using a positional isotopomer NMR tracer analysis method, Perry et al showed that leptin mediates a glucose-fatty acid cycle to maintain glucose homeostasis in starvation in rats [12]. Using a combination of metabolomics and transcriptomics, a recent published paper demonstrates that the carbohydrate, lipid and amino acid metabolic liver responses to glucose administration are broadly different between wild type and *ob/ob* mice [13].

Leptin and leptin receptor (lepr) are highly conserved and share extensive homology across vertebrates including all mammals and fish and have been studied in many model organisms [14, 15]. However, leptin functions in early development of vertebrates are largely unknown. Notwithstanding many reports indicate that leptin plays a key role in gestational diabetes and fetal development [16-20]. Further understanding of the function of leptin in these processes is hampered by the challenges of using rodent animal models for the study of fetal development. Zebrafish represents a robust animal model for early development because of its external fertilization, transparency of its larvae and large numbers of offspring. Since the zebrafish larvae are independent of feeding in the first five days after fertilization, it offers a great model for comparative leptin studies in fetal development with adult mammals. In zebrafish, there are two orthologs of the human leptin gene, *leptin a* (*lepa*) and *leptin b* (*lepb*). A zebrafish mutant line with *lepa* gene deficiency displays a phenotype of obesity and various deviations in behavior and circadian rhythm in the adult stage [21]. It was shown that *lepb* mutant zebrafish have more visceral fat and higher glucose level in male adult fish [22]. However, a zebrafish mutant for *lepr* was reported not to exhibit increased obesity in adult fish [23]. In larval studies, we have previously shown that *lepb* is one of the most affected genes after insulin injection [24]. However, how *lepb* gene affects the metabolic and transcriptomic level in zebrafish larvae is still unknown.

In this study, we have compared the metabolic changes resulting from leptin deficiency in blood of adult *ob/ob* mice, extracted and intact zebrafish larvae using MS, solution-state NMR and high-resolution magic-angle-spinning NMR (HR-MAS NMR) spectrometry. HR-MAS NMR is a noninvasive method that can be used for analysis of intact tissues at low temperature. In addition, we have compared the transcriptomic changes resulting from leptin deficiency in *ob/ob* mice heads,

a published dataset for *ob/ob* mice liver and *lepb* mutant zebrafish larvae. These comparisons show a remarkable similarity of the effects of leptin knockdown on the metabolomes and transcriptomes of adult mice and zebrafish larvae.

Results

Metabolic profiles of blood from *ob/ob* and wild type mice measured by MS

We first investigated the metabolic profiles of blood from *ob/ob* and wild type lean male mice at 14 weeks of age. Mice were kept on a standard diet for 8 weeks, after which the body weight of *ob/ob* mice was significantly higher than wild type C57BL/6 mice (**Supplementary Figure S1**). Metabolic profiles of the blood of the two groups were obtained by MS. Using a highly standardized platform we could measure 41 small amine-containing compounds. A Partial Least Squares Discriminant Analysis (PLS-DA) scores plot of the 41 identified metabolites showed clear differences between the *ob/ob* and the wild type mice, indicating metabolic alterations in the metabolism due to leptin deficiency (**Figure 1A**). Using a cut-off *p* value of 0.05, we could classify 30 out of the 41 identified small amine-containing compounds as associated with *ob/ob* mice. These 30 metabolites were significantly downregulated with a p value < 0.05 in *ob/ob* mice compared to wild type mice (**Figure 1B** and **Supplementary Table S1**). For 25 of these metabolites, we have previously shown that they are biomarkers for *mycobacterium tuberculosis* (*Mtb*)-infected mice (**Figure 1C**). Graphs showing the quantification of these 25 common metabolites revealed that both the original and normalized values were decreased in leptin-deficient *ob/ob* mice (**Supplementary Figure S2**).

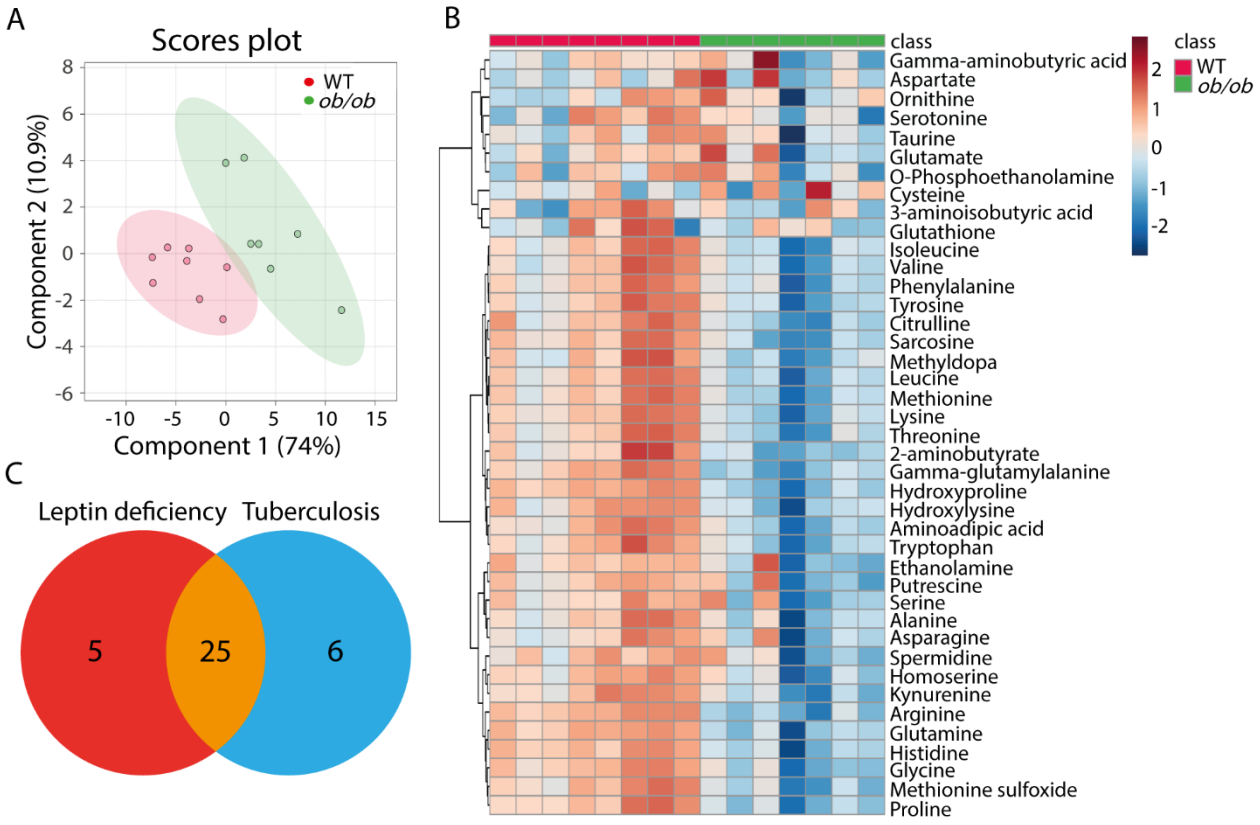

Figure 1. Metabolic profiles of blood from *ob/ob* and wild type C57BL/6 mice measured by mass spectrometry. **A** PLS-DA analysis of wild type and *ob/ob* mice, n = 15 in total, each replicate represents one mouse. *PLS-DA* partial least square discriminant analysis. *WT* wild type. **B** Heat map of 30 statistically significant biochemical markers profiled in this mice study. **C** A Venn diagram showing the overlap of the 30 metabolites of B with the set of wasting syndrome biomarkers published by Ding et al [26].

Metabolic profiles of extracts of *lepb* deficient and wild type zebrafish larvae measured by NMR

A *lepb* mutant zebrafish line was generated by CRISPR/CAS methodology [22]. Metabolic profiles of extracted zebrafish larvae from *lepb*$^{-/-}$ mutant and *lepb*$^{+/+}$ wild type siblings were measured by one-dimensional ^{1}H solution NMR. **Figure 2A** shows the representative ^{1}H NMR spectra of extracted metabolites in the two groups. The assignment was performed based on the peaks of reference metabolites from literature [6, 25] in the library of Chenomx 600 MHz (version 11). A PLS-DA scores plot showed differences between the *lepb*$^{-/-}$ and *lepb*$^{+/+}$ groups (**Figure 2B**), suggesting metabolic changes resulting from *lepb* deficiency in zebrafish larvae. We found 27 metabolites to be significantly changed with a p value < 0.05 in extracted *lepb*$^{-/-}$ zebrafish larvae compared to *lepb*$^{+/+}$ group. For 19 of these metabolites, we have previously shown that they are biomarkers for *Mycobacterium marinum*-infected zebrafish larvae (**Figure 2C**). Quantification of these 19 common metabolites showed that the levels of all the metabolites were decreased in *lepb* mutant zebrafish larvae (**Supplementary Figure S3**).

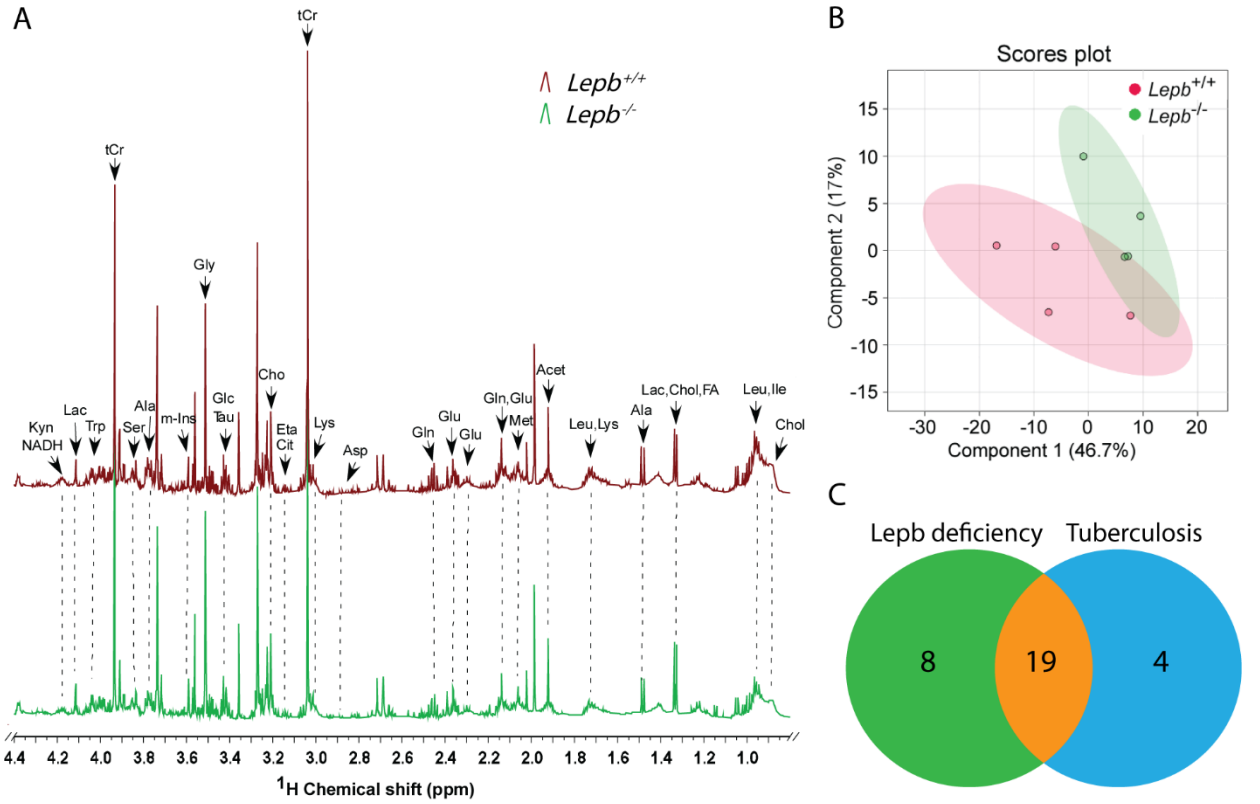

Figure 2. One-dimensional ^{1}H NMR spectra and PLS-DA analysis of extracted *lepb* mutant zebrafish larvae. A The representative spectra of extracted larvae from wild type and *lepb* mutant groups measured by solution NMR spectrometry. Spectra from chemical shift 0.5–4.4 were assigned to specific metabolites. *Acet* acetate, *Ala* alanine, *Arg* arginine, *Asp* aspartate, *Cho* choline, *Chol* cholesterol, *Cit* citrulline, *Eta* ethanolamine, *FA* fatty acid, *Glc* glucose, *Gln* glutamine, *Glu* glutamate, *Gly* glycine, Ile isoleucine, *Kyn* kynurenine, *Lac* lactate, *Leu* leucine, *Lys* lysine, *Met* methionine, *m-Ins* myo-inositol, *Ser* serine, *Tau* taurine, *tCr* total creatine (creatine + phosphocreatine), *Trp* tryptophan, *NMR* nuclear magnetic resonance. **B** PLS-DA analysis of wild type and *lepb* mutant groups, n = 4, each replicate represents 105 pooled larvae. *PLS-DA* partial least square discriminant analysis. **C** A Venn diagram is shown of the common 19 metabolites that changed significantly towards *lepb* deficiency in extracted zebrafish larvae and tuberculosis caused by *M. marinum* infection in extracted zebrafish larvae published by Ding et al [26].

Metabolic profiles of intact *lepb* deficient and wild type zebrafish larvae measured by HR-MAS NMR

Due to the possibility of degradation and selective loss of compounds because of the extraction method needed for solution NMR, we used HR-MAS NMR as a comparative method on intact zebrafish larvae. **Figure 3A** showed the comparison of metabolic profiles and the assignments of metabolites of representative spectra in *lepb* mutant and wild type siblings. It was shown that the intensities of many peaks were lower in the mutant group. A PLS-DA scores plot showed clear discrimination between the *lepb*$^{-/-}$ and *lepb*$^{+/+}$ groups (**Figure 3B**). To compare the methods of solution NMR and HR-MAS NMR, we showed a Venn diagram of the significantly changed metabolites in the mutant and control siblings. The result revealed that there were 25 common

metabolites significantly changed in both measurements (**Figure 3C**). These 25 metabolites include the small amines alanine, asparagine, aspartate, citrulline, cysteine, ethanolamine, glutamate, glutamine, glycine, histidine, isoleucine, kynurenine, leucine, methionine, phenylalanine, putrescine, serine, threonine and tyrosine (**Figure 4A**, **C**). In addition, the concentration of ATP, glucose, mannose, acetate, lactate and myo-inositol were changed significantly (**Figure 4B**, **D**). For 21 of the 25 metabolites, both methods showed the same result: lower measurements of 20 metabolites and higher glucose level in the mutant group. However, kynurenine, tyrosine, ATP and mannose were detected at a decreased level in the mutant group with extracted larvae while at an increased level using intact larvae (**Figure 4**).

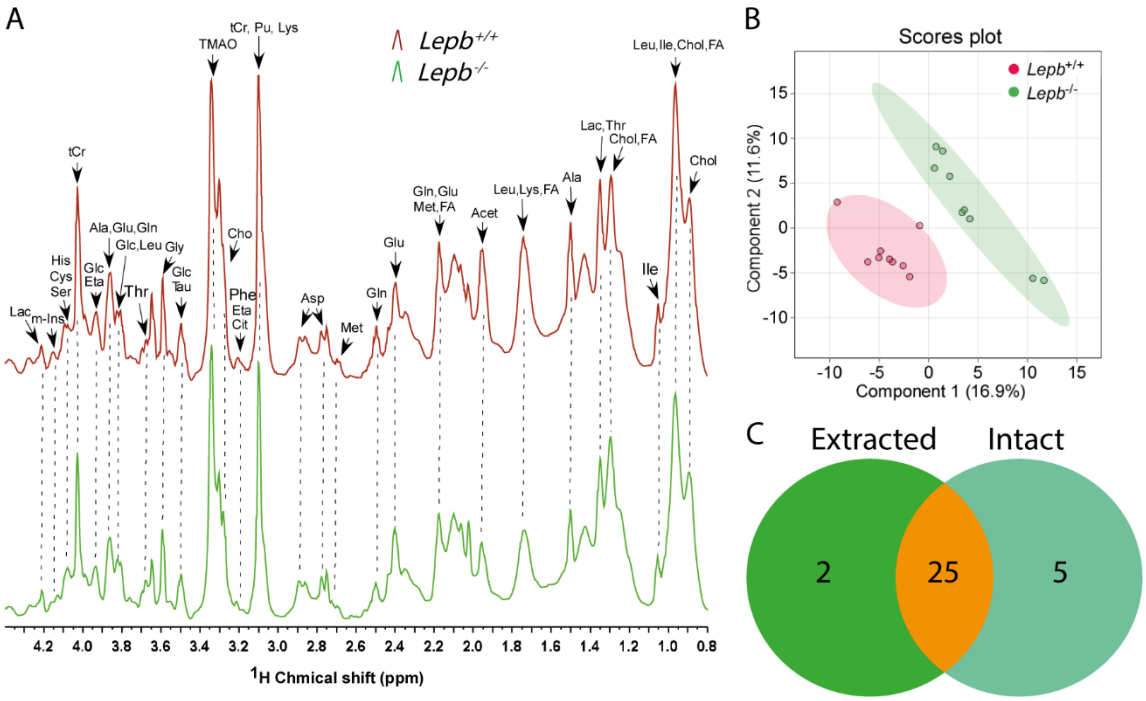

Figure 3. One-dimensional ^{1}H HR-MAS NMR spectra and PLS-DA analysis of intact *lepb* mutant zebrafish larvae. A The representative spectra of intact larvae from wild type and *lepb* mutant groups measured by HR-MAS NMR spectrometry. Spectra from chemical shift 0.5–4.4 were assigned to specific metabolites. *Acet* acetate, *Ala* alanine, *Asp* aspartate, *Cho* choline, Chol cholesterol, *Cit* citrulline, *Cys* cysteine, *Eta* ethanolamine, *FA* fatty acid, *Glc* glucose, *Gln* glutamine, *Glu* glutamate, *Gly* glycine, *His* histidine, *Ile* isoleucine, *Lac* lactate, *Leu* leucine, *Lys* lysine, *Met* methionine, *m-Ins* myo-inositol, *Pu* putrescine, *Ser* serine, *Tau* taurine, *tCr* total creatine (creatine + phosphocreatine), *Thr* threonine, *TAMO* trimethylamine N-oxide, *HR-MAS NMR* high-resolution magic-angle-spinning nuclear magnetic resonance. **B** PLS-DA analysis of intact larvae from wild type and *lepb* mutant groups, n = 3, three times measurements, each replicate represents 120 pooled larvae. *PLS-DA* partial least square discriminant analysis. **C** A Venn diagram is shown of the common 25 metabolites that are significantly changed both in extracted zebrafish larvae measured by ^{1}H solution NMR and intact larvae measured by ^{1}H HR-MAS NMR.

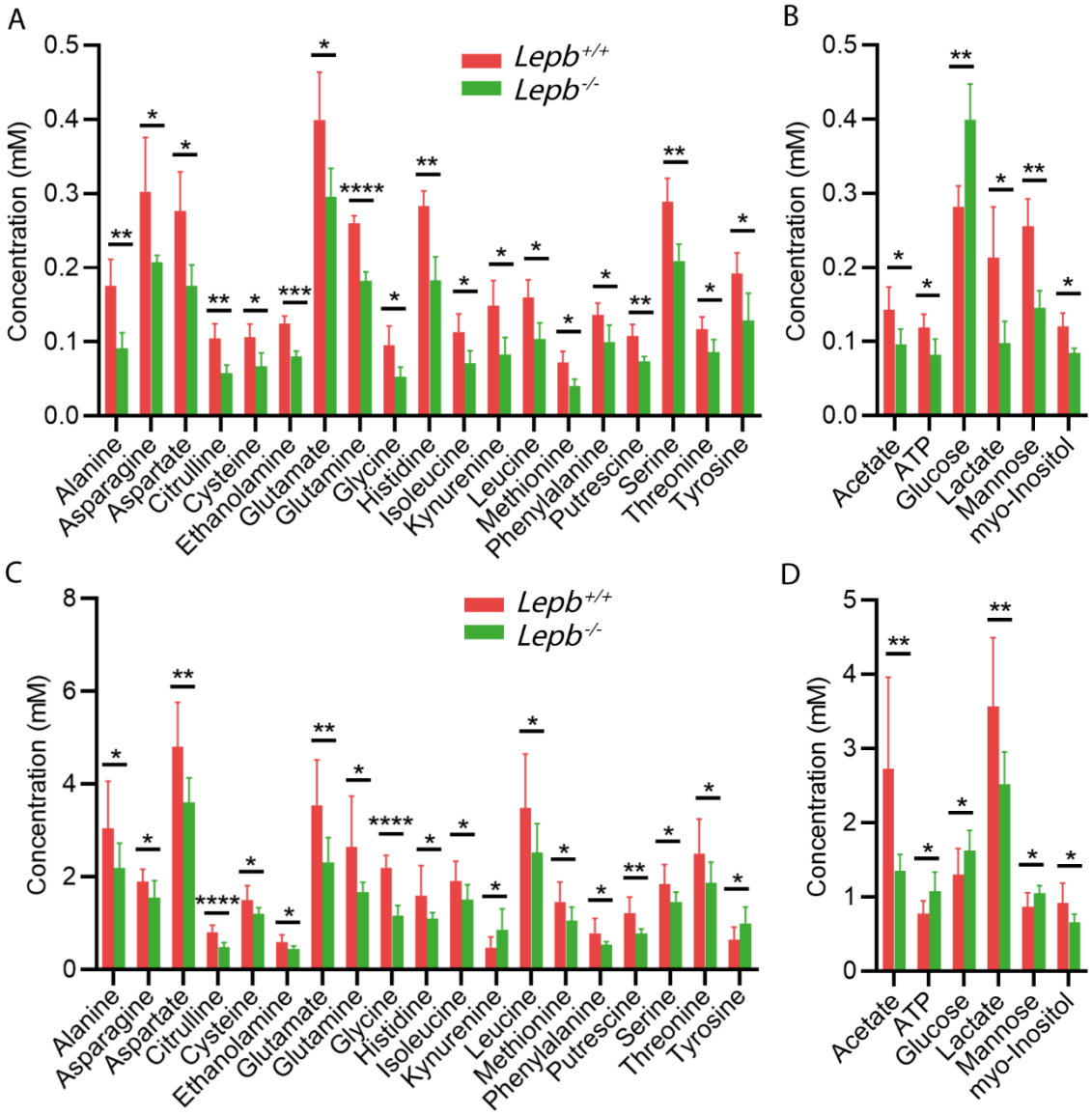

Figure 4. Quantification of the common 25 metabolites that are significantly changed in zebrafish larvae. **A** The concentration of amino acids and amines of wild type and *lepb* mutant in extracted larvae. **B** The concentration of ATP, carbohydrates and organic acids of wild type and *lepb* mutant in extracted larvae. **C** The concentration of amino acids and amines of wild type and *lepb* mutant in intact larvae. **D** The concentration of ATP, carbohydrates and organic acids of wild type and *lepb* mutant in intact larvae. *p < 0.05, **p < 0.01, ***p < 0.0005, ****p < 0.0001.

A core set of metabolites are markers for leptin deficiency in mice and zebrafish larvae

A common set of 13 metabolites were significantly changed in *ob/ob* mice blood, extracted *lepb* mutant and intact *lepb* mutant zebrafish larvae compared to their respective wild type controls (**Figure 5A**). These 13 common metabolites were alanine, citrulline, ethanolamine, glutamine, glycine, histidine, isoleucine, leucine, methionine, phenylalanine, putrescine, serine and threonine

(**Figure 5B**). The concentrations of these 13 metabolites were reduced in a mutant compared to wild types for all the three metabolomic data sets (**Figure 5B**). Of these metabolites, the following 6 are also reported as markers for tuberculosis infection in human, mice and zebrafish larvae based on mass spectrometry: citrulline, ethanolamine, leucine, methionine, phenylalanine, serine and threonine [26].

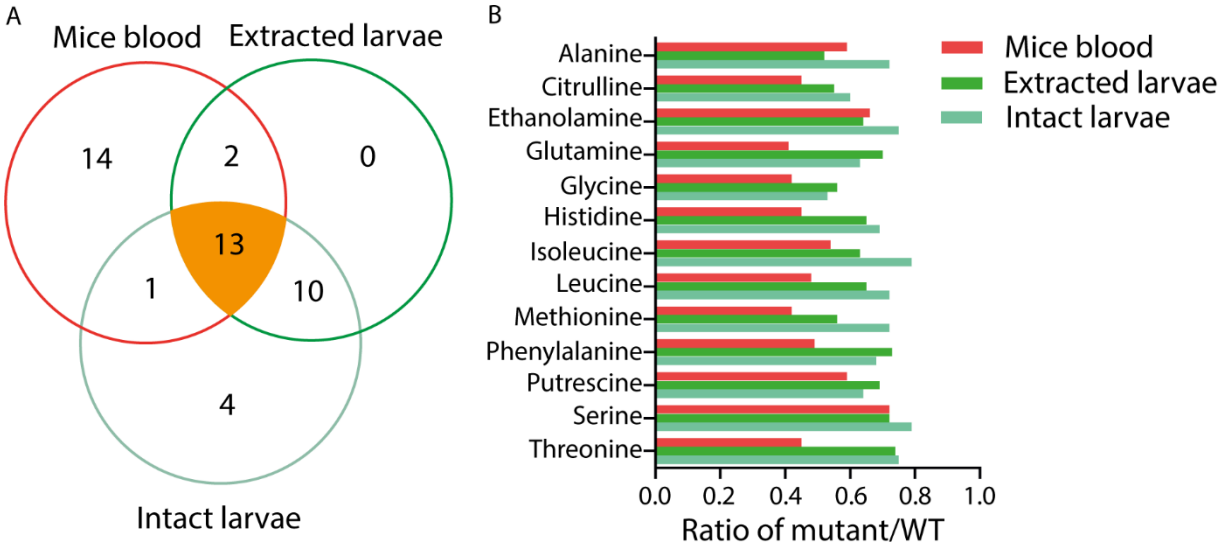

Figure 5. Common biomarkers for leptin deficiency in *ob/ob* mice, extracted and intact zebrafish larvae. **A** A Venn diagram shows that 13 common metabolites are significantly changed after leptin knockdown in mice blood, extracted and intact zebrafish larvae. **B** The ratio of leptin mutant versus wild type of the 13 common metabolites in the three metabolomic datasets.

Lipid profiles of *lepb*-deficient zebrafish larvae

To investigate whether lipid metabolism is influenced by leptin deficiency at the early stage of zebrafish development, lipids were extracted from pooled 5 days post fertilization (dpf) zebrafish larvae in the *lepb* mutant and sibling control groups and then measured with ^{1}H solution NMR (**Figure 6A**). A PLS-DA scores plot of the tetramethylsilane (TMS) normalized spectra showed a clear separation of the lipid profiles of the two groups (**Figure 6B**), which indicated lipid metabolism was altered in *lepb* mutant zebrafish larvae. Twenty-two lipid signals could be assigned from chemical shift 0.5 to 5.5 in the spectra of both groups (**Figure 6A** and **Supplementary Table S2**). Based on the quantification of normalized peaks, we can conclude that saturated lipids were significantly increased in the *lepb* mutant zebrafish larvae (**Figure 6C**, **D**). In addition, the polyunsaturated fatty acid (PUFA) docosahexaenoic acid (DHA) was found in a higher abundance in the mutant group (**Figure 6E**).

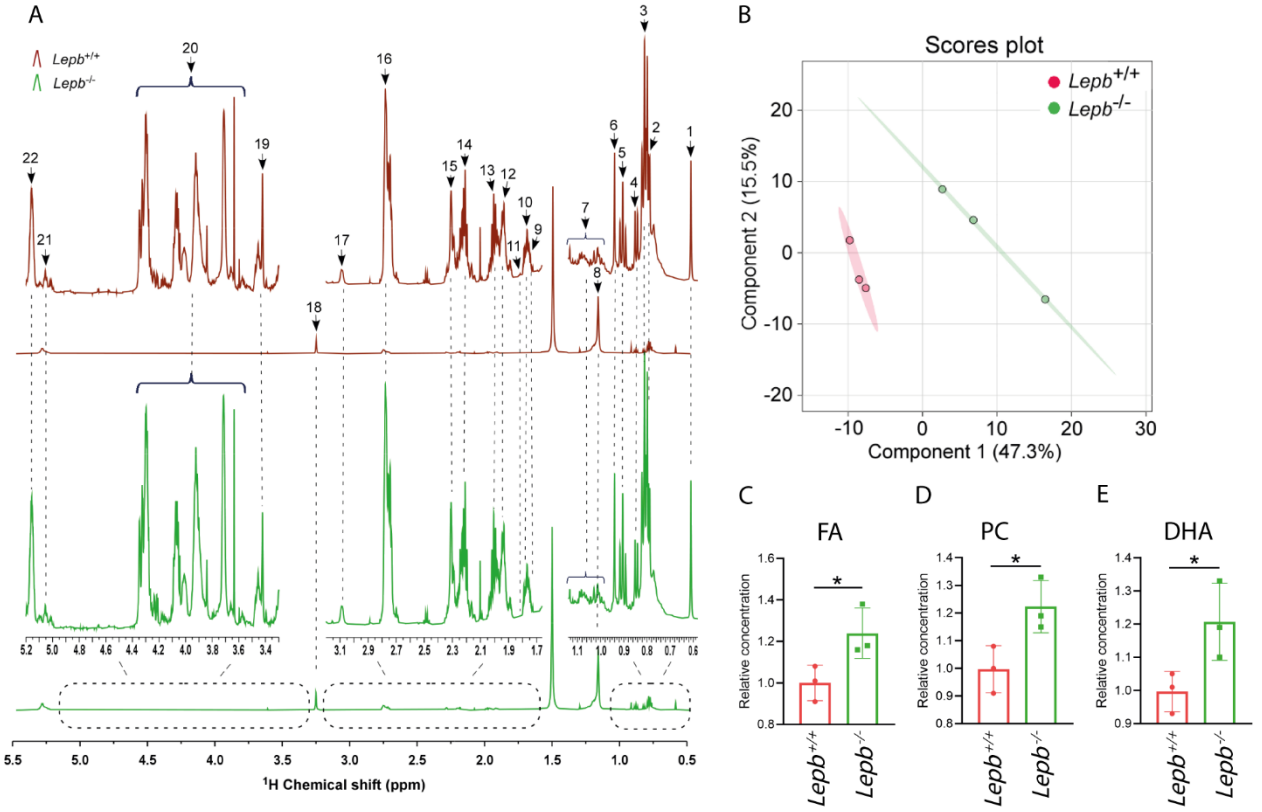

Figure 6. Lipid profiles of *lepb* mutant zebrafish larvae compared to wild type siblings. **A** The representative spectra of total lipid extracts from wild type and *lepb* mutant zebrafish larvae obtained by ^{1}H NMR spectroscopy. The assignments of the peak numbers were shown in Additional file 1: Table S2. *NMR* nuclear magnetic resonance. **B** PLS-DA analysis of *lepb* mutant and wild type zebrafish larvae, n = 3, each replicate represents 105 pooled larvae. *PLS-DA* partial least square discriminant analysis. **C** The relative concentration of the signal 14 FA in A. *FA* fatty acids. **D** The relative concentration of the signal 18 PC in A. *PC* phosphatidylcholines. **E** The relative concentration of the signal 15 DHA in A. *DHA* docosahexaenoic acid. *$p < 0.05$.

Deep sequencing of transcriptomes of leptin deficient mice and zebrafish larvae

We investigated the effects of leptin deficiency at the transcriptome level in mice and zebrafish larvae by using deep RNA sequencing methods. Samples were taken from the same experimental groups as used for the metabolomic analysis described above. Mice heads were taken as a body part of interest because of the known classical signaling of leptin in the brain. A volcano plot showed that 5658 genes significantly regulated at a p value < 0.05 in *ob/ob* mice compared to wild type C57BL/6 mice (**Figure 7A**). A recent paper published by Kokaji et al. reported the transcriptomes of mice liver from ten-week-old male *ob/ob* mutant and C57BL/6 wild type mice [13]. The comparison of the two mice liver groups showed 6693 genes significantly regulated at a p value < 0.05 (**Supplementary Figure S4**). The two gene sets encompassing 5658 and 6693 genes of the transcriptomes in mice head and mice liver, respectively, showed an overlap of 1865 genes (**Figure**

7B). Gene ontology (GO) enrichment analysis using DAVID showed a large group of GO terms. In **Figure 7C**, we showed a selected set of GO terms (biological process) with the lowest *p* adjusted values and the highest numbers of genes representatives. The GO term nervous system development was in line with the function of leptin in the brain. The GO enrichment of the overlap sets in **Figure 7B** gave comparable results as with the mouse head GO terms, with the exception of ion transport and nervous system development (**Figure 7C**). This could be explained by the relatively large number of neuronal cells in the head compared to liver.

For zebrafish larvae, there were 2718 genes significantly regulated at a p value < 0.05 in *lepb* mutant zebrafish larvae compared to wild type siblings (**Figure 7E**). We validated the mRNA expression level of a few representative genes in the $lepb^{+/+}$ and $lepb^{-/-}$ zebrafish larvae with qPCR (**Supplementary Figure S5**). The human orthologs of this zebrafish larvae gene set and of the mice head transcriptome *ob/ob* signature set showed an overlap of 470 genes (**Figure 7F**). The GO enrichment analysis of **Figure 7G** showed the top 8 GO terms (biological process) with lowest *p* adjusted values and highest numbers of genes representatives in the signature set of zebrafish larvae (**Figure 7G**). The GO enrichment of the overlap set gave a similar result as in the zebrafish larvae terms with the exception of DNA replication, cell division and mitotic nuclear division. As shown in the **Figure 7C** and **Figure 7G**, one of the top GO terms in the signature set of mice heads, zebrafish larvae and the overlap was proteolysis. We also found the GO term proteolysis to be significantly enriched in the overlap of mice head and liver *ob/ob* signature set (**Figure 7C**). The genes linked to this GO term were proteases which could be classified as aspartyl protease, carboxypeptidase, cysteine protease, metallopeptidase, serine protease, and threonine protease (**Figure 7D**, **H**, **Supplementary Table S3** and **Supplementary Table S4**). The pattern of the enriched gene numbers of those proteases in the signature sets of mice heads and zebrafish was similar in the up or down regulated groups (**Figure 7D**, **H**).

Figure 7 (following page). Transcriptome signature sets of mice and zebrafish larvae. **A** A Volcano plot showing a graphical representation of the significance ($p < 0.05$) in *ob/ob* mice head compared to C57BL/6 mice head. The transcripts with fold change over 1.5 are highlighted in red. Fifteen significant genes in mice head out of the fold change in X axis are excluded to make the graph look well. **B** A Venn diagram showing the comparison of the number of significantly changed genes between *ob/ob* mice head and mice liver published by Kokaji et al. **C** The top eight GO terms of biological process (BP) with lowest *p* adjusted values and highest numbers of genes representatives in mice head and the overlap of B. *GO* gene ontology. **D** Number of genes in classification of GO term proteolysis in the signature set of mice head. **E** A Volcano plot showing a graphical representation of the significance ($p < 0.05$) in *lepb* mutant zebrafish larvae compared to wild type siblings. The transcripts with fold change over 1.5 are highlighted in green. Twenty-two significant genes in zebrafish larvae out of the fold change in X axis are excluded to make the graph look well. **F** A Venn diagram showing the comparison of the number of significantly changed genes from human homologs of the signature gene sets of zebrafish larvae and *ob/ob* mice head. **G** The top eight GO terms of BP with lowest *p* adjusted values and highest numbers of genes representatives in zebrafish larvae and the overlap of F. **H** Number of genes in classification of GO term proteolysis in the signature set of zebrafish larvae.

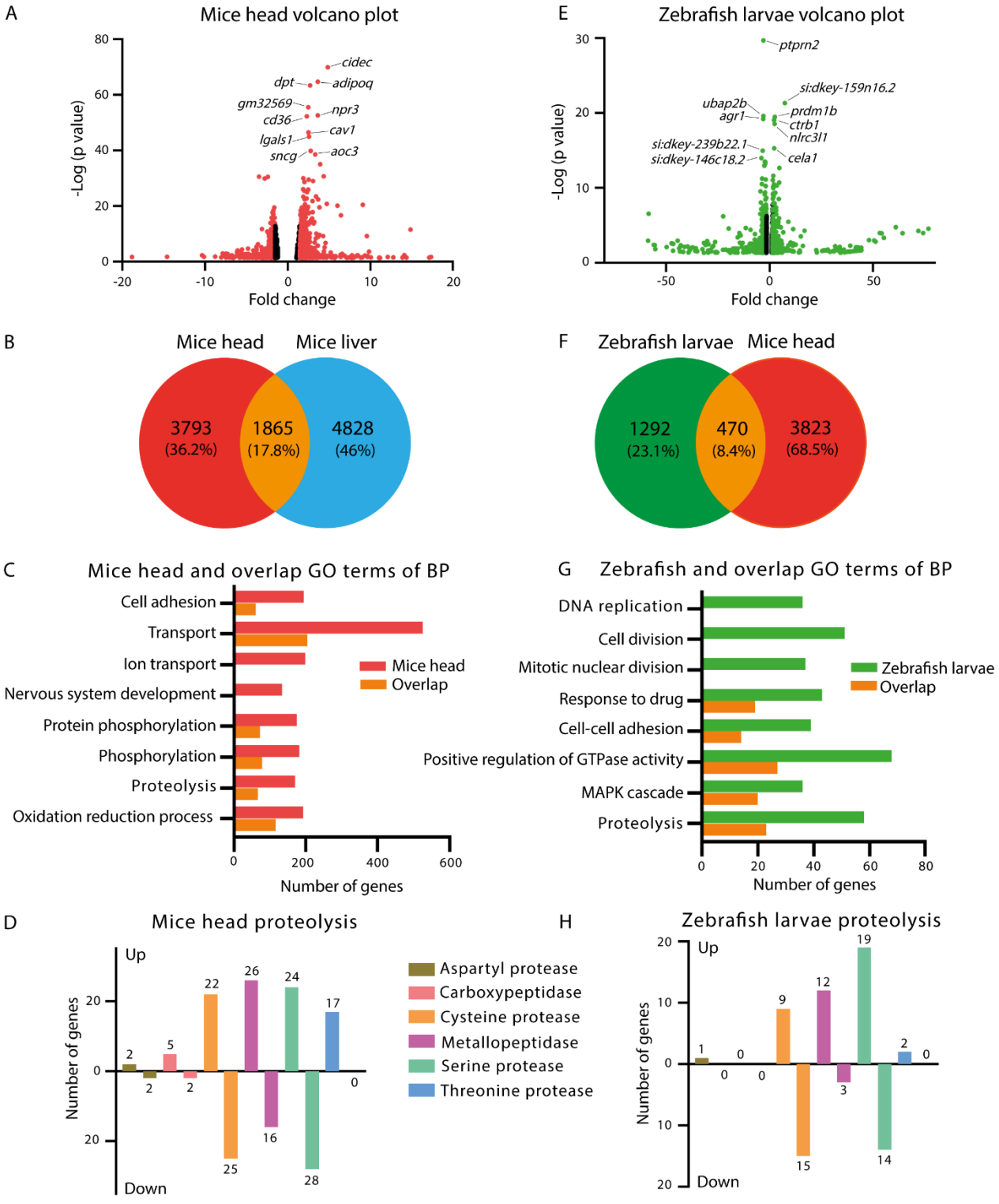
A
Mice head volcano plot
-Log (p value)
Fold change
cidec
dpt
adipoq
gm32569
npr3
cd36
cav1
lgals1
aoc3
sncg
E
Zebrafish larvae volcano plot
-Log (p value)
Fold change
ptprn2
si:dkey-159n16.2
ubap2b
agr1
prdm1b
ctrb1
nlrc3l1
si:dkey-239b22.1
si:dkey-146c18.2
cela1
B
Mice head
Mice liver
3793 (36.2%)
1865 (17.8%)
4828 (46%)
F
Zebrafish larvae
Mice head
1292 (23.1%)
470 (8.4%)
3823 (68.5%)
C
Mice head and overlap GO terms of BP
Cell adhesion
Transport
Ion transport
Nervous system development
Protein phosphorylation
Phosphorylation
Proteolysis
Oxidation reduction process
Mice head
Overlap
Number of genes
G
Zebrafish and overlap GO terms of BP
DNA replication
Cell division
Mitotic nuclear division
Response to drug
Cell-cell adhesion
Positive regulation of GTPase activity
MAPK cascade
Proteolysis
Zebrafish larvae
Overlap
Number of genes
D
Mice head proteolysis
Up
Down
Number of genes
Aspartyl protease
Carboxypeptidase
Cysteine protease
Metallopeptidase
Serine protease
Threonine protease
H
Zebrafish larvae proteolysis
Up
Down
Number of genes

As shown in Figure 6, fatty acids such as DHA were significantly increased in the *lepb* mutant zebrafish larvae compared to wild type siblings. Lipid metabolism disturbance is possibly associated with inflammation [27]. Obese leptin deficient *ob/ob* mice show a low-grade chronic inflammation [28]. Interestingly, we found another common enriched GO term using DAVID (KEGG pathway) in the signature sets of mice head, mice liver and zebrafish larvae was arachidonic acid (ARA) metabolism (**Supplementary Table S5**, **S6**, and **S7**). Arachidonic acid is a pro-inflammatory precursor that can mediate inflammatory responses via transforming into a variety of downstream products such as prostaglandins and leukotrienes. It is also an early indicator of inflammation [27]. Therefore, the human orthologs of the signature sets of mice head, mice liver and zebrafish larvae were projected on the drawn ARA metabolic pathway based on the human wikipathways data using Pathvisio (**Figure 8**). As shown in Figure 8, five genes in the pathway namely *ANXA1, ANXA5, ACSL3, MAP2K6, NFE2L2* were altered in all three datasets. Some other genes were significantly changed in only one or two datasets. However, the majority of the gene expression levels of the three datasets visualized in this pathway were not high (**Supplementary Table S8**). This indicates there might be only mild inflammation in the leptin deficient mice and zebrafish larvae.

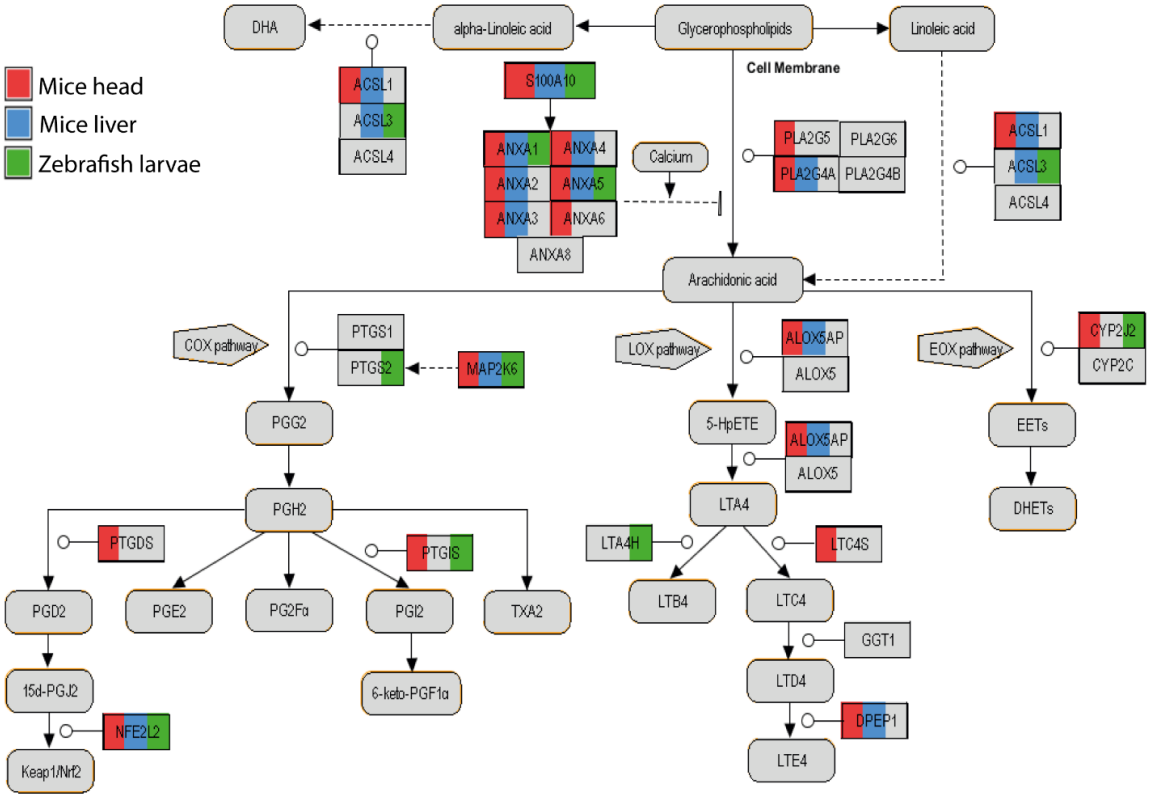

Figure 8. Genes involved in arachidonic acid pathway in human orthologs of the three transcriptome signature sets. Dashed lines means indirect regulation. Red color represents genes significantly changed in *ob/ob* mice head compared to control. Blue color represents genes significantly changed in *ob/ob* mice liver compared to wild type published by Kokaji et al. Green color represents genes significantly changed in *lepb* mutant zebrafish larvae compared to wild type siblings. *COX* cyclo-oxygenase, *LOX* lipoxygenase, *EOX* epoxygenase, *DHA* docosahexaenoic acid.

Discussion

In this study, we have compared the metabolic changes resulting from leptin deficiency in blood of adult mice and extracted as well as intact zebrafish larvae. We studied metabolism using three different technologies: mass spectroscopy (MS), nuclear magnetic resonance (NMR) and high-resolution magic-angle-spinning NMR (HR-MAS NMR) spectrometry. In addition, we have compared the transcriptomic changes resulting from leptin deficiency in *ob/ob* mice heads and published data sets for *ob/ob* mice liver and *lepb* mutant zebrafish larvae using deep RNA sequencing (RNA-seq). These comparisons using very different omics technologies all show a remarkable similarity of the effects of leptin knockdown on the metabolomes and transcriptomes of adult mice and zebrafish larvae. These similarities are surprising because the analyzed samples of this comparative study are in many respects extremely different: (1) Mice and zebrafish are very diverse examples of the vertebrate subphylum, e.g., metabolic rate, body size, body temperature and examined life stages vary greatly. (2) Samples of blood or body tissue, in the case of the mice experiments, are compared with the entire organism in the case of zebrafish larvae. (3) The environmental conditions are different in mice and zebrafish larvae. (4) The genetic variation within the studied populations is highly diverse in zebrafish test samples, whereas a highly inbred population is used in the case of mice. (5) For zebrafish larvae, there is no feeding of the organism involved and embryos are able to develop normally based on their reserves in the yolk until 5dpf. Nevertheless, also in a previous study, we showed remarkable similarities in small metabolite levels occurring in mice blood and zebrafish larvae after infection by mycobacteria [26]. The observed metabolic changes were mainly comprising a reduction of the levels of various amino acids that were also detected in human tuberculosis patients of several ethnical populations [26, 29, 30].

In the present study, we have also included HR-MAS NMR as a non-invasive method for analysis of metabolites in intact embryos. The results confirm the findings obtained with solution-state NMR analysis of extracted tissues. A few metabolites are changed in different directions measured by these two approaches, namely kynurenine, tyrosine, ATP and mannose. They are detected at a decreased level in the mutant group with extracted larvae while an increased level was detected with intact larvae using HR-MAS NMR (**Figure 4**). This might be due to the fact that samples detected by solution-state NMR require extraction and pretreatment. Therefore, solubility with the used extraction solvents plays a key role in the detectable concentration. In addition, some metabolites might get degraded and oxidized during the extraction process. Conversely, these limitations are not present with HR-MAS NMR as it works with natural, unaltered, and intact samples at low temperature. Therefore, it likely better mirrors the underlying biochemical activity and state. In the case of kynurenine, this has been reported to have a significant higher level in blood of tuberculosis patients possibly due to an increased level of the enzyme indoleamine 2,3 dioxygenase 1 (IDO1) that converts tryptophan [29]. Tyrosine and mannose levels were previously also shown to be increased in mice and zebrafish samples using NMR analyses [26, 31]. Considering that zebrafish larvae and mouse and human blood samples are very similar in their metabolite profiles after mycobacterial infection [26], the increased level of kynurenine, tyrosine and mannose seen using

HR-MAS NMR indicates an advantage of detecting metabolites directly in intact embryos using non-invasive HR-MAS NMR over extracted metabolites using solution NMR. However, a disadvantage of HR-MAS NMR compared to solution NMR is its lower resolution capacity for lipids.

As it is well known, rodents with leptin signaling deficiency show a typical phenotype of fat accumulation and obesity. Phospholipids and polyunsaturated fatty acids (PUFAs) including arachidonic acid and eicosapentaenoic acid are significantly increased in plasma and liver of *ob/ob* and *db/db* mice measured by MS [6]. Another study on obese Zucker and lean rats performed by ^{1}H NMR reported increased concentrations of total fatty acids and triglycerides, while the ratio of PUFAs/monounsaturated fatty acids (MUFAs) was decreased in liver and blood of obese rats [11]. In our larval zebrafish *lepb* mutant, we also found that many lipid peaks are generally higher, for instance levels of DHA and phosphatidylcholines are significantly increased in *lepb* mutant larvae compared to the wild type siblings (**Figure 6**). These observations demonstrate that *lepb* deficiency in zebrafish leads to lipid accumulation even at the organismal level at the larval stage. The parental adult *lepb* mutant zebrafish display distinctly more visceral fat compared to wild type sibling fish measured by magnetic resonance imaging (MRI) [32]. As zebrafish larvae before 5dpf only use yolk as their nutrition supply, which comes from the mother, zebrafish larvae offer a promising model to investigate maternal effects of the adult parents on the metabolic state of their offspring in the absence of a feeding regime. We reported previously that adult *lepb* mutant zebrafish display features of type 2 diabetes mellitus (T2DM) including higher glucose levels and develop early signs of diabetic nephropathy [32]. In this study, we also found that the concentration of glucose is significantly elevated in $lepb^{-/-}$ zebrafish larvae compared to $lepb^{+/+}$ group in both ^{1}H NMR and HR-MAS NMR measurements. These observations in adult and larval zebrafish could lead to a better understanding of the effects of parents with gestational diabetes mellitus (GDM) on their offspring. GDM is one type of diabetes characterized by high blood pressure and high levels of glucose occurring only during pregnancy. Children from mothers suffering from GDM have a higher risk to develop obesity and T2DM, but also diabetic complications such as kidney disease. Unfortunately, it is impracticable to investigate maternal effects of GDM on offspring in humans and mammal animal models. Zebrafish larvae are therefore promising to explore the maternal effects of T2DM on their offspring as they develop outside the mother's body [33, 34].

In this study, we demonstrate that 6 of the 13 amino acid metabolites of which the levels are reduced in both mutant *ob/ob* mice and $lepb^{-/-}$ zebrafish larvae are also biomarkers for tuberculosis infection in human, mice and zebrafish larvae [26]. As it is well known, tuberculosis is also called a consumption disease with severe wasting syndrome symptoms at a later stage in TB patients. Therefore, the similarities between the deficiency of leptin and tuberculosis could be related to the occurrence of wasting syndrome in both *ob/ob* mice and *lepb* mutant zebrafish larvae. In this respect, metabolic changes due to leptin deficiency are also relevant for understanding T2DM that is accompanied by wasting syndrome. Of the 30 amino acids levels that we find reduced in the blood of *ob/ob* mice, several have been reported to be also changed in diabetic mice models in other

studies. A decrease in glucogenic amino acids such as alanine, serine, glycine and glutamine indicates a high level of gluconeogenesis in leptin deficient animals. Plasma levels of glycine and serine were found to be significantly decreased in *ob/ob* mice and *db/db* mice compared to their wild type controls [6]. Leucine and isoleucine are two branched- chain amino acids (BCAAs) which are reported to stimulate protein synthesis in muscle [35, 36]. In contrast to our study, BCAAs levels were reported to be increased in *ob/ob* mice and *db/db* mice [6]. However, a study of human plasma samples demonstrated that the concentrations of the BCAAs, alanine and glutamine were significantly decreased in the plasma of T2DM patients compared to healthy volunteer groups [37]. The similarity of amino acid level changes resulting from leptin deficiency between mammals and zebrafish larvae provides the potential utility of common metabolites as biomarkers for both diabetic parents and their offspring by providing prognostic markers for the early identification of the risks of GDM.

The similarities in changes in metabolite levels resulting from leptin deficiency in different model organisms provide a way to further investigate the mechanism underlying these changes. In a first step towards further functional studies, we investigated the effect of leptin deficiency on the transcriptomic level. Studies have shown that wasting syndrome occurred in obese animals as evidenced by muscle mass reduction was due to the activation of proteolytic pathways such as the caspase-3 and the ubiquitin-proteasome proteolytic pathways [38, 39]. We also observed the gene ontology (GO) term proteolysis as one of the top GO terms in the transcriptome signature sets of *ob/ob* mice heads compared to wild type lean mice heads. This GO term was also enriched in the overlap set of this signature set with a signature set that we derived from a published liver transcriptome study of *ob/ob* mice compared to wild type mice (**Figure 7C**). Genes involved in proteolysis can be classified as six types of proteases (**Figure 7D**). Multiple proteolytic pathways are shown to be involved in wasting syndrome, including the following enzyme families: cysteine proteases such as calpains, cathepsins, caspases, ubiquitin peptidase families, metallopeptidases, serine proteases and threonine proteases such as proteasome subunit families [40]. Similar to the results obtained with the *ob/ob* mice body parts, we found that the expression levels of the genes encoding these proteases are significantly changed in *lepb* mutant zebrafish larvae compared to their wild type siblings (**Figure 7H**). This is an indication that the *lepb* mutation leads to wasting syndrome even at an early stage of zebrafish larval development. It has been reported that amino acids are key regulators of protein turnover [41] and that the depletion of amino acids stimulates proteolysis in differentiated muscle cells [42]. The mechanisms underlying the observed reduced levels of amino acids in *ob/ob* mice and *lepb* mutant zebrafish larvae remains to be determined, but could be explained by protein degradation. The significant decrease of many amino acids in *ob/ob* mice and *lepb* mutant zebrafish might be a trigger for protein degradation to compensate for the loss of these amino acids.

In zebrafish larvae, both saturated fatty acids and polyunsaturated fatty acid DHA are increased in the *lepb* mutant group. DHA is an omega-3 fatty acid which is a precursor of eicosanoids such as resolvins and protectins with potential anti-inflammatory activity [43]. In contrast, omega-6 PUFA

arachidonic acid (ARA) is a key precursor for eicosanoids such as prostaglandins, thromboxanes and leukotrienes which mediate inflammatory response [44]. Peak 11 of the spectra (**Figure 6A**) could represent the PUFA arachidonic acid. However, the relatively low abundance and the overlap with the peak of eicosapentaenoic acid (EPA) made it hard to quantify the concentration in the two groups. In zebrafish larvae, genes such as *PTGS2*, *PTGIS*, involved in the generation of prostaglandins in the cyclo-oxygenase (COX) pathway are downregulated in *lepb*$^{-/-}$ compared to the *lepb*$^{+/+}$ group (**Figure 8** and **Supplementary Table S8**). This might be the result of the anti-inflammatory effect of an increased level of DHA observed in *lepb* mutant zebrafish larvae. In *ob/ob* mice head and liver, genes like *PLA2G4A*, *ALOX5AP*, *DPEP1* involved in the release of ARA from cell membrane and lipoxygenase (LOX) pathway are significantly upregulated (**Figure 8** and **Supplementary Table S8**). Therefore, more leukotrienes are expected to be produced, which leads to a potential inflammatory state. This is consistent with the generally accepted concept that obesity and type II diabetes are accompanied with chronic, low-grade inflammation [45]. This is in line with the previously shown correlation of leptin deficiency and diabetes with a higher susceptibility to tuberculosis [46]. Furthermore, it has been shown that zebrafish larvae and humans respond in a very similar way to infection with mycobacteria, for instance in the activation of the prostaglandin pathway [47, 48]. Therefore, the opportunities for future studies of the common mechanism underlying wasting syndrome in various disease such as T2DM and infectious disease in zebrafish larvae are extremely promising for leading to understand human diseases.

Conclusion

Leptin deficiency in adult mice and larval zebrafish leads to highly similar metabolic alterations in amino acid levels. These metabolic changes show the same key features as observed during progression of tuberculosis in human patients, rodents and zebrafish larvae. This conclusion is supported by different technologies, namely MS, solution-state NMR and HR-MAS NMR. Moreover, by studying the transcriptome, we found highly similar changes in gene regulation related to proteolysis and arachidonic acid pathways in these two test systems. These results show a remarkable similarity of the effects of leptin knockdown on the metabolomes and transcriptomes of adult mice and zebrafish larvae that might be related to wasting syndrome. Apparently, the metabolic control by leptin is similar in adult and embryonic stages in mammals and fish, respectively.

Material and methods

Biological materials

Mice

Male *ob/ob* mice and lean C57BL/6 wild type mice were obtained from Charles River Laboratories at 6 weeks of age (n=8 per group) and maintained for 8 weeks under specific pathogen free conditions in the animal facility of the Leiden University Medical Center (LUMC). Male mice were chosen because metabolic variation due to the hormonal cycle is limited. Mice were kept on a standard-chow diet with ad libitum access to food and water. One *ob/ob* mouse had to be sacrificed at an early stage due to malocclusion. Body weight of all mice was measured weekly. Mice were sacrificed at week 14 and blood was collected and heads were snap-frozen in liquid nitrogen and stored at -80^{0}C until RNA isolation. Mice heads were taken as a body part of interest because of the known classical signaling of leptin in the brain. Handling of mice was conducted in compliance with European Community Directive 86/609 for the care and use of laboratory animals and in accordance with the regulations set forward by the LUMC animal care committee.

Mouse serum sample preparation

Mouse serum samples were collected from clotted blood tubes and mixed with pre-heated 80% ethanol at a 1:3 ratio (end concentration: 60% ethanol) in polypropylene screwcap tubes. Samples were heated for 10 min at 90°C and subsequently chilled on ice for 10 minutes before centrifugation at 13.000 rpm for 10 minutes at 4°C. Supernatants were harvested and stored at -80°C for LC-MS analysis.

Zebrafish larvae

Zebrafish were handled in compliance with the local animal welfare regulations and maintained according to standard protocols (http://zfin.org). Mutant *lepb*$^{-/-}$ and wild type sibling *lepb*$^{+/+}$ zebrafish lines were generated, screened and raised as described previously [32]. A *lepb* mutant with a 7 base pair deletion encompassing TAGAGGG in exon 2 was used in this study. Zebrafish larvae at 5 dpf from *lepb*$^{-/-}$ and *lepb*$^{+/+}$ groups were collected and stored at -80°C until further analysis. For solution-state NMR measurement, 4 replicate samples per genotype comprised of 105 pooled larvae were taken. From the same batch, 3 replicate samples per group of 15 pooled larvae were used for RNA isolation and transcriptome analysis. For HR-MAS NMR measurement, 3 replicates of 120 pooled larvae were used (each sample was measured three times).

LC–MS/MS

Metabolite levels in mice serum were measured in individual replicates using a targeted LC-MS/MS platform as described before [26, 29]. Subject numbers were randomized and run in 5 batches which included a calibration line, QC samples and blanks. QC samples were analyzed every 10 samples. They were used to assess data quality and to correct for instrument responses.

The amine platform covers amino acids and biogenic amines employing an Accq-Tag derivatization strategy adapted from a previously published protocol [49]. Briefly, 5.0 µL of each sample was spiked with an internal standard solution. Then proteins were precipitated by the addition of MeOH. The supernatant was dried in a speedvac. The residue was reconstituted in borate buffer (pH 8.5) with AQC reagent. 1.0 µL of the reaction mixture was injected into the UPLC-MS/MS system. Chromatographic separation was achieved by an Agilent 1,290 Infinity II LC System on an Accq-Tag Ultra column. The UPLC was coupled to electrospray ionization on a triple quadrupole mass spectrometer (AB SCIEX Qtrap 6500). Analytes were detected in the positive ion mode and monitored in Multiple Reaction Monitoring (MRM) using nominal mass resolution. Acquired data were evaluated using MultiQuant Software for Quantitative Analysis (AB SCIEX, Version 3.0.2). The data are expressed as relative response ratios (target area/ISTD area; unit free) using proper internal standards. For analysis of amino acids, their 13C15N-labeled analogs were used. For other metabolites, the closest-eluting internal standard was employed. In-house developed algorithms were applied using the pooled QC samples to compensate for shifts in the sensitivity of the mass spectrometer over the batches. After quality control correction, metabolite targets complied with the acceptance criteria of RSDqc < 15%. Using this platform, we were able to identify 41 metabolites in blood samples from mice.

MS data analysis

Data was analyzed using the software package MetaboAnalyst 4.0 [50]. MetaboAnalyst offers the possibility to provide automated data reports which we used for archiving data sets. Default settings were used with log transformation and auto scaling of the data for normalization. Naming of the metabolites is based on reference compounds using standard nomenclature of the human metabolome database (https ://www.hmdb.ca/).

^{1}H solution NMR measurement of extracted larvae

For ^{1}H solution NMR spectroscopy, metabolites from pooled zebrafish larvae were extracted according to a previous study [26]. Zebrafish larvae were crushed and 1ml mixture of methanol: water (1:1, v/v) and 1ml chloroform were immediately added to the sample. The mixture was sonicated for 15 minutes and then centrifuged at 5000rpm for 5 minutes. After centrifugation, two layers were formed: the upper layer is methanol and water containing metabolites, the lower layer is chloroform containing lipids. Those two layers were separately collected and evaporated via nitrogen gas flow. The metabolite pellets were resuspended in 600µl of 100mM deuterated phosphate buffer (KD2PO4, PH=7.0) containing 0.02% trimethyl-silylpropanoic acid (TSP) as a reference and was subsequently centrifuged, and the supernatant was analyzed by solution NMR. The lipid pellets were resuspended in 600µl deuterated chloroform containing 0.03% TMS which was used as a reference. Metabolites and lipids in zebrafish larvae were measured with a Bruker DMX 600MHz NMR spectrometer at 4°C equipped with a 5mm inverse triple high-resolution probe with an actively shielded gradient coil. The ^{1}H NMR spectra were accumulated with 65,000

data points, a 2-s relaxation delay, a sweep width of 12.4 kHz, and 256 scans which were required to obtain a satisfactory signal-to-noise ratio.

^{1}H HR-MAS NMR measurement of intact larvae

Metabolic profiling by ^{1}H HR-MAS NMR spectroscopy was performed as adapted from previous studies [51-53]. Zebrafish larvae from *lepb*$^{+/+}$ and *lepb*$^{-/-}$ groups were carefully transferred to a 4-mm zirconium oxide MAS NMR rotor (Bruker BioSpin AG, Switzerland). As a reference (^{1}H chemical shift at 0 ppm), 10µl of 100mM deuterated phosphate buffer (KD_2PO4, PH=7.0) containing 0.1% (w/v) TSP was added to each sample. The rotor was then placed immediately inside the NMR spectrometer.

All HR-MAS NMR experiments were done on a Bruker DMX 600-MHz NMR spectrometer, which was equipped with a 4-mm HR-MAS dual inverse ^{1}H/^{13}C probe with a magic angle gradient and spinning rate of 6 kHz with a proton resonance frequency of 600MHz. Measurements were carried out at a temperature of 277 K using a Bruker BVT3000 control unit. Acquisition and processing of data were done with Bruker TOPSPIN software 2.1 (Bruker Analytische Messtechnik, Germany).

A rotor synchronized Carr–Purcell–Meiboom–Gill (CPMG) pulse sequence with water suppression was used for one-dimensional ^{1}H HR-MAS NMR spectra. Each one-dimensional spectrum was acquired applying a spectral width of 8000 Hz, domain data points of 16k, a number of averages of 512 with 8 dummy scans, a constant receiver gain of 2048, an acquisition time of 2 s, and a relaxation delay of 2 s. The relaxation delay was set to a small value to remove nascent short transverse (T_2) components due to the presence of lipids in intact embryo samples. All spectra were processed by an exponential window function corresponding to a line broadening of 1 Hz and zero-filled before Fourier transformation. NMR spectra were phased manually and automatically baseline corrected using TOPSPIN 2.1. The total analysis time (including sample preparation, optimization of NMR parameters, and data acquisition) of ^{1}H HR-MAS NMR spectroscopy for each sample was approximately 20 min.

NMR analysis

The one-dimensional ^{1}H solution NMR and HR-MAS NMR spectra obtained from *lepb*$^{-/-}$ and *lepb*$^{+/+}$ group were corrected for baseline, phase shifts and reference using the MestReNova software version 11.0 (Mestrelab Research S.L., Santiago de Compostela, Spain). The region of 4.8-4.9 (solution NMR) was excluded from the analysis to remove the water peak. The spectra were then subdivided in the range between 0 and 10 ppm into buckets of 0.04 ppm. The resulting data matrix was saved as the format of script: NMR CSV matrix (transposed) (*.CSV, *.txt). This was then imported into MetaboAnalyst 4.0 for multivariate analysis using PLS-DA. Correlation coefficients with $p < 0.05$ were considered statistically significant. Quantification of metabolites was performed using Chenomx NMR Suite 8.6 (Edmonton, Alberta, Canada), which allowed for qualitative and quantitative analysis of an NMR spectrum by fitting spectral signatures from HMDB database to the respective spectrum. Assignment of peaks was based on the chemical shifts of compounds of

interest in Chenomx software. The concentration of lipids was calculated by comparing the integral peak intensity of the lipids of interest with that of the reference TMS peak [54]. Statistical analysis (t-tests) of the NMR quantification results was performed with GraphPad Prism 8.0.1 (San Diego, CA, USA) and *p*-values < 0.05 were considered significantly.

RNA isolation

Frozen *ob/ob* and C57BL/6 mouse heads (n=4) were thawed in 30 ml of TRIzol Reagent (Life Technologies) and manually crushed in a mortar while zebrafish larvae from *lepb*$^{+/+}$ and *lepb*$^{-/-}$ groups (n=3) were resuspended and crushed in 0.5 ml of TRIzol Reagent. Subsequently, total RNA was extracted in accordance with the manufacturer's instructions. Contaminating genomic DNA was removed using DNase I digestion for 15min at 37°C. RNA concentration was determined by NanoDrop 2000 (Thermo Scientific, the Netherlands). RNA integrity (RIN) was assessed by bioanalyzer (Agilent) and samples with RIN values > 6 were used for further library construction and sequencing.

Deep sequencing

Mice

Deep sequencing of total RNA samples derived from *ob/ob* and lean C57BL/6 mice heads was performed at ZF-screens B.V. (Leiden, the Netherlands) as described in a previous study [55]. A total of 3 µg of RNA was used to generate RNA-seq libraries using the Illumina TruSeq RNA Sample Preparation Kit v2 (Illumina Inc., San Diego, USA). In the manufacturer's instructions two modifications were made: In the adapter ligation step 1 µl instead of 2.5 µl adaptor was used; In the library size selection step, the library fragments were isolated using a double Ampure XP purification with a 0.7x beads to library ratio. The resulting mRNA-seq libraries were sequenced using an Illumina HiSeq2000 instrument according to the manufacturer's description with a read length of 50 nucleotides. Image analysis and base calling were done by the Illumina HCS version 1.15.1. At least 15 million reads were obtained that could be mapped to the mouse genome version GRCm38.

Zebrafish larvae

Deep sequencing of the zebrafish larvae RNA from *lepb*$^{+/+}$ and *lepb*$^{-/-}$ groups was performed by GenomeScan B.V. (Leiden, the Netherlands). The NEBNext Ultra II Directional RNA Library Prep Kit for Illumina (NEB #E7760S/L) was used to process the samples. Briefly, mRNA was isolated from total RNA using oligo-dT magnetic beads. After fragmentation of the mRNA, a cDNA synthesis was performed. This was used for ligation of the sequencing adapters and PCR amplification of the resulting product. The quality and yield after sample preparation was measured with Fragment Analyzer. The size of the resulting products was consistent with the expected size distribution (a broad peak between 300-500 bp). Clustering and DNA sequencing using the NovaSeq6000 was performed according to manufacturer's protocols. A concentration of 1.1 nM of

DNA was used. For the zebrafish larval samples, data sets of paired end reads of 150 nucleotides were obtained with at least 20 million reads of reads that could be mapped to the zebrafish genome version GRCz11.

Deep sequencing data mapping and analysis

Sequencing data of mice heads were aligned and mapped to the mouse genome GRCm38.p6 using Genetiles server [55]. Sequencing data of zebrafish larvae were aligned and mapped to the zebrafish genome GRCz11 using Salmon v1.2.1, and differential gene expression was analyzed using DESeq2 v1.21.1. Gene Ontology (GO) term enrichment and KEGG pathway analysis were performed in DAVID Bioinformatics Resources 6.8 (https://david.ncifcrf.gov/). The arachidonic acid pathway of Figure 8 was drawn in Pathvisio software based on the wikipathways eicosanoid synthesis, eicosanoid metabolism via cytochrome P450 mono-oxygenases (CYP), prostaglandin synthesis, and omega3 and omega6 fatty acids synthesis [56]. Genes MAP2K6 and Nfe2l2 were added to the pathway based on literature [57, 58].

qPCR

Zebrafish larvae cDNA was generated from the same RNA samples of RNAseq by using iScript cDNA synthesis kit (Bio-Rad). qPCR experiment was performed by following a protocol of SsoAdvanced Universal SYBR® Green Supermix kit (Bio-Rad). qPCR measurement was detected on a CFX96 machine (Bio-Rad). The Cq values of targeted genes were normalized to a zebrafish housekeeping gene *Tsp* as the expression level was not changed due to *lepb* mutation. The relative expression level were analyzed by using $2^{-\Delta\Delta Ct}$ method. We selected the representative genes based on the fold change, expression level, *p* adjusted value and the ease to make good primers. The forward and reverse primer sequences of tested genes in zebrafish larvae are showing below. *LO018181.1:* TGAAGCGACTGGGATGCTG/TGGATCTCTTCGTTCAAGGGTT.

Si:dkey-14d8.6: ACTCCTATGATCAGCCCCTG/TTACAGCCAAACTCCCACACC.

Amy2al2: AGCACAACCCAAACACGAAA/CTGAACTCCTCCATAGCCGT.

Tsp: CCTGCCCATTTTCAGTC/TGTTGTTGCCTCTGTTGCTC.

Declarations

Ethics approval

Experiments in mice were performed under ethical license number DEC 14080 (10-07-2014) of Leiden University. Zebrafish lines were handled in accordance with the local animal welfare regulations and maintained according to standard protocols (https://zfin.org). This local regulation serves as the implementation of Guidelines on the protection of experimental animals by the Council of Europe, Directive 86/609/EEC, which allows zebrafish embryos to be used up to the

moment of free-living (5 days after fertilization). Since embryos used in this study were no more than 5 days old, no license is required by the Council of Europe (1986), Directive 86/609/EEC or the Leiden University ethics committee.

Consent for publication

Not applicable

Availability of data and materials

All data generated or analyzed during this study are included in this published article and its supplementary information files.

Competing interests

The authors declare that they have no competing interests.

Funding

Y. Ding and J. He are funded by China Scholarship Council. M.N.H. Eeza is funded by the Deutscher Akademischer Austauschdienst (DAAD).

Authors' contributions

YD: Conceptualization, Methodology, Statistic analysis, Experimental and bioinformatic investigation, Visualization, Writing - Original Draft. MC.H: Resources, Experimental investigation, Writing - Review & Editing. GFC: bioinformatic investigation. JH, NN, AC.H and MN.H.E: Experimental investigation. A.A: Conceptualization, Methodology, Supervision, Writing - Review & Editing. TH and JM: Resources. HP.S: Initialization of the study, Conceptualization, Bioinformatic investigation, Supervision, Writing - Review & Editing, Project administration, Funding acquisition. All authors have read and approved the final version of the manuscript.

Acknowledgements

We thank Alfons Lefeber helping measuring samples with solution-state NMR. Y. Ding and J. He acknowledge the support of China Scholarship Council for fellowship. M.N.H. Eeza acknowledges the support by the Deutscher Akademischer Austauschdienst (DAAD) for fellowship.

References

[1] Zhang Y, Proenca R, Maffei M, Barone M, Leopold L, Friedman JM. Positional cloning of the mouse obese gene and its human homologue. Nature 1994;372(6505):425-32.

[2] Perakakis N, Farr OM, Mantzoros CS. Leptin in Leanness and Obesity: JACC State-of-the-Art Review. Journal of the American College of Cardiology 2021;77(6):745-60.

[3] Paz-Filho G, Mastronardi C, Delibasi T, Wong M-L, Licinio J. Congenital leptin deficiency: diagnosis and effects of leptin replacement therapy. Arquivos Brasileiros de Endocrinologia & Metabologia 2010;54:690-7.

[4] Meehan CA, Cochran E, Kassai A, Brown RJ, Gorden P. Metreleptin for injection to treat the complications of leptin deficiency in patients with congenital or acquired generalized lipodystrophy. Expert Rev Clin Pharmacol 2016;9(1):59-68.

[5] Wang B, Chandrasekera PC, Pippin JJ. Leptin- and leptin receptor-deficient rodent models: relevance for human type 2 diabetes. Current diabetes reviews 2014;10(2):131-45.

[6] Giesbertz P, Padberg I, Rein D, Ecker J, Hofle AS, Spanier B, et al. Metabolite profiling in plasma and tissues of ob/ob and db/db mice identifies novel markers of obesity and type 2 diabetes. Diabetologia 2015;58(9):2133-43.

[7] Won EY, Yoon MK, Kim SW, Jung Y, Bae HW, Lee D, et al. Gender-specific metabolomic profiling of obesity in leptin-deficient ob/ob mice by 1H NMR spectroscopy. PLoS One 2013;8(10):e75998.

[8] Gogiashvili M, Edlund K, Gianmoena K, Marchan R, Brik A, Andersson JT, et al. Metabolic profiling of ob/ob mouse fatty liver using HR-MAS (1)H-NMR combined with gene expression analysis reveals alterations in betaine metabolism and the transsulfuration pathway. Anal Bioanal Chem 2017;409(6):1591-606.

[9] Gipson GT, Tatsuoka KS, Ball RJ, Sokhansanj BA, Hansen MK, Ryan TE, et al. Multi-platform investigation of the metabolome in a leptin receptor defective murine model of type 2 diabetes. Mol Biosyst 2008;4(10):1015-23.

[10] Connor SC, Hansen MK, Corner A, Smith RF, Ryan TE. Integration of metabolomics and transcriptomics data to aid biomarker discovery in type 2 diabetes. Mol Biosyst 2010;6(5):909-21.

[11] Serkova NJ, Jackman M, Brown JL, Liu T, Hirose R, Roberts JP, et al. Metabolic profiling of livers and blood from obese Zucker rats. J Hepatol 2006;44(5):956-62.

[12] Perry RJ, Wang Y, Cline GW, Rabin-Court A, Song JD, Dufour S, et al. Leptin Mediates a Glucose-Fatty Acid Cycle to Maintain Glucose Homeostasis in Starvation. Cell 2018;172(1-2):234-48 e17.

[13] Kokaji T, Hatano A, Ito Y, Yugi K, Eto M, Morita K, et al. Transomics analysis reveals allosteric and gene regulation axes for altered hepatic glucose-responsive metabolism in obesity. Science Signaling 2020;13(660):eaaz1236.

[14] Gorissen M, Bernier NJ, Nabuurs SB, Flik G, Huising MO. Two divergent leptin paralogues in zebrafish (Danio rerio) that originate early in teleostean evolution. J Endocrinol 2009;201(3):329-39.

[15] Prokop JW, Duff RJ, Ball HC, Copeland DL, Londraville RL. Leptin and leptin receptor: analysis of a structure to function relationship in interaction and evolution from humans to fish. Peptides 2012;38(2):326-36.

[16] Araújo JR, Keating E, Martel F. Impact of Gestational Diabetes Mellitus in the Maternal-to-Fetal Transport of Nutrients. Current Diabetes Reports 2015;15(2):1.

[17] Guelfi KJ, Ong MJ, Li S, Wallman KE, Doherty DA, Fournier PA, et al. Maternal circulating adipokine profile and insulin resistance in women at high risk of developing gestational diabetes mellitus. Metabolism 2017;75:54-60.

[18] Kampmann FB, Thuesen ACB, Hjort L, Bjerregaard AA, Chavarro JE, Frystyk J, et al. Increased leptin, decreased adiponectin and FGF21 concentrations in adolescent offspring of women with gestational diabetes. European Journal of Endocrinology 2019;181(6):691.

[19] Radaelli T, Varastehpour A, Catalano P, Hauguel-de Mouzon S. Gestational Diabetes Induces Placental Genes for Chronic Stress and Inflammatory Pathways. Diabetes 2003;52(12):2951-8.

[20] Yamashita H, Shao J, Ishizuka T, Klepcyk PJ, Muhlenkamp P, Qiao L, et al. Leptin Administration Prevents Spontaneous Gestational Diabetes in Heterozygous Leprdb/+ Mice: Effects on Placental Leptin and Fetal Growth*. Endocrinology 2001;142(7):2888-97.

[21] Audira G, Sarasamma S, Chen JR, Juniardi S, Sampurna BP, Liang ST, et al. Zebrafish Mutants Carrying Leptin a (lepa) Gene Deficiency Display Obesity, Anxiety, Less Aggression and Fear, and Circadian Rhythm and Color Preference Dysregulation. Int J Mol Sci 2018;19(12).

[22] He J, Ding Y, Nowik N, Jager C, Eeza MNH, Alia A, et al. Leptin deficiency affects glucose homeostasis and results in adiposity in zebrafish. Journal of Endocrinology 2021;249(2):125-34.

[23] Michel M, Page-McCaw PS, Chen W, Cone RD. Leptin signaling regulates glucose homeostasis, but not adipostasis, in the zebrafish. Proc Natl Acad Sci U S A 2016;113(11):3084-9.

[24] Marín-Juez R, Jong-Raadsen S, Yang S, Spaink HP. Hyperinsulinemia induces insulin resistance and immune suppression via Ptpn6/Shp1 in zebrafish. Journal of Endocrinology 2014;222(2):229.

[25] Menni C, Fauman E, Erte I, Perry JR, Kastenmuller G, Shin SY, et al. Biomarkers for type 2 diabetes and impaired fasting glucose using a nontargeted metabolomics approach. Diabetes 2013;62(12):4270-6.

[26] Ding Y, Raterink RJ, Marin-Juez R, Veneman WJ, Egbers K, van den Eeden S, et al. Tuberculosis causes highly conserved metabolic changes in human patients, mycobacteria-infected mice and zebrafish larvae. Sci Rep 2020;10(1):11635.

[27] Sztolsztener K, Chabowski A, Harasim-Symbor E, Bielawiec P, Konstantynowicz-Nowicka K. Arachidonic Acid as an Early Indicator of Inflammation during Non-Alcoholic Fatty Liver Disease Development. Biomolecules 2020;10(8).

[28] Sáinz N, Rodríguez A, Catalán V, Becerril S, Ramírez B, Gómez-Ambrosi J, et al. Leptin Administration Downregulates the Increased Expression Levels of Genes Related to Oxidative Stress and Inflammation in the Skeletal Muscle of ob/ob Mice. Mediators of Inflammation 2010;2010:784343.

[29] Vrieling F, Alisjahbana B, Sahiratmadja E, van Crevel R, Harms AC, Hankemeier T, et al. Plasma metabolomics in tuberculosis patients with and without concurrent type 2 diabetes at diagnosis and during antibiotic treatment. Sci Rep 2019;9(1):18669.

[30] Weiner J, 3rd, Maertzdorf J, Sutherland JS, Duffy FJ, Thompson E, Suliman S, et al. Metabolite changes in blood predict the onset of tuberculosis. Nat Commun 2018;9(1):5208.

[31] Shin J-H, Yang J-Y, Jeon B-Y, Yoon YJ, Cho S-N, Kang Y-H, et al. 1H NMR-based Metabolomic Profiling in Mice Infected with Mycobacterium tuberculosis. Journal of Proteome Research 2011;10(5):2238-47.

[32] He J, Ding Y, Nowik N, Jager C, H. Eeza MN, Alia A, et al. Leptin deficiency affects glucose homeostasis and results in adiposity in zebrafish. Journal of Endocrinology 2021.

[33] Pelegri F. Maternal factors in zebrafish development. Developmental Dynamics 2003;228(3):535-54.
[34] Lee MT, Bonneau AR, Giraldez AJ. Zygotic genome activation during the maternal-to-zygotic transition. Annu Rev Cell Dev Biol 2014;30:581-613.
[35] O'Connell TM. The complex role of branched chain amino acids in diabetes and cancer. Metabolites 2013;3(4):931-45.
[36] Anthony JC, Reiter AK, Anthony TG, Crozier SJ, Lang CH, MacLean DA, et al. Orally Administered Leucine Enhances Protein Synthesis in Skeletal Muscle of Diabetic Rats in the Absence of Increases in 4E-BP1 or S6K1 Phosphorylation. Diabetes 2002;51(4):928-36.
[37] van Doorn M, Vogels J, Tas A, van Hoogdalem EJ, Burggraaf J, Cohen A, et al. Evaluation of metabolite profiles as biomarkers for the pharmacological effects of thiazolidinediones in Type 2 diabetes mellitus patients and healthy volunteers. Br J Clin Pharmacol 2007;63(5):562-74.
[38] Sishi B, Loos B, Ellis B, Smith W, du Toit EF, Engelbrecht AM. Diet-induced obesity alters signalling pathways and induces atrophy and apoptosis in skeletal muscle in a prediabetic rat model. Exp Physiol 2011;96(2):179-93.
[39] Wang X, Hu Z, Hu J, Du J, Mitch WE. Insulin resistance accelerates muscle protein degradation: Activation of the ubiquitin-proteasome pathway by defects in muscle cell signaling. Endocrinology 2006;147(9):4160-8.
[40] Pasiakos SM, Carbone JW. Assessment of skeletal muscle proteolysis and the regulatory response to nutrition and exercise. IUBMB Life 2014;66(7):478-84.
[41] Kadowaki M, Kanazawa T. Amino Acids as Regulators of Proteolysis. The Journal of Nutrition 2003;133(6):2052S-6S.
[42] Bechet D, Tassa A, Combaret L, Taillandier D, Attaix D. Regulation of skeletal muscle proteolysis by amino acids. J Ren Nutr 2005;15(1):18-22.
[43] Yan Y, Jiang W, Spinetti T, Tardivel A, Castillo R, Bourquin C, et al. Omega-3 Fatty Acids Prevent Inflammation and Metabolic Disorder through Inhibition of NLRP3 Inflammasome Activation. Immunity 2013;38(6):1154-63.
[44] Kuehl F, Egan R. Prostaglandins, arachidonic acid, and inflammation. Science 1980;210(4473):978-84.
[45] Hotamisligil GS. Inflammation and metabolic disorders. Nature 2006;444(7121):860-7.
[46] Dooley KE, Chaisson RE. Tuberculosis and diabetes mellitus: convergence of two epidemics. The Lancet Infectious Diseases 2009;9(12):737-46.
[47] Tobin DM, Roca FJ, Ray JP, Ko DC, Ramakrishnan L. An enzyme that inactivates the inflammatory mediator leukotriene b4 restricts mycobacterial infection. PLoS One 2013;8(7):e67828.
[48] Tobin David M, Roca Francisco J, Oh Sungwhan F, McFarland R, Vickery Thad W, Ray John P, et al. Host Genotype-Specific Therapies Can Optimize the Inflammatory Response to Mycobacterial Infections. Cell 2012;148(3):434-46.
[49] Noga MJ, Dane A, Shi S, Attali A, van Aken H, Suidgeest E, et al. Metabolomics of cerebrospinal fluid reveals changes in the central nervous system metabolism in a rat model of multiple sclerosis. Metabolomics 2012;8(2):253-63.
[50] Chong J, Xia J. Using MetaboAnalyst 4.0 for Metabolomics Data Analysis, Interpretation, and Integration with Other Omics Data. Methods Mol Biol 2020;2104:337-60.

[51] Berry JP, Roy U, Jaja-Chimedza A, Sanchez K, Matysik J, Alia A. High-Resolution Magic Angle Spinning Nuclear Magnetic Resonance of Intact Zebrafish Embryos Detects Metabolic Changes Following Exposure to Teratogenic Polymethoxyalkenes from Algae. Zebrafish 2016;13(5):456-65.

[52] Roy U, Conklin L, Schiller J, Matysik J, Berry JP, Alia A. Metabolic profiling of zebrafish (Danio rerio) embryos by NMR spectroscopy reveals multifaceted toxicity of beta-methylamino-L-alanine (BMAA). Sci Rep 2017;7(1):17305.

[53] Zuberi Z, Eeza MNH, Matysik J, Berry JP, Alia A. NMR-Based Metabolic Profiles of Intact Zebrafish Embryos Exposed to Aflatoxin B1 Recapitulates Hepatotoxicity and Supports Possible Neurotoxicity. Toxins (Basel) 2019;11(5).

[54] van Amerongen YF, Roy U, Spaink HP, de Groot HJ, Huster D, Schiller J, et al. Zebrafish brain lipid characterization and quantification by (1)H nuclear magnetic resonance spectroscopy and MALDI-TOF mass spectrometry. Zebrafish 2014;11(3):240-7.

[55] Veneman WJ, de Sonneville J, van der Kolk KJ, Ordas A, Al-Ars Z, Meijer AH, et al. Analysis of RNAseq datasets from a comparative infectious disease zebrafish model using GeneTiles bioinformatics. Immunogenetics 2015;67(3):135-47.

[56] Pico AR, Kelder T, van Iersel MP, Hanspers K, Conklin BR, Evelo C. WikiPathways: Pathway Editing for the People. PLOS Biology 2008;6(7):e184.

[57] Itoh K, Mochizuki M, Ishii Y, Ishii T, Shibata T, Kawamoto Y, et al. Transcription Factor Nrf2 Regulates Inflammation by Mediating the Effect of 15-Deoxy-Δ^{12,14}-Prostaglandin J₂. Molecular and Cellular Biology 2004;24(1):36-45.

[58] Oyeniran C, Tanfin Z. MAPK14 Cooperates with MAPK3/1 to Regulate Endothelin-1-Mediated Prostaglandin Synthase 2 Induction and Survival in Leiomyoma but Not in Normal Myometrial Cells1. Biology of Reproduction 2011;84(3):495-504.

Supplementary materials

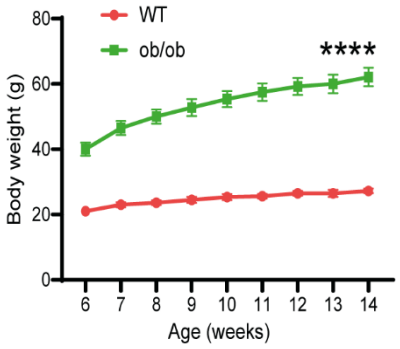

Supplementary Figure S1. Body weight of *ob/ob* and wild type C57BL/6 mice from week 6 to week 14. WT: Wild type. ****p < 0.0001.

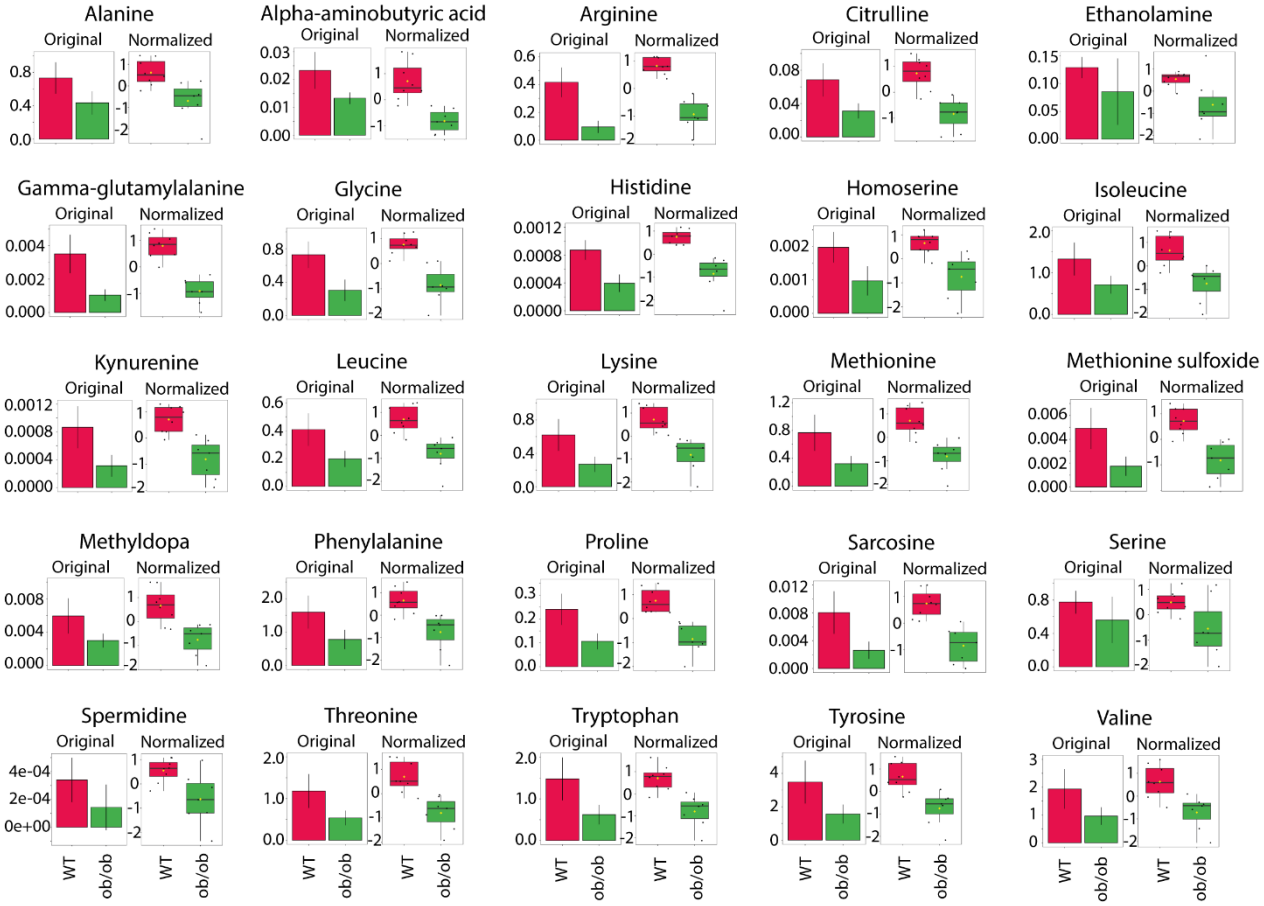

Supplementary Figure S2. Quantifications of the common biomarkers of the blood from *ob/ob* mice and wild type mice. The original and normalized value of the 25 biomarkers showing in Figure 1C were significantly (p < 0.05) decreased in *ob/ob* mice blood compared to wild type mice blood. Sample normalization was performed automatically by chosen log transformation and auto scaling in MetaboAnalyst 4.0. WT: Wild type.

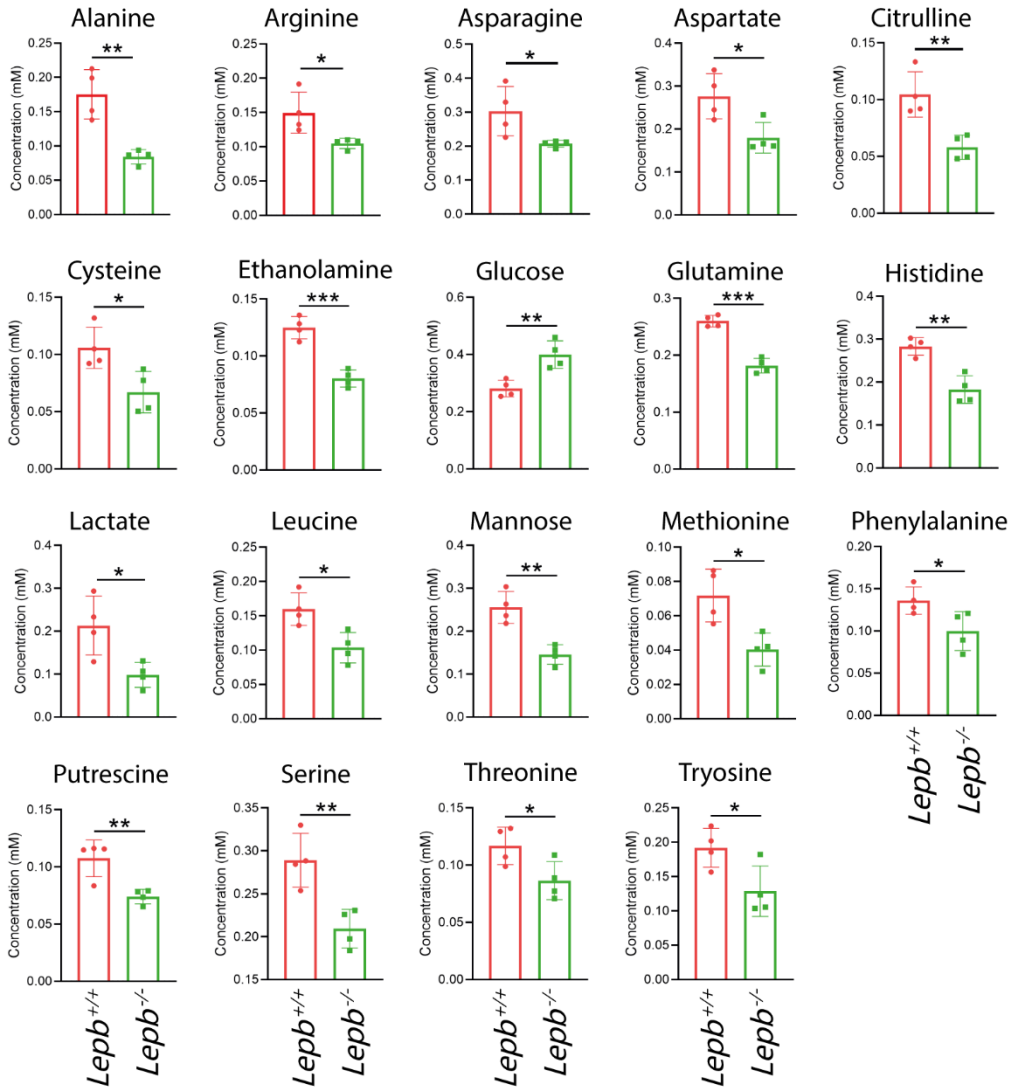

Supplementary Figure S3. Quantifications of the common biomarkers from extracted *lepb* mutant zebrafish larvae and wild type siblings. Quantifications of the common 19 biomarkers in Figure 2C that are significantly changed in *lepb* mutant zebrafish larvae versus wild type. WT: Wild type. *$p < 0.05$, **$p < 0.01$, ***$p < 0.0001$.

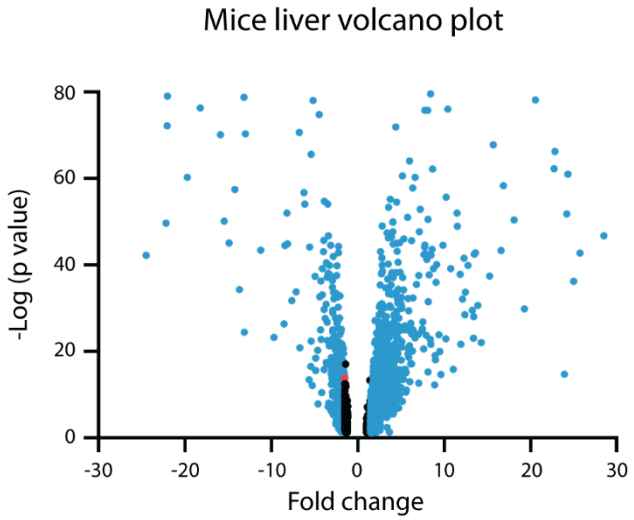

Supplementary Figure S4. A Volcano plot of published transcriptomes of mice liver. A Volcano plot showing a graphical representation of the significance ($p < 0.05$) in *ob/ob* mice liver compared to C57BL/6 mice liver. The transcripts with fold change over 1.5 are highlighted in blue. Thirty-six significant genes in mice liver out of the fold change in X axis were excluded to make the graph look well.

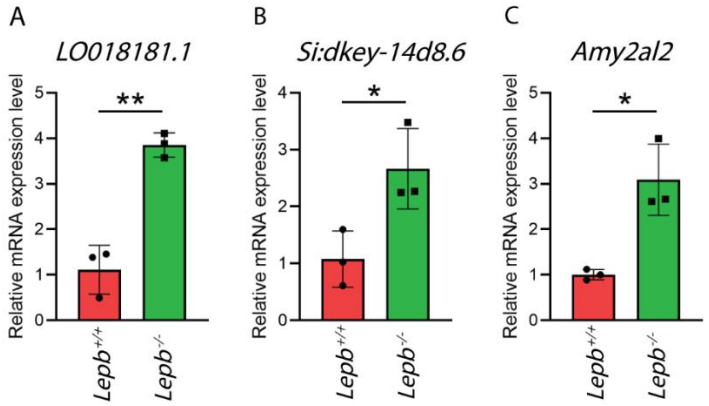

Supplementary Figure S5. Validation of gene mRNA expression level from RNAseq data in Zebrafish larvae using qPCR. A. Gene *LO018181.1*, ensembl code ENSDARG00000113971**. B**. Gene *Si:dkey-14d8.5*, ensembl code ENSDARG00000045835. **C.** Gene *Amy2al2*, ensembl code, ENSDARG00000009443. *$p < 0.05$, **$p < 0.01$.

Supplementary Table S1

Metabolite	HMDB code	FC	*p* value
Arginine	HMDB00517	0.23	3.00E-06
Hydroxyproline	HMDB00725	0.29	6.00E-06
Gamma-glutamylalanine	HMDB06248	0.30	1.00E-05
Glutamine	HMDB00641	0.41	5.00E-05
Histidine	HMDB00177	0.45	1.00E-04
Glycine	HMDB00123	0.42	1.00E-04
Proline	HMDB00162	0.44	1.00E-04
Sarcosine	HMDB00271	0.33	2.00E-04
Citrulline	HMDB00904	0.45	3.00E-04
Methionine sulfoxide	HMDB02005	0.36	3.00E-04
2-Aminobutyrate	HMDB00510	0.32	4.00E-04
Lysine	HMDB00182	0.43	5.00E-04

Alpha-aminobutyric acid	HMDB00452	0.57	5.00E-04
Methionine	HMDB00696	0.42	5.00E-04
Kynurenine	HMDB00183	0.36	5.00E-04
Tryptophan	HMDB00929	0.42	6.00E-04
Hydroxylysine	HMDB00450	0.46	7.00E-04
Leucine	HMDB00687	0.48	7.00E-04
Threonine	HMDB00167	0.45	8.00E-04
Tyrosine	HMDB00158	0.45	2.00E-03
Methyldopa	HMDB11754	0.50	2.00E-03
Phenylalanine	HMDB00159	0.49	2.00E-03
Isoleucine	HMDB00172	0.54	2.00E-03
Homoserine	HMDB00719	0.49	2.00E-03
Valine	HMDB00883	0.50	4.00E-03
Alanine	HMDB00161	0.59	5.00E-03
Spermidine	HMDB01257	0.42	2.00E-02
Ethanolamine	HMDB00149	0.66	2.00E-02
Putrescine	HMDB01414	0.59	2.00E-02
Serine	HMDB00187	0.72	4.00E-02

Supplementary Table S1. Ratio of metabolite quantities in blood of *ob/ob* mice compared to the control group. The levels of 30 metabolites are significantly decreased in the *ob/ob* mice compared to the wild type C57BL/6 mice.

Supplementary Table S2

Peak no.	Assignments	Zebrafish larvae	
		Multiplicity	Chemical shifts (ppm) 600MHz
1	Chol (C18)	s	0.62 .. 0.60
2	Chol (C26,27)	dd	0.81 .. 0.78
3	w-6 FA -CH3 (terminal)	d	0.83 .. 0.81
4	Chol (C21)	d	0.86 .. 0.83
5	w-3 FA -CH3 (terminal)	t	0.92 .. 0.89
6	Chol (C19)	s	0.95 .. 0.93
7	Chol	m	1.12 .. 0.98
8	Chol+FA (CH2)	s	1.28 .. 1.15
9	Chol+FA (CH2)	m	1.76 .. 1.73
10	FA (CH2)	bs	1.80 .. 1.76
11	Chol+FA (CH2)	d	1.89 .. 1.88

12	FA (CH2)–Chol	m	1.96 .. 1.91
13	FA (CH2)	quin	2.05 .. 1.96
14	FA (CH2)–Chol	dt	2.25 .. 2.19
15	FA (CH2)–DHA	m	2.33 .. 2.28
16	FA (CH2)–PUFA	dd	2.81 .. 2.72
17	PLs	bs	3.13 .. 3.05
18	PC	s	3.29 .. 3.26
19	Chol (C3)	m	3.49 .. 3.41
20	Phosphotidylglycerol	bm	4.38 .. 3.55
21	Sphingolipids	m	5.11 .. 4.99
	Dolichols		
	Plasmalogens		
22	FA (-CH = CH-) and Chol	m	5.19 .. 5.12

Supplementary Table S2. Overview of assigned lipid signals in Figure 6 from zebrafish larvae. S: singlet, d: doublet, t: triplet, m: multiplet, quin: quintet; dd: double doublet, bs: broad singlet, bm: broad multiplet, Chol: cholesterol, EPA: eicosapentaenoic acid, AA: arachidonic acid, DHA: docosahexaenoic acid, FA: fatty acids, PC: phosphatidylcholine, PLs: phospholipids, PUFA: polyunsaturated fatty acid.

Supplementary Table S3

Mice ID	Mice gene name	Human homolog	Meas/Ctrl or -Ctrl/Meas (scaled)	*p*-value	Classification
ENSMUSG00000070645	Ren1	ENSG00000143839	-2.89	8.16E-04	Aspartic peptidase
ENSMUSG00000032086	Bace1	ENSG00000186318	-1.17	1.60E-03	Aspartic peptidase
ENSMUSG00000007891	Ctsd	ENSG00000117984	1.11	3.43E-02	Aspartic peptidase
ENSMUSG00000058499	Pip		1.48	4.56E-02	Aspartic peptidase
ENSMUSG00000039070	Cpa4	ENSG00000128510	-2.67	3.05E-02	Carboxypeptidase
ENSMUSG00000020841	Cpd	ENSG00000108582	-1.28	4.34E-05	Carboxypeptidase
ENSMUSG00000039007	Cpq	ENSG00000104324	1.22	4.13E-03	Carboxypeptidase
ENSMUSG00000020473	Aebp1	ENSG00000106624	1.24	8.91E-03	Carboxypeptidase
ENSMUSG00000027408	Cpxm1	ENSG00000088882	1.40	2.04E-05	Carboxypeptidase
ENSMUSG00000001865	Cpa3	ENSG00000163751	1.90	9.45E-08	Carboxypeptidase
ENSMUSG00000036596	Cpz	ENSG00000109625	2.20	1.20E-07	Carboxypeptidase
ENSMUSG00000034342	Cbl	ENSG00000110395	-1.64	8.07E-06	Cysteine peptidase
ENSMUSG00000037326	Capn15	ENSG00000103326	-1.35	9.53E-04	Cysteine peptidase
ENSMUSG00000022637	Cblb	ENSG00000114423	-1.18	1.47E-02	Cysteine peptidase
ENSMUSG00000026509	Capn2	ENSG00000162909	1.12	2.24E-02	Cysteine peptidase
ENSMUSG00000001794	Capns1	ENSG00000126247	1.12	3.57E-02	Cysteine peptidase

ENSMUSG00000021939	Ctsb	ENSG00000164733	1.15	4.73E-04	Cysteine peptidase
ENSMUSG00000083282	Ctsf	ENSG00000174080	1.15	2.17E-02	Cysteine peptidase
ENSMUSG00000028015	Ctso	ENSG00000256043	1.25	1.63E-04	Cysteine peptidase
ENSMUSG00000032359	Ctsh	ENSG00000103811	1.25	4.55E-03	Cysteine peptidase
ENSMUSG00000038642	Ctss	ENSG00000163131	1.27	4.31E-04	Cysteine peptidase
ENSMUSG00000054083	Capn12	ENSG00000182472	1.30	3.85E-03	Cysteine peptidase
ENSMUSG00000016256	Ctsz	ENSG00000101160	1.31	6.93E-05	Cysteine peptidase
ENSMUSG00000079418	Atg4a	ENSG00000101844	1.33	1.47E-02	Cysteine peptidase
ENSMUSG00000025888	Casp1	ENSG00000137752	1.37	4.14E-02	Cysteine peptidase
ENSMUSG00000021477	Ctsl	ENSG00000136943	1.45	1.07E-11	Cysteine peptidase
ENSMUSG00000033538	Casp4	ENSG00000137757	1.96	3.68E-03	Cysteine peptidase
ENSMUSG00000028111	Ctsk	ENSG00000143387	2.36	9.17E-08	Cysteine peptidase
ENSMUSG00000035606	Ky	ENSG00000174611	-1.89	1.10E-08	Cysteine peptidase
ENSMUSG00000090115	Usp49	ENSG00000164663	-1.33	6.72E-04	Cysteine peptidase
ENSMUSG00000031010	Usp9x	ENSG00000124486	-1.31	7.73E-05	Cysteine peptidase
ENSMUSG00000051306	Usp42	ENSG00000106346	-1.29	3.12E-03	Cysteine peptidase
ENSMUSG00000056900	Usp13	ENSG00000058056	-1.28	3.14E-04	Cysteine peptidase
ENSMUSG00000042444	Fam63b	ENSG00000128923	-1.26	1.10E-05	Cysteine peptidase
ENSMUSG00000051527	Usp29	ENSG00000131864	-1.25	7.69E-03	Cysteine peptidase
ENSMUSG00000033909	Usp36	ENSG00000055483	-1.23	2.77E-03	Cysteine peptidase
ENSMUSG00000028514	Usp24	ENSG00000162402	-1.20	8.01E-04	Cysteine peptidase
ENSMUSG00000056342	Usp34	ENSG00000115464	-1.19	1.38E-03	Cysteine peptidase
ENSMUSG00000036712	Cyld	ENSG00000083799	-1.17	1.01E-02	Cysteine peptidase
ENSMUSG00000062627	Mysm1	ENSG00000162601	-1.17	3.83E-02	Cysteine peptidase
ENSMUSG00000040455	Usp45	ENSG00000123552	-1.16	3.76E-02	Cysteine peptidase
ENSMUSG00000045210	Vcpip1	ENSG00000175073	-1.16	2.16E-02	Cysteine peptidase
ENSMUSG00000043411	Usp48	ENSG00000090686	-1.16	4.90E-03	Cysteine peptidase
ENSMUSG00000054814	Usp46	ENSG00000109189	-1.15	1.43E-02	Cysteine peptidase
ENSMUSG00000038495	Otud7b	ENSG00000264522	-1.15	2.14E-02	Cysteine peptidase
ENSMUSG00000052917	Senp7	ENSG00000138468	-1.13	4.32E-02	Cysteine peptidase
ENSMUSG00000020124	Usp15	ENSG00000135655	-1.12	4.54E-02	Cysteine peptidase
ENSMUSG00000027363	Usp8	ENSG00000138592	-1.10	3.45E-02	Cysteine peptidase
ENSMUSG00000027364	Usp50	ENSG00000170236	-1.10	4.55E-02	Cysteine peptidase
ENSMUSG00000019124	Scrn1	ENSG00000136193	-1.10	3.06E-02	Cysteine peptidase
ENSMUSG00000028964	Park7	ENSG00000116288	1.12	3.67E-02	Cysteine peptidase
ENSMUSG00000028560	Usp1	ENSG00000162607	1.14	4.06E-02	Cysteine peptidase
ENSMUSG00000029223	Uchl1	ENSG00000154277	1.16	7.50E-03	Cysteine peptidase
ENSMUSG00000050994	Adgb	ENSG00000118492	1.22	2.90E-02	Cysteine peptidase
ENSMUSG00000021190	Lgmn	ENSG00000100600	1.22	4.86E-06	Cysteine peptidase
ENSMUSG00000019850	Tnfaip3	ENSG00000118503	1.32	7.28E-03	Cysteine peptidase
ENSMUSG00000028776	Tinagl1	ENSG00000142910	1.34	9.20E-03	Cysteine peptidase
ENSMUSG00000050345	4930486L24Rik	ENSG00000135047	3.01	2.15E-02	Cysteine peptidase
ENSMUSG00000008438	Adam21	ENSG00000139985	-1.78	3.85E-02	Metallopeptidase

ENSMUSG00000023845	Lnpep	ENSG00000113441	-1.67	1.96E-05	Metallopeptidase
ENSMUSG00000050663	Trhde	ENSG00000072657	-1.64	1.82E-10	Metallopeptidase
ENSMUSG00000053399	Adamts18	ENSG00000140873	-1.59	9.55E-03	Metallopeptidase
ENSMUSG00000006403	Adamts4	ENSG00000158859	-1.57	5.24E-06	Metallopeptidase
ENSMUSG00000073530	Pappa2	ENSG00000116183	-1.55	3.79E-03	Metallopeptidase
ENSMUSG00000028226	Mmp16	ENSG00000156103	-1.45	2.68E-04	Metallopeptidase
ENSMUSG00000022449	Adamts20	ENSG00000173157	-1.42	3.50E-03	Metallopeptidase
ENSMUSG00000040537	Adam22	ENSG00000008277	-1.37	2.55E-09	Metallopeptidase
ENSMUSG00000025964	Adam23	ENSG00000114948	-1.36	2.12E-08	Metallopeptidase
ENSMUSG00000020926	Adam11	ENSG00000073670	-1.29	3.39E-05	Metallopeptidase
ENSMUSG00000011256	Adam19	ENSG00000135074	-1.26	5.04E-03	Metallopeptidase
ENSMUSG00000029436	Mmp17	ENSG00000198598	-1.22	5.86E-05	Metallopeptidase
ENSMUSG00000024299	Adamts10	ENSG00000142303	-1.22	2.72E-02	Metallopeptidase
ENSMUSG00000027612	Mmp24	ENSG00000125966	-1.21	2.12E-03	Metallopeptidase
ENSMUSG00000054693	Adam10	ENSG00000137845	-1.15	1.13E-02	Metallopeptidase
ENSMUSG00000030884	Uqcrc2	ENSG00000140740	1.10	4.75E-02	Metallopeptidase
ENSMUSG00000029017	Pmpcb	ENSG00000105819	1.12	4.74E-02	Metallopeptidase
ENSMUSG00000063931	Pepd	ENSG00000124299	1.13	4.97E-02	Metallopeptidase
ENSMUSG00000020681	Ace	ENSG00000159640	1.20	1.88E-02	Metallopeptidase
ENSMUSG00000031029	Eif3f	ENSG00000175390	1.23	4.69E-05	Metallopeptidase
ENSMUSG00000039062	Anpep	ENSG00000166825	1.24	4.93E-03	Metallopeptidase
ENSMUSG00000024644	Cndp2	ENSG00000133313	1.26	8.50E-05	Metallopeptidase
ENSMUSG00000054555	Adam12	ENSG00000148848	1.27	2.76E-02	Metallopeptidase
ENSMUSG00000036545	Adamts2	ENSG00000087116	1.36	1.14E-03	Metallopeptidase
ENSMUSG00000000957	Mmp14	ENSG00000157227	1.41	3.44E-04	Metallopeptidase
ENSMUSG00000029061	Mmp23	ENSG00000189409	1.52	4.02E-03	Metallopeptidase
ENSMUSG00000025355	Mmp19	ENSG00000123342	1.54	2.63E-05	Metallopeptidase
ENSMUSG00000025473	Adam8	ENSG00000151651	1.56	3.03E-03	Metallopeptidase
ENSMUSG00000029718	Pcolce	ENSG00000106333	1.62	1.11E-07	Metallopeptidase
ENSMUSG00000070867	Trabd2b	ENSG00000269113	1.62	1.78E-05	Metallopeptidase
ENSMUSG00000019278	Dpep1	ENSG00000015413	1.71	2.59E-07	Metallopeptidase
ENSMUSG00000050578	Mmp13	ENSG00000137745	1.85	3.59E-09	Metallopeptidase
ENSMUSG00000031740	Mmp2	ENSG00000087245	1.88	9.13E-05	Metallopeptidase
ENSMUSG00000053687	Dpep2	ENSG00000167261	1.93	3.73E-02	Metallopeptidase
ENSMUSG00000057457	Phex	ENSG00000102174	2.10	1.08E-02	Metallopeptidase
ENSMUSG00000024481	Lvrn	ENSG00000172901	2.20	3.85E-03	Metallopeptidase
ENSMUSG00000022894	Adamts5	ENSG00000154736	2.41	6.19E-20	Metallopeptidase
ENSMUSG00000017737	Mmp9	ENSG00000100985	2.55	4.54E-18	Metallopeptidase
ENSMUSG00000043613	Mmp3	ENSG00000149968	3.40	5.21E-09	Metallopeptidase
ENSMUSG00000049723	Mmp12	ENSG00000262406	9.10	3.43E-21	Metallopeptidase
ENSMUSG00000025917	Cops5	ENSG00000121022	1.17	6.01E-03	Metallopeptidase
ENSMUSG00000063177	Klk1b27		-7.46	1.42E-03	Serine peptidase
ENSMUSG00000063089	Klk1b8		-7.26	2.11E-03	Serine peptidase

ENSMUSG00000030713	Klk7	ENSG00000169035	-6.89	3.68E-02	Serine peptidase
ENSMUSG00000038968	Klk1b16		-5.78	1.85E-03	Serine peptidase
ENSMUSG00000063133	Klk1b1	ENSG00000167751	-5.47	1.90E-03	Serine peptidase
ENSMUSG00000066516	Klk1b21	ENSG00000167751	-4.96	2.68E-03	Serine peptidase
ENSMUSG00000059042	Klk1b9	ENSG00000167751	-4.96	2.09E-03	Serine peptidase
ENSMUSG00000063713	Klk1b24	ENSG00000167751	-4.88	3.06E-03	Serine peptidase
ENSMUSG00000066515	Klk1b3	ENSG00000167751	-4.61	3.70E-03	Serine peptidase
ENSMUSG00000053719	Klk1b26		-4.27	4.73E-03	Serine peptidase
ENSMUSG00000044485	Klk1b11	ENSG00000167751	-4.26	4.65E-03	Serine peptidase
ENSMUSG00000060177	Klk1b22	ENSG00000167751	-4.17	6.65E-03	Serine peptidase
ENSMUSG00000066513	Klk1b4	ENSG00000167751	-4.09	3.66E-03	Serine peptidase
ENSMUSG00000061780	Cfd	ENSG00000197766	-2.40	3.07E-31	Serine peptidase
ENSMUSG00000006179	Prss16	ENSG00000112812	-2.16	2.71E-02	Serine peptidase
ENSMUSG00000016493	Cd46	ENSG00000117335	-1.52	1.26E-03	Serine peptidase
ENSMUSG00000070695	Cntnap5a	ENSG00000155052	-1.51	4.74E-07	Serine peptidase
ENSMUSG00000042453	Reln	ENSG00000189056	-1.42	2.02E-07	Serine peptidase
ENSMUSG00000037129	Tmprss13	ENSG00000137747	-1.38	2.38E-02	Serine peptidase
ENSMUSG00000028979	Masp2	ENSG00000009724	-1.35	5.29E-05	Serine peptidase
ENSMUSG00000032393	Dpp8	ENSG00000074603	-1.29	2.28E-05	Serine peptidase
ENSMUSG00000031995	St14	ENSG00000149418	-1.29	3.87E-02	Serine peptidase
ENSMUSG00000036098	Myrf	ENSG00000124920	-1.27	2.90E-04	Serine peptidase
ENSMUSG00000021587	Pcsk1	ENSG00000175426	-1.21	4.27E-02	Serine peptidase
ENSMUSG00000001229	Dpp9	ENSG00000142002	-1.20	1.20E-03	Serine peptidase
ENSMUSG00000024127	Prepl	ENSG00000138078	-1.19	3.01E-03	Serine peptidase
ENSMUSG00000061576	Dpp6	ENSG00000130226	-1.16	9.53E-03	Serine peptidase
ENSMUSG00000025246	Tbl1x	ENSG00000092377	-1.13	2.86E-02	Serine peptidase
ENSMUSG00000047866	Lonp2	ENSG00000102910	1.14	6.23E-03	Serine peptidase
ENSMUSG00000000278	Scpep1	ENSG00000121064	1.17	3.49E-02	Serine peptidase
ENSMUSG00000006205	Htra1	ENSG00000166033	1.17	2.64E-02	Serine peptidase
ENSMUSG00000017760	Ctsa	ENSG00000064601	1.18	5.18E-04	serine peptidase
ENSMUSG00000024713	Pcsk5	ENSG00000099139	1.22	1.61E-03	Serine peptidase
ENSMUSG00000021822	Plau	ENSG00000122861	1.25	3.64E-02	Serine peptidase
ENSMUSG00000027188	Pamr1	ENSG00000149090	1.27	3.85E-03	Serine peptidase
ENSMUSG00000020323	Prss57	ENSG00000185198	1.46	1.85E-02	Serine peptidase
ENSMUSG00000033491	Prss35	ENSG00000146250	1.51	1.57E-03	Serine peptidase
ENSMUSG00000000392	Fap	ENSG00000078098	1.54	1.07E-06	Serine peptidase
ENSMUSG00000055172	C1ra	ENSG00000159403	1.59	2.50E-05	Serine peptidase
ENSMUSG00000098470	C1rb	ENSG00000159403	1.70	1.63E-04	Serine peptidase
ENSMUSG00000038521	C1s1	ENSG00000182326	1.70	3.05E-09	Serine peptidase
ENSMUSG00000090231	Cfb	ENSG00000243649	2.31	1.94E-23	Serine peptidase
ENSMUSG00000029096	Htra3	ENSG00000170801	2.54	3.35E-30	Serine peptidase
ENSMUSG00000021492	F12	ENSG00000131187	2.63	2.46E-02	Serine peptidase
ENSMUSG00000041534	Rbp3	ENSG00000265203	2.76	2.92E-04	Serine peptidase

ENSMUSG00000061068	Mcpt4		3.01	1.67E-22	Serine peptidase
ENSMUSG00000033825	Tpsb2	ENSG00000095917, ENSG00000172236, ENSG00000197253	3.02	1.72E-18	Serine peptidase
ENSMUSG00000023031	Cela1	ENSG00000139610	3.48	8.79E-11	Serine peptidase
ENSMUSG00000022225	Cma1	ENSG00000092009	3.85	2.95E-20	Serine peptidase
ENSMUSG00000049719	Prss46	ENSG00000261603	4.82	1.12E-02	Serine peptidase
ENSMUSG00000031443	F7	ENSG00000057593	5.27	1.33E-02	Serine peptidase
ENSMUSG00000031722	Hp	ENSG00000261701	7.95	1.62E-147	Serine peptidase
ENSMUSG00000026750	Psmb7	ENSG00000136930	1.12	1.50E-02	Threonine peptidase
ENSMUSG00000030751	Psma1	ENSG00000256206	1.12	4.82E-02	Threonine peptidase
ENSMUSG00000068749	Psma5	ENSG00000143106	1.15	4.69E-02	Threonine peptidase
ENSMUSG00000030591	Psmd8	ENSG00000099341	1.16	2.00E-03	Threonine peptidase
ENSMUSG00000042541	Shfm1		1.16	3.58E-02	Threonine peptidase
ENSMUSG00000022193	Psmb5	ENSG00000100804	1.16	1.74E-02	Threonine peptidase
ENSMUSG00000015671	Psma2	ENSG00000256646	1.18	1.23E-03	Threonine peptidase
ENSMUSG00000027566	Psma7	ENSG00000101182	1.19	3.32E-04	Threonine peptidase
ENSMUSG00000039033	Tasp1	ENSG00000089123	1.20	2.12E-02	Threonine peptidase
ENSMUSG00000005779	Psmb4	ENSG00000159377	1.20	1.58E-04	Threonine peptidase
ENSMUSG00000014769	Psmb1	ENSG00000008018	1.20	3.07E-04	Threonine peptidase
ENSMUSG00000031897	Psmb10	ENSG00000205220	1.21	1.07E-02	Threonine peptidase
ENSMUSG00000021024	Psma6	ENSG00000100902	1.21	7.23E-04	Threonine peptidase
ENSMUSG00000024338	Psmb8	ENSG00000204264	1.22	4.43E-02	Threonine peptidase
ENSMUSG00000018286	Psmb6	ENSG00000142507	1.24	8.80E-05	Threonine peptidase
ENSMUSG00000028837	Psmb2	ENSG00000126067	1.30	6.18E-06	Threonine peptidase
ENSMUSG00000006344	Ggt5	ENSG00000099998	1.59	2.00E-03	Threonine peptidase

Supplementary Table S3: Gene lists and classification of GO term proteolysis from transcriptomes of mice head.

Supplementary Table S4

Zebrafish ID	Zebrafish gene name	Human homolog	Meas/Ctrl or -Ctrl/Meas (scaled)	*p*-value	Classification
ENSDARG00000057698	ctsd	ENSG00000117984	1.15	3.20E-02	Aspartic peptidase
ENSDARG00000008165	caspa		-2.08	4.23E-03	Cysteine protease
ENSDARG00000052039	caspb		-2.04	1.50E-05	Cysteine protease
ENSDARG00000052917	si:ch211-202f3.3	ENSG00000214711	-1.84	1.15E-03	Cysteine protease
ENSDARG00000005595	adgb	ENSG00000118492	-1.75	2.08E-02	Cysteine protease

ENSDARG00000013771	ctss2.2	ENSG00000163131	-1.68	2.27E-02	Cysteine protease
ENSDARG00000034211	capn2l	ENSG00000162909	-1.68	3.87E-04	Cysteine protease
ENSDARG00000012341	capn9	ENSG00000135773	-1.54	7.25E-03	Cysteine protease
ENSDARG00000045641	usp3	ENSG00000140455	-1.49	1.75E-02	Cysteine protease
ENSDARG00000098239	zgc:85932		-1.46	2.26E-03	Cysteine protease
ENSDARG00000091699	capn2a		-1.42	1.87E-03	Cysteine protease
ENSDARG00000030177	uchl3	ENSG00000118939	-1.40	2.22E-03	Cysteine protease
ENSDARG00000055045	casp3b	ENSG00000164305	-1.37	2.73E-02	Cysteine protease
ENSDARG00000040990	usp37	ENSG00000135913	-1.31	6.36E-03	Cysteine protease
ENSDARG00000035329	capns1a	ENSG00000126247	-1.31	2.15E-02	Cysteine protease
ENSDARG00000013804	capns1b	ENSG00000126247	-1.23	2.72E-02	Cysteine protease
ENSDARG00000089861	usp44	ENSG00000136014	1.19	4.32E-02	Cysteine protease
ENSDARG00000063190	zranb1b	ENSG00000019995	1.19	2.87E-02	Cysteine protease
ENSDARG00000079198	usp13	ENSG00000058056	1.28	1.63E-02	Cysteine protease
ENSDARG00000102705	otud6b	ENSG00000155100	1.30	2.81E-02	Cysteine protease
ENSDARG00000019595	senp8	ENSG00000166192	1.82	3.25E-02	Cysteine protease
ENSDARG00000101051	ctsbb	ENSG00000136943	1.92	4.83E-05	Cysteine protease
ENSDARG00000052578	c6ast4		1.97	1.26E-08	Cysteine protease
ENSDARG00000069748	capn5b	ENSG00000149260	2.02	4.80E-02	Cysteine protease
ENSDARG00000088145	atg4db	ENSG00000130734	4.19	1.55E-02	Cysteine protease
ENSDARG00000042816	mmp9	ENSG00000100985	-3.26	5.48E-03	Metallopeptidase
ENSDARG00000059029	mmp28	ENSG00000271447	-2.30	2.67E-02	Metallopeptidase
ENSDARG00000045887	mmp30		-1.66	4.76E-08	Metallopeptidase
ENSDARG00000034693	mysm1	ENSG00000162601	1.23	3.98E-02	Metallopeptidase
ENSDARG00000067545	adam19b	ENSG00000135074	1.24	3.16E-02	Metallopeptidase
ENSDARG00000062363	phex	ENSG00000102174	1.24	4.58E-02	Metallopeptidase
ENSDARG00000068187	spg7	ENSG00000197912	1.25	4.21E-02	Metallopeptidase
ENSDARG00000079166	ace	ENSG00000264813	1.32	1.78E-02	Metallopeptidase
ENSDARG00000007813	rnpepl1	ENSG00000142327	1.36	1.19E-02	Metallopeptidase
ENSDARG00000006901	si:ch1073-459j12.1	ENSG00000106624	1.40	5.42E-03	Metallopeptidase
ENSDARG00000061737	ece1	ENSG00000117298	1.52	1.38E-04	Metallopeptidase
ENSDARG00000043722	cpa4	ENSG00000158516	1.60	2.81E-03	Metallopeptidase
ENSDARG00000006029	lta4h	ENSG00000111144	1.88	3.17E-04	Metallopeptidase
ENSDARG00000057644	adam8b	ENSG00000151651	2.05	4.07E-04	Metallopeptidase
ENSDARG00000079983	agbl2	ENSG00000165923	4.57	2.56E-03	Metallopeptidase
ENSDARG00000059026	zgc:123217	ENSG00000189099	-6.64	3.52E-02	Serine peptidase
ENSDARG00000077540	f2rl1.2	ENSG00000164251	-1.98	2.11E-02	Serine peptidase
ENSDARG00000039579	cfd	ENSG00000197766	-1.90	2.20E-04	Serine peptidase
ENSDARG00000038891	AL954146.1		-1.86	4.30E-02	Serine peptidase
ENSDARG00000079393	tmprss15		-1.79	1.10E-02	Serine peptidase

ENSDARG00000055014	si:dkey-33m11.8		-1.65	1.46E-02	Serine peptidase
ENSDARG00000004748	zgc:100868	ENSG00000103355	-1.65	1.62E-05	Serine peptidase
ENSDARG00000095807	hp	ENSG00000263639	-1.59	1.56E-02	Serine peptidase
ENSDARG00000032831	htra1a	ENSG00000166033	-1.52	1.56E-02	Serine peptidase
ENSDARG00000102332	spint1a	ENSG00000243543	-1.49	6.25E-04	Serine peptidase
ENSDARG00000058593	sri	ENSG00000075142	-1.38	3.03E-03	Serine peptidase
ENSDARG00000089138	si:ch1073-440b2.1	ENSG00000170500	-1.32	4.82E-03	Serine peptidase
ENSDARG00000061173	st14a		-1.32	1.80E-02	Serine peptidase
ENSDARG00000100691	prss35	ENSG00000146250	-1.30	2.69E-02	Serine peptidase
ENSDARG00000037783	proza	ENSG00000126231	1.15	3.49E-02	Serine peptidase
ENSDARG00000029063	clpxa	ENSG00000166855	1.23	3.80E-04	Serine peptidase
ENSDARG00000088581	f10	ENSG00000126218	1.24	1.31E-02	Serine peptidase
ENSDARG00000075048	lonrf1		1.29	4.25E-03	Serine peptidase
ENSDARG00000037883	prcp	ENSG00000137509	1.45	2.48E-02	Serine peptidase
ENSDARG00000073742	prss59.2		1.62	1.27E-02	Serine peptidase
ENSDARG00000045544	hgfa	ENSG00000019991	1.65	1.46E-02	Serine peptidase
ENSDARG00000078567	lonrf1l	ENSG00000154359	1.67	2.69E-06	Serine peptidase
ENSDARG00000093844	zgc:136461	ENSG00000168928	1.78	6.57E-11	Serine peptidase
ENSDARG00000056765	ela2l	ENSG00000142615	1.82	2.41E-12	Serine peptidase
ENSDARG00000042993	prss1	ENSG00000204983	1.84	1.10E-10	Serine peptidase
ENSDARG00000068680	ctrl	ENSG00000141086	1.89	1.72E-09	Serine peptidase
ENSDARG00000007276	ela3l		1.90	1.12E-09	Serine peptidase
ENSDARG00000079274	prss59.1		1.95	1.41E-09	Serine peptidase
ENSDARG00000056744	ela2	ENSG00000142615	2.03	2.05E-02	Serine peptidase
ENSDARG00000090428	ctrb1	ENSG00000168925	2.19	8.72E-20	Serine peptidase
ENSDARG00000094741	HTRA2 (1 of many)	ENSG00000115317	2.21	4.19E-02	Serine peptidase
ENSDARG00000017314	CELA1 (1 of many)	ENSG00000139610	2.27	5.10E-16	Serine peptidase
ENSDARG00000043173	CELA1 (1 of many)	ENSG00000139610	3.87	6.95E-03	Serine peptidase
ENSDARG00000002240	psmb6	ENSG00000142507	1.39	7.79E-03	Threonine peptidase
ENSDARG00000043781	psmb10	ENSG00000205220	1.93	5.73E-03	Threonine peptidase

Supplementary Table S4: Gene lists and classification of GO term proteolysis from transcriptomes of zebrafish larvae.

Supplementary Table S5

Mouse ID	Mouse gene_name	Human gene stable ID	Meas/Ctrl or -Ctrl/Meas (scaled)	*p*-value	*p*-adj
ENSMUSG00000025479	Cyp2e1	ENSG00000130649	-3.45	2.60E-31	3.66E-28
ENSMUSG00000060675	Pla2g16	ENSG00000176485	1.4	3.29E-11	4.28E-09
ENSMUSG00000028597	Gpx7	ENSG00000116157	1.85	3.54E-07	1.55E-05
ENSMUSG00000015090	Ptgds	ENSG00000107317	1.25	6.88E-07	2.78E-05
ENSMUSG00000020377	Ltc4s	ENSG00000213316	2.45	1.74E-06	6.17E-05
ENSMUSG00000017969	Ptgis	ENSG00000124212	1.43	3.72E-05	7.88E-04
ENSMUSG00000041193	Pla2g5	ENSG00000127472	1.67	7.24E-05	1.36E-03
ENSMUSG00000018339	Gpx3	ENSG00000211445	1.27	2.94E-04	4.25E-03
ENSMUSG00000063856	Gpx1	ENSG00000233276	1.28	7.91E-04	9.20E-03
ENSMUSG00000034579	Pla2g3	ENSG00000100078	-1.26	1.34E-03	1.41E-02
ENSMUSG00000021760	Gpx8	ENSG00000164294	1.31	1.92E-03	1.86E-02
ENSMUSG00000006344	Ggt5	ENSG00000099998	1.59	2.00E-03	1.92E-02
ENSMUSG00000022040	Ephx2	ENSG00000120915	1.27	2.47E-03	2.24E-02
ENSMUSG00000098488	Pla2g4b	ENSG00000168970	-1.72	2.50E-03	2.26E-02
ENSMUSG00000022947	Cbr3	ENSG00000159231	1.31	9.26E-03	5.94E-02
ENSMUSG00000029059	Fam213b	ENSG00000157870	1.18	1.12E-02	6.79E-02
ENSMUSG00000027999	Pla2g12a	ENSG00000123739	1.19	1.48E-02	8.27E-02
ENSMUSG00000042808	Gpx2	ENSG00000176153	1.33	2.20E-02	1.09E-01
ENSMUSG00000056220	Pla2g4a	ENSG00000116711	1.33	2.20E-02	1.09E-01
ENSMUSG00000020891	Alox8	ENSG00000179593	-1.5	2.31E-02	1.13E-01
ENSMUSG00000052914	Cyp2j6	ENSG00000134716	1.16	3.04E-02	1.36E-01

Supplementary Table S5: Gene lists of GO term arachidonic acid metabolism from transcriptomes of mice head.

Supplementary Table S6

Mouse ID	Mouse gene name	Human gene stable ID	MEAS/CTRL or -CTRL/MEAS (scaled)	*p* value	*p*-adj
ENSMUSG00000006344	Ggt5	ENSG00000099998	1.56	2.14E-03	2.60E-03
ENSMUSG00000009646	Pla2g12b	ENSG00000138308	1.57	1.35E-03	1.74E-03
ENSMUSG00000018339	Gpx3	ENSG00000211445	2.56	4.80E-16	4.35E-15
ENSMUSG00000022040	Ephx2	ENSG00000120915	-1.57	1.49E-11	8.59E-11
ENSMUSG00000022947	Cbr3	ENSG00000159231	13.91	2.33E-31	5.53E-30
ENSMUSG00000024055	Cyp4f13	ENSG00000186526	-1.51	2.12E-14	1.65E-13

ENSMUSG00000024292	Cyp4f14	ENSG00000186115	-1.73	2.32E-12	1.48E-11
ENSMUSG00000025002	Cyp2c55	ENSG00000108242	4.51	2.08E-24	3.47E-23
ENSMUSG00000025003	Cyp2c39		3.16	5.14E-31	1.19E-29
ENSMUSG00000025004	Cyp2c40		1.78	8.28E-03	8.27E-03
ENSMUSG00000025197	Cyp2c23		-3.84	1.62E-55	1.17E-53
ENSMUSG00000025479	Cyp2e1	ENSG00000130649	-1.48	5.25E-10	2.51E-09
ENSMUSG00000026820	Ptges2	ENSG00000148334	1.34	4.51E-03	4.95E-03
ENSMUSG00000027983	Cyp2u1	ENSG00000155016	-2.61	1.72E-14	1.36E-13
ENSMUSG00000028597	Gpx7	ENSG00000116157	2.48	3.39E-06	8.52E-06
ENSMUSG00000028712	Cyp4a31	ENSG00000186204	-4.29	1.03E-25	1.83E-24
ENSMUSG00000028715	Cyp4a14		-2.02	1.69E-20	2.21E-19
ENSMUSG00000029919	Hpgds	ENSG00000163106	3.37	1.28E-09	5.76E-09
ENSMUSG00000029925	Tbxas1	ENSG00000059377	2.32	5.19E-06	1.26E-05
ENSMUSG00000030483	Cyp2b10		-1.33	4.18E-02	3.20E-02
ENSMUSG00000032808	Cyp2c38		1.82	6.04E-10	2.86E-09
ENSMUSG00000040660	Cyp2b9		79.13	1.13E-46	5.73E-45
ENSMUSG00000042248	Cyp2c37		-3.39	1.76E-47	9.41E-46
ENSMUSG00000042632	Pla2g6	ENSG00000184381	1.95	1.23E-07	4.06E-07
ENSMUSG00000047250	Ptgs1	ENSG00000095303	1.34	3.18E-03	3.66E-03
ENSMUSG00000051483	Cbr1	ENSG00000159228	2.26	4.09E-10	1.98E-09
ENSMUSG00000052520	Cyp2j5		-1.14	3.47E-03	3.96E-03
ENSMUSG00000054827	Cyp2c50		-1.74	1.71E-09	7.60E-09
ENSMUSG00000056220	Pla2g4a	ENSG00000116711	1.24	2.08E-03	2.54E-03
ENSMUSG00000063856	Gpx1	ENSG00000233276	1.48	4.96E-03	5.35E-03
ENSMUSG00000063929	Cyp4a32	ENSG00000186204	-1.95	2.11E-19	2.56E-18
ENSMUSG00000066072	Cyp4a10	ENSG00000186204	-2.10	3.56E-16	3.31E-15
ENSMUSG00000067225	Cyp2c54		-4.10	8.56E-34	2.24E-32
ENSMUSG00000071072	Ptges3	ENSG00000110958	-1.21	3.96E-04	5.99E-04
ENSMUSG00000074882	Cyp2c68		1.54	1.35E-05	3.00E-05
ENSMUSG00000078597	Cyp4a12b		-5.43	2.94E-17	3.02E-16

Supplementary Table S6: Gene lists of GO term arachidonic acid metabolism from transcriptomes of published mice liver.

Supplementary Table S7

Zebrafish ID	Fish gene_name	Human gene stable ID	Meas/Ctrl or -Ctrl/Meas (scaled)	*p*-value	*p*-adj
ENSDARG00000060094	ptgis	ENSG00000124212	-2.21	4.57E-02	4.37E-01
ENSDARG00000004539	ptgs2a	ENSG00000073756	-1.66	1.21E-03	5.49E-02

ENSDARG00000010276	ptgs2b	ENSG00000073756	-1.60	2.86E-03	9.78E-02
ENSDARG00000027088	ptgdsb.1		-1.52	7.38E-05	7.29E-03
ENSDARG00000021149	cbr1l		-1.48	8.79E-04	4.48E-02
ENSDARG00000069463	alox12	ENSG00000108839	-1.27	4.13E-02	4.19E-01
ENSDARG00000089626	ptges3b	ENSG00000110958	-1.24	2.18E-02	3.07E-01
ENSDARG00000006029	lta4h	ENSG00000111144	1.88	3.17E-04	2.16E-02
ENSDARG00000009153	pla2g1b		2.15	4.19E-02	4.22E-01
ENSDARG00000042090	si:ch73-55i23.1	ENSG00000105499	2.81	3.51E-02	3.88E-01

Supplementary Table S7: Gene lists of GO term arachidonic acid metabolism from transcriptomes of zebrafish larvae.

Supplementary Table S8

Human homologs	Human gene name	Mice id	Mice head ratio	Mice head *p*-value	Mice liver ratio	Mice liver *p*-value	Fish ID	Fish ratio	Fish *p*-value
ENSG00000127472	PLA2G5	ENSMUSG00000041193	1.67	7.24E-05					
ENSG00000116711	PLA2G4A	ENSMUSG00000056220	1.33	2.20E-02	1.24	2.08E-03			
ENSG00000179593	ALOX15B	ENSMUSG00000020891	-1.50	2.31E-02					
ENSG00000132965	ALOX5AP	ENSMUSG00000060063	1.74	1.81E-06	1.76	1.04E-02			
ENSG00000213316	LTC4S	ENSMUSG00000020377	2.45	1.74E-06					
ENSG00000015413	DPEP1	ENSMUSG00000019278	1.71	2.59E-07	1.59	5.63E-03			
ENSG00000107317	PTGDS	ENSMUSG00000015090	1.25	6.88E-07					
ENSG00000151726	ACSL1	ENSMUSG00000018796	1.31	2.80E-06	-1.34	2.65E-05			
ENSG00000182718	ANXA2	ENSMUSG00000032231	1.63	2.56E-13	10.01	3.36E-90			
ENSG00000138772	ANXA3	ENSMUSG00000029484	1.48	1.82E-06	1.82	3.72E-06			
ENSG00000196975	ANXA4	ENSMUSG00000029994	1.33	1.24E-04	1.40	1.80E-04			
ENSG00000197043	ANXA6	ENSMUSG00000018340	1.10	4.38E-02					
ENSG00000123983	ACSL3	ENSMUSG00000032883			1.42	4.74E-14	ENSDARG00000032079	2.23	2.61E-02
ENSG00000073756	PTGS2						ENSDARG00000004539	-1.66	1.21E-03
ENSG00000073756	PTGS2						ENSDARG00000010276	-1.60	2.86E-03
ENSG00000100344	PNPLA3						ENSDARG00000102020	1.58	6.74E-05
ENSG00000111144	LTA4H						ENSDARG00000006029	1.88	3.17E-04

ENSG000 00108839	ALOX12						ENSDARG0 0000069463	-1.27	4.13E-02
ENSG000 00197747	S100A10	ENSMUSG0 0000041959	1.44	8.09E-11	2.65	2.06E-12	ENSDARG0 0000055589	-1.69	8.71E-05
ENSG000 00134716	CYP2J2	ENSMUSG0 0000052914	1.16	3.04E-02			ENSDARG0 0000098803	-5.70	2.52E-03
ENSG000 00135046	ANXA1	ENSMUSG0 0000024659	1.67	6.86E-08			ENSDARG0 0000100095	-3.40	4.54E-08
ENSG000 00135046	ANXA1	ENSMUSG0 0000024659	1.67	6.86E-08	2.32	5.94E-08	ENSDARG0 0000026726	-2.57	6.82E-03
ENSG000 00116044	NFE2L2	ENSMUSG0 0000015839	1.15	1.72E-02	1.65	4.46E-06	ENSDARG0 0000042824	-2.25	3.39E-02
ENSG000 00124212	PTGIS	ENSMUSG0 0000017969	1.43	3.72E-05			ENSDARG0 0000060094	-2.21	4.57E-02
ENSG000 00164111	ANXA5	ENSMUSG0 0000027712	1.24	5.46E-05	3.60	4.04E-54	ENSDARG0 0000026406	-1.65	1.03E-02
ENSG000 00108984	MAP2K6	ENSMUSG0 0000020623	-1.29	4.66E-04	-1.62	2.28E-04	ENSDARG0 0000099184	-1.20	1.28E-02

Supplementary Table S8: Gene signature sets of mice head, mice liver and zebrafish larvae in Figure 8.

Chapter 5

Leptin mutation and mycobacterial infection leads non-synergistically to a similar metabolic syndrome

Yi Ding[1], Mariëlle C Haks[2], Tom H. M. Ottenhoff[2], Amy C. Harms[3], Thomas Hankemeier[3], Muhamed N. H. Eeza[4, 5], Jörg Matysik[4], A. Alia[5,6], Herman P. Spaink[1*]

[1] Institute of Biology, Leiden University, The Netherlands

[2] Department of Infectious Diseases, Leiden University Medical Center, The Netherlands

[3] Leiden Academic Centre for Drug Research, Leiden University, The Netherlands

[4] Institute of Analytical Chemistry, University of Leipzig, Linnéstraße 3, D-04103, Leipzig, Germany

[5] Institute for Medical Physics and Biophysics, University of Leipzig, 04107 Leipzig, Germany.

[6] Leiden Institute of Chemistry, Leiden University, 2333 Leiden, The Netherlands.

*Corresponding author, email: h.p.spaink@biology.leidenuniv.nl

Manuscript in preparation

ABSTRACT

The leptin signaling pathway, originally discovered as one of the major factors that controls food intake, has been subsequently shown to play an evolutionary conserved role in regulating glucose homeostasis and system metabolism. Furthermore, it plays an important role as a key regulator of cellular and systemic inflammatory responses. In accordance, the leptin gene plays a role in many diseases such as cancer, tuberculosis and diabetes. In this study, we investigated the metabolism of a leptin mutant in the absence and presence of mycobacterial infection in mice and zebrafish larvae. Metabolites in the blood of *ob/ob* mice and entire *lepb* mutant zebrafish larvae were studied using mass spectrometry and HR-MAS NMR spectrometry, respectively. The results show that leptin mutation leads to a similar metabolic syndrome as caused by mycobacterial infection in the two species, characterized by the decrease of 11 amine metabolites. In both species, this metabolic syndrome is not aggravated when the leptin mutant is infected by mycobacteria. Therefore, we conclude that leptin and mycobacterial infection are both impacting metabolism non-synergistically. In addition, we studied the transcriptomes of *lepb* mutant zebrafish larvae and wild type siblings after mycobacterial infection. The transcriptome studies in zebrafish larvae show that mycobacteria induce a very distinct transcriptome signature in the *lepb* mutant compared to the wild type sibling control. Apparently, different transcriptomic responses can lead to the same metabolic end states.

Introduction

Tuberculosis (TB) is an infectious disease which causes around 10 million cases and 1.2 million deaths reported to the World Health Organization in 2019 [1]. Approximately one quarter of the world's population is latently infected with *Mycobacterium tuberculosis (Mtb)*, the causative agent of TB [1]. In around 10% of these latent infections progresses to active TB disease [2]. TB is often associated with severe wasting syndrome accompanied by loss of whole body mass and increased risk of death [3]. The metabolic abnormalities underlying the wasting syndrome in TB have been studied in humans and TB animal models [4, 5]. TB causes metabolic reprogramming characterized by decrease of many metabolites in the blood of patients from Africa [4], China [6], Indonesia [7] and the Netherlands [5]. The metabolic responses towards mycobacterial infection in the blood of mice are highly similar to that in TB patients [5]. We have shown that even in entire zebrafish larvae, infection with *M. marinum*, a natural fish pathogen and a close relative of *Mtb*, leads to a very similar metabolic syndrome as observed in mice and patients after infection with *Mtb* [5]. Ten small amines were identified as common biomarkers of mycobacterial infection in TB patients, mice and zebrafish larvae [5].

One of the risk factors for the development of TB is type 2 diabetes mellitus (T2DM) [8]. T2DM patients are three times more likely to develop progressive tuberculosis infection than normoglycemic people [9]. TB accompanied by T2DM leads to higher *Mtb* bacillary loads in sputum compared with TB patients without T2DM [10]. This might be due to the defects in the immune responsiveness in diabetic patients [11]. Alternatively, the changes in system metabolism associated with T2DM could lead to a higher risk of TB [12]. Interestingly, both TB and T2DM can lead to a similar metabolic syndrome that is companied by muscle wasting [12, 13]. Mouse and zebrafish mutants in leptin signaling genes are used to study metabolic alterations associated with T2DM [14-17]. These studies have shown that leptin in addition to its function in controlling of food intake plays an evolutionarily conserved role in regulating glucose homeostasis [16, 17]. Leptin has also been shown to have a function in mediating a glucose-fatty acid cycle to maintain glucose homeostasis under starvation condition in rats [18]. We previously find that leptin deficiency causes similar metabolite alterations in both mice and zebrafish larvae [19]. These metabolic changes show similar features as observed during progression of tuberculosis in human patients, mice and zebrafish larvae [19]. Studies in a mouse leptin mutant have provided evidence that leptin plays a role in the early immune response to *Mtb* infection [20]. Several studies have shown a correlation between the serum level of leptin and the risk of acquiring active TB [21-24]. The function of leptin in the susceptibility of TB and T2DM is linked to the important role of leptin as a major player in inflammatory processes and to its function as a regulator of system metabolism [7, 25]. However, the connections between the mechanisms underlying the role of leptin in TB and T2DM are still unknown.

In this study, we investigated the metabolic response in leptin mutants in the absence and presence of mycobacterial infection in mice and zebrafish larvae. We compared the effects of mycobacterial infection in the leptin mutant zebrafish larvae and mice using metabolomics. Our results showed that leptin mutations and mycobacterial infection led to a similar metabolic syndrome. This metabolic syndrome, however, was not more severe after mycobacterial infection in the leptin mutant. Subsequent transcriptome studies in zebrafish larvae showed that mycobacteria induced a very distinct transcriptome signature in the leptin mutant compared to the wild type sibling control. Apparently, different transcriptomic responses can lead to the same metabolic end states. Therefore, we conclude that leptin and mycobacterial infection control metabolism in different ways despite share metabolic features.

Results

Measurement of bacterial burden and metabolic profiles of *lepb* mutant and control zebrafish larvae in the absence and presence of *M. marinum* infection.

Lepb mutant (*lepb*$^{-/-}$) zebrafish larvae and their wild type siblings (*lepb*$^{+/+}$) were injected in the yolk with mWasabi-labeled *M. marinum* strain M or mock-injected with 2% polyvinylpyrrolidone 40 (PVP 40) at 4 hours post fertilization (hpf). Images of the four groups of zebrafish larvae were acquired at 5 days post infection (dpi) and the representative images are shown in **Figure 1A**. The images showed that most bacteria after *M. marinum* infection in both *lepb*$^{+/+}$ and *lepb*$^{-/-}$ larvae were present in yolk but were also detectable in the tail (**Figure 1A**). Pixel count quantification of bacterial burden in entire larvae was significantly higher in the *lepb*$^{-/-}$ infected zebrafish larvae than in the *lepb*$^{+/+}$ siblings (**Figure 1B).** Metabolic profiles of the four groups of pooled zebrafish larvae were measured by high-resolution magic-angle-spinning nuclear magnetic resonance (HR-MAS NMR) spectroscopy. A partial least squares discriminant analysis (PLS-DA) scores plot on the metabolic profiles of zebrafish larvae showed three separate clusters (**Figure 1C**). The *lepb*$^{+/+}$ infected cluster overlapped with the other three clusters (**Figure 1C**). The HR-MAS NMR spectra were divided into two major regions: 0.8-4.4 ppm and 6.7-8.2 ppm. Peak assignment was performed according to earlier literature and the chemical shift of the metabolites in the HMDB database (**Figure 1D**). There were 27 metabolites assigned, including alanine, lysine, lactate and phenylalanine (**Figure 1D**). The fold change and *p* value of all the measured metabolites in different comparisons were shown in **Supplementary Table S1**.

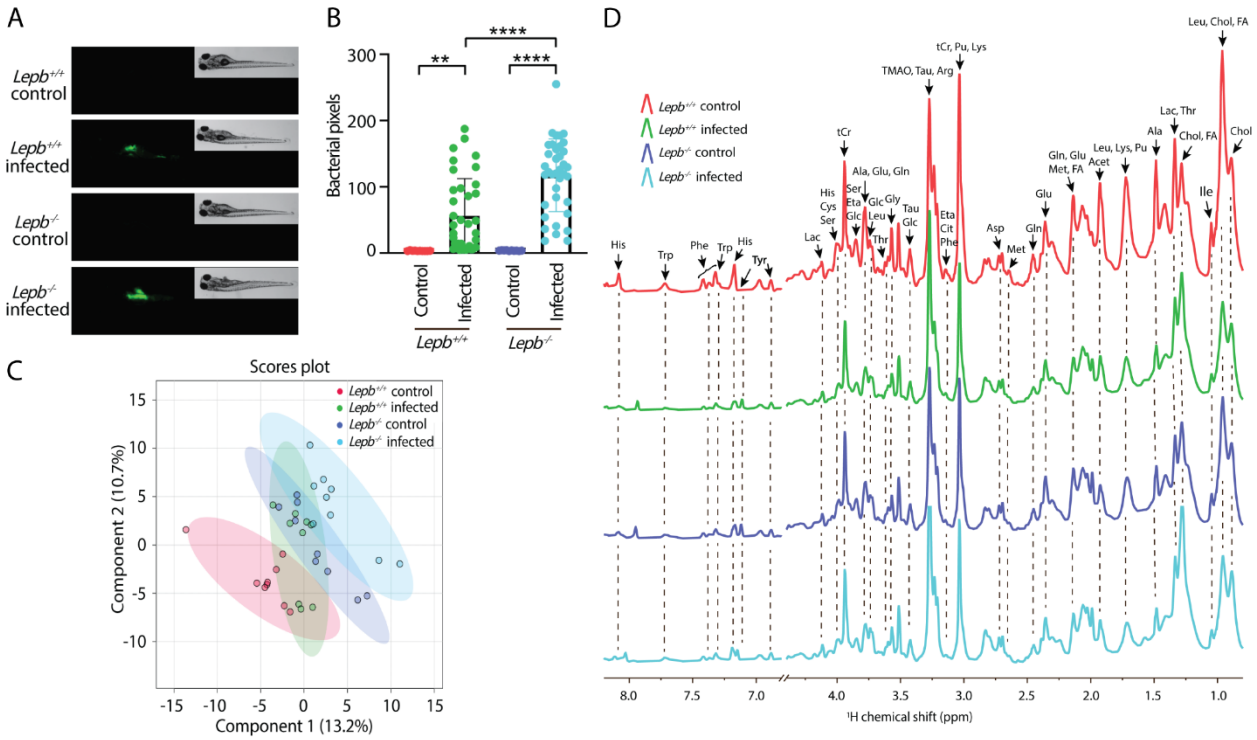

Figure 1. Bacterial loads and metabolic profiles of *lepb*$^{+/+}$ and *lepb*$^{-/-}$ zebrafish larvae with and without *M. marinum* infection. A. Representative bright field and fluorescent images of 5dpf zebrafish larvae from the *lepb*$^{+/+}$ and *lepb*$^{-/-}$ group in the absence and presence of infection. **B**. Quantifications of bacterial pixels of the four groups. ***p*<0.01, *****p*<0.0001. **C**. PLS-DA analysis of metabolic profiles from the four groups. PLS-DA: Partial least square discriminant analysis. **D**. The representative HR-MAS NMR spectra of the four groups. Acet: acetate, Ala: alanine, Arg: arginine, Asp: aspartate, Chol: cholesterol, Cit: citrulline, Cys: cysteine, Eta: ethanolamine, FA: fatty acid, Glc: Glucose, Gln: glutamine, Glu: glutamate, Gly: glycine, His: Histidine, Ile: isoleucine, Lac: lactate, Leu: leucine, Lys: lysine, Met: methionine, Phe: phenylalanine, Pu: putrescine, Ser: serine, Tau: taurine, Thr: threonine, tCr: total creatine (creatine + phosphocreatine), Trp: Tryptophan, Tyr: tyrosine, NMR: Nuclear magnetic resonance.

Mutation of the *lepb* gene and *M. marinum* infection lead non-synergistically to a similar metabolic syndrome in zebrafish larvae

Firstly, we compared the result of the wild type *M. marinum* infection in our current HR-MAS NMR study with previously published infection in zebrafish larvae using solution NMR [5] (**Supplementary Figure S1**). The result showed 20 common metabolites in the two data sets, confirming most of the previously reported biomarkers for infection in zebrafish larvae (**Supplementary Figure S1**). Secondly, we generated Venn diagrams to compare the metabolic effects of infection in the *lepb* mutant compared to the wild type sibling control at a *p* value <0.05 with and without applying a 1.5-fold change (FC) filter. The Venn diagrams of **Figure 2A** and **2C** showed that the number of metabolites of which the levels were changed after infection in the *lepb*$^{-}$

$^{/-}$ mutant was lower than in the *lepb*$^{+/+}$ sibling control (**Figure 2C** and **2E**). The Venn diagrams of **Figure 3A** and **3B** showed that the number of metabolites of which the levels were different between the *lepb* mutant and wild type in the absence of infection was much higher than in the presence of infection. As can be seen in **Figure 2E** and **3D**, this is the consequence of many of the metabolite levels decreasing in response to infection in the wild type were already decreased in the absence of infection in the mutant compared to the wild type. In conclusion, infection in the *lepb* mutant does not lead to lowering of the levels of the infection biomarker metabolites. Therefore, we can conclude that there is no clear synergy of the effects of *lepb* mutation and *M. marinum* infection on metabolism. The *lepb* mutation, therefore, does not exacerbate the metabolic wasting syndrome caused by *M. marinum* infection. However, there were a few metabolite levels that were specifically changing in the mutant after infection. The level of a metabolite namely lactate was specifically higher in the mutant group after infection while it was lower in the wild type after infection (**Figure 2A** and **2B**). Two other metabolites, trimethylamine N-oxide and mannose had a higher level in the *lepb*$^{-/-}$ than *lepb*$^{+/+}$ zebrafish larvae after infection (**Figure 2D** and **Figure 3C**).

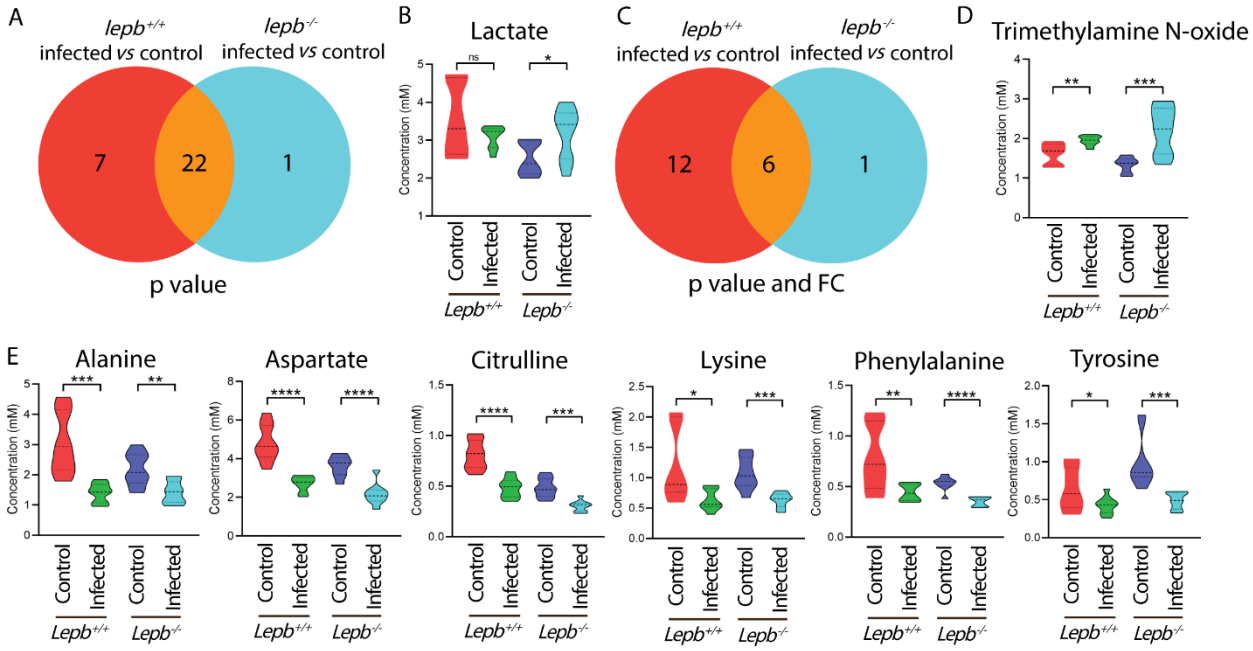

Figure 2. Venn diagrams show the number of metabolites in response to infection in the *lepb*$^{+/+}$ and *lepb*$^{-/-}$ zebrafish larvae. A. A Venn diagram shows the number of metabolites in response to *M. marinum* infection in the *lepb*$^{+/+}$ and *lepb*$^{-/-}$ larvae with $p<0.05$. **B**. Quantification of the one metabolite lactate in Figure 2A. *$p<0.05$. ns, non-significant. **C.** A Venn diagram shows the number of metabolites in response to *M. marinum* infection in the *lepb*$^{+/+}$ and *lepb*$^{-/-}$ larvae with $p<0.05$ and $|FC|>1.5$. FC: fold change. **D**. Quantification of the one metabolite trimethylamine N-oxide in Figure 2C. **$p<0.01$, ***$p<0.001$. **E**. Quantification of the common 6 metabolites in Figure 2C. ****$p<0.0001$.

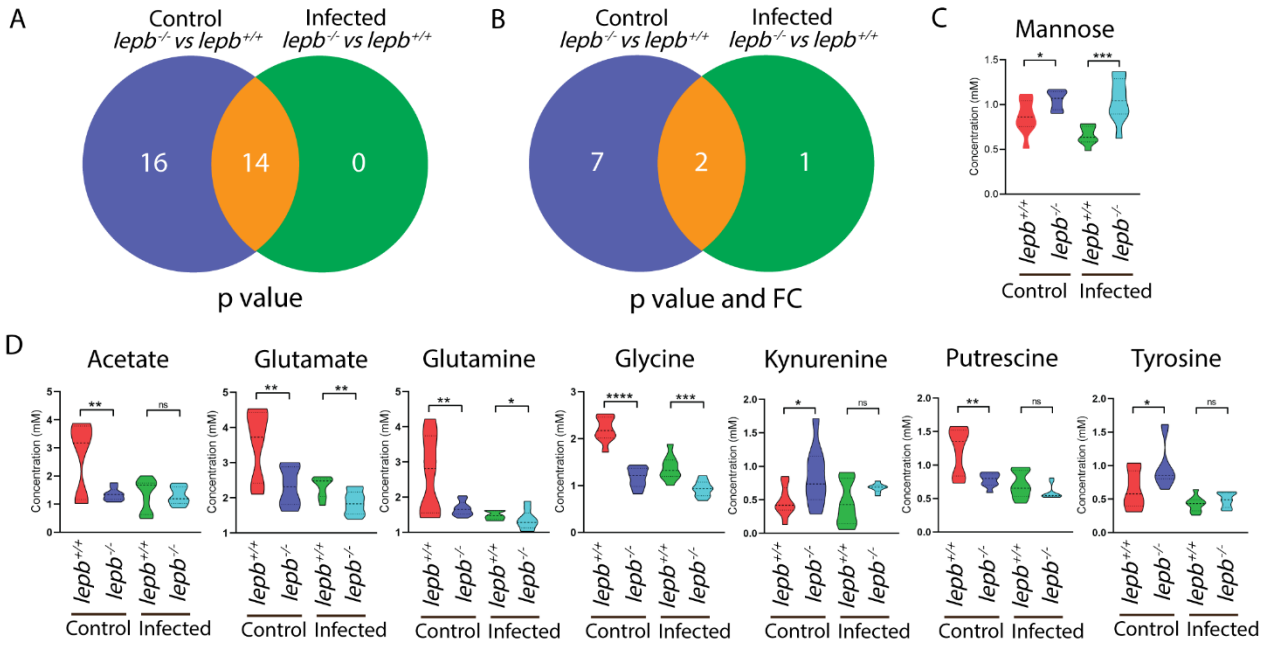

Figure 3. Venn diagrams show the number of metabolites between the *lepb*$^{-/-}$ and *lepb*$^{+/+}$ in the uninfected control and infected conditions. A. A Venn diagram shows the number of metabolites between the *lepb*$^{-/-}$ and *lepb*$^{+/+}$ in the uninfected control and infected conditions with $p<0.05$. **B**. A Venn diagram shows the number of metabolites between the *lepb*$^{-/-}$ and *lepb*$^{+/+}$ in the uninfected control and infected conditions with $p<0.05$ and $|FC|>1.5$. FC: fold change. **C**. Quantification of the one metabolite mannose in Figure 3B. *$p<0.05$, ***$p<0.001$. **D**. Quantification of the seven metabolites in Figure 3B. **$p<0.01$, ****$p<0.0001$. ns, non-significant.

Metabolic profiles of the blood of leptin mutant *ob/ob* and wild type mice in the absence and presence of *Mtb* infection.

Leptin deficient *ob/ob* mice and lean C57BL/6 mice, as a wild type control, were nasally infected with *M. tuberculosis (Mtb)*. After 8 weeks, the lungs and spleens were collected and were analyzed for bacterial colony-forming unit (CFU). Plating of bacteria from the isolated organ materials showed that the mice were systemically infected by *Mtb* in both *ob/ob* and wild type mice (**Figure 4A** and **B**). There was more infection in the lungs of *ob/ob* mice than that in the wild type mice, but not in the spleen (**Figure 4A** and **B**). The metabolic profiles of the blood of these mice were measured by mass spectrometry (MS). A PLS-DA scores plot showed that the data sets of the *ob/ob* and wild type mice could be separated based on two principal components (**Figure 4C**). However, the control and infected data sets were not be completely separated in the *ob/ob* and wild type mice (**Figure 4C**). A heatmap showed the abundances of 41 metabolites which were significantly changed in the comparison of infected versus uninfected in the two groups of mice (**Figure 4D**). It reveals that the levels of a majority of those metabolites were reduced in the wild type mice after

Mtb infection (**Figure 4D**). The levels of the metabolites in *ob/ob* mice were not obviously altered due to infection (**Figure 4D**).

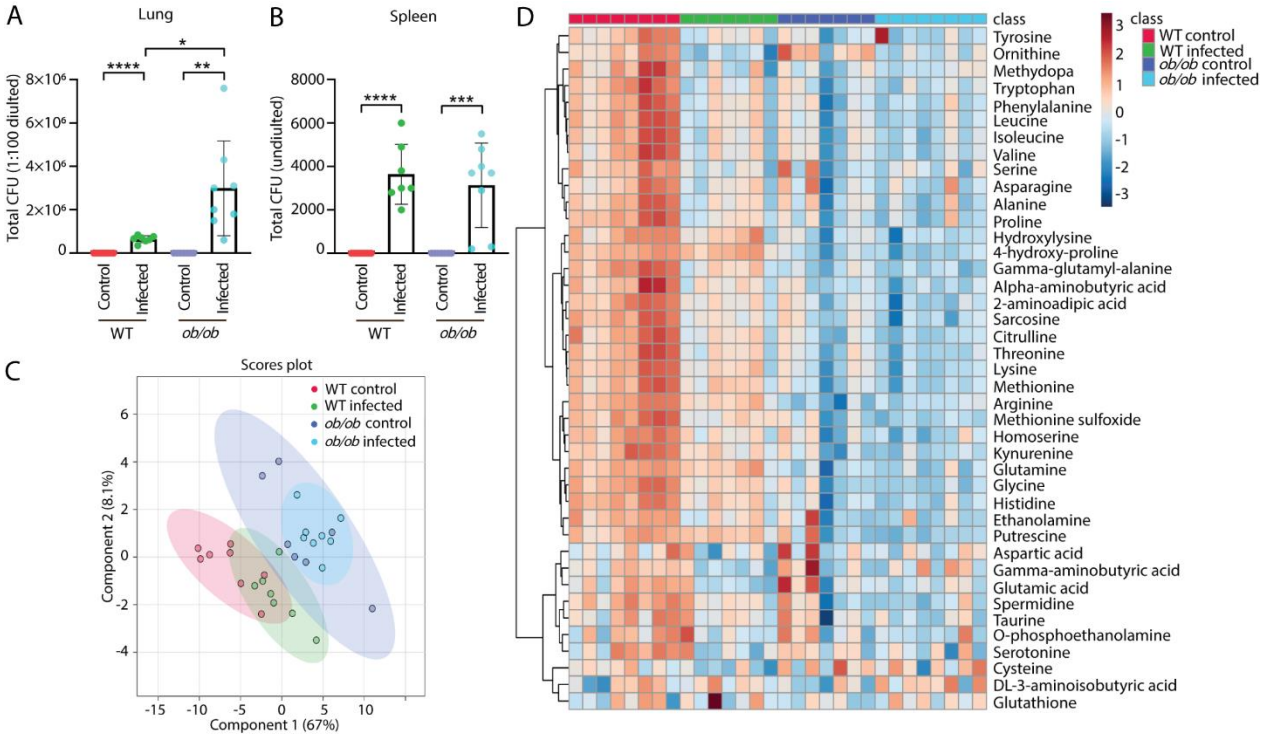

Figure 4. Bacterial loads and metabolic profiles of the blood of wild type and *ob/ob* mice with and without *Mtb* infection. A. Total CFU (1:100 diluted) of the lungs from the WT and *ob/ob* mice in the absence and presence of infection. CFU: colony-forming unit. WT: wild type. **p*<0.05,***p*<0.01, *****p*<0.0001. **B**. Total CFU (undiluted) of the spleen from the four groups. ****p*<0.001. **C**. PLS-DA analysis of the blood metabolic profiles of the four groups. PLS-DA: Partial least square discriminant analysis. **D**. Heatmap analysis of the four groups.

Mutation of the leptin gene and *Mtb* infection lead non-synergistically to a similar metabolic syndrome in mice

Venn diagrams were generated to compare the metabolic effect of infection in the *ob/ob* mutant mice as compared to the wild type control at a *p* value <0.05 with and without applying a 1.5-FC filter. The Venn diagrams of **Figure 5A** and **5D** showed that the number of metabolites of which the levels were changed after infection in the *ob/ob* mutant mice was much lower than in the wild type control. After applying 1.5-FC filter, only one metabolite, namely ornithine, was commonly lower after infection in both wild type and *ob/ob* mice (**Figure 5C**). The Venn diagrams of **Figure 6A** and **6B** showed that the number of metabolites of which the levels were different between the *ob/ob* mutant and wild type in the absence of infection was higher than in the presence of infection.

This is because the concentrations of a majority of the metabolites were decreased already as a result of leptin mutation compared to wild type mice. *Mtb* infection thus did not enhance the metabolic effects of leptin mutation. In conclusion, infection in the *ob/ob* mutant does not lead to lowering of the levels of the infection biomarker metabolites. Therefore, we conclude there is no clear synergy of the effects of leptin mutation and *Mtb* infection on metabolism. The leptin mutation, therefore, does not exacerbate the metabolic wasting syndrome caused by *Mtb* infection. However, two metabolites 3-aminoisobutyric acid and putrescine were significantly changed in *ob/ob* mice but not in wild type mice after infection (**Figure 5B** and **6C**). Although arginine levels were lower as a result of *Mtb* infection in the wild type, they were higher in the *ob/ob* mice (**Figure 5C**).

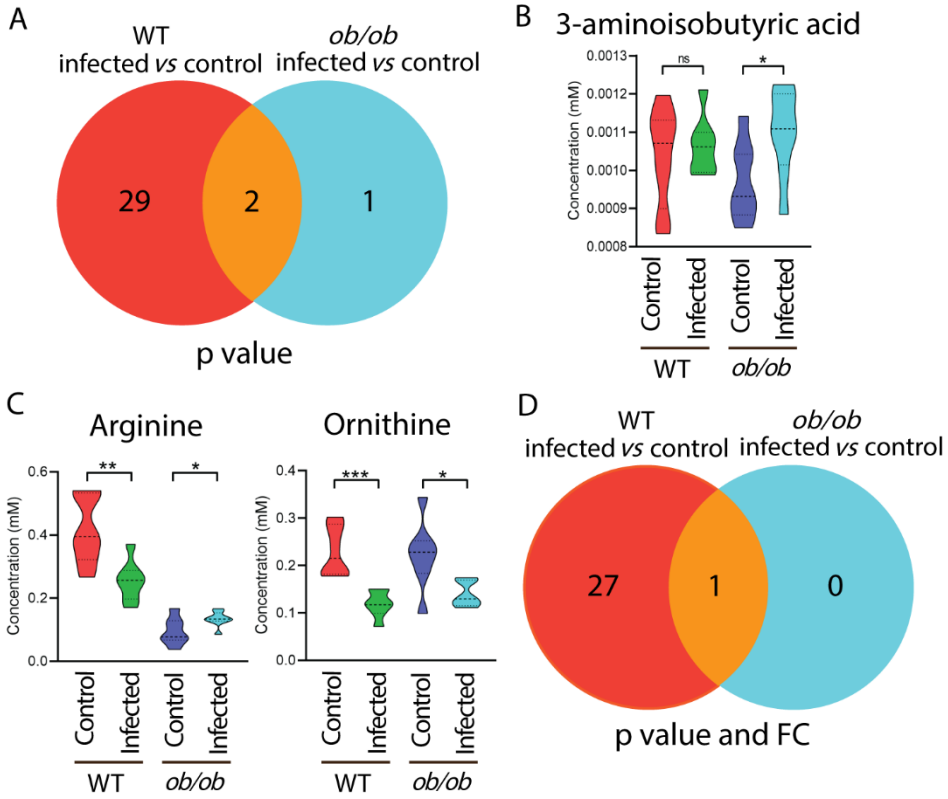

Figure 5. Venn diagrams show the number of metabolites in response to infection in the wild type and *ob/ob* mice. A. A Venn diagram shows the number of metabolites in response to *Mtb* infection in the WT and *ob/ob* mice with $p<0.05$. WT, wild type. **B**. Quantification of the one metabolite 3-aminoisobutyric acid in Figure 5A. *$p<0.05$. ns, non-significant. **C.** Quantification of the two common metabolites arginine and ornithine in Figure 5A. *$p<0.05$,**$p<0.01$, ***$p<0.001$. **D.** A Venn diagram shows the number of metabolites in response to *Mtb* infection in the wild type and *ob/ob* mice with $p<0.05$ and $|FC|>1.5$. FC: fold change.

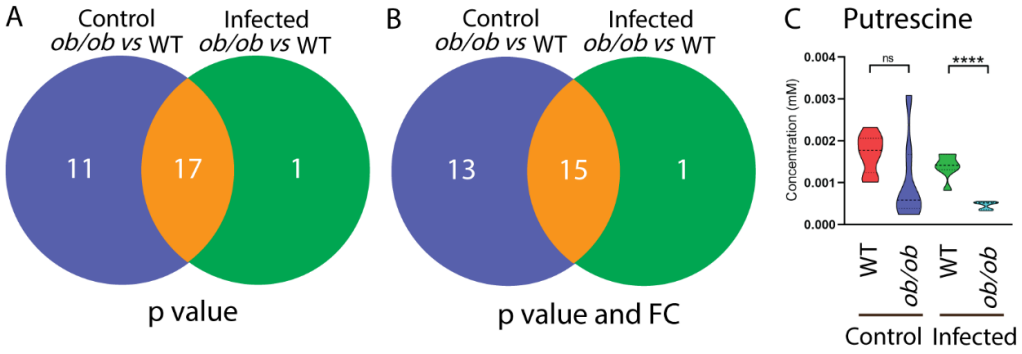

Figure 6. Venn diagrams show the number of metabolites between the wild type and *ob/ob* mice in the uninfected control and infected conditions. A. A Venn diagram shows the number of metabolites between the WT and *ob/ob* mice in the uninfected control and infected conditions with $p<0.05$. WT, wild type. **B**. A Venn diagram shows the number of metabolites between the WT and *ob/ob* mice in the uninfected control and infected conditions with $p<0.05$ and $|FC|>1.5$. FC: fold change. **C**. Quantification of the one metabolite putrescine in Figure 6A and B. ****$p<0.0001$. ns, non-significant.

The metabolic syndrome caused by leptin mutation and mycobacterial infection is similar in zebrafish and mice

We analyzed whether leptin mutation and mycobacterial infection caused similar metabolic effects in zebrafish and mice (**Supplementary Table S1**). By applying either a *p* value or a FC filter, 9 metabolites were changed in the same pattern in zebrafish larvae and mice in response to infection in the leptin mutant and wild type (**Table 1**). There were 4 metabolites of which the level was no longer significantly changed in the leptin mutant after infection in both zebrafish larvae and mice (**Table 1**). The 4 metabolites were methionine, asparagine, isoleucine and tryptophan. In conclusion, the metabolic effects caused by leptin mutation and mycobacterial infection are highly conserved in zebrafish larvae and mice.

Metabolite	Infected *vs* control			
	Zebrafish		Mice	
	lepb $^{+/+}$	*lepb* $^{-/-}$	WT	*ob/ob*
Glycine	↓	↓	↓	×
Histidine	↓	↓	↓	×
Leucine	↓	↓	↓	×
Threonine	↓	↓	↓	×
Cysteine	↓	↓	↓	×
Methionine	↓	×	↓	×
Asparagine	↓	×	↓	×
Isoleucine	↓	×	↓	×
Tryptophan	↓	×	↓	×

Table 1. The changes of 9 common metabolites in response to infection between the wild type and leptin mutant in zebrafish larvae and mice. ↑p<0.05, upregulated, FC<1.5; ↓p<0.05, downregulated, |FC|>1.5; ↓p<0.05, downregulated, |FC|<1.5; ✕ nonsignificant.

Deep sequencing of transcriptome response to infection of *lepb*$^{-/-}$ and *lepb*$^{+/+}$ zebrafish larvae

We investigated the transcriptomic profiles of *lepb* mutation and wild type siblings in the absence and presence of *M. marinum* infection in zebrafish larvae by using RNAseq (**Figure 7A** and **B**). Using significance cutoffs of $p<0.05$ and 1.5-fold change (FC), the results showed that the mRNA levels of 1009 genes were significantly changed in *lepb*$^{+/+}$ infected zebrafish larvae compared to the *lepb*$^{+/+}$ uninfected control (**Figure 7C**). Using the same p and FC cutoff values, the result showed that the mRNA levels of 1648 genes were significantly changed in *lepb*$^{-/-}$ infected zebrafish larvae compared to the *lepb*$^{-/-}$ uninfected control (**Figure 7C**). The number of differentially expressed genes (DEGs) in the *lepb*$^{-/-}$ larvae in response to infection was therefore higher than in the *lepb*$^{+/+}$ larvae (**Figure 7C**). The Venn diagram of Figure 7C showed 151 common genes in the two signature gene sets. Gene ontology (GO) enrichment analysis using DAVID resulted in significantly ($p<0.05$) enriched GO terms for biological process of the three different groups in the Venn diagram of Figure 7C (**Supplementary Figure S3A** and **S3B**). The significantly enriched GO terms of the 151 common genes include "response to bacterium" and "inflammatory response" (**Supplementary Figure S3B**). In Figure 7D, we illustrated the FC and p value of the three groups of genes, shown in Figure 3C, belonging to these two GO terms. A few genes, namely *il1b, il12a, cxl34a.4, saa, irg1l, mmp9* and *cebpb*, were significantly upregulated by infection in the common 151 signature set (**Figure 7D**). More genes related to chemokine signaling were significantly changed in *lepb*$^{+/+}$ compared to *lepb*$^{-/-}$ larvae after infection. However, the number of significantly regulated genes related to cytokine signaling, the complement cascade and matrix remodeling was higher in *lepb*$^{-/-}$ than in *lepb*$^{+/+}$ larvae after infection (**Figure 7D**).

Figure 7 (following page). Transcriptome signature sets of *lepb*$^{-/-}$ and *lepb*$^{+/+}$ zebrafish larvae in the absence and presence of *M. marinum* infection. **A**. A volcano plot of the signature set of *lepb*$^{+/+}$ infected larvae compared to the *lepb*$^{+/+}$ uninfected control. We used $p<0.05$ and |FC|>1.5 as cutoff values for all the figures. **B**. A volcano plot of the signature set of *lepb*$^{-/-}$ infected larvae compared to the *lepb*$^{-/-}$ uninfected control. **C**. A Venn diagram shows the number of differentially expressed genes (DEGs) in response to infection in the *lepb*$^{+/+}$ and *lepb*$^{-/-}$ larvae. **D**. The FC and p value of the three groups of genes, shown in Figure 7C, belonging to the two GO terms "response to bacterium" and "inflammatory responses". **E**. A volcano plot of the signature set of *lepb*$^{-/-}$ compared to *lepb*$^{+/+}$ larvae in the uninfected control situation. **F**. A volcano plot of the signature set of *lepb*$^{-/-}$ compared to *lepb*$^{+/+}$ larvae in the infected situation. **G**. A Venn diagram shows the number of DEGs between the *lepb*$^{-/-}$ and *lepb*$^{+/+}$ in the uninfected

control and infected conditions. **H**. The FC and *p* value of the three groups of genes, shown in Figure 7G, belonging to the two GO terms “response to bacterium” and “inflammatory responses”.

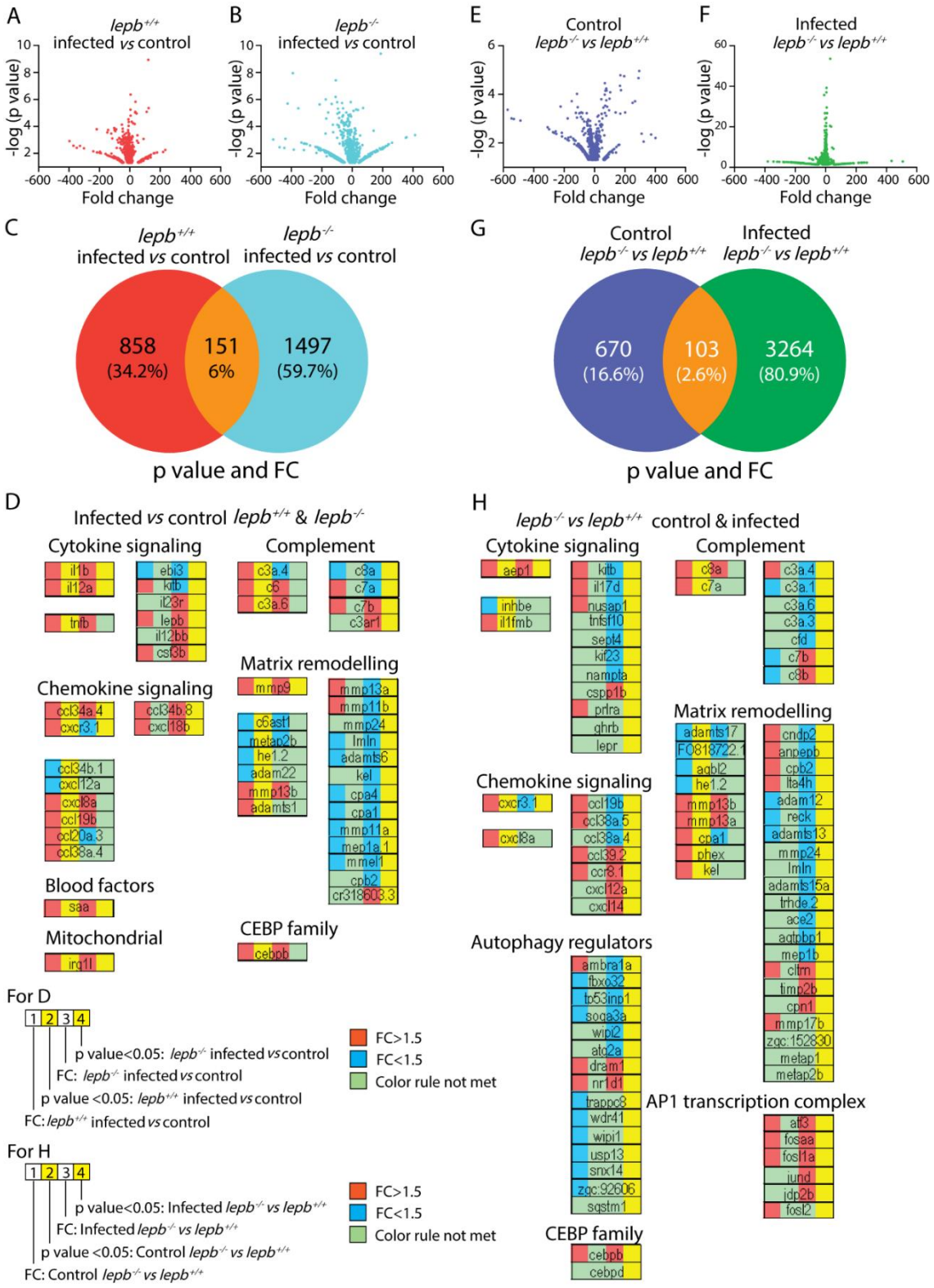

Next, we compared the number of genes that are differentially regulated between the mutant and the wild type in the absence of infection (see volcano plot **Figure 7E**) with the number of differentially regulated genes in the presence of infection (see volcano plot **Figure 7F**). There were 773 genes differentially regulated in the absence of infection at $p<0.05$ and 1.5-FC (**Figure 7G**). However, there were 3367 genes differentially regulated at the same *p* value and FC cutoff in infected *lepb*$^{-/-}$ larvae compared to infected *lepb*$^{+/+}$ siblings (**Figure 7G**). The two signature sets encompassing 773 and 3367 genes showed an overlap of 103 genes (**Figure 7G**). In Figure 7H, we illustrated the FC and *p* value of the three groups of genes, shown in **Figure 7G**, belonging to the two GO terms "response to bacterium" and "inflammatory response". In the uninfected condition, there were 16 genes differentially regulated between the mutant and the wild type with these GO terms, whereas in the infected condition there were 70 genes (**Figure 7H**). In conclusion, the mutation of the *lepb* gene and *M. marinum* infection cause synergistic effects in the transcription of inflammation related genes. We also performed the same comparisons with the genes in glycolysis and gluconeogenesis pathway because of the finding of the metabolomic analysis (**Figure 8**). The result showed that only a few genes were differentially expressed after infection in both the mutant and the wild type (**Figure 8A**). *PCK1*, a key marker for gluconeogenesis, was significantly upregulated in *lepb*$^{+/+}$ infected group, whereas it was not significantly changed in the *lepb*$^{-/-}$ infected group (**Figure 8A**). In the uninfected condition, there were no genes differentially regulated between the mutant and the wild type in this pathway, whereas in the infected condition there were 14 genes (**Figure 8B**). In addition, *PCK1* was significantly lower in the infected *lepb*$^{-/-}$ larvae compared to infected *lepb*$^{+/+}$ larvae (**Figure 8B**).

Figure 8 (following page). Genes regulated in glycolysis and gluconeogenesis pathway. A. The differentially expressed genes (DEGs) in response to infection in the *lepb*$^{+/+}$ and *lepb*$^{-/-}$ larvae. **B**. The DEGs between the *lepb*$^{-/-}$ and *lepb*$^{+/+}$ in the uninfected control and infected conditions.

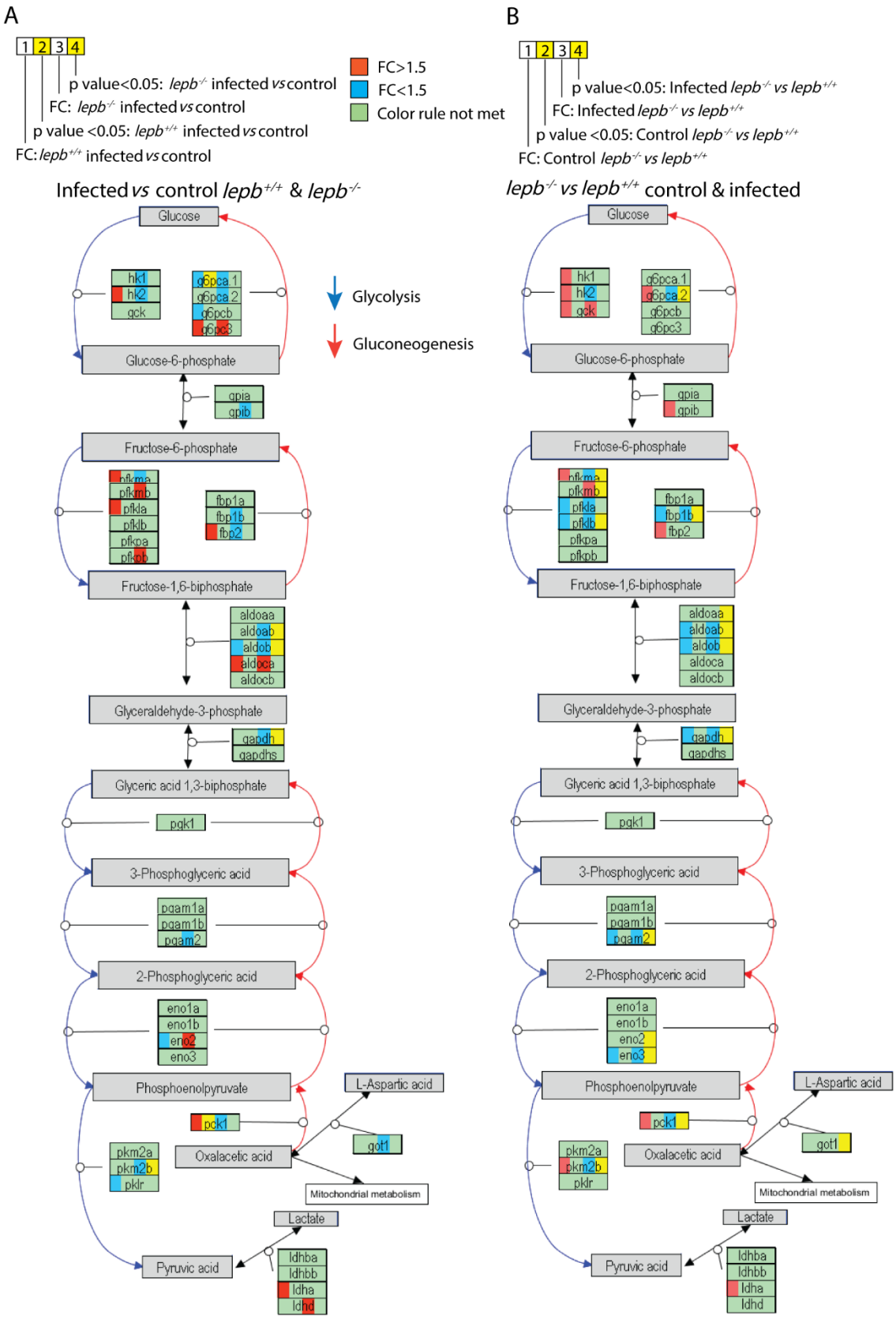
A
1 2 3 4
p value<0.05: lepb-/- infected vs control
FC: lepb-/- infected vs control
p value <0.05: lepb+/+ infected vs control
FC: lepb+/+ infected vs control
FC>1.5
FC<1.5
Color rule not met
Infected vs control lepb+/+ & lepb-/-
Glycolysis
Gluconeogenesis
Glucose
hk1
hk2
gck
g6pca.1
g6pca.2
g6pcb
g6pc3
Glucose-6-phosphate
gpia
gpib
Fructose-6-phosphate
pfkma
pfkmb
pfkla
pfklb
pfkpa
pfkpb
fbp1a
fbp1b
fbp2
Fructose-1,6-biphosphate
aldoaa
aldoab
aldob
aldoca
aldocb
Glyceraldehyde-3-phosphate
gapdh
gapdhs
Glyceric acid 1,3-biphosphate
pgk1
3-Phosphoglyceric acid
pgam1a
pgam1b
pgam2
2-Phosphoglyceric acid
eno1a
eno1b
eno2
eno3
Phosphoenolpyruvate
L-Aspartic acid
pck1
got1
pkm2a
pkm2b
pklr
Oxalacetic acid
Mitochondrial metabolism
Lactate
Pyruvic acid
ldhba
ldhbb
ldha
ldhd
B
1 2 3 4
p value<0.05: Infected lepb-/- vs lepb+/+
FC: Infected lepb-/- vs lepb+/+
p value <0.05: Control lepb-/- vs lepb+/+
FC: Control lepb-/- vs lepb+/+
lepb-/- vs lepb+/+ control & infected
Glucose
hk1
hk2
gck
g6pca.1
g6pca.2
g6pcb
g6pc3
Glucose-6-phosphate
gpia
gpib
Fructose-6-phosphate
pfkma
pfkmb
pfkla
pfklb
pfkpa
pfkpb
fbp1a
fbp1b
fbp2
Fructose-1,6-biphosphate
aldoaa
aldoab
aldob
aldoca
aldocb
Glyceraldehyde-3-phosphate
gapdh
gapdhs
Glyceric acid 1,3-biphosphate
pgk1
3-Phosphoglyceric acid
pgam1a
pgam1b
pgam2
2-Phosphoglyceric acid
eno1a
eno1b
eno2
eno3
Phosphoenolpyruvate
L-Aspartic acid
pck1
got1
pkm2a
pkm2b
pklr
Oxalacetic acid
Mitochondrial metabolism
Lactate
Pyruvic acid
ldhba
ldhbb
ldha
ldhd

Discussion

In this study, we studied the connections between the role of leptin in TB and T2DM. Therefore, we investigated the effects of mycobacterial infection in leptin deficient *lepb*$^{-/-}$ mutant zebrafish larvae and *ob/ob* mutant mice using metabolomics and transcriptomic techniques. We observed that there were higher bacterial loads in the lungs of *ob/ob* mice infected with *M. tuberculosis* (*Mtb*) bacteria, compared to the wild type infected controls (**Figure 4A**). This observation is consistent with infection studies in *ob/ob* and leptin receptor (*db/db*) mutant mice. Wieland et al. [20] observed a remarkably higher *Mtb* load in the lungs of *ob/ob* mice in comparison with the wild type controls after 5 and 10 weeks of infection. Lemos et al. [26] made the same observation in *db/db* mice infected with *Mtb*. Leptin signaling was also shown to play a key role in macrophage infection by other pathogens such as *Salmonella* Typhimurium [27]. However, since in the study of Fischer et al [27], *lepr* ablation reduced bacterial burden, this indicates that leptin signaling might play a different role in defense towards infections by different species of microbes. For this study, we have used the zebrafish larval model infection system, which has the advantage of a non-feeding system in which the functional adaptive immune system is not yet present and therefore simplifies studies of the innate immune and metabolic responses to infection. Interestingly, we found that there were also higher mycobacterial loads in the *lepb*$^{-/-}$ mutant zebrafish larvae compared to the wild type siblings (**Figure 1B**). This shows that *lepb*$^{-/-}$ mutant zebrafish larvae recapitulate the mice *ob/ob* and *db/db* phenotypes of susceptibility towards mycobacteria infection.

We found that leptin mutation and mycobacterial infection lead to a similar metabolic syndrome in zebrafish larvae as well as in mice (**Table 1**). This similarity could be explained by the occurrence of wasting syndrome in both the leptin mutants and during tuberculosis [5, 19]. In addition to wasting syndrome, *ob/ob* mice exhibit a phenotype of hyperglycemia, similar to human T2DM patients, indicating that leptin plays an important role in regulating glucose metabolism [28]. Plasma leptin level is reduced in conditions of prolonged fasting [29] and leptin has been shown to be a key factor during starvation [18]. In this study, we found that there were significantly higher glucose levels in the *lepb*$^{-/-}$ mutant zebrafish larvae as well as in the condition of *M. marinum* infection (**Supplementary table S1**). *Pck1*, a marker of gluconeogenesis, was observed to be upregulated after infection in the wild type but not in the *lepb*$^{-/-}$ mutant (**Figure 8A**). Consistently, we found that *pck1* expression was lower in the infected *lepb*$^{-/-}$ mutant compared with the infected *lepb*$^{+/+}$ siblings (**Figure 8B**). The expression levels of several other genes in the infected group associated with the glycolysis pathway (**Figure 8B**) were also found to be lower in the *lepb*$^{-/-}$ mutant than in the wild type. Considering the lack of knowledge on the control of gluconeogenesis by infection and leptin signaling, it is hard to speculate on the relevance of these differences of the transcriptional responses of the *lepb*$^{-/-}$ mutant to infection. In any case, it is possible that the higher bacterial loads in the infected *lepb*$^{-/-}$ group lead to extreme limitations of carbon sources for

gluconeogenesis and thereby might have triggered feed-back mechanisms. In support of this hypothesis, the decrease of the levels of many amino acids in the *lepb*$^{-/-}$ mutant zebrafish larvae and *ob/ob* mutant mice indicates that the supply of the glucogenic amino acids in the mutants is limiting.

However, in both species, the decrease in the levels of amino acids is not getting more pronounced when the leptin mutant is infected by mycobacteria. We only see very few metabolites, namely trimethylamine N-oxide (**Figure 2D**), mannose (**Figure 3C**), 3-aminoisobutyric acid (**Figure 5B**) and putrescine (**Figure 6C**) of which the levels are changed more severely in the leptin mutant zebrafish larvae and mice in the presence of infection as compared to the wild type. Therefore, we conclude that leptin and mycobacterial infection are non-synergistically controlling metabolism, but lead to a similar metabolic reprogramming. Nevertheless, it is possible that after infection of the leptin mutants as compared to the wild types, more energy is drained from long term storage supplies or depletion of muscle mass, as observed in severe wasting syndrome. This could explain the difference in responses of the *lepb*$^{-/-}$ mutant to infection found at the transcriptome level.

At the transcriptome level in zebrafish larvae, we observed that the number of genes of which the expression was significantly changed following *M. marinum* infection was higher in the *lepb*$^{-/-}$ mutant than in the sibling control (**Figure 7A**, **B** and **C**). GO term enrichment analysis shows that in both the *lepb*$^{-/-}$ mutant and wild type siblings, inflammatory responses to infection were highly enriched (**Supplementary Figure S3**). However, there was a larger set of genes associated with inflammation responding to infection in the *lepb*$^{-/-}$ mutant than in the sibling control (**Figure 7D**). This larger gene signature set includes genes of various cytokines, chemokines and genes involved in matrix remodeling and the complement cascade. When comparing the number of genes that are differentially expressed between the mutant and the wild type in the absence of infection with the number of differentially expressed genes in the presence of infection, we also observe larger differences (**Figure 7E**, **F** and **G**). In the absence of infection, the difference in transcriptional levels of inflammatory genes between the mutant and wild type is very limited (**Figure 7G** and **H**). In contrast, in the presence of infection many inflammatory genes have a much stronger response in the *lepb*$^{-/-}$ mutant than in the wild type siblings. In addition to the cytokines, chemokines and genes involved in matrix remodeling and the complement cascade, we now also observe various genes of the AP1 transcription complex and genes involved in autophagy regulation to be stronger responding in the mutant (**Figure 7H**).

These data are in seeming contrast with the observations that leptin functions as a proinflammatory cytokine and plays a key role in immunity and inflammatory response in immune cells [25, 30]. Therefore, it has been used as an explanation why leptin deficiency leads to increased susceptibility of infection and it is a risk factor for many infectious diseases including TB [31]. Our data shows that the function of leptin is very complex in that mutation of the *lepb* gene in an infection model

leads to a very different signature set for inflammatory responses. Although there are common transcriptional responses that are still functional in the mutant, a particular set of response factors are selectively activated or inhibited. This is very different from what we found with the metabolic basic state and responses to infection in the mutant and wild type.

In summary it has been published that leptin deficiency increases susceptibility towards mycobacterial infection, impairs immune functions and dysregulates inflammatory responses [30, 32, 33]. Many publications indicate that these effects of leptin deficiency could be due to a direct role in controlling cellular immunity. Our results confirm that there is a very different response in many inflammatory genes transcripts after infection in a zebrafish leptin mutant. The effect of the leptin mutation on the response to infection is very specific for a particular gene signature set and is not a general effect on all inflammatory genes. However, at the metabolism level, there is a general effect of the mutation on the levels of glucose and the glycolysis pathway and a pronounced function in metabolic reprogramming related to wasting syndrome. This effect of the mutation is highly similar to the effect of mycobacterial infection and is not synergistic. Therefore, we can conclude that the function of leptin in defense against mycobacteria is highly complex and is likely to be based on control of both inflammatory and system metabolism. Our metabolic and transcriptomic response signature sets of infection in the leptin mutant and wild type controls can assist in further studies of the mechanisms underlying the role of leptin in glucose homeostasis, wasting syndrome and defense against infection. It thereby could provide further insights in the mechanisms of the connections between immunity and systems metabolism that are still poorly understood.

Methods

Mice

Male *ob/ob* mice and lean C57BL/6 wild type (WT) mice were obtained from Charles River Laboratories. Eight mice per group were nasally infected with *Mtb* strain H37Rv and another eight mice per group were mock infected at 6-week age. The mice were kept under standard conditions for 8 weeks in the animal facility of the Leiden University Medical Center (LUMC). Male mice were chosen because metabolic variation due to the hormonal cycle is limited. The mice were kept on a standard-chow diet with ad libitum access to food and water. One *ob/ob* mouse and one WT infected mouse had to be sacrificed at an early stage due to malocclusion. The mice were sacrificed at week 14 and blood, lung and spleen were collected. Mouse serum samples were collected from clotted blood tubes and mixed with pre-heated 80% ethanol at a 1:3 ratio (end concentration: 60% ethanol) in polypropylene screwcap tubes. Samples were heated for 10 min at 90°C and subsequently chilled on ice for 10 minutes before centrifugation at 13.000 rpm for 10 minutes at

4°C. Supernatants were harvested and stored at -80°C for LC-MS analysis. Handling of mice was conducted in compliance with European Community Directive 86/609 for the care and use of laboratory animals and in accordance with the regulations set forward by the LUMC animal care committee.

Zebrafish larvae

Zebrafish were handled in compliance with the local animal welfare regulations and maintained according to standard protocols (http://zfin.org). Zebrafish breeding and embryo collection were performed as described previously [34]. Mutant *lepb*$^{-/-}$ and wild type sibling *lepb*$^{+/+}$ zebrafish lines were generated, screened and raised as described previously [14]. A *lepb* mutant with a 7 base pair deletion encompassing TAGAGGG in exon 2 was used in this study. Zebrafish *lepb*$^{+/+}$ and *lepb*$^{-/-}$ embryos were collecting from 6-month-old wild type and *lepb* mutant parents, respectively. The embryos were injected into yolk with *M. marinum* strain M labelled with mWasabi plasmid pTEC15 vector22 or mock injected with 2% polyvinylpyrrolidone 40 (PVP40) at 4 to 6 hour post fertilization (hpf). *M. marinum* preparation and automatic microinjection were followed by the protocol of a previous study [35, 36]. Zebrafish larvae at 5 days post fertilization (dpf) were collected and stored at -80°C until further analysis. For HR-MAS NMR measurement, 3 replicates of 120 pooled larvae were used and each sample was measured three times to avoid technique issues.

LC–MS/MS

Metabolite levels in mice serum were measured in individual replicates using a targeted LC-MS/MS platform as described before [5]. Subject numbers were randomized and run in 5 batches which included a calibration line, QC samples and blanks. QC samples were analyzed every 10 samples. They were used to assess data quality and to correct for instrument responses.

The amine platform covers amino acids and biogenic amines employing an Accq-Tag derivatization strategy adapted from a previously published protocol [37]. Briefly, 5.0 µL of each sample was spiked with an internal standard solution. Then proteins were precipitated by the addition of MeOH. The supernatant was dried in a speedvac. The residue was reconstituted in borate buffer (pH 8.5) with AQC reagent. 1.0 µL of the reaction mixture was injected into the UPLC-MS/MS system. Chromatographic separation was achieved by an Agilent 1,290 Infinity II LC System on an Accq-Tag Ultra column. The UPLC was coupled to electrospray ionization on a triple quadrupole mass spectrometer (AB SCIEX Qtrap 6500). Analytes were detected in the positive ion mode and monitored in Multiple Reaction Monitoring (MRM) using nominal mass resolution. Acquired data were evaluated using MultiQuant Software for Quantitative Analysis (AB SCIEX, Version 3.0.2). The data are expressed as relative response ratios (target area/ISTD area; unit free) using proper internal standards. For analysis of amino acids, their 13C15N-labeled analogs were used. For other metabolites, the closest-eluting internal standard was employed. In-house developed algorithms were applied using the pooled QC samples to compensate for shifts in the sensitivity of the mass spectrometer over the batches. After quality control correction,

metabolite targets complied with the acceptance criteria of RSDqc < 15%. Using this platform, we were able to identify 41 metabolites in blood samples from mice.

MS data analysis

Data was analyzed using the software package MetaboAnalyst 5.0 [38]. MetaboAnalyst offers the possibility to provide automated data reports which we used for archiving data sets. Default settings were used with log transformation and auto scaling of the data for normalization. Naming of the metabolites is based on reference compounds using standard nomenclature of the human metabolome database (https://hmdb.ca/).

^{1}H HR-MAS NMR measurement of intact zebrafish larvae

Metabolic profiling by ^{1}H HR-MAS NMR spectroscopy was performed as described in a previous study [19]. Zebrafish larvae were carefully transferred to a 4-mm zirconium oxide MAS NMR rotor (Bruker BioSpin GmbH, Germany). As a reference (^{1}H chemical shift at 0 ppm), 10µl of 100mM deuterated phosphate buffer (KD_2PO4, PH=7.0) containing 0.1% (w/v) trimethyl-silylpropanoic acid (TSP) was added to each sample. The rotor was then placed immediately inside the NMR spectrometer.

All HR-MAS NMR experiments were performed on a Bruker DMX 600-MHz NMR spectrometer, which was equipped with a 4-mm HR-MAS dual inverse ^{1}H/^{13}C probe with a magic angle gradient and spinning rate of 6 kHz with a proton resonance frequency of 600MHz. Measurements were carried out at a temperature of 277 K using a Bruker BVT3000 control unit. Acquisition and processing of data were done with Bruker TOPSPIN software 2.1 (Bruker BioSpin GmbH, Germany).

A standard pulse sequence “ZGPR” (from Bruker's pulse program library) with water pre-saturation was used for measuring one-dimensional ^{1}H HR-MAS NMR spectra. Each one-dimensional spectrum was acquired applying a spectral width of 12 kHz, time domain data points of 8k, number of averages of 128, an acquisition time of 170 msec and a relaxation delay of 2 s. All spectra were processed by an exponential window function corresponding to a line broadening of 1 Hz and zero-filled before Fourier transformation. NMR spectra were phased manually and automatically baseline corrected using TOPSPIN 2.1 (Bruker BioSpin GmbH, Germany). The total analysis time (including sample preparation, optimization of NMR parameters, and data acquisition) of ^{1}H HR-MAS NMR spectroscopy for each sample was approximately 20 min.

NMR analysis

The one-dimensional ^{1}HR-MAS NMR spectra were corrected for baseline, phase shifts and reference using TOPSPIN 2.1 (Bruker BioSpin GmbH, Germany). Subsequently, the spectra were subdivided in the range between 0 and 10 ppm into buckets of 0.04 ppm using MestReNova software version 11.0 (Mestrelab Research S.L., Santiago de Compostela, Spain). The resulting data matrix was saved as the format of script: NMR CSV matrix (transposed) (*.CSV, *.txt). This was

then imported into MetaboAnalyst 5.0 for multivariate analysis using Partial Least Squares Discriminant Analysis (PLS-DA). Correlation coefficients with $p<0.05$ were considered statistically significant. Quantification of metabolites was performed using Chenomx NMR Suite 8.6 (Edmonton, Alberta, Canada), which allowed for qualitative and quantitative analysis of an NMR spectrum by fitting spectral signatures from HMDB database to the respective spectrum. Assignment of peaks was based on the chemical shifts of compounds of interest in Chenomx software. Statistical analysis (t-tests) of the NMR quantification results was performed with GraphPad Prism 8.0.1 (San Diego, CA, USA) and $p<0.05$ were considered significant.

RNA isolation

Zebrafish larvae from *lepb*$^{+/+}$ and *lepb*$^{-/-}$ infected and control groups (n=3) were resuspended and crushed in 0.5 ml of TRIzol Reagent. Subsequently, total RNA was extracted in accordance with the manufacturer's instructions. Contaminating genomic DNA was removed using DNase I digestion for 15min at 37°C. RNA concentration was determined by NanoDrop 2000 (Thermo Scientific, the Netherlands). RNA integrity (RIN) was assessed by bioanalyzer (Agilent) and samples with RIN values>6 were used for further library construction and sequencing.

Deep sequencing of zebrafish larvae

Deep sequencing of the zebrafish larvae was performed by GenomeScan B.V. (Leiden, the Netherlands). The NEBNext Ultra II Directional RNA Library Prep Kit for Illumina (NEB #E7760S/L) was used to process the samples. Briefly, mRNA was isolated from total RNA using oligo-dT magnetic beads. After fragmentation of the mRNA, a cDNA synthesis was performed. This was used for ligation of the sequencing adapters and PCR amplification of the resulting product. The quality and yield after sample preparation was measured with Fragment Analyzer. The size of the resulting products was consistent with the expected size distribution (a broad peak between 300-500 bp). Clustering and DNA sequencing using the NovaSeq6000 was performed according to manufacturer's protocols. A concentration of 1.1 nM of DNA was used. For the zebrafish larval samples, data sets of paired end reads of 150 nucleotides were obtained with at least 20 million reads of reads that could be mapped to the zebrafish genome version GRCz11.

Deep sequencing data mapping and analysis

Sequencing data of zebrafish larvae were aligned and mapped to the zebrafish genome GRCz11 using CLC Genomics, and differential gene expression was analyzed using DESeq2 v1.21.1. Gene Ontology (GO) term enrichment and KEGG pathway analysis were performed in DAVID Bioinformatics Resources 6.8 (https://david.ncifcrf.gov/).

Ethical licenses

Experiments in mice were performed under ethical license number DEC 14080 (10-07-2014) of Leiden University. Zebrafish lines were handled in accordance with the local animal welfare regulations and maintained according to standard protocols (https://zfin.org). This local regulation

serves as the implementation of Guidelines on the protection of experimental animals by the Council of Europe, Directive 86/609/EEC, which allows zebrafish embryos to be used up to the moment of free-living (5 days after fertilization). Since embryos used in this study were no more than 5 days old, no license is required by the Council of Europe (1986), Directive 86/609/EEC or the Leiden University ethics committee.

References

[1] World Health Organization. Global Tuberculosis Report. 2020.

[2] Kiazyk S, Ball TB. Latent tuberculosis infection: An overview. Can Commun Dis Rep 2017;43(3-4):62-6.

[3] Paton NI, Ng YM. Body composition studies in patients with wasting associated with tuberculosis. Nutrition (Burbank, Los Angeles County, Calif) 2006;22(3):245-51.

[4] Weiner J, Maertzdorf J, Sutherland JS, Duffy FJ, Thompson E, Suliman S, et al. Metabolite changes in blood predict the onset of tuberculosis. Nature Communications 2018;9(1):5208.

[5] Ding Y, Raterink R-J, Marín-Juez R, Veneman WJ, Egbers K, van den Eeden S, et al. Tuberculosis causes highly conserved metabolic changes in human patients, mycobacteria-infected mice and zebrafish larvae. Scientific Reports 2020;10(1):11635.

[6] Deng J, Liu L, Yang Q, Wei C, Zhang H, Xin H, et al. Urinary metabolomic analysis to identify potential markers for the diagnosis of tuberculosis and latent tuberculosis. Archives of Biochemistry and Biophysics 2021;704:108876.

[7] Vrieling F, Alisjahbana B, Sahiratmadja E, van Crevel R, Harms AC, Hankemeier T, et al. Plasma metabolomics in tuberculosis patients with and without concurrent type 2 diabetes at diagnosis and during antibiotic treatment. Scientific Reports 2019;9(1):18669.

[8] Dooley KE, Chaisson RE. Tuberculosis and diabetes mellitus: convergence of two epidemics. Lancet Infect Dis 2009;9(12):737-46.

[9] Restrepo Blanca I, Schlossberg D. Diabetes and Tuberculosis. Microbiol Spectr 2016;4(6):4.6.48.

[10] Andrade BB, Kumar NP, Sridhar R, Banurekha VV, Jawahar MS, Nutman TB, et al. Heightened Plasma Levels of Heme Oxygenase-1 and Tissue Inhibitor of Metalloproteinase-4 as Well as Elevated Peripheral Neutrophil Counts Are Associated With TB-Diabetes Comorbidity. Chest 2014;145(6):1244-54.

[11] Ronacher K, Joosten SA, van Crevel R, Dockrell HM, Walzl G, Ottenhoff THM. Acquired immunodeficiencies and tuberculosis: focus on HIV/AIDS and diabetes mellitus. Immunological Reviews 2015;264(1):121-37.

[12] Salgado-Bustamante M, Rocha-Viggiano AK, Rivas-Santiago C, Magaña-Aquino M, López JA, López-Hernández Y. Metabolomics applied to the discovery of tuberculosis and diabetes mellitus biomarkers. Biomarkers in Medicine 2018;12(9):1001-13.

[13] Vrieling F, Ronacher K, Kleynhans L, van den Akker E, Walzl G, Ottenhoff THM, et al. Patients with Concurrent Tuberculosis and Diabetes Have a Pro-Atherogenic Plasma Lipid Profile. EBioMedicine 2018;32:192-200.

[14] He J, Ding Y, Nowik N, Jager C, Eeza MNH, Alia A, et al. Leptin deficiency affects glucose homeostasis and results in adiposity in zebrafish. Journal of Endocrinology 2021;249(2):125-34.

[15] Giesbertz P, Padberg I, Rein D, Ecker J, Höfle AS, Spanier B, et al. Metabolite profiling in plasma and tissues of ob/ob and db/db mice identifies novel markers of obesity and type 2 diabetes. Diabetologia 2015;58(9):2133-43.

[16] Tups A, Benzler J, Sergi D, Ladyman SR, Williams LM. Central Regulation of Glucose Homeostasis. Comprehensive Physiology 2017:741-64.

[17] Michel M, Page-McCaw PS, Chen W, Cone RD. Leptin signaling regulates glucose homeostasis, but not adipostasis, in the zebrafish. Proceedings of the National Academy of Sciences 2016;113(11):3084-9.

[18] Perry RJ, Wang Y, Cline GW, Rabin-Court A, Song JD, Dufour S, et al. Leptin Mediates a Glucose-Fatty Acid Cycle to Maintain Glucose Homeostasis in Starvation. Cell 2018;172(1):234-48.e17.

[19] Alia; Herman P. Spaink YDMCHGF-CJHNNACHTHMNHEJMA. Metabolomic and transcriptomic profiling of adult mice and larval zebrafish leptin mutants reveal a common pattern of changes in metabolites and signaling pathways. Cell & Bioscience 2021.

[20] Wieland CW, Florquin S, Chan ED, Leemans JC, Weijer S, Verbon A, et al. Pulmonary Mycobacterium tuberculosis infection in leptin-deficient ob/ob mice. International Immunology 2005;17(11):1399-408.

[21] Soh AZ, Tan CTY, Mok E, Chee CBE, Yuan JM, Larbi A, et al. Adipokines and the risk of active TB: a nested case-control study. The international journal of tuberculosis and lung disease : the official journal of the International Union against Tuberculosis and Lung Disease 2021;25(1):31-5.

[22] Ye M, Bian L-F. Association of serum leptin levels and pulmonary tuberculosis: a meta-analysis. J Thorac Dis 2018;10(2):1027-36.

[23] van Crevel R, Karyadi E, Netea MG, Verhoef H, Nelwan RHH, West CE, et al. Decreased Plasma Leptin Concentrations in Tuberculosis Patients Are Associated with Wasting and Inflammation. The Journal of Clinical Endocrinology & Metabolism 2002;87(2):758-63.

[24] Mansour O, Khames A, I. Radwan E, Yousif M, Elkhatib M. Study of serum leptin in patients with active pulmonary tuberculosis. Menoufia Medical Journal 2019;32(1):217-20.

[25] Pérez-Pérez A, Sánchez-Jiménez F, Vilariño-García T, Sánchez-Margalet V. Role of Leptin in Inflammation and Vice Versa. International Journal of Molecular Sciences 2020;21(16).

[26] Lemos MP, Rhee KY, McKinney JD. Expression of the Leptin Receptor outside of Bone Marrow-Derived Cells Regulates Tuberculosis Control and Lung Macrophage MHC Expression. The Journal of Immunology 2011;187(7):3776.

[27] Fischer J, Gutièrrez S, Ganesan R, Calabrese C, Ranjan R, Cildir G, et al. Leptin signaling impairs macrophage defenses against Salmonella Typhimurium. Proc Natl Acad Sci U S A 2019;116(33):16551-60.

[28] Wang B, Chandrasekera PC, Pippin JJ. Leptin- and leptin receptor-deficient rodent models: relevance for human type 2 diabetes. Curr Diabetes Rev 2014;10(2):131-45.

[29] Sonnenberg GE, Krakower GR, Hoffmann RG, Maas DL, Hennes MMI, Kissebah AH. Plasma Leptin Concentrations during Extended Fasting and Graded Glucose Infusions: Relationships with Changes in Glucose, Insulin, and FFA. The Journal of Clinical Endocrinology & Metabolism 2001;86(10):4895-900.

[30] Maurya R, Bhattacharya P, Dey R, Nakhasi HL. Leptin Functions in Infectious Diseases. Frontiers in Immunology 2018;9:2741.

[31] Maurya R, Bhattacharya P, Dey R, Nakhasi HL. Leptin Functions in Infectious Diseases. Frontiers in immunology 2018;9:2741-.

[32] Iikuni N, Lam QLK, Lu L, Matarese G, La Cava A. Leptin and Inflammation. Curr Immunol Rev 2008;4(2):70-9.

[33] Lord GM, Matarese G, Howard JK, Baker RJ, Bloom SR, Lechler RI. Leptin modulates the T-cell immune response and reverses starvation-induced immunosuppression. Nature 1998;394(6696):897-901.

[34] Avdesh A, Chen M, Martin-Iverson MT, Mondal A, Ong D, Rainey-Smith S, et al. Regular care and maintenance of a zebrafish (Danio rerio) laboratory: an introduction. J Vis Exp 2012(69):e4196-e.

[35] Au - Benard EL, Au - van der Sar AM, Au - Ellett F, Au - Lieschke GJ, Au - Spaink HP, Au - Meijer AH. Infection of Zebrafish Embryos with Intracellular Bacterial Pathogens. JoVE 2012(61):e3781.
[36] Spaink HP, Cui C, Wiweger MI, Jansen HJ, Veneman WJ, Marín-Juez R, et al. Robotic injection of zebrafish embryos for high-throughput screening in disease models. Methods 2013;62(3):246-54.
[37] Noga MJ, Dane A, Shi S, Attali A, van Aken H, Suidgeest E, et al. Metabolomics of cerebrospinal fluid reveals changes in the central nervous system metabolism in a rat model of multiple sclerosis. Metabolomics 2012;8(2):253-63.
[38] Pang Z, Chong J, Zhou G, de Lima Morais DA, Chang L, Barrette M, et al. MetaboAnalyst 5.0: narrowing the gap between raw spectra and functional insights. Nucleic acids research 2021.

Supplementary materials

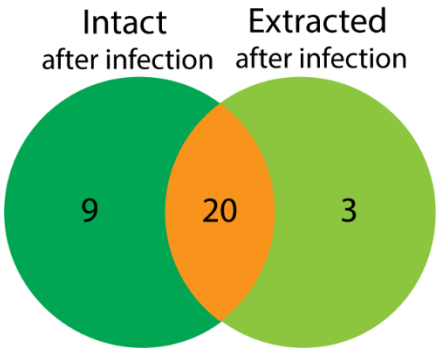

Supplementary Figure 1. Comparison of the number of biomarkers in intact and extracted zebrafish larvae due to *M. marinum* infection. A Venn diagram is shown of the overlap of the 20 metabolites of Intact wild type zebrafish larvae after *M.marinum* infection measured by HR-MAS NMR in this study with the set of infection biomarkers in extracted zebrafish larvae measured by solution NMR published by Ding et al, 2020.

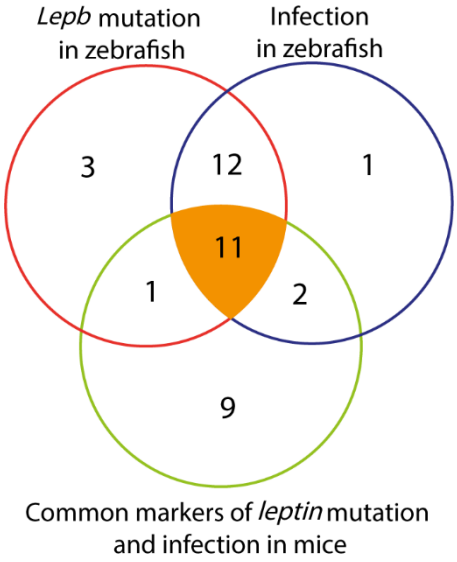

Supplementary Figure 2. Common biomarkers for leptin mutation and mycobacteria infection in zebrafish larvae and mice. A Venn diagram shows that 11 common metabolites are significantly changed in both leptin mutation and mycobacteria infection in zebrafish larvae and mice. Common biomarkers of leptin mutation and infection in mice are from Ding et al, 2021. The 11 common metabolites are alanine, citrulline, ethanolamine, glycine, histidine, isoleucine, leucine, methionine, phenylalanine, serine and threonine. Three anti-correlated metabolites namely ATP, tyrosine and tryptophan are excluded.

A

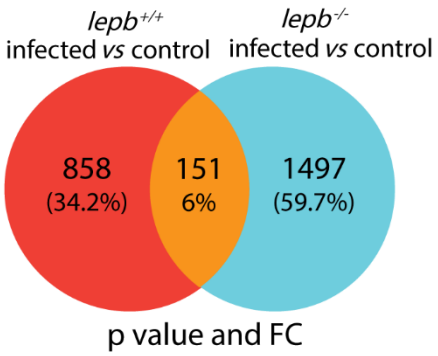

B

Infection signature *lepb* +/+ specific	Common genes	Infection signature *lepb* -/- specific
Axon development	Response to bacterium	Transport
Chemokine-mediated signaling pathway	Proteolysis	Proteolysis
Muscle contraction	Glycine biosynthetic process, by transamination of glyoxylate	Thrombin receptor singaling pathway
Neutrophil chemotaxis	Negative regulation of apoptotic process	Axon extension involved in axon guidance
Monocyte chemotaxis	Regulation of mitotic cell cycle	Cellular response to peptide hormone stimulus
Lymphocyte chemotaxis	Protein autophosphorylation	Glucocorticoid biosynthetic process
Cellular response to interferon-gamma	Inflammatory response	Collagen fibril organization
JAK-STAT cascade	Leukocyte migration	Cortisol metabolic process
Cellular response to interleukin-1	Inflammatory response to wounding	Ion transport
lar response to tumor necrosis f	Fin regeneration	Potassium ion import
Base-excision repair	Response to molecule of bacterial origin	Roundabout signaling pathway
Cilium organization	Defense response to bacterium	Secondary metabolite biosynthetic process
Bone mineralization	Response to exgenous dsRNA	Response to steroid hormone
Inflammatory response		Cell recognition
Positive regulation of ERK1 and ERK2 cascade		Cholesterol metabolic process
Homophilic cell adhesion via plasma membrane adhesion molecules		Potassium ion transport
		Regulation of axonogenesis
		Cell development
		SMAD protein signal transduction
		Blood coagulation
		Negative regulation of axon extension involved in axon guidance

Supplementary Figure S3. A Venn diagram and GO terms. **A**. A Venn diagram shows the number of differentially expressed genes (DEGs) in response to infection in the *lepb*$^{+/+}$ and *lepb*$^{-/-}$ larvae with $p<0.05$ and 1.5-FC. **B**. Gene ontology (GO) enrichment analysis using DAVID resulted in significantly ($p<0.05$) enriched GO terms for biological process of the three different groups in the Venn diagram of Supplementary Figure S3A.

Supplementary table S1

Metabolite	*Lepb* $^{+/+}$_infected *vs* control		*Lepb* $^{-/-}$_infected *vs* control		Control_*lepb* $^{-/-}$ *vs* *lepb* $^{+/+}$		Infected_*lepb* $^{-/-}$ *vs* *lepb* $^{+/+}$	
	FC	*p* value	FC	*p* value	FC	*p* value	FC	*p* value
2-Aminobutyrate	-1.25	*	-1.12	ns	-1.13	ns	-1.01	ns
Acetate	-2.08	**	-1.04	ns	-2.02	**	-1.01	ns
Alanine	-2.16	***	-1.54	**	-1.39	*	1.01	ns
Arginine	-1.22	*	-1.47	*	1.29	ns	1.07	ns
Asparagine	-1.40	**	1.04	ns	-1.22	*	1.20	ns
Aspartate	-1.77	****	-1.66	****	-1.33	**	-1.25	*
ATP	-1.13	ns	-1.21	ns	1.38	*	1.29	ns
Choline	-1.74	***	-1.38	*	-1.45	**	-1.15	ns
Citrulline	-1.68	****	-1.60	***	-1.67	****	-1.59	***
Creatine	-1.18	ns	1.01	ns	-1.21	*	-1.02	ns
Cysteine	-1.79	****	-1.27	*	-1.24	*	1.13	ns
Ethanolamine	-1.26	*	-1.35	**	-1.33	*	-1.42	**
Glucose	1.29	*	1.22	**	1.25	*	1.18	*
Glutamate	-1.53	**	-1.24	*	-1.53	**	-1.24	**
Glutamine	-1.75	**	-1.26	**	-1.58	*	-1.14	*
Glycine	-1.60	****	-1.25	*	-1.88	****	-1.47	***
Histidine	-1.89	**	-1.42	****	-1.46	*	-1.10	ns
Isoleucine	-1.42	**	-1.03	ns	-1.26	*	1.10	ns
Kynurenine	-1.06	ns	-1.27	ns	1.81	*	1.50	ns
Lactate	-1.16	ns	1.26	*	-1.41	**	1.03	ns
Leucine	-1.59	**	-1.33	*	-1.38	*	-1.15	*
Lysine	-1.90	*	-1.69	***	-1.14	ns	-1.01	ns
Mannose	-1.32	*	1.00	ns	1.21	*	1.60	***
Methionine	-1.64	**	1.06	ns	-1.39	*	1.25	*
myo-Inositol	-1.92	**	-1.28	*	-1.39	*	1.08	ns
NADH	-1.39	ns	-1.16	ns	1.01	ns	1.21	ns
Phenylalanine	-1.77	**	-1.51	****	-1.47	*	-1.25	*
Putrescine	-1.73	**	-1.31	**	-1.57	**	-1.19	ns
Sarcosine	-1.13	ns	-1.04	ns	-1.00	ns	1.07	ns
Serine	-1.42	**	-1.41	***	-1.26	*	-1.26	*
Taurine	-1.47	***	-1.36	**	-1.18	*	-1.10	ns
Threonine	-1.58	**	-1.37	**	-1.34	*	-1.16	*
Trimethylamine N-oxide	1.21	**	1.65	***	-1.21	*	1.14	ns
Tryptophan	-1.38	*	-1.06	ns	1.73	**	2.24	****
Tyrosine	-1.50	*	-2.03	***	1.55	*	1.15	ns

Supplementary table S1. The fold change and *p* value of all the 35 quantified metabolites in the four different comparisons in zebrafish larvae. ns, not significant. *p<0.05, **p<0.01, ***p<0.001, ****p<0.0001.

Supplementary table S2

Metabolite	WT_infected *vs* control		*ob/ob* _infected *vs* control		Control_*ob/ob* *vs* WT		Infected_*ob/ob* *vs* WT	
	FC	*p* value	FC	*p* value	FC	*p* value	FC	*p* value
2-aminoadipic acid	-2.53	**	-1.68	ns	-3.11	**	-2.07	**
3-aminoisobutyric acid	1.03	ns	1.13	*	-1.06	ns	1.03	ns
4-hydroxy-proline	-1.13	ns	-1.16	ns	-3.51	****	-3.59	****
Alanine	-1.64	**	-1.19	ns	-1.69	**	-1.22	ns
Alpha-aminobutyric acid	-1.53	**	-1.14	ns	-1.75	**	-1.30	**
Arginine	-1.63	**	1.41	*	-4.36	****	-1.90	***
Asparagine	-1.44	*	-1.10	ns	-1.39	ns	-1.06	ns
Aspartic acid	-1.20	ns	-1.27	ns	1.09	ns	1.02	ns
Citrulline	-1.76	**	-1.21	ns	-2.20	***	-1.51	**
Cysteine	-1.04	*	-1.01	ns	1.01	ns	1.04	ns
Ethanolamine	-1.48	**	-1.21	ns	-1.51	ns	-1.23	ns
Gamma-aminobutyric acid	-1.76	**	-1.34	ns	1.19	ns	1.57	ns
gamma-glutamyl-alanine	-2.13	**	-1.22	ns	-3.38	***	-1.93	**
Glutamic acid	-1.56	*	-1.52	ns	1.01	ns	1.04	ns
Glutamine	-1.20	ns	1.06	ns	-2.43	****	-1.90	***
Glutathione	1.05	ns	1.06	ns	-1.04	ns	-1.04	ns
Glycine	-1.59	**	-1.19	ns	-2.41	****	-1.79	****
Histidine	-1.52	***	-1.06	ns	-2.21	****	-1.55	**
Homoserine	-1.70	**	-1.20	ns	-2.02	***	-1.43	*
Hydroxylysine	-1.34	ns	-1.18	ns	-2.17	***	-1.91	**
Isoleucine	-1.75	**	-1.15	ns	-1.87	**	-1.22	ns
Kynurenine	-1.83	**	-1.15	ns	-2.78	***	-1.74	***
Leucine	-1.82	**	-1.14	ns	-2.07	***	-1.30	ns
Lysine	-1.68	**	-1.28	ns	-2.30	***	-1.75	**
Methionine	-1.58	*	-1.20	ns	-2.38	**	-1.81	***
Methionine sulfoxide	-1.95	**	-1.26	ns	-2.81	***	-1.82	****
Methyldopa	-1.92	**	1.01	ns	-1.99	**	-1.03	ns
O-Phosphoethanolamine	-1.28	ns	-1.54	ns	-1.19	ns	-1.43	ns
Ornithine	-1.94	***	-1.59	*	-1.04	ns	1.18	ns
Phenylalanine	-1.78	**	-1.07	ns	-2.05	**	-1.23	ns
Proline	-1.89	***	-1.05	ns	-2.26	***	-1.26	ns
Putrescine	-1.23	ns	-2.19	ns	-1.69	ns	-3.01	****
Sarcosine	-2.82	***	-1.67	ns	-3.06	***	-1.82	**
Serine	-1.58	***	-1.13	ns	-1.38	ns	1.01	ns
Serotonine	-3.25	ns	-1.17	ns	-4.56	*	-1.64	ns
Spermidine	-2.03	*	-1.80	ns	-2.38	*	-2.11	ns
Taurine	-1.23	ns	-1.26	ns	-1.28	ns	-1.31	ns
Threonine	-1.85	**	-1.29	ns	-2.20	**	-1.54	**
Tryptophan	-2.10	**	-1.05	ns	-2.38	**	-1.19	ns
Tyrosine	-1.94	**	1.44	ns	-2.22	**	1.26	ns
Valine	-1.85	**	-1.21	ns	-2.01	**	-1.31	ns

Supplementary table S2. The fold change and *p* value of all the 41 detectable metabolites in the four different comparisons in mice. ns, not significant. *p<0.05, **p<0.01, ***p<0.001, ****p<0.0001.

Supplementary table S3

Category	Metabolite	Infected *vs* control			
		Zebrafish		Mice	
		lepb $^{+/+}$	*lepb* $^{-/-}$	WT	*ob/ob*
Cat.1	Glycine	↓	↓	↓	×
	Histidine	↓	↓	↓	×
	Leucine	↓	↓	↓	×
	Threonine	↓	↓	↓	×
	Cysteine	↓	↓	↓	×
	Methionine	↓	×	↓	×
	Asparagine	↓	×	↓	×
	Isoleucine	↓	×	↓	×
	Tryptophan	↓	×	↓	×
Cat.2	Alanine	↓	↓	↓	↓
	Citrulline	↓	↓	↓	×
	Lysine	↓	↓	↓	×
	Phenylalanine	↓	↓	↓	×
	Tyrosine	↓	↓	↓	×
	Ethanolamine	↓	↓	↓	×
	Serine	↓	↓	↓	×
	Arginine	↓	↓	↓	↑
	Sarcosine	×	×	↓	×
	Kynurenine	×	×	↓	×
Cat.3	Putrescine	↓	↓	×	×
	Taurine	↓	↓	×	×
	Glutamine	↓	↓	×	×

Supplementary table S3. The changes of 22 common metabolites in zebrafish and mice in response to infection between the wild type and leptin mutants. ↑ p<0.05, upregulated, FC<1.5; ↓ p<0.05, downregulated, |FC|>1.5; ↓ p<0.05, downregulated, |FC|<1.5; × nonsignificant.

Chapter 6

General discussion and future perspectives

Yi Ding[1], Herman P. Spaink[1]

[1] Institute of Biology, Leiden University, The Netherlands

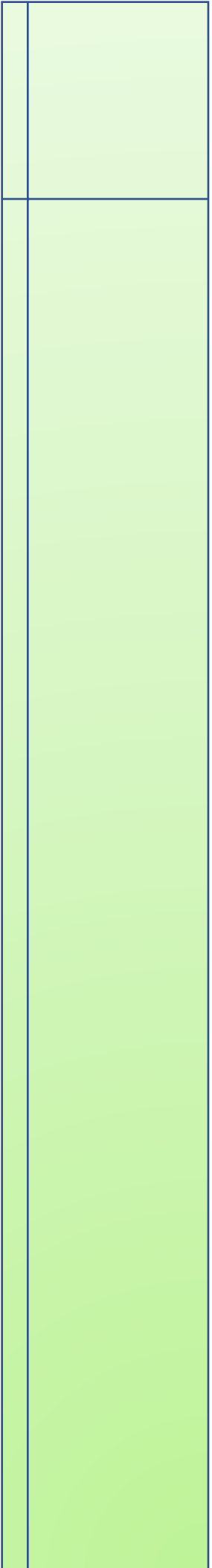

Zebrafish models for metabolic diseases

The zebrafish (Danio rerio) is an emerging model organism for studying acquired diseases including cancer and microbial infections, as well as metabolic diseases as it has many advantages [1, 2]. Zebrafish are genetically tractable and with high frequency can produce large numbers of larvae that are optically transparent which allows their real time imaging for tracking pathogenesis of diseases [3]. Zebrafish share approximately 70% genetic similarity with human beings [4, 5] and the basic cellular processes and molecular functions are highly conserved between mammals and zebrafish [6]. The growing availability of transgenic lines with fluorescent labels for instance in immune cells makes it possible to non-invasively and directly visualize the process of pathogenesis in the transparent zebrafish larvae [7]. Versatile zebrafish models for studying tuberculosis (TB) have been developed and are commonly used [8, 9]. In Figure 2 of **Chapter 1**, it is shown that *M. marinum* infection in zebrafish embryos results in characteristic necrotic granulomas, which recapitulates the process leading to human TB. Furthermore, the application of automatic robotic injection of *M. marinum* pathogens into the zebrafish yolk with a speed of up to 1000 embryos within 20 minutes at very high accuracy, contributes to a high-throughput level of screening [10-12]. The availability of a collection of large numbers of zebrafish samples upon infection also compensates for the relatively low sensitivity of NMR measurements. Therefore, the zebrafish model for TB continues to yield important insights into the discovery of new biomarkers for TB, early diagnosis of the disease and screening for new therapeutic treatments.

Rodent animal models with leptin or leptin receptor deficiency are well established and widely used for studies of obesity and diabetes mellitus (DM) [13]. Leptin and leptin receptor are highly conserved in fish and mammals [14, 15]. In the research described in **Chapter 3**, a *lepb* mutant zebrafish line is generated using CRISPR-CAS technology. The study of this zebrafish line shows that leptin deficiency in adult zebrafish at 1.5-year-old age leads to the development of DM and early signs of diabetic nephropathy as well as a significant accumulation of visceral fat measured by magnetic resonance imaging (MRI) [16]. A recent published paper show that no obesity is found in *lepr* and *lepa* zebrafish mutants compared to their respective controls [17]. The controversial results observed by different groups might be explained by different breeding schemes [17-20]. Wild type and *lep* or *lepr* mutant zebrafish raised together in the same tank show no significant differences in growth phenotypes [18, 20]. However, significant growth differences between genotypes are observed when they are raised in separate tanks despite the absence of consistent obesity phenotype [17]. This might be due to the differences in terms of food competition, background variation, or stress sensitivity between genotypes when different breeding schemes are used [17, 21]. It is also possible that during breeding, compensatory genetic mechanisms have led to differences in phenotypes. Such compensatory mechanisms have been reported to occur in various zebrafish mutant lines, although the molecular basis for these mechanisms is still not fully

understood [22]. Considering the lack of knowledge of function of the duplication of the leptin genes in zebrafish, the occurrence of compensatory mechanisms in *lepa* or *lepb* mutants is difficult to exclude. It is therefore highly interesting to generate *lepa* and *lepb* double mutants in future research. Furthermore, it is recommended that the various leptin mutants generated in different laboratories are exchanged between laboratories and subjected to comparative studies.

Conserved metabolic changes resulting from tuberculosis and leptin deficiency across species

In this thesis we have shown that metabolic alterations resulting from both TB and leptin mutation are highly conserved across mammals and non-mammals. It gives support for the hypothesis that there is a common molecular mechanism underlying wasting syndrome in all vertebrates. In **Chapter 2**, it is shown that a metabolic reprogramming processes during TB infection are conserved in humans, mice and zebrafish larvae. In **Chapter 4**, it is shown that leptin deficiency in adult mice and larval zebrafish leads to highly similar metabolic alterations in amino acid levels as well as in regulation of genes involved in the proteolysis and arachidonic acid pathways. In **Chapter 5,** it is shown that leptin mutation and mycobacterial infection lead to a similar metabolic syndrome in mice as well as in zebrafish larvae. The metabolic changes resulting from both TB and leptin mutation between different species are very striking considering the variety of differences between the analyzed samples. (1) Human, mice and zebrafish are very diverse examples of the vertebrate subphylum, e.g., metabolic rate, body size, body temperature and examined life stages vary greatly. (2) Samples of blood or body tissue, in the case of the human and mice experiments, are compared with the entire organism in the case of zebrafish larvae. (3) The environmental conditions are different in the three species. (4) Metabolic profiles are detected by different metabolomics technologies with different sample handling. (5) The genetic variation within the studied populations is highly diverse in zebrafish test samples, whereas a highly inbred population is used in the case of mice. (6) Since zebrafish larvae are not yet fed during the timeframe of the experiments, but solely use their yolk for nutrition, this shows that differences in food intake are not involved in the observed metabolic changes. The metabolic similarities, in spite of the many differences in the analyzed samples listed above, give important information and many new insights. Comparative analyses between mammals and non-mammals at metabolomics and transcriptomics levels provide essential information for further biological studies of tuberculosis and diabetes and drug engineering. The metabolic similarities and conserved pathways found in metabolic diseases among different species yield advances in various aspects. Firstly, it can give new insights in the evolution of controlling mechanisms of metabolism in vertebrates; Secondly, it offers new possibilities to study the mechanisms of metabolic alterations in the zebrafish larval model system; Thirdly, it shows the translatability of biomarkers from zebrafish and rodents to human diseases.

The role of leptin in tuberculosis

Tuberculosis patients usually suffer from anorexia and malnutrition, resulting in severe weight loss including extremely consumption of fat and muscle tissues [23]. Leptin is a key regulator of body weight, energy balance and immunity [24], therefore it might also play an essential role to defense against *Mtb* infection. Plasma leptin level is found to be lower in TB patients than in healthy controls [25-27]. Its concentration is increased after anti-TB treatment [28]. In contrast, leptin level is also found to be higher in TB patients than in controls [29]. To investigate the role of leptin in defense against mycobacteria infection, in **Chapter 5**, we look into the effects of mycobacterial infection in leptin deficient *lepb*$^{-/-}$ mutant zebrafish larvae and *ob/ob* mutant mice. Higher bacterial loads are observed in the *lepb*$^{-/-}$ zebrafish larvae as well as in the lungs of *ob/ob* mice upon mycobacteria infection, compared to the respective wild type infected controls. This observation is consistent with infection studies in *ob/ob* and *db/db* mutant mice [30, 31]. It is reported that leptin-deficiency is correlated with dysregulation of cytokines secretion, which increases susceptibility to infectious diseases including TB [32, 33]. However, in both species, the decrease in the levels of metabolites is not getting more pronounced when the leptin mutant is infected by mycobacteria. Therefore, we conclude that leptin and mycobacterial infection are non-synergistically controlling metabolism, but lead to a similar metabolic reprogramming. This is the consequence of many of the metabolite levels decreasing in response to infection in the wild type are already decreased in the absence of infection in the mutant compared to the wild type. The fact that the effect of infection by mycobacteria on metabolism is similar to that of a mutation in the leptin gene could be used as an argument that the bacteria are not directly responsible for the observed metabolic changes, but that their effect is indirect via the host system. Apparently, the wasting syndrome that is the result of a mutation of the leptin gene can't be further aggravated by consumption of metabolites by mycobacteria after infection of the leptin mutant.

The potential utility of leptin deficient zebrafish for gestational diabetes mellitus studies

In **Chapter 4**, it is shown that leptin deficiency in adult mice and zebrafish larvae lead to similar metabolite changes. The similarity of metabolic changes resulting from leptin deficiency between blood of adult mice and entire zebrafish larvae provides the potential to use common metabolites as biomarkers. These biomarkers could be indicators for the onset of diabetes in adults but also in their offspring, providing prognostic markers for the early identification of the risks of gestational diabetes mellitus (GDM). In this respect, it can be expected that the metabolic state of the parents can even influence the development of the second-generation offspring since the germ line cells are already developed before birth and at the larval stages in fish. We are planning to investigate this in more details in zebrafish, for instance by paying attention to epigenetic factors that could play a role in maternal or paternal influences on the offspring in the first and second generation. To

investigate the role of the age of diabetic parents on development of their offspring, we are currently analysing RNAseq data from the 5dpf offspring of different ages (0.5, 1 and 1.5 years old) of adult *lepb* mutant zebrafish and their wild type siblings. In addition, to see if there are gene expression differences caused by two *lepb* gene deletions (7bp and 8bp), RNAseq data from 5dpf offspring of *lepb*7 and *lepb*8 at 1.5-year-old will be investigated as well. Moreover, the offspring and muscle tissues collected from 2-year-old *lepb*7 and *lepb*8 adult zebrafish are currently sequenced by bulk RNA barcoding and sequencing (BRB-seq). BRB-seq is a novel high-throughput transcriptomics sequencing approach which is quicker and 20 times cheaper than conventional commercial RNAseq technologies [34, 35]. By studying the correlation of transcriptome changes caused by leptin mutation in adult zebrafish and their offspring, we aim to obtain more knowledge of parental effects of leptin deficiency on their off-spring and thereby provide new insights in the mechanisms underlying GDM.

Perspectives for future studies

The application of PINTA and μMRI in zebrafish

NMR spectroscopic analysis of biological samples often makes use of isotopic tracers [36, 37]. For instance, Perry et al. reported a method called positional isotopomer Nuclear Magnetic Resonance (NMR) tracer analysis (PINTA) [38]. This method allows non-invasively to model metabolism *in vivo* [38, 39] by combining NMR and gas chromatography-mass spectrometry (GC-MS) analysis of plasma following an infusion of [3-^{13}C] lactate and glucose tracer [38]. This method can be used for instance to examine the role of hepatic glucose, fat and amino acid metabolism in a physiological state in humans as well as in animal models. In a future study, we are interested in applying the PINTA approach for the real time investigation of hepatic metabolism in zebrafish. The use to adult zebrafish is relatively difficult due to ethic issues. Zebrafish larvae might be suitable as an alternative model by injection of [3-^{13}C] lactate and glucose tracer into blood vessels and then subsequent analysis by the combination of NMR and GC-MS.

In addition, magnetic resonance microimaging (μMRI) has been reported to be useful for imaging of intact zebrafish. It was used to detect tumors in live adult zebrafish despite the very small size of the cellular structures [40]. We are planning to develop an application of the μMRI technique to image younger zebrafish even at larval stage. For this, the micro-coil technology reported by Schadewijk et al. can be employed [41]. Using such technology it should be possible to image noninvasively the fat distribution and muscle volumes *in vivo*. This would allow us to investigate which tissues are affected by wasting syndrome at an early stage of zebrafish development and also open path for longitudinal MRI studies from larvae till adult stage. Furthermore, chemical shift imaging and localized MR spectroscopy at larval stage can provide the possibility to map the distribution of various metabolites *in vivo*.

Wasting analysis in zebrafish larvae

In **Chapter 4**, it is shown that the level of many metabolites in leptin mutant zebrafish larvae is decreased compared to the wild type siblings. The metabolic changes are similar with what we observed in leptin signalling-deficient mice which exhibit muscle loss and muscle weakness [42]. In future studies, we are interested in whether there is muscle wasting in the early development of *lepb* mutant zebrafish larvae. To study this, we can use the vertebrate automated screening technology (VAST) bioimager platform that has been developed and established for advanced volume imaging by Guo et al [43]. It allows to load zebrafish larvae automatically into the system and it enables 360 degrees rotation of zebrafish larvae during imaging [44, 45]. Due to the optical transparency of zebrafish larvae, most zebrafish organs including muscle can be visualized three-dimensionally. Bright field as well as fluorescent images of zebrafish larvae can be acquired. Muscles from zebrafish larvae can for instance be labelled using rhodamine-phalloidin. By reconstruction of fluorescent muscle images from different orientations of the larvae, muscle volume as well as the ratio of muscle and body volume can be determined. We want to use this method for high throughput measurements of muscle wasting during development in mycobacterial-infected wild type and leptin mutant zebrafish larvae.

Analysis of fatty acids in zebrafish larvae

Unpublished data from our laboratory show that *lepb* mutant zebrafish embryos display more fat vesicles than the wild type siblings at around 9 hours post fertilization detected by electron microscopy. Furthermore, oil red staining shows differences between 5dpf *lepb* mutant and wild type zebrafish larvae. We are investigating the amount of fat and fat distribution resulting from leptin mutation in more details by testing different time points of larval development. Furthermore, in **Chapter 4**, it is shown that the arachidonic acid pathway is enriched both in the transcriptomes of heads of *ob/ob* mice and *lepb* mutant zebrafish larvae. To further study this, a robust and sensitive targeted analysis platform: high performance liquid chromatography coupled to tandem mass spectrometry (HPLC-MS/MS) using a dynamic multiple reaction monitoring (dMRM) mode, is available at Leiden [46-48]. The dMRM mode has short retention time windows and is highly sensitive [46]. This platform allows the quantitative measurements of arachidonic acid and its downstream derived eicosanoids down to nanomolar levels [46]. The application of this robust platform to the zebrafish model systems used in this thesis will provide important information on the role of eicosanoid signalling in the inflammatory processes underlying diabetes and mycobacterial infection.

References

[1] Lieschke GJ, Currie PD. Animal models of human disease: zebrafish swim into view. Nature Reviews Genetics 2007;8(5):353-67.

[2] Seth A, Stemple DL, Barroso I. The emerging use of zebrafish to model metabolic disease. Dis Model Mech 2013;6(5):1080-8.

[3] Berg RD, Ramakrishnan L. Insights into tuberculosis from the zebrafish model. Trends in molecular medicine 2012;18(12):689-90.

[4] Howe K, Clark MD, Torroja CF, Torrance J, Berthelot C, Muffato M, et al. The zebrafish reference genome sequence and its relationship to the human genome. Nature 2013;496(7446):498-503.

[5] Santoriello C, Zon LI. Hooked! Modeling human disease in zebrafish. J Clin Invest 2012;122(7):2337-43.

[6] Shehwana H, Konu O. Comparative Transcriptomics Between Zebrafish and Mammals: A Roadmap for Discovery of Conserved and Unique Signaling Pathways in Physiology and Disease. Front Cell Dev Biol 2019;7:5-.

[7] Meijer AH, Spaink HP. Host-pathogen interactions made transparent with the zebrafish model. Curr Drug Targets 2011;12(7):1000-17.

[8] Myllymäki H, Bäuerlein CA, Rämet M. The Zebrafish Breathes New Life into the Study of Tuberculosis. Frontiers in Immunology 2016;7:196.

[9] van Leeuwen LM, van der Sar AM, Bitter W. Animal models of tuberculosis: zebrafish. Cold Spring Harb Perspect Med 2014;5(3):a018580-a.

[10] Spaink HP, Cui C, Wiweger MI, Jansen HJ, Veneman WJ, Marín-Juez R, et al. Robotic injection of zebrafish embryos for high-throughput screening in disease models. Methods 2013;62(3):246-54.

[11] Cordero-Maldonado ML, Perathoner S, van der Kolk KJ, Boland R, Heins-Marroquin U, Spaink HP, et al. Deep learning image recognition enables efficient genome editing in zebrafish by automated injections. PloS one 2019;14(1):e0202377.

[12] Carvalho R, de Sonneville J, Stockhammer OW, Savage NDL, Veneman WJ, Ottenhoff THM, et al. A High-Throughput Screen for Tuberculosis Progression. PloS one 2011;6(2):e16779.

[13] Wang B, Chandrasekera PC, Pippin JJ. Leptin- and leptin receptor-deficient rodent models: relevance for human type 2 diabetes. Curr Diabetes Rev 2014;10(2):131-45.

[14] Prokop JW, Duff RJ, Ball HC, Copeland DL, Londraville RL. Leptin and leptin receptor: analysis of a structure to function relationship in interaction and evolution from humans to fish. Peptides 2012;38(2):326-36.

[15] Londraville RL, Prokop JW, Duff RJ, Liu Q, Tuttle M. On the Molecular Evolution of Leptin, Leptin Receptor, and Endospanin. Frontiers in Endocrinology 2017;8:58.

[16] He J, Ding Y, Nowik N, Jager C, Eeza MNH, Alia A, et al. Leptin deficiency affects glucose homeostasis and results in adiposity in zebrafish. The Journal of endocrinology 2021;249(2):125-34.

[17] Bagivalu Lakshminarasimha A, Page McCaw P, Möckel D, Gremse F, Michel M. Leptin system loss of function in the absence of obesity in zebrafish. The Journal of endocrinology 2021.

[18] Ahi EP, Brunel M, Tsakoumis E, Schmitz M. Transcriptional study of appetite regulating genes in the brain of zebrafish (Danio rerio) with impaired leptin signalling. Scientific reports 2019;9(1):20166.

[19] Audira G, Sarasamma S, Chen JR, Juniardi S, Sampurna BP, Liang ST, et al. Zebrafish Mutants Carrying Leptin a (lepa) Gene Deficiency Display Obesity, Anxiety, Less Aggression and Fear, and

Circadian Rhythm and Color Preference Dysregulation. International journal of molecular sciences 2018;19(12).

[20] Michel M, Page-McCaw PS, Chen W, Cone RD. Leptin signaling regulates glucose homeostasis, but not adipostasis, in the zebrafish. Proceedings of the National Academy of Sciences of the United States of America 2016;113(11):3084-9.

[21] Deck CA, Honeycutt JL, Cheung E, Reynolds HM, Borski RJ. Assessing the functional role of leptin in energy homeostasis and the stress response in vertebrates. Frontiers in endocrinology 2017;8:63.

[22] El-Brolosy MA, Kontarakis Z, Rossi A, Kuenne C, Günther S, Fukuda N, et al. Genetic compensation triggered by mutant mRNA degradation. Nature 2019;568(7751):193-7.

[23] Gupta KB, Gupta R, Atreja A, Verma M, Vishvkarma S. Tuberculosis and nutrition. Lung India 2009;26(1):9-16.

[24] Park H-K, Ahima RS. Physiology of leptin: energy homeostasis, neuroendocrine function and metabolism. Metabolism: clinical and experimental 2015;64(1):24-34.

[25] van Crevel R, Karyadi E, Netea MG, Verhoef H, Nelwan RHH, West CE, et al. Decreased Plasma Leptin Concentrations in Tuberculosis Patients Are Associated with Wasting and Inflammation. The Journal of Clinical Endocrinology & Metabolism 2002;87(2):758-63.

[26] Buyukoglan H, Gulmez I, Kelestimur F, Kart L, Oymak FS, Demir R, et al. Leptin levels in various manifestations of pulmonary tuberculosis. Mediators Inflamm 2007;2007:64859-.

[27] Ye M, Bian L-F. Association of serum leptin levels and pulmonary tuberculosis: a meta-analysis. J Thorac Dis 2018;10(2):1027-36.

[28] Mexitalia M, Dewi YO, Pramono A, Anam MS. Effect of tuberculosis treatment on leptin levels, weight gain, and percentage body fat in Indonesian children. Korean J Pediatr 2017;60(4):118-23.

[29] Zheng Y, Ma A, Wang Q, Han X, Cai J, Schouten EG, et al. Relation of leptin, ghrelin and inflammatory cytokines with body mass index in pulmonary tuberculosis patients with and without type 2 diabetes mellitus. PloS one 2013;8(11):e80122.

[30] Wieland CW, Florquin S, Chan ED, Leemans JC, Weijer S, Verbon A, et al. Pulmonary Mycobacterium tuberculosis infection in leptin-deficient ob/ob mice. International immunology 2005;17(11):1399-408.

[31] Lemos MP, Rhee KY, McKinney JD. Expression of the leptin receptor outside of bone marrow-derived cells regulates tuberculosis control and lung macrophage MHC expression. Journal of immunology (Baltimore, Md : 1950) 2011;187(7):3776-84.

[32] Maurya R, Bhattacharya P, Dey R, Nakhasi HL. Leptin Functions in Infectious Diseases. Front Immunol 2018;9(2741).

[33] Pérez-Pérez A, Sánchez-Jiménez F, Vilariño-García T, Sánchez-Margalet V. Role of Leptin in Inflammation and Vice Versa. International journal of molecular sciences 2020;21(16):5887.

[34] Alpern D, Gardeux V, Russeil J, Mangeat B, Meireles-Filho ACA, Breysse R, et al. BRB-seq: ultra-affordable high-throughput transcriptomics enabled by bulk RNA barcoding and sequencing. Genome Biology 2019;20(1):71.

[35] Alpern D, Gardeux V, Russeil J, Deplancke B. Time-and cost-efficient high-throughput transcriptomics enabled by Bulk RNA Barcoding and sequencing. bioRxiv 2018:256594.

[36] Lane AN, Fan TWM. NMR-based Stable Isotope Resolved Metabolomics in systems biochemistry. Archives of biochemistry and biophysics 2017;628:123-31.

[37] Gowda GAN, Shanaiah N, Raftery D. Isotope enhanced approaches in metabolomics. Adv Exp Med Biol 2012;992:147-64.
[38] Perry RJ, Peng L, Cline GW, Butrico GM, Wang Y, Zhang XM, et al. Non-invasive assessment of hepatic mitochondrial metabolism by positional isotopomer NMR tracer analysis (PINTA). Nat Commun 2017;8(1):798.
[39] Perry RJ, Wang Y, Cline GW, Rabin-Court A, Song JD, Dufour S, et al. Leptin Mediates a Glucose-Fatty Acid Cycle to Maintain Glucose Homeostasis in Starvation. Cell 2018;172(1):234-48.e17.
[40] Kabli S, He S, Spaink HP, Hurlstone A, Jagalska ES, De Groot HJ, et al. In vivo magnetic resonance imaging to detect malignant melanoma in adult zebrafish. Zebrafish 2010;7(2):143-8.
[41] Schadewijk RV, Berg T, Gupta K, Ronen I, de Groot HJM, Alia A. Non-invasive magnetic resonance imaging of oils in Botryococcus braunii green algae: Chemical shift selective and diffusion-weighted imaging. PloS one 2018;13(8):e0203217.
[42] Wang X, Hu Z, Hu J, Du J, Mitch WE. Insulin resistance accelerates muscle protein degradation: Activation of the ubiquitin-proteasome pathway by defects in muscle cell signaling. Endocrinology 2006;147(9):4160-8.
[43] Guo Y, Veneman WJ, Spaink HP, Verbeek FJ. Three-dimensional reconstruction and measurements of zebrafish larvae from high-throughput axial-view in vivo imaging. Biomedical optics express 2017;8(5):2611-34.
[44] Pardo-Martin C, Chang T-Y, Koo BK, Gilleland CL, Wasserman SC, Yanik MF. High-throughput in vivo vertebrate screening. Nat Methods 2010;7(8):634-6.
[45] Chang T-Y, Pardo-Martin C, Allalou A, Wählby C, Yanik MF. Fully automated cellular-resolution vertebrate screening platform with parallel animal processing. Lab on a Chip 2012;12(4):711-6.
[46] Strassburg K, Huijbrechts AML, Kortekaas KA, Lindeman JH, Pedersen TL, Dane A, et al. Quantitative profiling of oxylipins through comprehensive LC-MS/MS analysis: application in cardiac surgery. Anal Bioanal Chem 2012;404(5):1413-26.
[47] Ellero-Simatos S, Beitelshees AL, Lewis JP, Yerges-Armstrong LM, Georgiades A, Dane A, et al. Oxylipid Profile of Low-Dose Aspirin Exposure: A Pharmacometabolomics Study. Journal of the American Heart Association;4(10):e002203.
[48] Astarita G, McKenzie JH, Wang B, Strassburg K, Doneanu A, Johnson J, et al. A Protective Lipidomic Biosignature Associated with a Balanced Omega-6/Omega-3 Ratio in fat-1 Transgenic Mice. PloS one 2014;9(4):e96221.

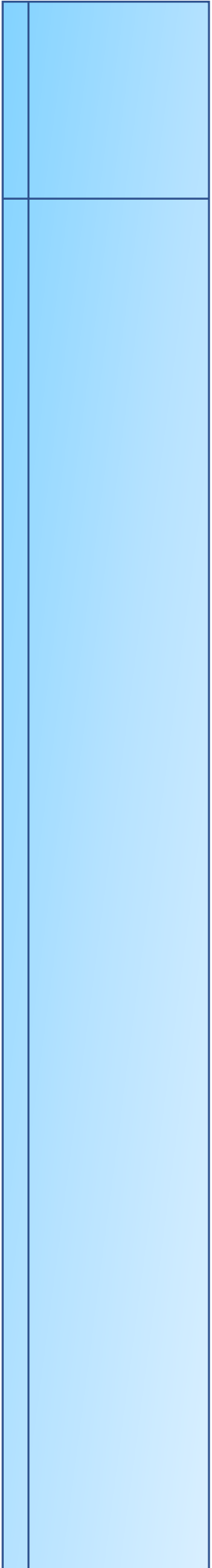

Summary

Chapter 1 provides a general background of metabolic wasting syndrome (also called cachexia), functions of the leptin gene, and the main omics technologies and an outline of this thesis. We particularly focus on two diseases resulting in cachexia at a later stage: tuberculosis (TB) and diabetes mellitus (DM). TB remains a big threat to global public health and one of the most important means to control the disease is to develop new efficient, reproducible and cost-effective diagnostic methods. Here we show that omics-based approaches are promising for biomarker discovery of TB as well as for prediction of disease therapy outcomes. DM is a chronic metabolic disease caused by defects in insulin signaling. Leptin has been extensively studied in DM because of its crucial role in control of body weight, energy homeostasis and metabolism. Leptin has also been implicated to play a role in the progression of tuberculosis. We illustrate that zebrafish is a versatile animal model to study the progression and the pathogenic mechanisms of TB and DM and functions of leptin in wasting syndrome. Furthermore, we compare the strengths and weaknesses of the most common used analytical tools: mass spectrometry and nuclear magnetic resonance spectroscopy. We also summarize the currently most common short-reading RNAseq methods and the future possibilities for the extensive use of long-reading sequencing methods.

Tuberculosis is a highly infectious and potentially fatal disease accompanied by wasting symptoms, which cause severe metabolic changes in infected people. Measurements of metabolites in human TB patients have shown to be a promising method for diagnostic purposes. In **Chapter 2**, we have compared the effects of mycobacterial infection on the level of metabolites in blood of humans and mice and whole zebrafish larvae using one highly standardized mass spectrometry pipeline, ensuring technical comparability of the results. Quantification of a range of circulating small amines show that the levels of the majority of these compounds were significantly decreased in all three groups of infected organisms. Our study identifies 10 common biomarkers for tuberculosis disease in humans, mice and zebrafish comprising: methionine, asparagine, cysteine, threonine, serine, tryptophan, leucine, citrulline, ethanolamine and phenylalanine. Furthermore, we use the zebrafish model to further investigate the metabolic changes after infection using NMR analyses based on a large number of specimens. The NMR analysis of zebrafish larvae confirms the MS data and also identifies new markers for infection including identifying general effects on metabolism such as a change of glucose levels. Our results show across-species conservation of metabolic reprogramming processes during TB infection and disease in humans, mice and zebrafish. Apparently, the mechanisms underlying these processes are independent of environmental, developmental and vertebrate evolutionary factors. The zebrafish larval model is highly suited to further investigate the mechanism of metabolic reprogramming and the connection with wasting syndrome due to infection by mycobacteria.

Summary

Leptin is a hormone which functions in the regulation of energy homeostasis via suppression of appetite. In zebrafish, there are two paralogous genes encoding leptin, called *lepa* and *lepb*. In a gene expression study, we found that the *lepb* gene was significantly downregulated under the state of insulin-resistance in zebrafish larvae, suggesting that the *lepb* plays a role in glucose homeostasis. In **Chapter 3**, we generate *lepb*-deficient zebrafish by using the CRISPR/CAS9 gene editing approach. This study aims to investigate whether the disruption of the *lepb* gene would result in the development of type 2 diabetes mellitus (T2DM) and diabetic complications in adult zebrafish. To address this question, we examined the body weight and length, blood glucose levels, and the body fat distribution in 1.5 years old *lepb*$^{-/-}$ adult zebrafish and compared them to age-matched wild type controls. Furthermore, we examine the renal histopathologic changes of these zebrafish by performing hematoxylin and eosin (HE) or periodic-acid schiff (PAS) staining, and transmission electron microscopy (TEM) methods. We observe that *lepb*$^{-/-}$ adult zebrafish have an increase in body weight, length and visceral fat accumulation, compared to age-matched control zebrafish. In addition, *lepb*$^{-/-}$ zebrafish have significantly higher blood glucose levels compared to control zebrafish. These data collectively indicate that *lepb*$^{-/-}$ adult zebrafish display the features of T2DM. Furthermore, we show that *lepb*$^{-/-}$ adult zebrafish have glomerular hypertrophy and thickening of the glomerular basement membrane, compared to control zebrafish, suggesting that *lepb*$^{-/-}$ adult zebrafish develop early signs of diabetic nephropathy. In conclusion, our results demonstrate that *lepb* regulates glucose homeostasis and adiposity in zebrafish, and suggest that *lepb*$^{-/-}$ mutant zebrafish are a promising model to investigate the role of leptin in the development of T2DM and are an attractive model to perform mechanistic and therapeutic research in T2DM and its complications.

Leptin plays a critical role in the regulation of metabolic homeostasis. However, the molecular mechanism and cross talks between leptin and metabolic pathways leading to metabolic homeostasis across different species are not clear. In **Chapter 4,** we have compared the metabolic changes resulting from leptin deficiency in blood of adult *ob/ob* mice and extracted and intact zebrafish larvae using MS, solution-state NMR and high-resolution magic-angle spinning NMR (HR-MAS NMR) spectrometry. In addition, we have compared the transcriptomic changes resulting from leptin deficiency in *ob/ob* mice heads, a published dataset for *ob/ob* mice liver and *lepb* mutant zebrafish larvae using deep RNA sequencing (RNA-seq). Thirteen metabolites were identified as common biomarkers discriminating *ob/ob* mice and *lepb*$^{-/-}$ zebrafish larvae from their respective wild type controls: alanine, citrulline, ethanolamine, glutamine, glycine, histidine, isoleucine, leucine, methionine, phenylalanine, putrescine, serine and threonine. Moreover, we also observe that glucose and lipid levels are increased in *lepb*$^{-/-}$ zebrafish larvae compared to the *lepb*$^{+/+}$ group. RNAseq show that many genes involved in proteolysis and arachidonic acid metabolism are dysregulated in *ob/ob* mice heads and *lepb* mutant zebrafish larvae compared to their wild type controls, respectively. Leptin deficiency in adult mice and larval zebrafish leads to highly similar metabolic alterations in amino acid levels. These metabolic changes show the same key features as

observed during progression of tuberculosis in human patients, rodents and zebrafish larvae. Moreover, by studying the transcriptome, we found highly similar changes in gene regulation related to proteolysis and arachidonic acid pathways in these two test systems. These results show a remarkable similarity of the effects of leptin knockdown on the metabolomes and transcriptomes of adult mice and zebrafish larvae that might be related to wasting syndrome. Apparently, the metabolic control by leptin is similar in adult and embryonic stages in mammals and fish, respectively.

Leptin plays an evolutionary conserved role in regulating glucose homeostasis and system metabolism as well as cellular and systemic inflammatory responses. In accordance, the leptin gene plays a role in many diseases such as cancer, tuberculosis and diabetes. In **Chapter 5**, we investigate the metabolism of leptin mutants in the absence and presence of mycobacterial infection in mice and zebrafish larvae. Metabolites in the blood of *ob/ob* mice and entire *lepb* mutant zebrafish larvae are studied using mass spectrometry and HR-MAS NMR spectroscopy, respectively. Our results show that leptin mutations and mycobacterial infection lead to a similar metabolic syndrome, characterized by the decrease of 11 amine metabolites. In both species, this metabolic syndrome is not aggravated when the leptin mutant was infected by mycobacteria. Therefore, we conclude that leptin and mycobacterial infection are both impacting metabolism non-synergistically. Subsequent transcriptome studies in zebrafish larvae showe that mycobacteria induced a very distinct transcriptome signature in the leptin mutant compared to the wild type sibling control. Apparently, different transcriptomic responses can lead to the same metabolic end states. Therefore, we conclude that leptin and mycobacterial infection control metabolism in different ways despite share metabolic features.

In **Chapter 6**, we discuss the major findings described in the previous chapters of this thesis and present perspectives for future studies. We demonstrate that zebrafish are an excellent animal model for studies of metabolic diseases including tuberculosis and diabetes due to various particular advantages. The effects of *lep* or *lepr* mutation on obesity in zebrafish as reported by different research groups are controversial. We postulate that differences in breeding schemes and compensatory genetic mechanisms might be responsible for the reported inconsistencies. Subsequently, we discuss that the metabolic changes in leptin mutants and infectious disease reported in this thesis are highly conserved in several species and different developmental stages considering the following points. Firstly, metabolic changes resulting from mycobacterial infection is highly similar in human, mice and zebrafish larvae. Secondly, metabolic and transcriptomic changes resulting from leptin mutation is very similar in mice and zebrafish larvae. Thirdly, metabolic changes resulting from mycobacterial infection and leptin mutation are highly similar in mice and zebrafish larvae. Fourthly, metabolic changes are shown to be highly similar based on different sample preparation and metabolomics technologies: mass spectrometry and nuclear magnetic resonance spectroscopy. Furthermore, we discuss the role of leptin in tuberculosis and

the potential utility of leptin deficient zebrafish for gestational diabetes mellitus studies and ongoing work that is currently performed. Finally, we provide perspectives of three additional technologies for future studies of new research questions resulting from this study. (1) Potential applications of a method called positional isotopomer nuclear magnetic resonance tracer analysis (PINTA) and magnetic resonance microimaging (μMRI) are proposed for further studies in zebrafish. (2) A vertebrate automated screening technology (VAST) bioimager platform will be applied for high throughput measurements of muscle wasting during development in mycobacteria-infected wild type and leptin mutant zebrafish larvae. (3) A sensitive targeted analysis HPLC-MS/MS platform can be used for studies of fatty acids, especially derivatives from arachidonic acid signaling pathway. By using these advanced platforms, we aim to provide new insights into the mechanisms of metabolic changes underlying tuberculosis and diabetes.

Nederlandse samenvatting

Hoofdstuk 1 geeft een algemene achtergrond van het metabool wasting-syndroom (ook wel cachexie genoemd), functies van het leptine-gen en de belangrijkste omics-technologieën en een overzicht van dit proefschrift. We richten ons met name op twee ziekten die in een later stadium tot cachexie leiden: tuberculose (TB) en diabetes mellitus (DM). TB blijft een grote bedreiging voor de wereldwijde volksgezondheid en een van de belangrijkste middelen om de ziekte onder controle te houden, is het ontwikkelen van nieuwe efficiënte, reproduceerbare en kosteneffectieve diagnostische methoden. Hier laten we zien dat op omics gebaseerde benaderingen veelbelovend zijn voor de ontdekking van tbc met biomarkers en voor het voorspellen van de uitkomst van de therapie. DM is een chronische stofwisselingsziekte die wordt veroorzaakt door defecten in de insuline signalering. Leptine is uitgebreid bestudeerd bij diabetes vanwege zijn cruciale rol bij de regulatie van het lichaamsgewicht, de energiehomeostase en het metabolisme. Leptine is ook geïmpliceerd om een rol te spelen bij de progressie van tuberculose. We illustreren dat de zebravis een veelzijdig diermodel is om de progressie en de pathogene mechanismen van TB en DM en functies van leptine in het wasting-syndroom te bestuderen. Verder vergelijken we de sterke en zwakke punten van de meest gebruikte analytische instrumenten: massaspectrometrie en nucleaire magnetische resonantie. We vatten ook de momenteel meest voorkomende short-reading RNAseq-methoden samen en de toekomstige mogelijkheden voor het omvangrijke gebruik van long-reading sequencing methoden.

Tuberculose is een zeer besmettelijke en mogelijk dodelijke ziekte die gepaard gaat met slopende symptomen, die ernstige metabole veranderingen veroorzaken bij geïnfecteerde mensen. Metingen van metabolieten bij menselijke tbc-patiënten is een veelbelovende methode gebleken voor diagnostische doeleinden. In **Hoofdstuk 2** hebben we het effect van mycobacteriële infectie op het niveau van metabolieten in het bloed van mensen en muizen en hele zebravislarven vergeleken met behulp van één zeer gestandaardiseerde massaspectrometrie pijplijn, waardoor technische vergelijkbaarheid van de resultaten is gegarandeerd. Kwantificering van een reeks circulerende kleine amines toonde aan dat de niveaus van de meeste van deze verbindingen significant waren verlaagd in alle drie de groepen geïnfecteerde organismen. Onze studie identificeerde 10 algemene biomarkers voor tuberculoseziekte bij mensen, muizen en zebravissen, waaronder: methionine, asparagine, cysteïne, threonine, serine, tryptofaan, leucine, citrulline, ethanolamine en fenylalanine. Verder hebben we het zebravismodel gebruikt om de metabolische veranderingen na infectie verder te onderzoeken met behulp van NMR-analyses op basis van een groot aantal exemplaren. De NMR-analyse van zebravislarven bevestigde de MS-gegevens en identificeerde ook nieuwe markers voor infectie, waaronder het identificeren van algemene effecten op het metabolisme, zoals een verandering van glucosespiegels. Onze resultaten laten het behoud van metabole herprogrammeringsprocessen tussen soorten zien tijdens tbc-infectie en ziekte bij mensen, muizen en zebravissen. Blijkbaar zijn de mechanismen die ten grondslag liggen aan deze processen

onafhankelijk van omgevings-, ontwikkelings- en gewervelde evolutionaire factoren. Het zebravislarvenmodel is zeer geschikt om het mechanisme van metabole herprogrammering en het verband met het wasting-syndroom door infectie door mycobacteriën verder te onderzoeken.

Leptine is een hormoon dat functioneert bij de regulatie van energiehomeostase via onderdrukking van de eetlust. In de zebravis zijn er twee paraloge genen die coderen voor leptine, genaamd lepa en lepb. In een genexpressiestudie ontdekten we dat het *lepb*-gen significant gedownreguleerd was onder de staat van insulineresistentie in zebravislarven, wat suggereert dat de lepb een rol speelt bij glucosehomeostase. In **Hoofdstuk 3** hebben we *lepb*-deficiënte zebravissen gegenereerd met behulp van de CRISPR/CAS9-genediting-aanpak. Deze studie heeft tot doel te onderzoeken of de verstoring van het *lepb*-gen zou resulteren in de ontwikkeling van type 2 diabetes mellitus (T2DM) en diabetische complicaties T2DM bij volwassen zebravissen. Om deze vraag te beantwoorden, onderzochten we het lichaamsgewicht en de lengte, de bloedglucosespiegels en de verdeling van lichaamsvet bij 1,5 jaar oude *lepb*$^{-/-}$ volwassen zebravissen en vergeleken ze met WT-controles van dezelfde leeftijd. Verder onderzochten we de renale histopathologische veranderingen van deze zebravissen door hematoxyline en eosine (HE) of Periodic acid Schiff (PAS) kleuring en transmissie-elektronenmicroscopie (TEM) methoden uit te voeren. We hebben waargenomen dat *lepb*$^{-/-}$ volwassen zebravissen een toename in lichaamsgewicht, lengte en viscerale vetophoping hadden, in vergelijking met leeftijd-gematchte controle zebravissen. Bovendien had de *lepb*$^{-/-}$-zebravis significant hogere bloedglucosewaarden in vergelijking met controle-zebravissen. Deze gegevens geven gezamenlijk aan dat *lepb*$^{-/-}$ volwassen zebravissen de kenmerken van T2DM vertonen. Verder toonden we aan dat *lepb*$^{-/-}$ volwassen zebravissen glomerulaire hypertrofie en verdikking van het glomerulaire basale membraan hadden, in vergelijking met controle zebravissen, wat suggereert dat *lepb*$^{-/-}$ volwassen zebravissen vroege tekenen van diabetische nefropathie ontwikkelen. Concluderend tonen onze resultaten aan dat lepb glucosehomeostase en adipositas bij zebravissen reguleert, en suggereren ze dat *lepb*$^{-/-}$ mutante zebravissen een veelbelovend model zijn om de rol van leptine in de ontwikkeling van T2DM te onderzoeken en dat ze een aantrekkelijk model zijn om mechanistisch en therapeutisch onderzoek in T2DM en de complicaties ervan uit te voeren.

Leptine speelt een cruciale rol bij de regulatie van metabole homeostase. Het moleculaire mechanisme en de cross-talks tussen leptine en metabole routes die leiden tot metabole homeostase bij verschillende soorten zijn echter niet duidelijk. In **Hoofdstuk 4** hebben we de metabole veranderingen vergeleken die het gevolg zijn van leptine-deficiëntie in het bloed van volwassen ob/ob-muizen en geëxtraheerde en intacte zebravislarven met behulp van MS, NMR in oplossingstoestand en NMR met hoge resolutie magic-angle spinning (HR-MAS NMR) spectrometrie. Daarnaast hebben we de transcriptomische veranderingen vergeleken die het gevolg zijn van leptine-deficiëntie in ob/ob-muizenkoppen, een gepubliceerde dataset voor ob/ob-muizenlever en *lepb*-mutante zebravislarven met behulp van deep RNA-sequencing (RNA-seq). Dertien metabolieten werden geïdentificeerd als algemene biomarkers die ob/ob-muizen en *lepb*$^{-/-}$-

zebravislarven onderscheiden van hun respectievelijke wildtype-controles: alanine, citrulline, ethanolamine, glutamine, glycine, histidine, isoleucine, leucine, methionine, fenylalanine, putrescine, serine en threonine. Bovendien hebben we ook waargenomen dat glucose- en lipideniveaus verhoogd waren in *lepb*$^{-/-}$ zebravislarven in vergelijking met de *lepb*$^{+/+}$ groep. RNAseq toonde aan dat veel genen die betrokken zijn bij proteolyse en arachidonzuurmetabolisme ontregeld waren in respectievelijk ob/ob-muizenkoppen en lepb-mutante zebravislarven in vergelijking met hun wildtype-controles. Leptine-deficiëntie bij volwassen muizen en larvale zebravissen leidt tot zeer vergelijkbare metabole veranderingen in aminozuurniveaus. Deze metabole veranderingen vertonen dezelfde hoofdkenmerken als waargenomen tijdens de progressie van tuberculose bij menselijke patiënten, knaagdieren en zebravislarven. Bovendien vonden we, door het transcriptoom te bestuderen, zeer vergelijkbare veranderingen in genregulatie gerelateerd aan proteolyse en arachidonzuurroutes in deze twee testsystemen. Deze resultaten laten een opmerkelijke overeenkomst zien tussen de effecten van leptine-knockdown op de metabolomen en transcriptomen van volwassen muizen en zebravislarven die mogelijk verband houden met het wasting-syndroom. Blijkbaar is de metabole controle door leptine vergelijkbaar in respectievelijk volwassen en embryonale stadia bij zoogdieren en vissen.

Leptine speelt een evolutionair geconserveerde rol bij het reguleren van glucosehomeostase en systeemmetabolisme, evenals cellulaire en systemische ontstekingsreacties. In overeenstemming hiermee speelt het leptine-gen een rol bij veel ziekten zoals kanker, tuberculose en diabetes. In **Hoofdstuk 5** onderzochten we het metabolisme van een leptinemutant in de aan- en afwezigheid van mycobacteriële infectie in muizen en zebravislarven. Metabolieten in het bloed van *ob/ob*-muizen en volledige *lepb*-mutante zebravislarven werden bestudeerd met respectievelijk massaspectrometrie en HR-MAS NMR-spectrometrie. Onze resultaten laten zien dat leptine mutaties en mycobacteriële infectie leiden tot een vergelijkbaar metabool syndroom, gekenmerkt door de afname van 11 aminemetabolieten. Bij beide soorten werd dit metabool syndroom niet verergerd wanneer de leptinemutant werd geïnfecteerd door mycobacteriën. Daarom concluderen we dat leptine en mycobacteriële infectie beide het metabolisme niet-synergetisch beïnvloeden. Daaropvolgende transcriptoom studies in zebravislarven toonden aan dat mycobacteriën een zeer duidelijke transcriptoom signatuur induceerden in de leptinemutant in vergelijking met de wildtype broer of zus-controle. Blijkbaar kunnen verschillende transcriptomische reacties leiden tot dezelfde metabole eindtoestanden. Daarom concluderen we dat leptine en mycobacteriële infectie het metabolisme op verschillende manieren beheersen, ondanks gedeelde metabole kenmerken.

In **Hoofdstuk 6** bespreken we de belangrijkste bevindingen beschreven in de voorgaande hoofdstukken van dit proefschrift en presenteren we perspectieven voor toekomstig onderzoek. We tonen aan dat zebravissen een uitstekend diermodel zijn voor studies van metabole ziekten, waaronder tuberculose en diabetes vanwege verschillende specifieke voordelen. De effecten van lep- of lepr-mutatie op obesitas bij zebravissen, zoals gerapporteerd door verschillende

onderzoeksgroepen, zijn controversieel. We veronderstellen dat verschillen in fokschema's en compenserende genetische mechanismen verantwoordelijk kunnen zijn voor de gerapporteerde inconsistenties. Vervolgens bespreken we dat de metabole veranderingen in leptinemutanten en infectieziekten die in dit proefschrift worden beschreven, in hoge mate geconserveerd zijn in verscheidene diersoorten en verschillende ontwikkelingsstadia, rekening houdend met de volgende punten. Ten eerste zijn metabole veranderingen als gevolg van mycobacteriële infectie sterk vergelijkbaar in mensen, muizen en zebravis larven. Ten tweede lijken metabole en transcriptomische veranderingen als gevolg van leptine mutatie erg op elkaar bij muizen en zebravislarven. Ten derde lijken metabole veranderingen als gevolg van mycobacteriële infectie en leptine mutatie sterk op elkaar bij muizen en zebravislarven. Ten vierde is aangetoond dat metabole veranderingen zeer vergelijkbaar zijn op basis van verschillende monstervoorbereiding en metabolomics-technologieën: massaspectrometrie en nucleaire magnetische resonantiespectroscopie. Verder bespreken we de rol van leptine bij tuberculose en het potentiële nut van leptine-deficiënte zebravissen voor studies naar zwangerschapsdiabetes mellitus en lopend werk dat momenteel wordt uitgevoerd. Ten slotte bieden we perspectieven van 3 aanvullende technologieën voor toekomstige studies van nieuwe onderzoeksvragen die voortvloeien uit deze studie. (1) Potentiële toepassingen van een methode genaamd positionele isotopomeer nucleaire magnetische resonantie tracer analyse (PINTA) en magnetische resonantie microimaging (μMRI) worden voorgesteld voor verder onderzoek bij zebravissen. (2) Een geautomatiseerde screeningtechnologie (VAST) bioimager-platform voor gewervelde dieren zal worden toegepast voor high-throughput-metingen van spierafbraak tijdens de ontwikkeling in met mycobacteriële geïnfecteerde wildtype en leptine-mutante zebravislarven. (3) Een gevoelig HPLC-MS/MS-platform voor gerichte analyse kan worden gebruikt voor studies van vetzuren, met name derivaten van de arachidonzuursignaleringsroute. Door deze geavanceerde platforms te gebruiken, willen we nieuwe inzichten bieden in de mechanismen van metabole veranderingen die ten grondslag liggen aan tuberculose en diabetes.

Curriculum Vitae

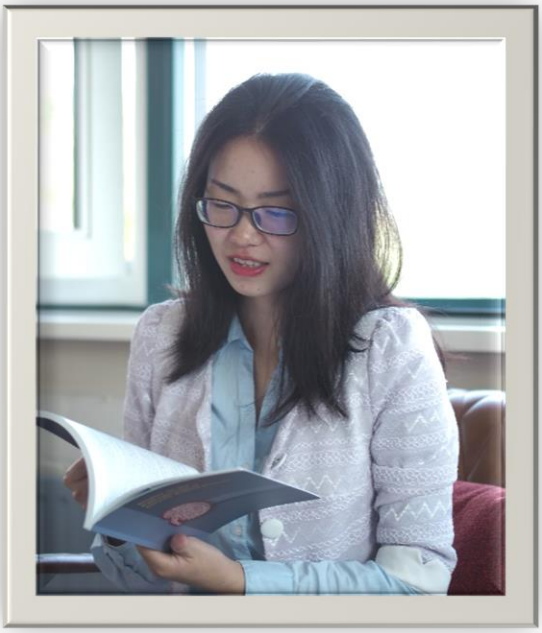

Yi Ding (Chinese: 丁义) was born in Chongqing, the People's Republic of China on 25th June, 1989. In September 2009 after graduating from high school, she started her bachelor studies at the College of Life Science, Hebei Normal University in Shijiazhuang, China. She did her internship in a middle school for six months and obtained a quantification certificate for high school teaching. In June 2013, she gained a bachelor diploma in biology. After that, she was admitted to the State key laboratory of biotherapy, Sichuan University in Chengdu, China. She was successful to get a scholarship at Sichuan University for her master studies. Her thesis project was about N-Acetylcysteine improvement of palmitate-induced myotube loss in skeletal muscle cells and high fat diet-induced muscle wasting in mice, under the supervision of Prof. dr. H. Xiao. In June 2016, she obtained a master diploma in cell biology. Subsequently, she worked in two biotechnical companies in China from July 2016 to August 2017. In September 2017, she was awarded a four-year grant from China Scholarship Council for PhD studies at the Institute of Biology, Leiden University, the Netherlands. The PhD projects focused on exploring the functions of leptin resulting from metabolic reprograming of tuberculosis and diabetes in mice and zebrafish, under the supervision of Prof. dr. H. P. Spaink and Prof. dr. A. Alia. The work of her PhD research is presented in this thesis. Currently from September 2021, she is working at the same institute as a post-doctoral fellow studying immune responses to *Mycobacterium avium* infection using zebrafish models.

List of publications

Ding Y, Haks MC, Forn-Cuní G, He J, Nowik N, Harms AC, Hankemeier T, Eeza MNH, Matysik J, Alia A, Spaink HP. Metabolomic and transcriptomic profiling of adult mice and larval zebrafish leptin mutants reveal a common pattern of changes in metabolites and signaling pathways. Cell Biosci. 2021 Jul 7;11(1):126.

He J*, **Ding Y***, Nowik N, Jager C, Eeza MNH, Alia A, Baelde HJ, Spaink HP. Leptin deficiency affects glucose homeostasis and results in adiposity in zebrafish. J Endocrinol. 2021 May;249(2):125-134.

Ding Y, Raterink RJ, Marín-Juez R, Veneman WJ, Egbers K, van den Eeden S, Haks MC, Joosten SA, Ottenhoff THM, Harms AC, Alia A, Hankemeier T, Spaink HP. Tuberculosis causes highly conserved metabolic changes in human patients, mycobacteria-infected mice and zebrafish larvae. Sci Rep. 2020 Jul 15;10(1):11635.

Ding Y, Haks MC, Ottenhoff THM, Harms AC, Hankemeier T, Eeza MNH, Matysik J, Alia A & Spaink HP. Leptin mutation and mycobacterial infection leads non-synergistically to the same metabolic syndrome.
Manuscript in preparation.

*Authors contributed equally.